Generation and characterisation of ultrashort diode laser pulses

Thesis presented for the degree of

Doctor of Philosophy

To the University of St. Andrews

By

David J. L. Birkin, MEng

April 2001

Generation and characterisation of ultrashort diode laser pulses

Thesis presented for the degree of

Doctor of Philosophy

To the University of St. Andrews

By

David J. L. Birkin, MEng

April 2001

Declarations.

I, David J. L. Birkin, hereby certify that this thesis, which is approximately forty seven thousand words in length, has been written by me, that it is the record of work carried out by me and that it has not been submitted in any previous application for a higher degree.

I was admitted as a research student and as a candidate for the degree of Doctor of Philosophy in October 1996; the higher study for which this is a record was carried out at the University of St. Andrews between 1996 and 2001.

In submitting this thesis to the University of St. Andrews I understand that I am giving permission for it to made available for use in accordance with the regulations of the University Library for the time being in force, subject to any copyright vested in the work not being affected thereby. I also understand that the title and abstract will be published, and that a copy of the work may be made and supplied to any *bona fide* library or research worker.

Signature of candidate. Date. 27/04/2007

I hereby certify that the candidate has fulfilled the conditions of the Resolution and Regulations appropriate for the degree of Doctor of Philosophy in the University of St. Andrews and that the candidate is qualified to submit this thesis in application for that degree.

Signature of supervisor. Date. 27-04-01

To my mother.

For all the sacrifices you've made over the past twenty-eight years.

Abstract.

This thesis is concerned with the development of a compact diode laser source of picosecond optical pulses having enhanced average powers. This is realised by the application of a large amplitude sinusoidal modulation to a single-contact, single-mode, narrow stripe, InGaAs/GaAs ridge-waveguide diode laser. The operational characteristics of the device when in continuous wave and gain-switched regimes are presented.

In the gain-switched regime, a minimum pulse duration of $30ps$ is demonstrated, at average and peak powers up to $\approx 150mW$ and $\approx 1.8W$ respectively. A sonogram technique is employed to determine the sign and magnitude of the frequency chirp in the optical pulses. On the basis of this information aperiodic gratings are designed and fabricated in germanosilicate optical fibres and lithium niobate crystals to realise temporal pulse compression and efficient second harmonic generation respectively.

The effect of self-injection optical feedback is described, along with the corresponding realisation in the reduction in the spectral bandwidth of the optical pulses from $\approx 11nm$ to $0.05nm$. When the optical feedback is provided by a standard diffraction grating, a tuning range of $70nm$ is demonstrated. The addition of a second grating results in two independently tunable outputs, with an adjustable spectral separation of up to $53nm$.

Bragg gratings are fabricated in the cores of photosensitive germanosilicate optical fibres. It is demonstrated that when such a fibre is used in an external cavity configuration, both temporal and spectral compression of the optical pulses is observed.

Direct frequency conversion of the diode laser output by using quasi-phase matched crystals of lithium niobate and KTP is demonstrated. High efficiencies are obtained with a KTP crystal containing a waveguide structure and a Bragg grating section to provide optical feedback to the diode laser. By this approach impressively high average second harmonic powers of up to $7.3mW$ in the blue spectral region are achieved for this frequency-doubled picosecond diode laser.

Abbreviations.

AML	Active mode locking.
AR	Antireflection.
a-PPLN	aperiodically poled lithium niobate.
a-FBG	aperiodic fibre Bragg grating.
E_g	Bandgap energy.
COD	Catastrophic optical damage.
^oC	Celsius.
l_c	Coherence length.
CPS	Coherent photon seeding.
CW	Continuous wave.
I	Current.
dB	Decibel.
DBR	Distributed Bragg reflector.
DC	Direct current.
DFB	Distributed feedback.
DH	Double hetrostructure.
DSO	Digital sampling oscilloscope.
DTDM	Distributed time-domain model.
d_{eff}	Effective nonlinear coefficient.
EOS	Electro-optic sampling.
eV	Electron-volt.
e	Electronic charge.
P_{elec}	Electrical power.
E	Energy.
f_{ext}	External cavity frequency.
L_{ext}	External cavity length.

L_B^{ext}	External cavity length for blue spectral components.
L_R^{ext}	External cavity length for red spectral components.
FBG	Fibre Bragg grating.
f	Femto.
E_F	Fermi energy.
FIBE	Focused ion beam etching.
f, ω	Frequency.
FDPM	Frequency domain phase measurement.
FROG	Frequency resolved optical gating.
FWHM	Full width at half maximum.
G	Giga.
GRIN	Gradient index.
HML	Hybrid mode locking.
HR	High reflection.
Hz	Hertz.
k	Kilo
L	Light.
LED	Light emitting photodiode.
α	Linewidth enhancement factor.
MOPA	Master oscillator and power amplifier.
M	Mega.
m	Metre.
μ	Micro.
f_{mod}	Modulation frequency.
MCP	Multi-channel plate.
n	Nano.
Ω	Ohm.
f_{opt}	Optical frequency.

OMA	Optical multi-channel analyser.
P_{opt}	Optical power.
OTDM	Optical time domain multiplexed.
OSA	Optical spectrum analyser.
PML	Passive mode locking.
Λ	Period.
PPLN	periodically poled lithium niobate.
PP-KTP	periodically poled potassium titanyl phosphate.
p	Pico.
Δk	Phase mismatch.
PMT	Photo multiplier tube.
S	Photon density.
$h\omega$	Photon energy.
KTP	potassium titanyl phosphate.
PID	Proportional, integral, derivative.
$\Delta\tau$	Pulse duration.
QPM	Quasi-phase matching.
n	Refractive index or carrier density.
RC	Resistance * capacitance product.
RF	Radio frequency.
SEM	Scanning electron microscope.
s	Second.
2ω	Second harmonic frequency.
SHG	Second harmonic generation.
SPM	Self phase modulation.
SCH-QW	Separate confinement hetrostructure quantum well.
$\Delta\lambda$	Spectral bandwidth.
c	Speed of light.
TEC	Thermo-electric cooler.

I_{th}	Threshold current.
TPA	Two-photon absorption.
UV	Ultraviolet.
V	Voltage.
W	Watts.
λ	Wavelength.

Figures.

Tables.

Contents.

Chapter 1.
Introduction.

1.1. Introduction.

The ideas underpinning light amplification in semiconductor devices were shown by Von Neumann in 1953.[1] Several independent groups subsequently demonstrated operational devices in the late 1950's and early 1960's. Although these first devices were rather crude by modern standards, they heralded a completely new direction for laser physics and technology. Since then, diode lasers have matured considerably and are now of great interest in many diverse aspects of modern life. Indeed, many technologies that we now take for granted (such as long-haul optical telecommunications and CD players) would be significantly more expensive and less practical if it were not for diode lasers. This intense commercial interest, together with much fundamental science interest means that there is extensive worldwide research in this topic.

Many physical attributes make diode lasers especially attractive. These include, ease of mass production using the existing fabrication technology from the semiconductor industry, direct electrical injection and modulation with associated high overall efficiencies, wide range of emission wavelengths and high output powers. Interestingly also, their small physical dimensions mean that they can be integrated directly into opto-electronics circuitry. No other laser source can claim such versatility or compatibility with modern technologies.

1.2. Semiconductor physics.

The underlying physics of semiconductor diode lasers is described comprehensively in the literature,[2-4] but for clarity some key issues will be briefly discussed here.

Consider the distribution of electrons within the energy levels of the conduction and valence bands of a semiconductor material. Under conditions of thermal equilibrium Fermi-Dirac statistics defines the occupation of an energy state with energy, E, as:[5]

$$F(E)=\left[1+\exp\left(\frac{E-E_F}{kT}\right)\right]^{-1} \qquad 1.1$$

where E_F is the Fermi energy, which marks the level of the carriers with the highest energy, and is constant for a given system at a particular temperature. In an undoped semiconductor in thermal equilibrium at zero Kelvin the Fermi energy level lies halfway between the valence and conduction bands.

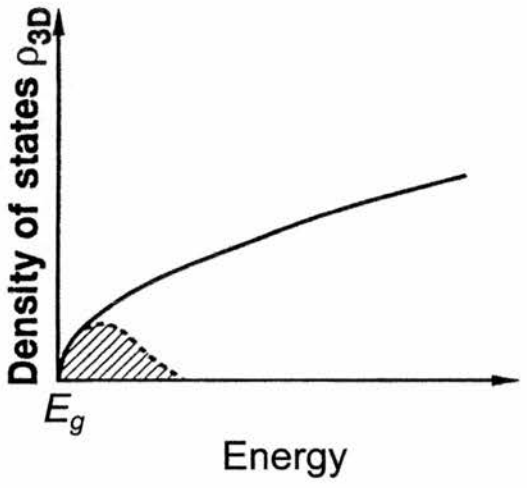

Figure 1.2.1. Density of states as a function of energy for a bulk material.[6]

From the Fermi function follows the *density of states,* $D(E)$, which is the occupational probability for the possible states. The density of states for a bulk material is illustrated as the solid line in Figure 1.2.1. and is quadratic in form. The dashed area represents the filled states.

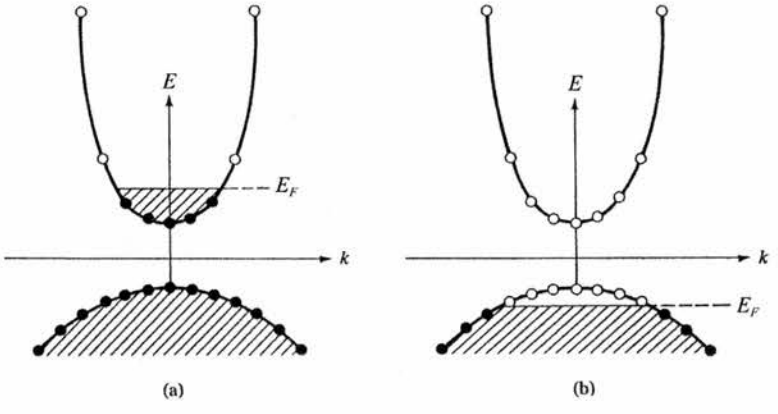

Figure 1.2.2. Energy band structure for *n*-doped (a) and *p*-doped (b) semiconductor at $0K$.[3]

Consider now the energy band diagrams of Figure 1.2.2. for a *degenerate* semiconductor material that is either doped *n*-type (a) or *p*-type (b). It should be

recognised that for high doping levels the respective Fermi energies are in the conduction and valance bands respectively.

In Figures 1.2.2. and 1.2.3. the open circles and none cross hashed areas depict holes, whereas the closed circles and the cross hashed areas depict electrons. Holes can be considered in a similar manner to electrons, but with an opposite charge, and because of this fill down the energy axis in contrast to electrons that fill up.

A junction formed from the combination of *n* and *p*-doped materials under non-thermal equilibrium conditions would have an energy band at the interface similar to that depicted in Figure 1.2.3. when subject to carrier injection. Two distinct Fermi levels now exist, one in the conduction band, E_{FC}, and one in the valance band, E_{FV}. The extent to which the Fermi levels impinge into the bands is dependent upon the doping.

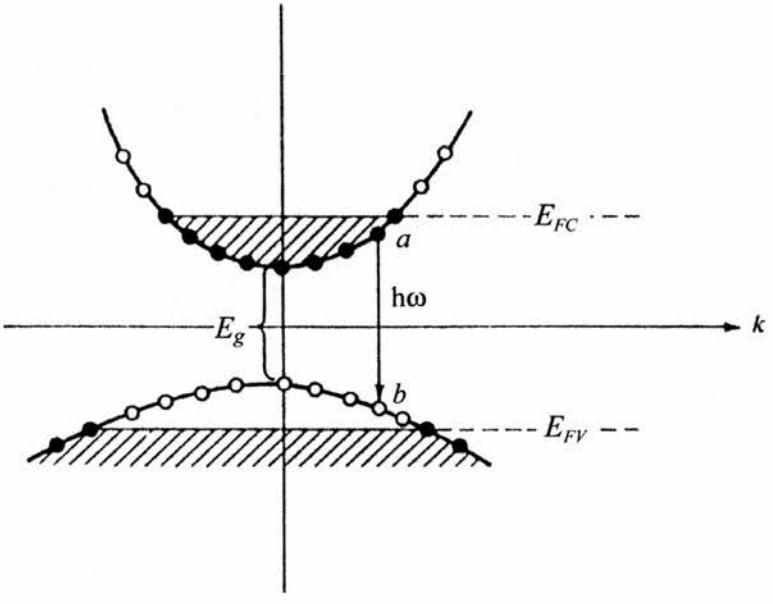

Figure 1.2.3. Energy bands for a doubly degenerate structure.[3]

If an incident photon has an energy, $h\omega$, that satisfies the condition:

$$E_g < h\omega < E_{FC} - E_{FV} \qquad 1.2$$

where E_g is bandgap, then that photon can induce the downward transition a → b as illustrated in Figure 1.2.3. This results in the production of a second photon of energy E that is coherent with the original. The above transition of a

→ b is for direct bandgap materials where the *k*-vectors are the same, and hence momentum is conserved. The transition a → b is however possible in indirect materials if a phonon is involved. The process outlined by Equation 1.2. results in optical gain for all frequencies that are satisfied.

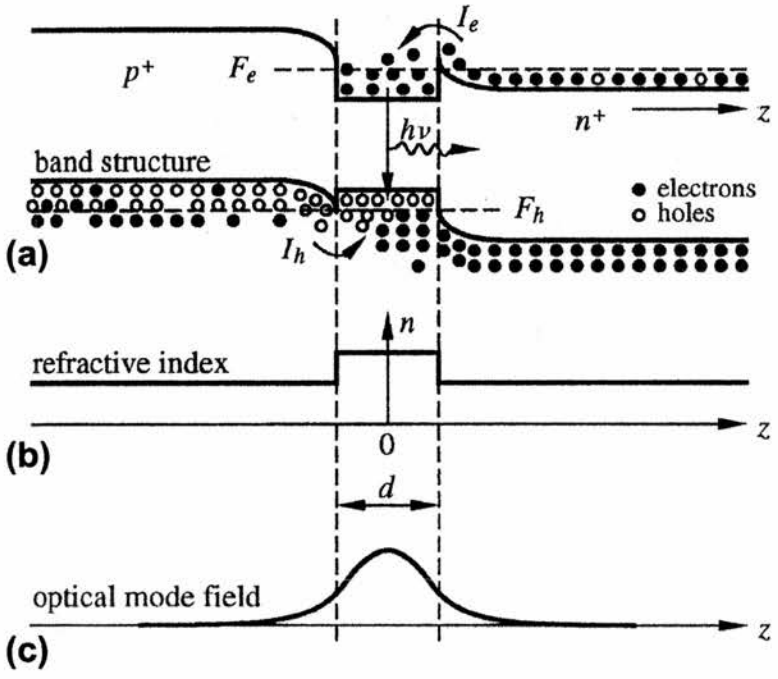

Figure 1.2.4. Schematic of a diode laser illustrating (a) the energy band of a double hetrostructure with (b) the refractive index profile and (c) the resultant optical mode.[7]

Shown schematically in Figure 1.2.4. are the energy band structure, refractive index profile and optical field for a bulk double hetrostructure (DH). It was a device based on a DH that resulted in a suitable reduction in the threshold carrier density such that room temperature operation was possible. In such bulk diode lasers, as shown in Figures 1.2.4. and 1.2.5. separate confinement mechanisms are established simultaneously for the injected carriers and optical field. Carrier confinement is provided by the difference in energy bandgap, reducing diffusion from the active region (Figure 1.2.5). Optical confinement is derived from the step change in the refractive index, confining the optical field mainly to the active region. In such a way both the injected carriers and optical field are confined to the same region of space, thus enhancing their interaction and lowering the threshold current density.

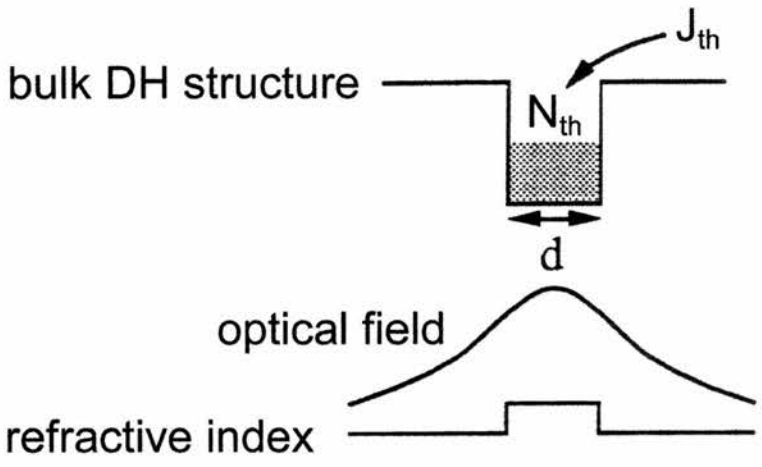

Figure 1.2.5. Schematic of a double hetrostructure showing (upper) carrier confinement, (middle) optical field and (lower) refractive index profile.[7]

An operational laser is formed through the enclosure of the gain mechanism within a suitable cavity. Such a cavity is obtained when a semiconductor crystal is cleaved along the *010* plane, (Figure 1.2.6.) thus forming a simple Fabry-Perot cavity with two parallel facets. Given the refractive index of, for example GaAs $(n = 3.6)$, the facets thus produced have a reflectivity suitable for lasing action (Equation 1.3.).

$$R = \left(\frac{n_{GaAs} - n_{air}}{n_{GaAs} + n_{air}} \right)^2 \simeq 0.32 \qquad 1.3$$

Although a reflectivity of 32% is satisfactory for lasing action, emission from both ends of the device will result. It is therefore standard that the facets of commercial devices are asymmetrically coated, with anti-reflecting (AR) on the output facet and high-reflecting (HR) on the rear.

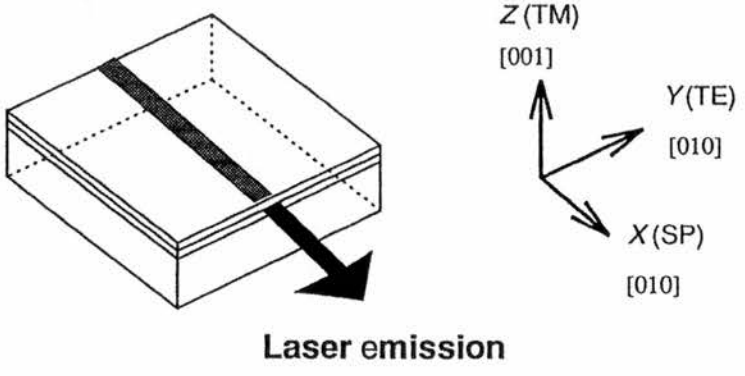

Figure 1.2.6. Crystallographic axes and planes.[8]

The threshold current density for a diode laser is given by Equation 1.4:[9]

$$J_{th} = \frac{8\pi v_0^2 ed\tau_{21}\Delta\nu n^2}{\tau_e c^2}\left[\gamma + \frac{1}{2l}\ln\left(\frac{1}{R_1 R_2}\right)\right] \qquad 1.4$$

The explanation for the terms used in Equation 1.4. can be found in Reference [9]. From Equation 1.4. it should be noted that the threshold current density scales with the active region thickness d perpendicular to the junction. It would therefore seem reasonable to assume that a reduction in J_{th} could simply be brought about by reducing d. However, if d is reduced below $\sim 10nm$ the optical confinement of the double hetrostructure illustrated in Figures 1.2.4. and 1.2.5. is reduced, with the consequence that the threshold current density starts to increase.[7] A structure through which a simultaneous reduction in both J_{th} and d can be achieved is the separate confinement hetrostucture quantum well (SCH-QW). The dimension d for a SCH-QW structure is reduced from the order of micrometres to that of nanometres. Such a reduction in d confines the carriers to a small region of *k*-space with the effect that the carrier energy and the density of states becomes quantised, as a result of which the density of states exhibits a step like profile (Figure 1.2.7.).

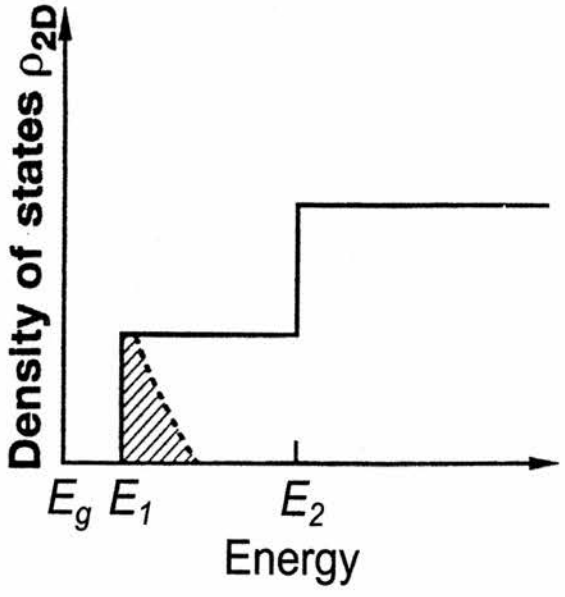

Figure 1.2.7. Density of states for a quantum well structure.[6]

Lasing action occurs between the sub-bands having the lowest energies. The photon energy, and hence the lasing wavelength, can be tailored by varying the well width and barrier height.[10,11] The carriers are still free to move parallel to the junction. A quantum well can be visualised as a 2D structure, with bulk being 3D. Further quantum confinement of the carriers is possible using quantum wires (1D)[12-17] and quantum dots (0D)[18-26] and is of interest due to the reduced threshold current densities that can thus be achieved.

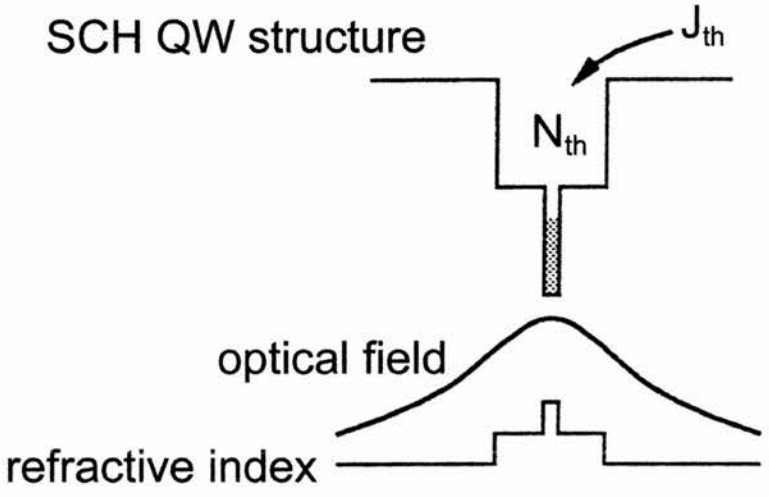

Figure 1.2.8. Schematic of a separate confinement hetrostructure showing (upper) carrier confinement, (middle) optical field and (lower) refractive index profile.[7]

Shown schematically in Figure 1.2.8. are the energy band, optical field and refractive index profile for a SCH-QW. The separate confinement features for the carriers and optical field of the SCH-QW are clearly visible when compared with the DH structure illustrated Figure 1.2.5.

1.3. Materials.

The diode laser is an exceedingly versatile source and through the use of appropriate materials and structures emission wavelengths from ~400nm to >200μm are possible with these limits being relaxed as material technology evolves. To span such a vast wavelength range, alloys from various elements in the periodic table are used, mainly being II-VI, III-V and IV-VI. Figure 1.3.1. illustrates many of the possible alloys and the possible emission wavelength ranges associated with each.

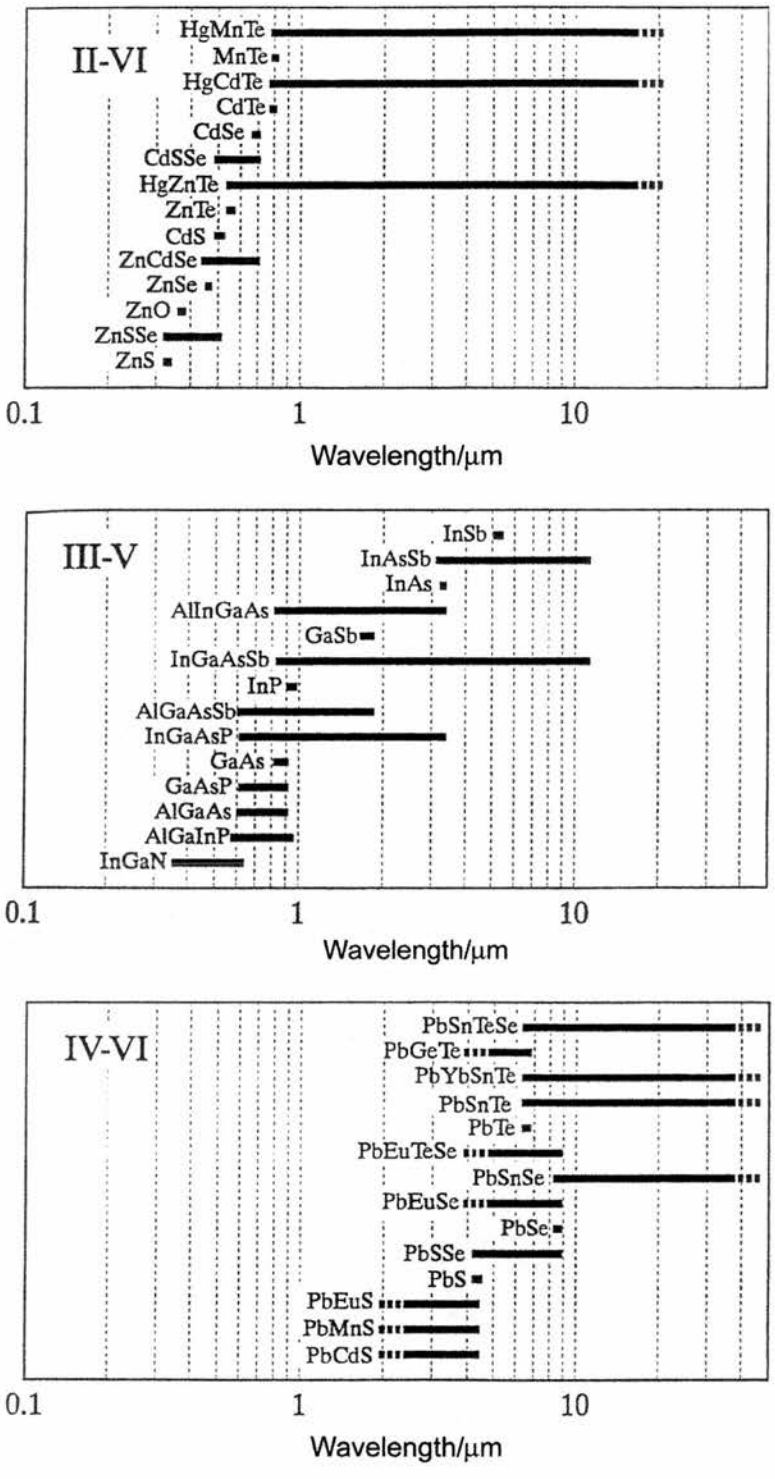

Figure 1.3.1. Material structures and their spectral coverage.[27]

Of particular interest is emission in the near infrared, because of its relevance to optical communications. The discussion that follows will focus on the particular alloy of the III-V quaternary compound $Ga_xIn_{1-x}As_{1-y}P_y$. Illustrated in Figure 1.3.2. is the lattice constant, a, (and emission wavelength) variation with

bandgap for this GaInAsP alloy. Those substrates that yield lattice matched growth are shown on the right hand side of the diagram with direct and in direct bandgap materials represented as solid and dashed lines respectively. The hashed area of the figure refers to quaternary alloys.

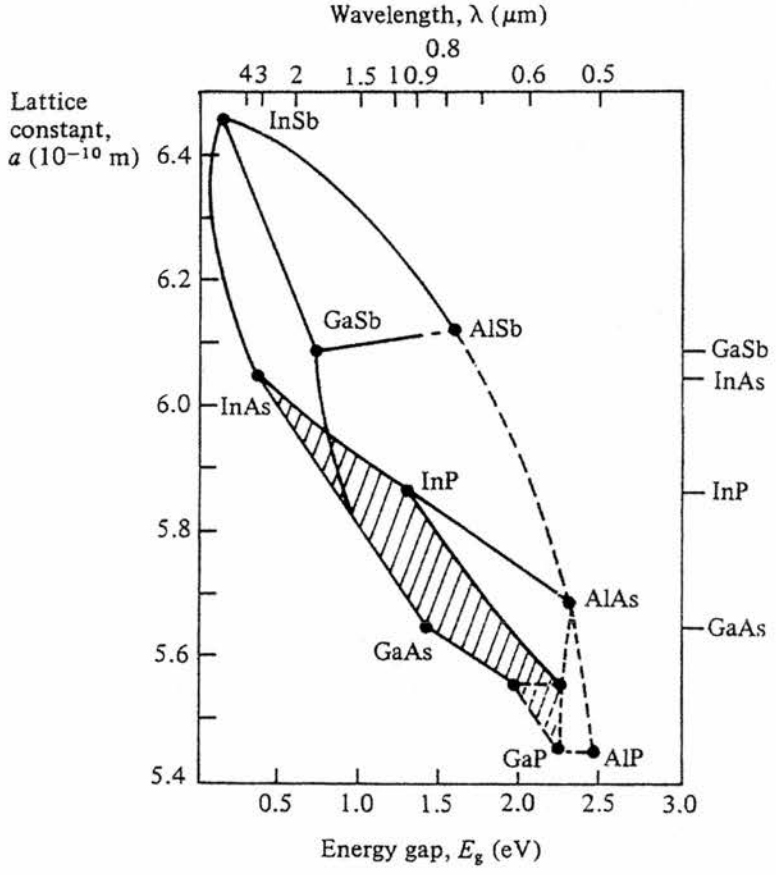

Figure 1.3.2. Lattice contstant versus energy gap for various III-V alloys.[9]

As shown in Figure 1.3.2, appropriate selection of parameters *x* and *y* results in a broad range of emission wavelengths. Table 1.3.1. lists the common emission wavelength ranges obtained when different active regions alloys are grown over a GaAs substrate.

Table 1.3.1. Emission wavelengths obtained for various active regions alloys grown on a GaAs substrate.

Active region alloy	Approximate wavelength range/nm
$Ga_xAl_{1-x}As$	780-850
GaAs	860-880
$Ga_xIn_{1-x}As$	940-1050

Typically the layers grown over the substrate have a lattice parameter roughly equal to that of the substrate, with any mismatch being $<0.1\%$. In this case, the layers are referred to as *lattice matched.* Such a small degree of mismatch is necessary to obtain defect-free growth, reducing the strain within subsequent layers. By varying the lattice parameter for a given substrate the emission wavelength may be adjusted. A certain amount of strain may be tolerated, although the mismatch $\Delta a/a$ may be no greater than 1.5%, where Δa is the difference in lattice parameters between the substrate and the overlying layers. As the introduced strain increases, the active region thickness must be reduced to ensure that the layers are free of dislocations. InGaAs and AlGaAsP form strained layers when grown over a GaAs substrate. Strained layers may be used effectively in quantum well lasers resulting in a reduced threshold carrier density due to a reduction in the density of states at the valance band maximum.[8]

1.3.1. Power versus performance.

Although diode lasers are used in many applications requiring low output powers, there are many circumstances where high output power devices are needed, such as metal machining and as a replacement for the flash lamps used for the excitation of solid-state lasers (e.g. Nd:YAG). Inherent to the design of diode laser is the difference in dimensions of the width and thickness of a typical active region. This causes the spatial output to be elliptical. Though the astigmatism is unavoidable it can be corrected through the use of various optical schemes including crossed cylindrical lenses, anamorphic prism pairs and optical fibre transmission. Reliability considerations, including catastrophic optical damage (COD) and accelerated degradation of the facets; kinks in the light/current (L/I) curve and thermal limitations all limit the output power of narrow stripe diffraction limited devices to several hundred milliwatts. The output may be increased without adversely affecting the lifetime by increasing the active region width, though this can result in filamentation. Various schemes have been employed to improve the transverse mode output from broad area devices including a bow-tie structure[28-31] and intracavity lenses

formed by focussed ion beam etching.[32] An output power of several watts may be obtained by combining several single emitters into an array that are then either individually fibre coupled into a single bundle or free-space combined using a beam reshaping optics.[33,34] This, however, is not ideal for all applications. High power diffraction limited outputs have been demonstrated[35-42] through the use of suitable master oscillator and power amplifier (MOPA) configurations and is analogous with similar approaches in electronics.

1.4. Short pulse generation from diode lasers.

Diode lasers may have large gain bandwidths, inferring that optical pulses with femtosecond durations should be possible. However, there are several mechanisms that will tend to broaden the pulses, thereby increasing the minimum duration that might otherwise be obtained. These pulse-broadening mechanisms include gain saturation, gain and group-velocity dispersion and frequency chirping.

The result of these pulse broadening mechanisms is that solitary pulsed diode lasers have typical durations of several picoseconds, though sub-picosecond durations have been demonstrated. There exist three generic methodologies with which the output from a diode laser may be pulsed. These are Q-switching; gain-switching and mode-locking techniques. A brief overview of these will now follow.

Shown in Equations 1.5 and1.6,[43] are the rate equations linking the carrier density, n, and photon density S. An analysis of these equations can provide an insight into the mechanisms involved in pulse generation from diode lasers.

$$\frac{dn}{dt} = \frac{j(t)}{ed} - g(n,S)v_g S - \frac{n}{\tau_s} \qquad 1.5$$

$$\frac{dS}{dt} = \Gamma g(n,S)v_g S - \frac{S}{\tau_{ph}} + \frac{\beta\Gamma n}{\tau_s} \qquad 1.6$$

where j is the time dependent current density, e is the electronic charge, d is the active layer thickness, $g(n,S)$ is the optical gain per unit length, v_g is the group velocity in the laser medium, τ_{ph} is the photon lifetime, β is the

spontaneous coupling factor, Γ is the optical confinement factor and τ_s is the carrier lifetime.

The photon lifetime is defined as:[43]

$$\tau_{ph} = \left(\frac{1}{v_g(\alpha_m + \alpha_i)} \right) \qquad 1.7$$

where α_m is the mirror loss divided by the cavity length, and α_i the internal cavity losses per unit length.

Equations 1.5 and 1.6 apply to a single mode condition and as such assume there is no distribution of S between cavity modes. They also assume that the gain is proportional to the carrier density, and that there is a uniform carrier distribution.

Spatial uniformity in the laser cavity is assumed such that:[43]

$$\frac{j(t)}{d} = \frac{i(t)}{V} \qquad 1.8$$

where $i(t)$ is the injection current and V is the active region volume.

It may be approximated that $g(n,S)$ is independent of S, and increases linearly with carrier concentration as:[43]

$$g(n,S) = g_0(n - n_t) \qquad 1.9$$

where g_0 is the gain cross section for stimulated emission and n_t the carrier density for transparency.

The optical gain g_0 can be considered to be constant for low photon densities, but tends to saturate at higher levels. This saturation results in increased damping of the small signal resonance peak[44] for high optical powers. The dependence of the optical gain on the nonlinear photon density is given by:[45]

$$g(n,S) = \frac{g_0(n - n_t)}{1 + \varepsilon S} \qquad 1.10$$

where g_0 and ε are determined from the small signal, high frequency modulation characteristics.[44]

The refractive index of the active region is linked to the carrier density, and from this it follows that a small increase in the carrier density shifts the gain peak to higher energies with a resultant shift of the emission to shorter wavelengths.[4] This wavelength shift (or frequency chirp) is described by $d\mu/dN$, which is related to the linear carrier dependant modulation of the refractive index. This leads to a parameter known as the linewidth enhancement factor,[46-48]

$$\alpha = -\frac{4\pi}{\lambda}\frac{d\mu/dN}{dg/dN} \qquad 1.11$$

As will be discussed later in this chapter in the context of gain-switching, chirp plays an important role in limiting the minimum pulse duration that may be obtained from such pulsed diode lasers.

During the evolution of a pulse the population inversion is depleted by carrier recombination, with a resultant change in the refractive index across the pulse, an affect known as self-phase modulation (SPM). SPM leads to frequency chirping of the pulses, which will be discussed in further detail in Chapter 4.

1.4.1. Gain-switching.

Gain-switching is the simplest method of producing short pulses directly from a diode laser. It has the further advantage that the modulation frequency can be easily varied. A diode laser is gain-switched by the direct application of a modulated electrical drive obtained from either a comb generator, picosecond photoconductive switch, avalanche transistor or sinusoidal modulation.

When a short electrical pulse is directly applied to a suitably pre-biased diode laser, optical relaxation oscillations occur. A single optical pulse will result if the duration of the electrical pulse is short enough that is has ceased before the onset of a secondary optical relaxation. The short length and high losses of a diode laser cavity result in a short photon lifetime. This means that an optical pulse can be much shorter than its electrical excitation pulse. An intense optical pulse can be obtained if before lasing action commences, a high gain situation is realised by the creation of a large inverted carrier density. Although stimulated emission quickly depletes the carrier density, a secondary optical

pulse with reduced amplitude can be produced if sufficient gain remains. However, these secondary pulses maybe eliminated if the carrier injection is adjusted such that the carrier density is only sufficient to provide gain for the main pulse, and after which the gain drops below threshold.

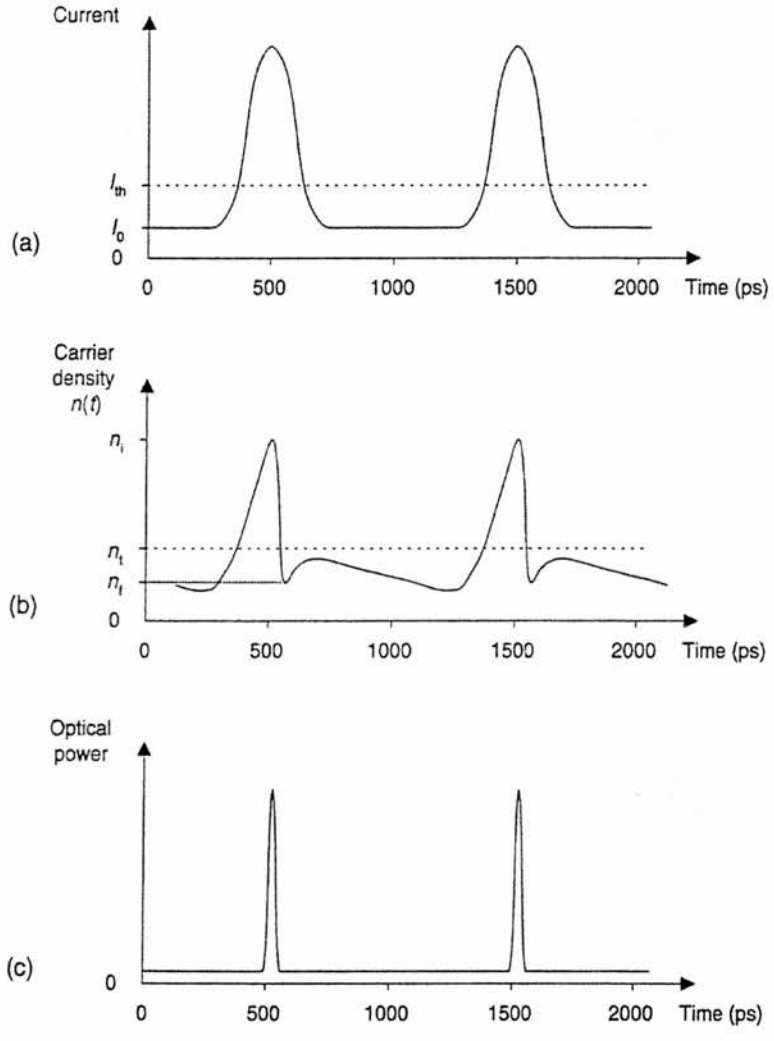

Figure 1.4.1. Time course of (a) electrical injection pulse, (b) carrier density and (c) optical output for a gain-switched device.[43]

Figure 1.4.1 illustrates the evolution of an optical pulse from a gain-switched diode laser pre-biased at some current, I_0, below threshold, I_{th}. The current pulse (a) quickly increases the carrier density (b) to a value greater than transparency, n_t, at which point lasing can commence. The carrier density follows the current pulse to reach a maximum value of n_i before decreasing, due to stimulated emission, to a value of n_f below the lasing threshold. The

optical pulses generated by gain switching may have pulse durations in the picosecond region, although femtosecond durations[49-51] have been obtained by the use of extra-cavity pulse compression. Gain switching can result in a viable and simple source of picosecond pulses at all diode laser wavelengths.

If S is large enough such that the final term of Equation 1.6 can be neglected,[43] then $S(t)$ increases exponentially through stimulated emission. Furthermore, if $n_i - n_t$ is large enough when lasing action commences then the middle term may also be neglected. Thus:[4,43]

$$\frac{1}{S}\frac{dS}{dt} = g_0 v_g \Gamma (n_i - n_t) \qquad 1.12$$

Najarajan and Bowers[52] illustrated how the rise time of an optical pulse from a gain-switched pulse was dependent upon the total charge , Q, contained within the electrical pulse and not the shape. Najarajan and Bowers[52] discussed how the optical pulses from a gain-switched diode laser can be approximated as two exponentials for the rise, τ_r, and fall, τ_f, times respectively:[52]

$$\tau_r = \frac{qV}{v_g g \Gamma Q} \qquad 1.13$$

and

$$\tau_f = \frac{1}{v_g g \Gamma (N_{th} - N_f)} \qquad 1.14$$

where q is the electronic charge, V is the volume of the active region, v_g is the mode velocity,[52] g is the differential gain, and Γ is the transverse optical confinement factor.

The fall time typically shows an exponential decay with a duration $\tau_f \approx \tau_r + \tau_{ph}$ that can be up to four times longer than the rise time as it is determined by the difference between the threshold and transparency densities, along with being limited by the energy transfer between the electron and photon populations. An expression for the optical pulse shape was suggested by Helkey and Arakawa[53] as being:

$$S(t) = \frac{2\hat{S}}{\exp(-t/\tau_r) + \exp(-t/\tau_f)} \qquad 1.15$$

Important considerations concerning the performance of a gain-switched diode laser are the phase noise (or timing jitter),[54-63] frequency chirping[63-69] and spectral bandwidth broadening. During the evolution of a gain-switched pulse, stimulated emission causes carrier recombination and a reduction of the carrier density in the conduction band. This gradual reduction of the carrier density results in a shift of the emission wavelength across the optical pulse due to a change in the refractive index of the active region. This shift of the emission wavelength gives rise to a pulse that is frequency chirped, where the wavelength shift is:[43]

$$\Delta\lambda \approx \frac{\lambda_0}{\mu_0}\frac{d\mu}{dn}\Delta n \qquad 1.16$$

Frequency chirping of the optical pulses from a gain-switched diode laser results in a time-bandwidth product greater than that of the Fourier-transform limit and may be expressed as:[70-73]

$$\Delta\tau\Delta\nu = k\left(1+\alpha^2\right)^{\frac{1}{2}} \qquad 1.17$$

where k is a constant dependent upon the assumed pulse shape and α is the linewidth enhancement factor expressed in Equation 1.11.

The rate equations presented earlier were for a single longitudinal mode laser. However, due to the dynamic overshoot of the electron concentration it is possible that multiple longitudinal modes may be generated even in a laser that would, under CW operating conditions be single-mode. The single-mode rate equations can be modified[74] to:[43]

$$\frac{dn}{dt} = \frac{j(t)}{ed} - v_g\sum g_m S_m - \frac{n}{\tau_s} \qquad 1.18$$

and

$$\frac{dS_m}{dt} = \Gamma g_m v_g S_m - \frac{S_m}{\tau_{ph}} + \frac{\beta\Gamma nD_m}{\tau_s} \qquad 1.19$$

where $g_m=(D_m n-n_t)g_0$, S_m is the photon density for the mth mode and D_m is the line-shape factor. The photon density is given by $S(t)=\sum S_m$.

The pulse energy from a gain-switched diode laser is limited by the charge of the electrical pulse, which is determined by the peak voltage of the external drive circuitry. The shortest optical pulses with the greatest energy may be obtained when the diode laser is DC biased at some level just below threshold.

1.4.2. Q-switching.

A cavity, be it microwave or optical, has an associated parameter referred to as the quality factor, Q. An optical cavity with a low round-trip loss is referred to as being high Q, whereas one with a high loss has a low Q. Q-switching involves switching the cavity Q from a low value to a high value over a relatively short period of time and this is brought about by a modulation of the cavity loss. Whilst the Q is low, electrical injection increases the carrier density that, since it is not depleted through stimulated emission, can increase to values greater than the threshold density. When the cavity Q is dramatically increased and lasing commences, the result is a high intensity optical pulse before the carrier density falls below the threshold value. The optical pulse duration is of the order of a few cavity round-trip period.

A Q-switched laser will consist of at least two discrete sections: a gain section and a loss section. The mechanism underpinning the loss modulation determines whether the Q-switching is active, passive or hybrid (a combination of the former two.)

Typically, active Q-switching involves modulating the loss of the diode laser cavity, be it an element external to the diode laser (such as a modulator) or a loss intrinsic to the actual device. The frequency of the external electrical drive applied to the loss section determines the repetition rate of the diode laser. It is more common for a two-section diode laser to be utilised with a modulation applied to a loss section and a DC bias applied to a gain section. An example of a Q-switched device is that of the *bow-tie* laser demonstrated by Williams and co-workers where a loss section was situated between two flared gain

regions.[29] A modulation was then applied to the central section whilst the outer sections were DC biased. The gain sections were flared in order to maximise the gain extraction of the optical mode and reduce the likelihood of COD due to the high pulse energies. Shown in Figure 1.4.2. is the temporal evolution of optical pulses from an actively Q-switched diode laser, where the cavity loss is modulated by application of an electrical pulse to a loss section of a two-section device.

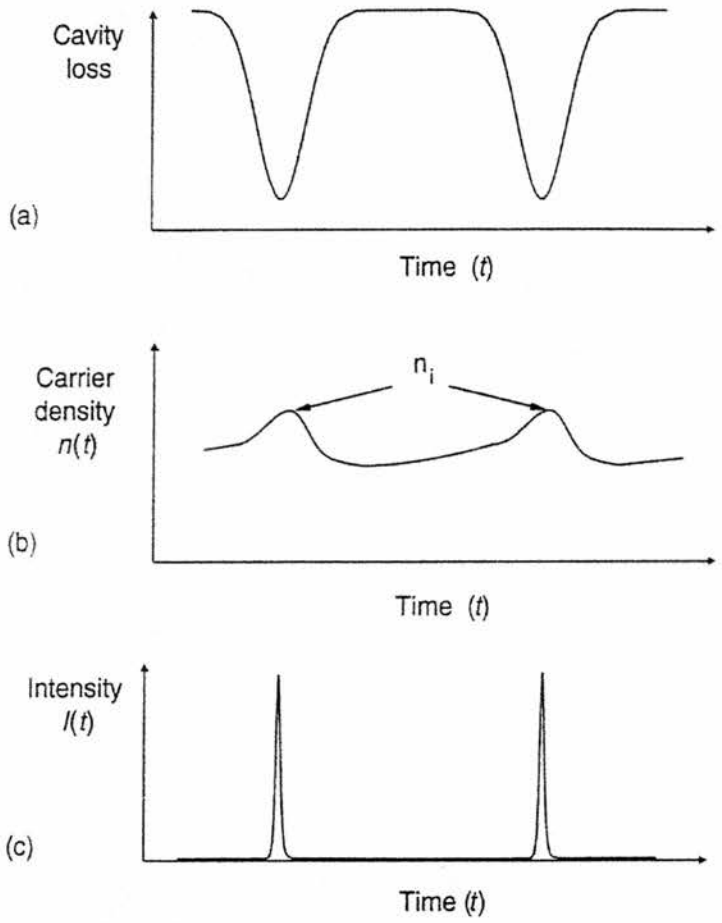

Figure 1.4.2 Time course of (a) cavity loss, (b) carrier density and (c) optical output for a Q switched device.[43]

Passive Q-switching,[75] also referred to as self-Q-switching, exploits intentional defects present within the diode laser structure which act as a saturable absorber. For low light intensities, the saturable absorber is strongly absorptive such that this represents a low cavity-Q condition. As the population inversion in the conduction band increases so does the rate of stimulated emission. The saturable absorber is then bleached resulting in a dramatic increase in the

cavity Q at which point laser emission can occur. As the saturable absorber recovers (via carrier recombination) it becomes highly absorbing ready for the cycle to re-commence.

Vasil'ev[4] illustrated that from the rate Equations of 1.5 and 1.6 the photon density for a Q-switched diode laser may be expressed as:

$$S(t) = n_i - n(t) - \frac{1}{g_o v_g \tau_{ph}} \ln\left[\frac{n_i - n_t}{n(t) - n_t}\right] \qquad 1.20$$

It then follows[43] that the pulse duration from a Q-switched diode laser can be expressed as:

$$\tau = \frac{rn\tau_{ph}}{(r - 1 - \ln r)} \qquad 1.21$$

where r is the inversion parameter defined as:[43]

$$r = g_0 v_g \tau_{ph}(n_i - n_t) \qquad 1.22$$

The loss section required for Q-switched operation can be realised in the design of the structure or a device can be post-processed. The post-processing techniques commonly utilised include focussed ion beam etching (FIBE) for the fabrication of actively Q-switched multi-section devices and ion implantation for the passively Q-switched devices.

1.4.3. Mode locking.

If one wishes to obtain the shortest optical pulses from a diode laser then mode-locking is the technique that must be employed. Only a brief overview of the technique will be presented here and for a more in-depth discussion on the subject the reader is referred to the following publications.[76-79]

Given that a typical diode laser cavity may have a length $\leq 1\text{mm}$ and a large gain-bandwidth there exists the possibility of many oscillating longitudinal modes, ν_n, where $n = 1,2,3...$ with a frequency of $\delta\nu$ between adjacent cavity modes. Only those modes for which the gain, g, exceeds the loss, α, will oscillate within the cavity. The output from the laser is then the sum of all the

individual frequency components, where the electric field may be given by the expression:

$$\mathrm{E}(t)=\sum_{n=0}^{N-1}(\mathrm{E}_0)_n \exp\left[j(\omega_n t+\delta_n)\right] \qquad 1.23$$

where E, ω and δ represent the amplitude, angular frequency and phase of the *n*th mode respectively.

With no outside influence, the longitudinal modes from a diode laser will have a random phase relationship with respect to one another. The output is continuous wave with an intensity given by the summation of the electric field of the individual modes.

If there are N modes oscillating incoherently then the total irradiance is given by:

$$I = N\mathrm{E}_0^2 \qquad 1.24$$

However, if it is arranged that the phases of the longitudinal modes maintain a constant relationship with one another, such that $\delta_n = \delta$, then the electric field will now be given by:

$$\mathrm{E}(t)=\mathrm{E}_0 \exp(j\delta)\sum_{n=0}^{N-1}\exp(j\omega_m t) \qquad 1.25$$

This results in the output from the laser being in the form of a periodic train of intense pulses:

$$\mathrm{E}(t)=\mathrm{E}_0 \exp\left[j(\omega t+\delta)\right]*\frac{\sin\frac{N\phi}{2}}{\sin\frac{\phi}{2}} \qquad 1.26$$

where $\phi=\frac{\pi \mathrm{ct}}{\mathrm{L}}$.

The irradiance, $\mathrm{I}=\mathrm{E}(\mathrm{t})\mathrm{E}^*(\mathrm{t})$, so Equation 1.26 maybe re-written as:

$$I(t)=\mathrm{E}_0^2\frac{\sin^2\left(\frac{N\phi}{2}\right)}{\sin^2\left(\frac{\phi}{2}\right)} \qquad 1.27$$

Equation 1.27 results in the emission of a series of intense optical pulses with a periodicity of $t=2L/c$ that is equal to the round-trip period of the laser cavity. The optical pulses have a duration $\Delta\tau$, which is inversely proportional to the lasing spectral bandwidth, $\Delta\nu$.

As N modes may oscillate simultaneously and omitting pulse shape considerations, the minimum pulse duration is given by:

$$\tau_{\min} = \frac{2L}{Nc} = \frac{1}{\Delta\nu} \qquad 1.28$$

This is an idealised situation, because in real laser systems $\Delta\nu \cdot \Delta\tau \neq 1$. The pulse shape must be taken into account when considering the time-bandwidth product, as the assumed pulse shape makes a significant difference to the pulse duration.

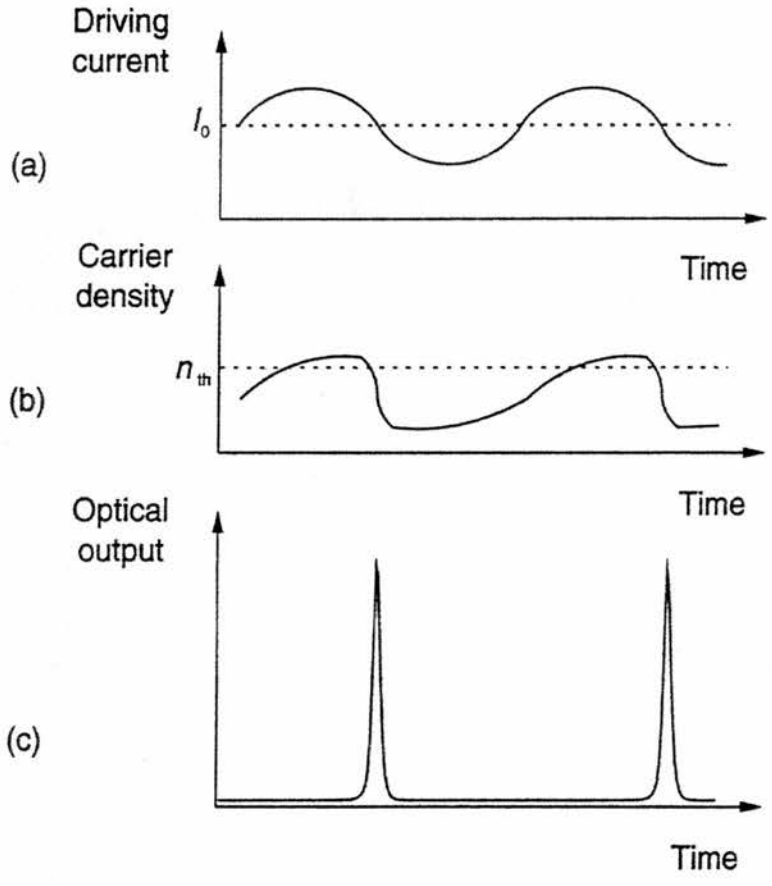

Figure 1 4 3 Time course of (a) sinusoidal current, (b) carrier density and (c) optical output for a mode-locked device.[43]

Various pulse shapes with their time-bandwidth products may be found in Table 1.5.1. Furthermore, Equation 1.28 illustrates that increasing the number of longitudinal modes that are locked together decreases the resultant pulse duration accordingly.

The principle of operation for active mode-locking a diode laser is illustrated in Figure 1.4.3. This involves modulating the gain (or loss) of the device at a frequency equal to the mode spacing. Typically a sinusoidal modulation is superimposed on a DC bias and applied to the device (Figure 1.4.3a.) producing a similar modulation in the carrier density (Figure 1.4.3b.). By suitable choice of both the sinusoidal modulation amplitude and DC bias it can be arranged that the carrier density exceed the lasing threshold (n_{th}) for only a short period of time during each cycle. The result is a sequence of intense optical pulse with a frequency corresponding to the round-trip time of the cavity.

Methodologies used for the realisation of mode-locking of diode lasers maybe broadly classified into two categories: active mode-locking (AML) and passive mode-locking (PML). A scheme that falls into both schemes is classified as hybrid mode locking (HML) and utilises techniques from both AML and PML.

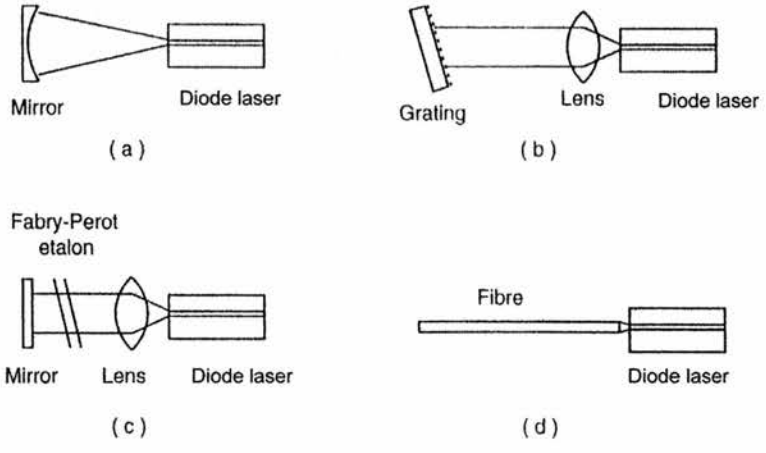

Figure 1.4.4. External cavity mode-locking of a diode laser using (a) mirror, (b) grating, (c) mirror and Fabry-Perot etalon and (d) fibre.[43]

Although mode-locking produces pulses with the shortest durations and highest peak powers, it is limited due to the fact that the repetition frequency of a solitary diode laser cannot be varied since it is determined by the cavity round trip time, or multiples thereof. The short cavity lengths of diode lasers yield a

cavity frequency that can be prohibitively high. To alleviate this problem, various schemes (Figure 1.4.4.) have been employed to increase the cavity length, thereby reducing the frequency. Prior to the implementation of an external cavity, element one facet of the diode laser is AR-coated.

1.5. Pulse characterisation.

In the course of this work several different techniques have been employed to directly observe the pulses in the time domain. Each measurement system has its own merits. These measurement systems will be discussed and their advantages and disadvantages highlighted.

1.5.1. Electron-optical streak camera.

Electron-optical streak cameras have been used for temporal measurements for many years. There is still considerable interest in this technology due its sensitivity and versatility. The streak camera converts an incoming temporal pulse directly into a spatial representation of that pulse, where the spatial brightness is directly related to the pulse intensity.

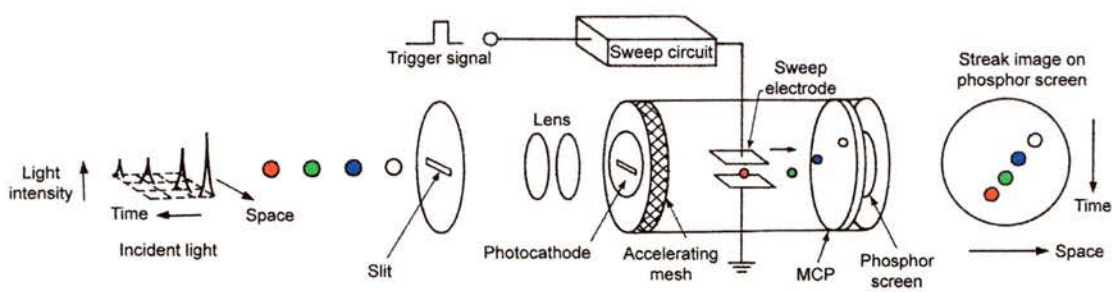

Figure 1.5.1. Schematic of a streak camera.

Figure 1.5.1. illustrates schematically the basic operational principles of a streak camera of this type. Incoming laser pulses that are separated in time illuminate a slit forming an image on a photocathode through the use of suitable optics. The photocathode converts the optical pulses into bursts of electrons, where the number of electrons is directly related to the intensity of the incident pulse. These photoelectrons are accelerated toward a phosphor screen by the application of suitable voltage gradients. Before impinging upon the phosphor screen the electrons pass through a microchannel plate (MCP) where they are

multiplied. Thus the image produced on the phosphor screen is a faithful representation of the pulse that produced it. The sweep electrodes spatially separate the temporal pulses by the application of a deflection voltage that is synchronised with the arrival of the photoelectrons. This sweep voltage determines the operation of the streak camera, which can be classified as either single-shot or synchroscan. In single-shot operation when triggered only one sweep is performed, whereas synchroscan operation involves a high-speed repetitive sweeping of the deflection voltage through the application of a sinusoid. For synchroscan operation it is necessary to synchronise the sinusoidal sweep voltage with incident laser pulses. It is possible to detect very faint events with a high signal-to-noise ratio and high dynamic range due to the repetitive nature.

The measured pulse duration of the laser pulse will be a convolution of the actual pulse duration and the streak camera response, as given by:

$$\tau_{measurement} = \sqrt{\left(\tau_{streakcamera}\right)^2 + \left(\tau_{actual}\right)^2} \qquad 1.29$$

where $\tau_{streakcamera}$ is the total impulse response of the streak camera.

When a streak camera is operated synchroscan the image on the phosphor screen is the accumulation of many individual pulses. If there is a slight fluctuation in the spatial representation of the pulses then the perceived duration will be increased over that of the actual duration. This process is caused by *jitter* and limits the temporal resolution of the streak camera. In spite of this, electron-optical streak cameras have been demonstrated with a temporal resolution of $\sim 500 fs$.[80]

The scanning nature of a streak camera enables *full frame* detection of weak optical phenomena, which has resulted in the use of the streak camera in many diverse applications including, amongst others, semiconductor physics, photochemistry, biomedical science, plasma physics and optical communications.

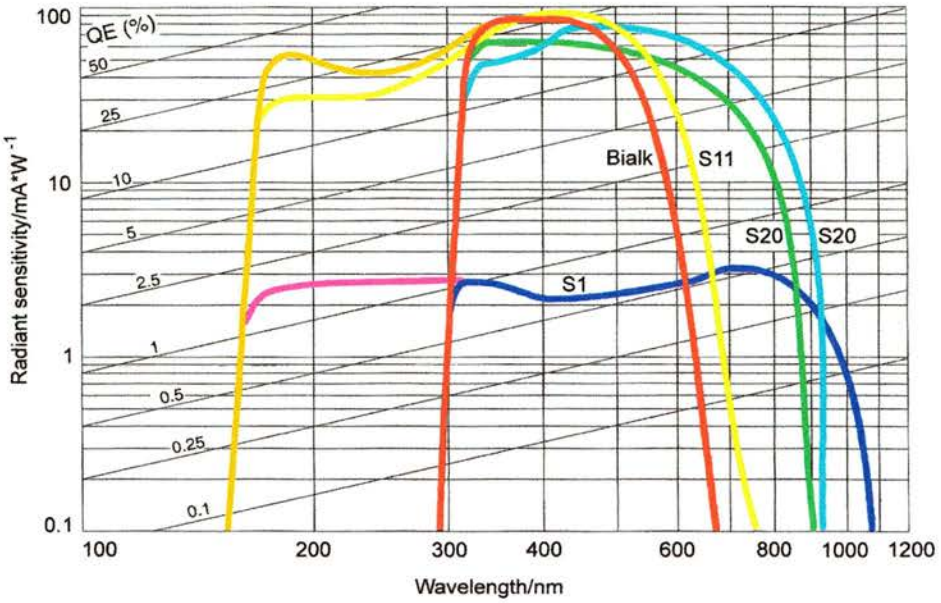

Figure 1.5.2. Spectral response curves for the main photocathode types.

The visual representation of the pulses on the phosphor screen is typically monitored using a suitable CCD camera or optical multichannel analyser (OMA) with a computer used for realtime analysis. The spectral response, and sensitivity is highly dependent upon the type of tube that is utilised. Illustrated in Figure 1.5.2 are the photo-sensitivity ranges for the typical photocathodes used. Temporal resolutions of $\sim 500 fs$ and the direct realtime detection of very weak optical emissions make streak cameras an attractive pulse measurement technique.

1.5.2. Autocorrelation.

An autocorrelator is based on a Michelson interferometer type of optical delay. The incoming pulse is split along two arms that have variable path length using a 50:50 beam splitter. At the end of these two arms are mirrors (or corner cubes), one of which is fixed whilst the other moves to sweep a delay. Whilst this may be suitable for femtosecond duration pulses where the delay required is small $(1\text{ps} \approx 3\text{mm})$ this is not the case for picosecond duration pulses. The longer delay required for an autocorrelator of pulses having durations of several picoseconds can be realised by mounting both mirrors (or corner cubes) on loudspeakers operating out of phase (Figure 1.5.3.). Upon reflection, the

returning beams pass through the beam-splitter and are focussed into a second harmonic generation (SHG) (non-zero χ_2) crystal, cut for type I phase matching, where they interfere. Due to the nonlinear response of the SHG crystal, the generated second harmonic is proportional to the temporal overlap between the two pulses. A filter blocks any unconverted fundamental from reaching the photo multiplier tube (PMT) used for detection. The electrical signal from the PMT is therefore related to the degree of overlap between the two beams from the individual arms.

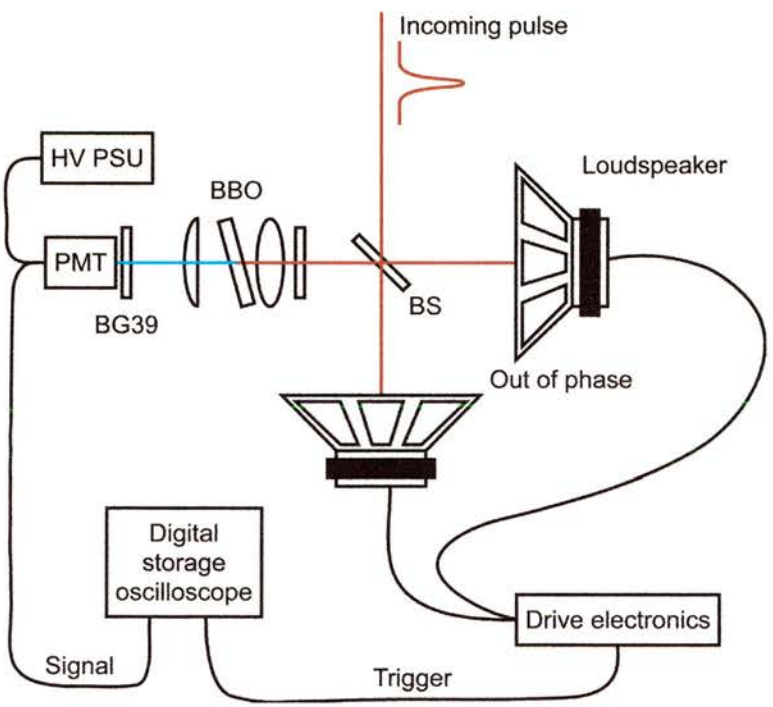

Figure 1.5.3. Autocorrelator suitable for the measurement of picosecond duration pulses.

If the PMT and oscilloscope to which it is connected are impedance matched then the measured autocorrelation will be interferometric $g(\tau)$, whereas if the system is not matched an intensity autocorrelation $G(\tau)$ will be measured.[81]

$$g(\tau)=\frac{\int_{-\infty}^{\infty}\left|\left[E(t)+E(t-\tau)\right]^2\right|^2 dt}{2\int_{-\infty}^{\infty}E^4(t)dt} \qquad 1.30$$

$$g(\tau)=1+\frac{2\int_{-\infty}^{\infty}E^3(t)E(t+\tau)dt+2\int_{-\infty}^{\infty}E(t)E^3(t+\tau)dt+3\int_{-\infty}^{\infty}E^2(t)E^2(t+\tau)dt}{\int_{-\infty}^{\infty}E^4(t)dt} \qquad 1.31$$

The intensity autocorrelation function $G(\tau)$, which is the time average of $g(\tau)$, is given by:[81]

$$G(\tau)=1+2\frac{\int_{-\infty}^{\infty}I(t)I(t-\tau)dt}{\int_{-\infty}^{\infty}I^2(t)dt} \qquad 1.32$$

where $I(t)=\mathrm{E}^2(t)$, and the signal-to-noise ratio should be 3:1.

The autocorrelator must be calibrated to establish the relative delay of the two arms with respect to one another. Moving one of the arms a known distance and recording the corresponding delay provides the calibration, τ, in the above equations. This calibration is valid until either the speaker amplitude or frequency is varied.

Table 1.5.1. Various pulse shapes with their respective time-bandwidth products.[81]

	Pulse profile $I(t)$ $(x\equiv t/T)$	Time-bandwidth product $\Delta\tau\cdot\Delta\nu$
Gaussian	$I(t)=e^{-x^2}$	0.4413
Diffraction function	$I(t)=\frac{\sin^2 x}{x^2}$	0.8859
Hyperbolic secant squared	$I(t)=\mathrm{sech}^2 x$	0.3148
Lorentzian	$I(t)=\frac{1}{1+x^2}$	0.2206

Of all the direct temporal measurement systems, the autocorrelator has the best temporal resolution and is therefore capable of monitoring the shortest pulses with durations as short as $\sim 5\,fs$. A potential major drawback of the autocorrelator is that a pulse shape must be *assumed* (Table 1.5.1.) and this

can be problematic if the measured pulses have asymmetric intensity profiles. Even with this limitation the autocorrelator has the possibility to provide useful information as it may highlight features that would otherwise go undetected if another technique were used. The excellent temporal resolution and convenience of autocorrelators make this a preferred method of ultrashort pulse characterisation.

The nonlinear crystal and PMT may be replaced with a semiconductor device in which a two-photon absorption (TPA) effect is utilised. For a semiconductor with a bandgap, E_g, an incident photon must have an energy greater than $h\nu$ if it is to create an electron-hole pair. However, if the incident beam is of sufficiently high intensity then two photons with energies of $\geq h\nu/2$ may excite electrons into the conduction band. The TPA effect is quadratic in nature and was first observed by Takagi and co-workers in Si and GaAsP photodiodes.[82]

Since then, TPA has been observed in diode lasers and light emitting diodes (LED's)[83]. Reid and co-workers used a commercial AlGaAs LED with a peak emission of $660nm$ as an unbiased photodetector. As the LED's bandgap was greater than the photon energy of the $800nm$ laser output, negligible photovoltage was observed when the laser was operated CW. The measured photovoltage increased by approximately two orders of magnitude when the laser was mode locked. The effect observed above was that of two-photon absorption and is now widely used in autocorrelators. It is worth noting that two-photon absorption in a waveguide is dependent upon the polarisation of the incoming radiation.[84]

1.5.3. High-speed photodiode.

At the time of writing, the *fastest photodiode* was a 370 GHz *p-i-n* travelling wave photodiode fabricated using low-temperature grown GaAs.[85] This photodiode fabricated by Chiu and co-workers had a recorded impulse response (measured using electro-optic sampling (EOS)[86]) of 1.1 ps FWHM at 800 nm, although the measured impulse response was asymmetrical. A 220 GHz photodiode fabricated by Ito and co-workers[85] had a symmetrical

impulse response of 1.44 ps FWHM at 1.55 μm. The bandwidth of such a photodiode may be increased by (1) reducing the physical dimension of the device that in turn decreases the *RC* product, (2) reduce the carrier lifetime of the materials and (3) minimise the transit time by reducing the electrode spacing. As the dimensions of the photodiode active area are reduced, the sensitivity of the device will suffer. Therefore, most high-speed photodiodes are single-mode optical fibre coupled in order to maximise the detection. This makes the high-speed photodiode of particular interest in telecommunications systems analysis. An important consideration for high-speed photodiodes is whether they are frequency- or time-domain optimised. The devices discussed above are not commercially available, and even if they were, digital sampling oscilloscopes are currently limited to 50 GHz.

The frequency domain is related to the time domain by:[87]

$$\tau_{FWHM} = \frac{0.44}{f_{3dB}} \qquad 1.33$$

where f_{3dB} is the frequency bandwidth at 3dB.

Using Equation 1.33, the τ_{FWHM} for a 50 GHz digital sampling oscilloscope would be 8.8 ps. This however is not the minimum pulse duration that could be measured, since the observed pulse duration depends upon the convolution of many bandwidths that will include the signal, photodiode and the oscilloscope. Thus, if a Gaussian pulse with a given FWHM duration were incident upon a fast photodiode connected to such a digital sampling oscilloscope, the duration of the pulse measurement may be obtained by summing the squares of the individual impulse responses. For example:

$$\tau_{measurement} = \sqrt{\left(\tau_{dso}\right)^2 + \left(\tau_{photodiode}\right)^2 + \left(\tau_{actual}\right)^2} \qquad 1.34$$

The individual impulse response of the components that make up Equation 1.34 are well defined such that they can be taken into consideration when the determining the actual pulse duration Another consideration when making a temporal measurement of a diode laser pulse with photodiode/DSO combination is jitter. As the oscilloscope trace is made up of the data from

many different optical pulses any timing differences between the individual pulses will increase the measured pulse duration. As jitter is random it is not easily eliminated, but for small values its influence on the pulse measurement can be minimised through the use of averaging.

1.6. Conclusions.

In summary, an overview of the underlying semiconductor physics and materials structures relevant to diode laser operation has been presented.

The basic principles of short pulse generation from a diode laser have been described. Q-switched and gain-switched operations in particular will be discussed in subsequent chapters.

The main direct pulse measurement techniques were summarised, and attention paid to their respective characteristics. Given the picosecond duration of the pulses generated in the work that follows, the high-speed photodiode provides a convenient method through which the pulse duration can be deduced in most instances.

1.7. References.

1. Dupuis, R. D., "An Introduction to the Development of the Semiconductor-Laser," *IEEE Journal of Quantum Electronics*, vol. 23, pp. 651-657, 1987.
2. Weisbuch, C. & Vinter, B. *Quantum semiconductor structures: Fundamentals and application* (Academic Press, 1991).
3. Yariv, A. *Optical Electronics* (Saunders College Publishing, 1991).
4. Vasilev, P. *Ultrafast diode lasers: fundamentals and applications* (Artech House, 1995).
5. Hawkes, J. & Latimer, I. *Lasers: Theory and Practice* (Prentice Hall, 1995).
6. Kapon, E. in *Semicondutor laser I: Fundamentals* (ed. Kapon, E.) 291-360 (Academic Press, 1999).
7. Zhao, B. & Yariv, A. in *Semicondutor laser I: Fundamentals* (ed. Kapon, E.) 1-121 (Academic Press, 1999).
8. Adams, A. R., OReilly, E. P. & Silver, M. in *Semicondutor laser I: Fundamentals* (ed. Kapon, E.) 123-176 (Academic Press, 1999).
9. Wilson, J. & Hawkes, J. F. B. *Optoelectronics: An introduction* (Prentice Hall, 1989).
10. Park, S. H., "Barrier-height effects on lasing characteristics of InGaAs/InGaAlAs strained quantum well lasers," *Journal of the Korean Physical Society*, vol. 32, pp. 713-717, 1998.
11. Hamp, M. J. *et al.*, "Effect of barrier height on the uneven carrier distribution in asymmetric multiple-quantum-well InGaAsP lasers," *IEEE Photonics Technology Letters*, vol. 10, pp. 1380-1382, 1998.
12. Kim, T. G. *et al.*, "Design and fabrication of a narrow stripe GaAs/AlGaAs quantum wire laser," *Journal of the Korean Physical Society*, vol. 30, pp. S123-S126, 1997.
13. Chavezpirson, A., Ando, H., Saito, H. & Kanbe, H., "Quantum-Wire Microcavity Laser Made From Gaas Fractional Layer Superlattices," *Applied Physics Letters*, vol. 64, pp. 1759-1761, 1994.
14. Tiwari, S. & Woodall, J. M., "Experimental Comparison of Strained Quantum-Wire and Quantum- Well Laser Characteristics," *Applied Physics Letters*, vol. 64, pp. 2211-2213, 1994.
15. Arakawa, Y., Vahala, K. & Yariv, A., "Quantum Noise and Dynamics in Quantum Well and Quantum Wire Lasers," *Applied Physics Letters*, vol. 45, pp. 950-952, 1984.
16. Kim, T. G., Suzuki, Y., Shimiz, M. & Ogura, M., "First demonstration of the gain switching characteristics of an AlGaAs/GaAs V-grooved quantum wire laser," *Solid-State Electronics*, vol. 43, pp. 2093-2096, 1999.
17. Wohlert, D. E., Cheng, K. Y. & Chou, S. T., "Temperature invariant lasing and gain spectra in self-assembled GaInAs quantum wire Fabry-Perot lasers," *Applied Physics Letters*, vol. 78, pp. 1047-1049, 2001.
18. Oraevskii, A. N., Scully, M. O. & Velichanskii, V. L., "Quantum dot laser," *Quantum Electronics*, vol. 28, pp. 203-208, 1998.
19. Sogawa, F., Nishioka, M., Kamiya, T. & Arakawa, Y., "Picosecond pulse generation in microcavity quantum dot lasers," *Physics of Low-Dimensional Structures*, vol. 12, pp. 125-129, 1997.
20. Kazi, Z. I., Egawa, T., Jimbo, T. & Umeno, M., "First room-temperature continuous-wave operation of self-formed InGaAs quantum dot-like laser on Si substrate grown by metalorganic chemical vapor deposition," *Japanese Journal of Applied Physics Part 1-Regular Papers Short Notes & Review Papers*, vol. 39, pp. 3860-3862, 2000.
21. Huang, X. D. *et al.*, "Very low threshold current density room temperature continuous wave lasing from a single-layer InAs quantum-dot laser," *IEEE Photonics Technology Letters*, vol. 12, pp. 227-229, 2000.

22. Newell, T. C. *et al.*, "Gain and linewidth enhancement factor in InAs quantum-dot laser diodes," *IEEE Photonics Technology Letters*, vol. 11, pp. 1527-1529, 1999.

23. Park, G., Shchekin, O. B., Csutak, S., Huffaker, D. L. & Deppe, D. G., "Room-temperature continuous-wave operation of a single-layered 1.3 mu m quantum dot laser," *Applied Physics Letters*, vol. 75, pp. 3267-3269, 1999.

24. Lester, L. F. *et al.*, "Optical characteristics of 1.24-mu m InAs quantum-dot laser diodes," *IEEE Photonics Technology Letters*, vol. 11, pp. 931-933, 1999.

25. Zhukov, A. E. *et al.*, "Power conversion efficiency of quantum dot laser diodes," *Semiconductors*, vol. 34, pp. 609-613, 2000.

26. Tachibana, K., Someya, T., Arakawa, Y., Werner, R. & Forchel, A., "Room-temperature lasing oscillation in an InGaN self-assembled quantum dot laser," *Applied Physics Letters*, vol. 75, pp. 2605-2607, 1999.

27. Eliseev, P. G. in *Semicondutor laser II: Materials and structures* (ed. Kapon, E.) 71-155 (Academic Press, 1999).

28. Williams, K. A., White, I. H., Penty, R. V. & Laughton, F. R., "Gain-switched dynamics of tapered waveguide bow-tie lasers: Experiment and theory," *IEEE Photonics Technology Letters*, vol. 9, pp. 167-169, 1997.

29. Williams, K. A. *et al.*, "Q-Switched Bow-Tie Lasers For High-Energy Picosecond Pulse Generation," *Electronics Letters*, vol. 30, pp. 320-321, 1994.

30. Sheem, S. K. & Vojak, B. A., "Broad-Area Semiconductor-Lasers With Gain-Length Variation For Lateral-Mode Control - the Bow-Tie Geometry Laser," *Journal of Applied Physics*, vol. 63, pp. 248-250, 1988.

31. Khrushchev, I. Y. *et al.*, "Picosecond Q-switched bow-tie laser diode array," *Electronics Letters*, vol. 33, pp. 426-428, 1997.

32. Rashed, A. M., Williams, K. A., Heard, P. J., Penty, R. V. & White, I. H., "Intracavity lens for low-divergence high-power laser diode operation," *Applied Physics Letters*, vol. 76, pp. 279-281, 2000.

33. Edwin, R. P., "Stripe Stacker For Use With Laser-Diode Bars," *Optics Letters*, vol. 20, pp. 222-224, 1995.

34. Clarkson, W. A. & Hanna, D. C., "Two-mirror beam-shaping technique for high-power diode bars," *Optics Letters*, vol. 21, pp. 375-377, 1996.

35. Goldberg, L., Weller, J. F., Mehuys, D., Welch, D. F. & Scifres, D. R., "12-W Broad Area Semiconductor Amplifier With Diffraction Limited Optical Output," *Electronics Letters*, vol. 27, pp. 927-929, 1991.

36. Mehuys, D., Welch, D. F. & Goldberg, L., "2.0w CW, Diffraction-Limited Tapered Amplifier With Diode Injection," *Electronics Letters*, vol. 28, pp. 1944-1946, 1992.

37. Welch, D. F. *et al.*, "1.1 W CW, Diffraction-Limited Operation of a Monolithically Integrated Flared-Amplifier Master Oscillator Power-Amplifier," *Electronics Letters*, vol. 28, pp. 2011-2013, 1992.

38. Mehuys, D., Welch, D. F., Goldberg, L. & Weller, J., "11.6-W Peak Power, Diffraction-Limited Diode-to-Diode Optical Amplifier," *Applied Physics Letters*, vol. 62, pp. 544-546, 1993.

39. Parke, R. *et al.*, "2.0 W CW, Diffraction-Limited Operation of a Monolithically Integrated Master Oscillator Power-Amplifier," *IEEE Photonics Technology Letters*, vol. 5, pp. 297-300, 1993.

40. Goldberg, L., Mehuys, D. & Welch, D., "High-Power Mode-Locked Compound Laser Using a Tapered Semiconductor Amplifier," *IEEE Photonics Technology Letters*, vol. 6, pp. 1070-1072, 1994.

41. Mehuys, D., Obrien, S., Lang, R. J., Hardy, A. & Weich, D. F., "5W, Diffraction-Limited, Tapered-Stripe Unstable Resonator Semiconductor-Laser," *Electronics Letters*, vol. 30, pp. 1855-1856, 1994.

42. Obrien, S., Schoenfelder, A. & Lang, R. J., "5W CW diffraction-limited InGaAs broad-area flared amplifier at 970 nm," *IEEE Photonics Technology Letters*, vol. 9, pp. 1217-1219, 1997.

43. Vasil'ev, P. P., White, I. H. & Gowar, J., "Fast phenomena in semiconductor lasers," *Reports On Progress in Physics*, vol. 63, pp. 1997-2042, 2000.

44. Downey, P. M., Bowers, J. E., Tucker, R. S. & Agyekum, E., "Picosecond Dynamics of a Gain-Switched Ingaasp Laser," *IEEE Journal of Quantum Electronics*, vol. 23, pp. 1039-1047, 1987.

45. Bowers, J. E., Hemenway, B. R., Gnauck, A. H. & Wilt, D. P., "High-Speed InGaAsP Constricted-Mesa Lasers," *IEEE Journal of Quantum Electronics*, vol. 22, pp. 833-844, 1986.

46. Henry, C. H., "Theory of the Linewidth of Semiconductor-Lasers," *IEEE Journal of Quantum Electronics*, vol. 18, pp. 259-264, 1982.

47. Vahala, K., Chiu, L. C., Margalit, S. & Yariv, A., "On the Linewidth Enhancement Factor-Alpha in Semiconductor Injection-Lasers," *Applied Physics Letters*, vol. 42, pp. 631-633, 1983.

48. Osinski, M. & Buus, J., "Linewidth Broadening Factor in Semiconductor-Lasers - an Overview," *IEEE Journal of Quantum Electronics*, vol. 23, pp. 9-29, 1987.

49. Matsui, Y., Pelusi, M. D. & Suzuki, A., "Generation of 20-fs optical pulses from a gain-switched laser diode by a four-stage soliton compression technique," *IEEE Photonics Technology Letters*, vol. 11, pp. 1217-1219, 1999.

50. Yatsu, R., Taira, K. & Tsuchiya, M., "High-quality sub-100-fs optical pulse generation by fiber-optic soliton compression of gain-switched distributed feedback laser diode pulses in conjunction with nonlinear optical fiber loops," *Optics Letters*, vol. 24, pp. 1172-1174, 1999.

51. Miyamoto, M., Tsuchiya, M., Liu, H. F. & Kamiya, T., "Generation of ultrashort (similar to 65fs) pulses from 1.55 mu m gain-switched distributed feedback (DFB) laser with soliton compression by dispersion arrangements," *Japanese Journal of Applied Physics Part 2-Letters*, vol. 35, pp. L1330-L1332, 1996.

52. Nagarajan, R. & Bowers, E. J. in *Semicondutor laser I: Fundamentals* (ed. Kapon, E.) 177-290 (Academic Press, 1999).

53. Helkey, R. J. & Arakawa, Y., "Cavity Optimization For Minimum Pulsewidth of Gain-Switched Semiconductor-Lasers," *IEEE Photonics Technology Letters*, vol. 7, pp. 272-274, 1995.

54. Pepeljugoski, P. K., Cutrer, D. M. & Lau, K. Y., "Parametric Dependence of Timing Jitter in Gain-Switched Semiconductor-Lasers," *Applied Physics Letters*, vol. 63, pp. 3556-3558, 1993.

55. Weber, A. G., Ronghan, W., Bottcher, E. H., Schell, M. & Bimberg, D., "Measurement and Simulation of the Turn-On Delay Time Jitter in Gain-Switched Semiconductor-Lasers," *IEEE Journal of Quantum Electronics*, vol. 28, pp. 441-446, 1992.

56. Bottcher, E. H. & Bimberg, D., "Detection of Pulse to Pulse Timing Jitter in Periodically Gain- Switched Semiconductor-Lasers," *Applied Physics Letters*, vol. 54, pp. 1971-1973, 1989.

57. Williams, K. A., White, I. H., Burns, D. & Sibbett, W., "Jitter reduction through feedback for picosecond pulsed InGaAsP lasers," *IEEE Journal of Quantum Electronics*, vol. 32, pp. 1988-1994, 1996.

58. Williams, K. A., White, I. H., Burns, D. & Sibbett, W., "Low Jitter Q-Switching Using Optoelectronic Feedback," *Electronics Letters*, vol. 30, pp. 1687-1688, 1994.

59. Taylor, A. J., Wiesenfeld, J. M., Eisenstein, G. & Tucker, R. S., "Timing Jitter in Mode-Locked and Gain-Switched Ingaasp Injection-Lasers," *Applied Physics Letters*, vol. 49, pp. 681-683, 1986.

60. Schell, M. *et al.*, "Jitter and Dynamics of Self-Seeded Fabry-Perot Laser-Diodes," *IEEE Journal of Selected Topics in Quantum Electronics*, vol. 1, pp. 528-534, 1995.

61. Seo, D. S., Kim, D. Y. & Liu, H. F., "Timing jitter reduction of gain-switched DFB laser by external injection-seeding," *Electronics Letters*, vol. 32, pp. 44-45, 1996.

62. Schell, M., Utz, W., Huhse, D., Kassner, J. & Bimberg, D., "Low Jitter Single-Mode Pulse Generation By a Self-Seeded, Gain- Switched Fabry-Perot Semiconductor-Laser," *Applied Physics Letters*, vol. 65, pp. 3045-3047, 1994.

63. Dellunde, J., Torrent, M. C., Sancho, J. M. & SanMiguel, M., "Frequency dynamics of gain-switched injection-locked semiconductor lasers," *IEEE Journal of Quantum Electronics*, vol. 33, pp. 1537-1542, 1997.

64. Tsuchiya, M., Takeshita, H. & Kamiya, T., "Precise analysis of linear and non-linear chirp parameters of gain switched distributed feedback laser pulses for the fibre optic compression scheme," *Optical and Quantum Electronics*, vol. 28, pp. 975-982, 1996.

65. Wiesenfeld, J. M., Tucker, R. S. & Downey, P. M., "Picosecond Measurement of Chirp in Gain-Switched, Single-Mode Injection-Lasers," *Applied Physics Letters*, vol. 51, pp. 1307-1309, 1987.

66. Barry, L. P., Dudley, J. M., Thomsen, B. C. & Harvey, J. D., "Frequency-resolved optical gating measurement of 1.4 THz beat frequencies from dual wavelength self-seeded gain-switched laser diode," *Electronics Letters*, vol. 34, pp. 988-990, 1998.

67. Wiesenfeld, J. M. *et al.*, "Gain-Switched GaAs Vertical-Cavity Surface-Emitting Lasers," *IEEE Journal of Quantum Electronics*, vol. 29, pp. 1996-2005, 1993.

68. Olsen, C. M., Izadpanah, H. & Lin, C., "Time-Resolved Chirp Evaluations of Gbit/S Nrz and Gain-Switched DFB Laser-Pulses Using Narrowband Fabry-Perot Spectrometer," *Electronics Letters*, vol. 25, pp. 1018-1019, 1989.

69. Chow, K. K. & Shu, C., "Switching dynamics between single-mode and dual-mode pulse emissions from a self-seeded laser diode," *Applied Physics Letters*, vol. 76, pp. 276-278, 2000.

70. Koch, T. L. & Bowers, J. E., "Nature of Wavelength Chirping in Directly Modulated Semiconductor-Lasers," *Electronics Letters*, vol. 20, pp. 1038-1040, 1984.

71. Buus, J., "Dynamic Line Broadening of Semiconductor-Lasers Modulated At High-Frequencies," *Electronics Letters*, vol. 21, pp. 129-131, 1985.

72. Koyama, F. & Suematsu, Y., "Analysis of Dynamic Spectral Width of Dynamic-Single-Mode (DSM) Lasers and Related Transmission Bandwidth of Single-Mode Fibers," *IEEE Journal of Quantum Electronics*, vol. 21, pp. 292-297, 1985.

73. Wada, K. & Cho, Y., "Improved Expression For the Time-Bandwidth Product of Picosecond Optical Pulses From Gain-Switched Semiconductor- Lasers," *Optics Letters*, vol. 19, pp. 1633-1635, 1994.

74. Marcuse, D. & Lee, T. P., "On Approximate Analytical Solutions of Rate-Equations For Studying Transient Spectra of Injection-Lasers," *IEEE Journal of Quantum Electronics*, vol. 19, pp. 1397-1406, 1983.

75. Vanderziel, J. P., Tsang, W. T., Logan, R. A., Mikulyak, R. M. & Augustyniak, W. M., "Subpicosecond Pulses From Passively Mode-Locked Gaas Buried Optical Guide Semiconductor-Lasers," *Applied Physics Letters*, vol. 39, pp. 525-527, 1981.

76. Bowers, J. E., Morton, P. A., Mar, A. & Corzine, S. W., "Actively Mode-Locked Semiconductor-Lasers," *IEEE Journal of Quantum Electronics*, vol. 25, pp. 1426-1439, 1989.

77. Corzine, S. W. *et al.*, "Actively Mode-Locked Gainasp Laser With Subpicosecond Output," *Applied Physics Letters*, vol. 52, pp. 348-350, 1988.

78. Yeung, J. A., "Theory of Active-Mode Locking of a Semiconductor-Laser in an External Cavity," *IEEE Journal of Quantum Electronics*, vol. 17, pp. 398-404, 1981.

79. Vanderziel, J. P., "Active-Mode Locking of Double Heterostructure Lasers in an External Cavity," *Journal of Applied Physics*, vol. 52, pp. 4435-4446, 1981.

80. Finch, A., Sleat, W. E. & Sibbett, W., "Subpicosecond Synchroscan Operation of a Photochron-Iv Streak Camera," *Review of Scientific Instruments*, vol. 60, pp. 839-844, 1989.

81. Sala, K. L., Kenney-Wallace, G. A. & Hall, G. E., "CW autocorrelation measurements of picosecond laser pulses," *IEEE Journal of Quantum Electronics*, vol. 16, pp. 990-996, 1980.

82. Takagi, Y., Kobayashi, T., Yoshihara, K. & Imamura, S., "Multiple-Shot and Single-Shot Autocorrelator Based On 2-Photon Conductivity in Semiconductors," *Optics Letters*, vol. 17, pp. 658-660, 1992.

83. Reid, D. T., Padgett, M., McGowan, C., Sleat, W. E. & Sibbett, W., "Light-emitting diodes as measurement devices for femtosecond laser pulses," *Optics Letters*, vol. 22, pp. 233-235, 1997.

84. Karkhanehchi, M. M., Marsh, J. H. & Hutchings, D. C., "Polarization dependence of two-photon absorption in an AlGaAs waveguide autocorrelator," *Applied Optics*, vol. 36, pp. 7799-7801, 1997.

85. Chiu, Y. J., Fleischer, S. B., Lasaosa, D. & Bowers, J. E., "Ultrafast (370 GHz bandwidth) p-i-n traveling wave photodetector using low-temperature-grown GaAs," *Applied Physics Letters*, vol. 71, pp. 2508-2510, 1997.

86. Weingarten, K. J., Rodwell, M. J. W. & Bloom, D. M., "Picosecond Optical-Sampling of Gaas Integrated-Circuits," *IEEE Journal of Quantum Electronics*, vol. 24, pp. 198-220, 1988.

87. Rush, K., Draving, S. & Kerley, J., "Characterizing High-Speed Oscilloscopes," *IEEE Spectrum*, vol. 27, pp. 38-39, 1990.

Chapter 2.
Focused ion beam etching procedures as applied to experimental diode lasers.

2.1. Introduction.

There are a number of areas where diode laser sources capable of producing high-energy, short optical pulses would be of significant interest. A number of routes are currently available to obtain such pulses from diode lasers, based on mode locking, gain-switching or Q-switching. Mode locking requires precise synchronisation of an external sinusoidal modulation with the diode laser cavity frequency, and the cavity length determines the pulse repetition frequency. With gain-switching it can prove difficult to obtain ultra short symmetrical optical pulses. Though Q-switching does not produce optical pulses with the shortest duration, it can yield the highest energies, and if an *active* technique is employed there is the added flexibility that the repetition rate is readily adjustable.

The multi-section devices required for active Q-switching are typically realised by using one of two distinct techniques. The multi-section device can be designed and fabricated as such,[1-4] or a single contact device may be post-processed using etching. The use of a focused ion beam etching (FIBE) procedure offers particular flexibility for interesting and novel device configurations. Reconfiguration is imparted to the device through the use of a suitably predetermined *mask*, which is used to control the ion beam effects. Focused ion beam etching is a versatile technique that can be used to tailor a device into virtually any conceivable configuration. There is however, a major constraint in such device processing because the time taken to perform a given task can be quite long for the etching rates currently available.

The basic principles for focused ion beam etching "FIBE" are as illustrated in Figure 2.1. At near normal incidence, a *gun* accelerates gallium ions on to the target to be etched. Upon impact, the high energy Ga^+ ions remove the surface material. The rate at which material is removed by the Ga^+ ions is determined by the splutter rate. Some typical splutter rates are outlined in Table 2.1. for a $25keV$ Ga^+ beam incident normally on a target surface.

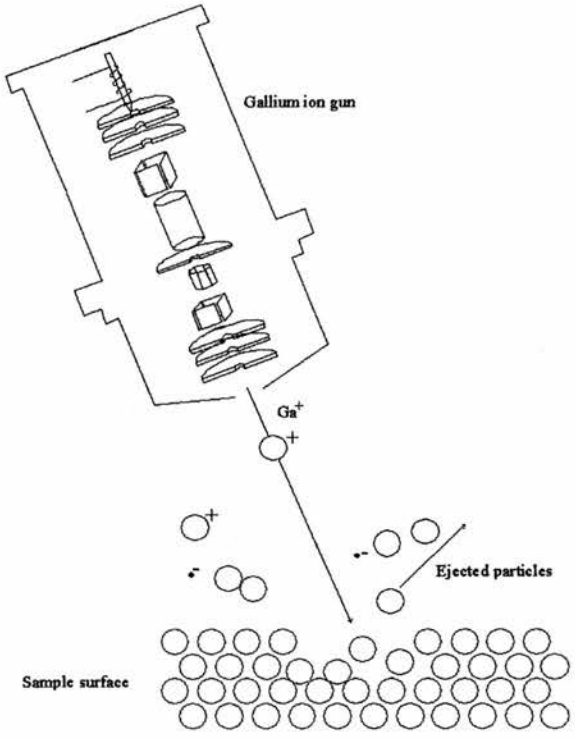

Figure 2.1. Fundamentals underlying focused ion beam etching.

Table 2.1. Splutter rates for various materials.

Material	Splutter rate $\mu m^3 * s^{-1} * nA^{-1}$
Al	0.43
$Al_{0.4}Ga_{0.6}As$	0.66
Au	1.52
C (graphite)	0.07
GaAs	0.94
GaN	0.52
InP	0.95
Si	0.25
SiO_2	0.22

The FIBE machine used in this work had a spatial resolution of $<100nm$, at a beam current of $50pA$, and a stability of $<50nm$. The beam current was adjustable in the range $2pA$ to $6nA$, with a stability of $<2\%/hr$.

2.2. Experimental.

When a single-contact diode laser is electrically pumped with a short high current pulse of duration $\geq 100ps$, the dynamic overshoot of the carriers within the device will result in an optical pulse that is not symmetrical.[5] Furthermore, the duration of the electrical pulse is such that sufficient gain can remain after the main optical pulse such that excitation of optical relaxation oscillations occur, leading to a *ringing* in the optical output pulse profile. The problem of relaxation oscillations can be avoided if short duration electrical pulses are

used. However, if the option of short duration electrical pulses is not readily available then an alternative is to modify the diode laser in some way so that further oscillations are suppressed. A practical involves multi-sectioning with the formation of distinct gain and loss sections. Through the use of a multi-section device, an improvement in the temporal output may be achieved by the application of a reverse DC bias to a *loss section*. If a short duration high current electrical pulse is applied to a *gain section* of a suitably biased two-section device, then the high photon density obtained at the peak of the electrical pulse is sufficient to overcome the loss inherent to the loss section, and lasing can commence. Following the evolution of the main optical pulse, the carrier and photon densities are greatly reduced; the loss section recovers inhibiting the occurrence of relaxation oscillations. As a consequence of the reverse DC bias applied to a loss section, an electrical pulse at an increased current can be applied to the gain section whilst maintaining an acceptable pulse profile, having enhanced average and peak powers. These operational parameters are attractive because good temporal profiles in picosecond pulse having high peak powers are often desired.

2.2.1. Temporal management.

Two different laser structures were etched for subsequent testing in a Q-switched configuration. One was a commercially available ridge-waveguide device with a stripe width of $\sim 3\mu m$ and a cavity length of $750\mu m$. This device was mounted *p*-side up on a copper submount and produced a CW output power of $\sim 210mW$.

The second device was a prototype (Marconi) seven element tapered array,[6] where each stripe width was $3\mu m$ at the HR-coated facet and $30\mu m$ at the AR-coated output facet. The device length was $1mm$. Although most standard commercially available devices are mounted *p*-side down on a submount, for this study the devices were specially supplied *p*-side up, to facilitate etching. The CW output power for the *p*-side down device was $\sim 5.6W$, but due to the increased thermal loading of *p*-side-up mounting, the devices were not subjected to high power operation. Both devices were based on the InGaAs/GaAs material structure and had emission wavelengths around $980nm$.

Subsequent to etching, the diode lasers were tested using one of two pulse generators. The first was built in-house with an electrical pulse duration of $\sim 1.8\text{ns}$, a repetition frequency up to 100kHz and a peak current of 1.6A. The second was a Kentech instruments commercial unit, which had a constant pulse duration of $\sim 150\text{ps}$, repetition frequency up to 1kHz and peak voltage of 2kV.

Typically the electrical pulse was applied to a more extended gain section, although with the narrow stripe laser, its operation was also tested when the electrical pulse was applied to the shorter loss section. Forward and reverse DC bias voltages were applied to the gain and loss sections respectively. Alternatively, a sinusoidal modulation from an Anritsu MG3633A frequency synthesiser was applied to either the gain or loss section. The frequency range was limited by the bandwidth of the power amplifier to the $1.00 \rightarrow 2.70 GHz$ range. The resultant optical pulses were measured using a fast free-space InGaAsP photodiode $\left(f_{3dB} \approx 15 GHz\right)$ and sampling oscilloscope. The temporal resolution of this scope/diode-based pulse characterisation system was $\sim 50\text{ps}$.

2.2.1.1. Narrow stripe devices.

The narrow stripe devices were etched such that two-sections were formed. A schematic of those etches performed in the device are shown in Figure 2.2.1, and the etching parameters may be found in Table 2.2.1.

Table 2.2.1. Narrow stripe device etching details.

Device number	X						Resistance/Ω
	Length /μm	Etch. Dose/pC*μm^{-2}, Current/nA					
		1	2	3	4	5	
1	100	10000, 6	10000, 6	1500, 1	9000, 6	9000, 6	256
2	200	9000, 6	9000, 6	2000, 1	9000, 6	9000, 6	56

As seen from Table 2.2.1. etching of the narrow stripe devices did not yield a particularly high inter-contact resistance. However, the resistance obtained for device number one was such as to allow Q-switched operation though the application of a forward DC bias to the gain section and a reverse DC bias to the loss section, with a supplementary sinusoidal modulation applied individually and alternatively between the two. In Figures 2.2.2. and 2.2.3. the upper (blue) line corresponds to the situation where no reverse DC bias was

applied to the loss section. The frequency of the sinusoidal modulation was $1.80GHz$, with a power level of $29dBm$.

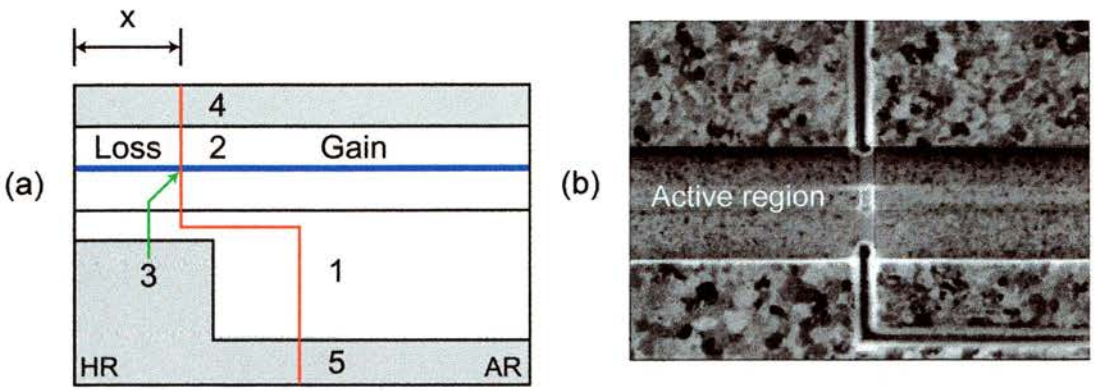

Figure 2.2.1. Multi-section etching of narrow stripe devices, illustrating (a) the individual etches and (b) a representative SEM image of the active region.

The radio frequency (RF) power actually applied to the diode laser was somewhat reduced due to the impedance mis-match that occurred between the device and 50Ω microwave cable.

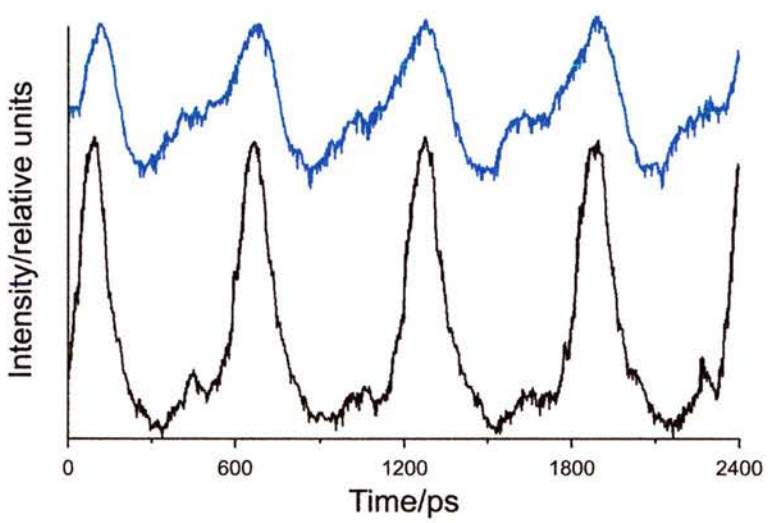

Figure 2.2.2. Temporal profiles for the output pulses from the etched narrow stripe device having forward DC bias with sinusoidal modulation applied to the gain section with the loss section disconnected (blue) or a reverse DC bias applied (black).

The result of this impedance mis-match was that a fraction of the RF power from the amplifier was reflected at the connection between the diode laser and 50Ω microwave cable. Impedance matching can somewhat improve the situation, a subject that is discussed further in Chapter 3.

Shown in Figure 2.2.2. are the pulse sequences from the two-section narrow stripe device when a sinusoidal modulation and forward DC bias were applied

to the gain section, with the loss section electrically disconnected (blue) or a reverse DC bias of $-12mA, 0.08V$ (black). The DC bias applied to the gain-section was $248mA$, which when combined with sinusoidal modulation resulted in a pulse duration of $200ps$ and an average optical output power of $52mW$. At this point there was no electrical connection to the loss section. When the loss section was connected, and a reverse DC bias applied, the pulse duration and average output power were reduced to $130ps$ and $33mW$ respectively.

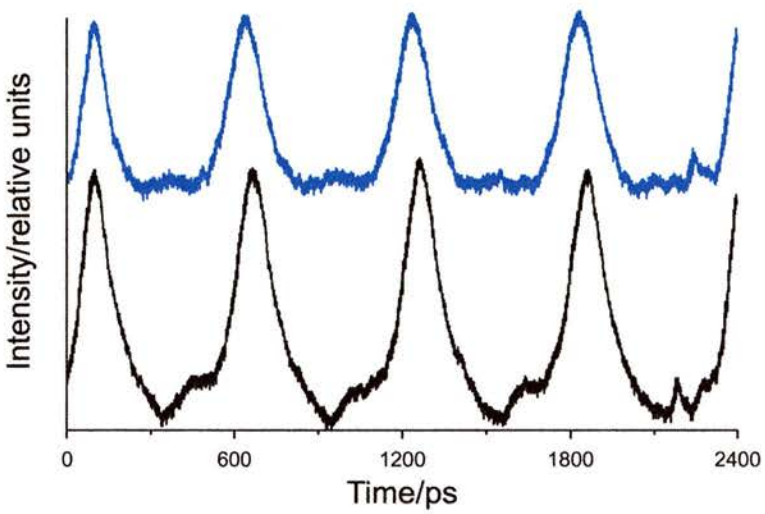

Figure 2.2.3. Temporal profiles for the output pulses from the etched narrow stripe device having forward DC bias applied to the gain section, with the loss section having sinusoidal modulation only (blue) or a combination of modulation and reverse DC bias (black).

Shown in Figure 2.2.3. are the pulse sequences from the two-section narrow stripe device when a forward DC bias was applied to the gain section, with sinusoidal modulation only applied to the loss section (blue) or a combination of modulation and reverse DC bias of $-3mA, 0V$ (black). The DC bias applied to the gain section was $256mA$. The resultant pulse duration was $140ps$, with an average output power of $43mW$. With the application of a reverse DC bias to the loss section, the pulse duration and average output power were reduced to $120ps$ and $33mW$ respectively. The improvement in the temporal profile, reduction in pulse duration and increased peak powers are clearly visible for both configurations. The stark difference observed in Figure 2.2.2. was due to there being no electrical connection to the loss section when the upper trace was recorded. The sinusoidal modulation applied to the loss section for Figure

2.2.3. resulted in carrier leakage between the two sections, which was unavoidable due to the low inter-contact resistance.

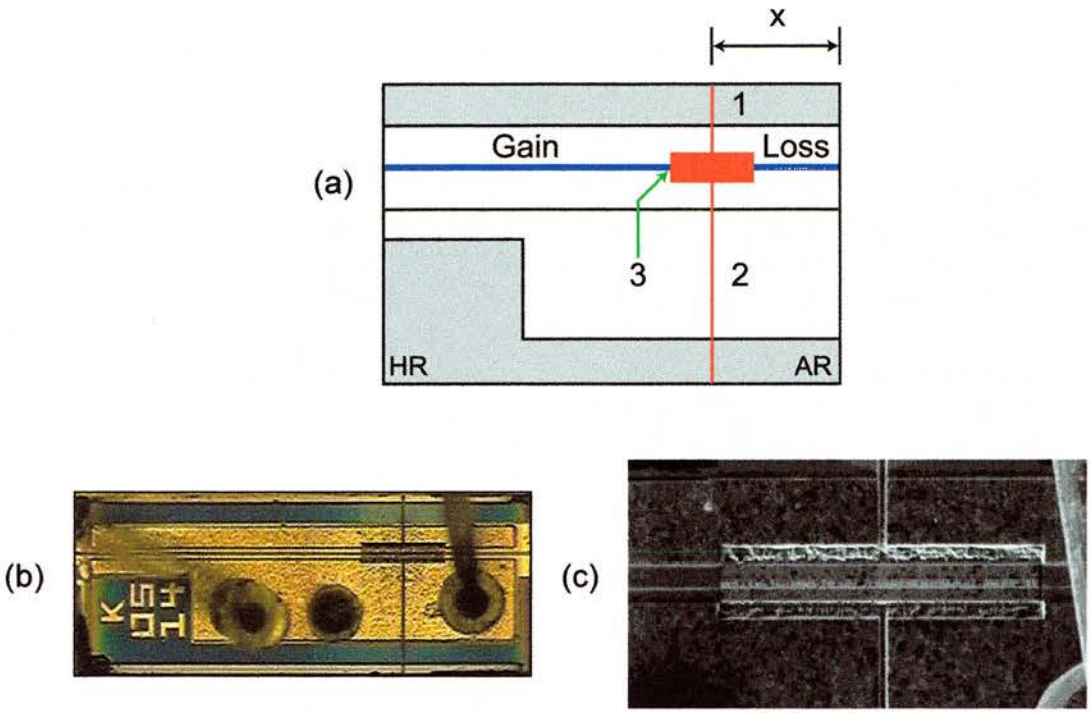

Figure 2.2.4. Alternative configuration showing (a) etch schematic, (b) post-etch device and (c) SEM image of active region.

In an attempt to increase the inter-contact resistance obtained from a two-section narrow stripe device, a large area over the active region was etched, rather than a single line. The etches performed in the device are shown in Figure 2.2.4a, where (1) and (2) were $10500 pC * \mu m^{-2}$ and (3) was $1220 pC * \mu m^{-2}$. Figures 2.2.4b. and 2.2.4c. illustrate the device after etching, clearly showing the etched area. Unfortunately, the inter-contact resistance was still low, at 62.5Ω. No further processing was performed on this device.

The inconsistent value for the inter-contact resistance, obtained from the narrow stripe devices, implied that the post-etching of these devices suffered a lack of repeatability. This was partly due to an absence of a detailed prior knowledge of the device structure, due to their commercial nature. Compared with unetched devices, the output power was severely and unacceptably compromised as a consequence of etching. Interestingly, there was no significant reduction in operational lifetime for all of the devices that survived the etching process. Etching of narrow stripe devices was discontinued and

another methodology for short optical pulse generation sought. The technique implemented was gain-switching, and this is discussed further in subsequent chapters.

2.2.1.2. Array devices.

Tapered array devices were etched to form the four distinctive configurations as illustrated in Figure 2.2.5. (The etch parameters may be found in Table 2.2.2.) Devices 1, 2, 4 and 5 were etched such that one of the seven array elements was isolated. By this means, the effect of subsequent etching could be investigated without the need to consider the performance of the array as a whole.

Table 2.2.2. Array device etching details.

Device number	X			Y			Isolation		Notes
	Length /μm	Etch. Dose/pC*μm^{-2}, Current/nA	R/Ω	Length /μm	Etch. Dose/pC*μm^{-2}, Current/nA	R/Ω	Etch. Dose/pC*μm^{-2}, Current/nA	R/Ω	
1	NA	NA	NA	NA	NA	NA	2000, 6	11	a
2	~150	5000, 2	6.5k	NA	NA	NA	2000, 6	40k	b
3	~220	2200, 2*c*	1k	NA	NA	NA	2000, 6	40k	
4	<200	2200, 2*d*	62	NA	NA	NA	NA	NA	e
5	250	2000, 2	1.42K	180	2000, 2	1.56k	2000, 2	0.7M	

a. Old batch, not etched multi-section.
b. Deep etch, two sections totally isolated.
c. An extra 100pc*μm^{-2} was used over the active region.
d. As c.
e. The whole array was etched.

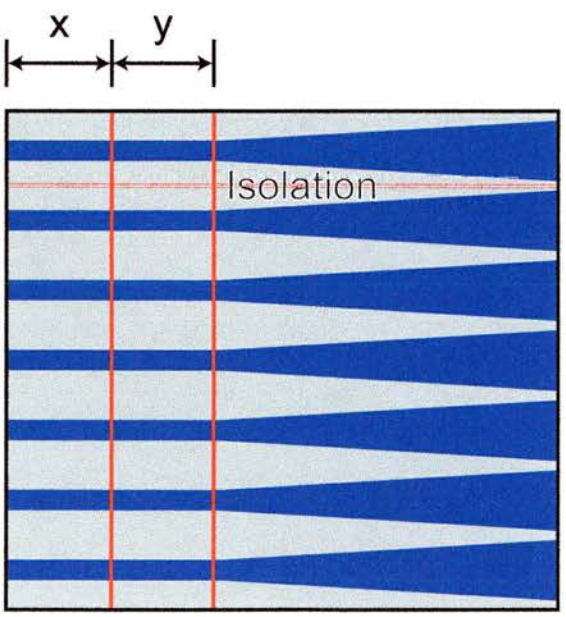

Figure 2.2.5. Illustration of the etches made in the array devices.

The inter-stripe resistance following isolation etching of the first experimental device was just 11Ω. This was deemed too low in comparison with subsequent devices, and as a consequence no further processing was performed.

After stripe isolation a second device was etched to yield a two-section device having a smaller loss section length of $\sim 150\mu m$. However, the dose of $5000 pC * \mu m^{-2}$ over the active region was too high and this led to device failure.

Active region etching on device number three was for a greatly reduced dose of $2000 pC * \mu m^{-2}$, resulting in a section of length $\sim 220\mu m$ with an inter-contact resistance of $1k\Omega$. The device was tested using the in-house built pulse generator, with the current measured at $370mA$. A secondary pulse seen in Figure 2.2.6a, when the loss section was unbiased, is no longer evident in Figure 2.2.6b. where a reverse DC bias was applied to the loss section. The optical pulse duration was measured to be $\sim 100 ps$, at a repetition frequency of $100kHz$. The average output powers from the device were $20\mu W$ and $15\mu W$ under the conditions of an unbiased and reverse biased loss section respectively. Its peak output powers were $2.0W$ and $1.5W$. The maximum average optical output power obtained from the device was $27\mu W$, with a peak power of $2.7W$, obtained for a $550mA$ current pulse and a reverse DC bias of $-3.8V$ on the loss section.

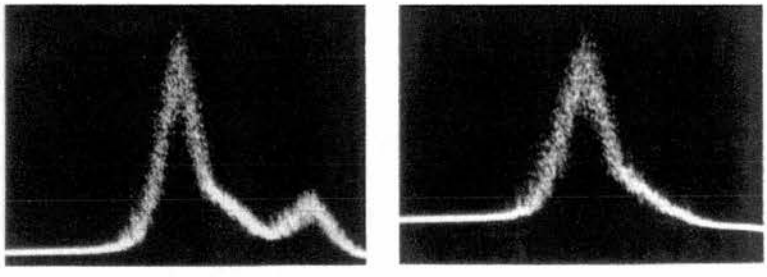

(a) (b)

Figure 2.2.6. The output pulse from a multi-section device for (a) zero and (b) reverse loss-section DC bias.

The inter-contact resistance of 62Ω obtained after etching device number four was such that successful Q-switched operation could not be achieved. No further processing was performed on this device.

A fifth device was initially etched to form a three-section device. However, due to the poor performance that resulted, the latter two sections were subsequently electrically connected yielding essentially a two section device. When an $800mA$ electrical pulse was applied to the gain section, with zero reverse DC bias applied to the loss section, an average optical power of $109\mu W$ was obtained, with a peak power of $10.9W$. When the loss section reverse DC bias was increased to $-4.3V$, the average and peak optical output powers became $87\mu W$ and $8.7W$ respectively. The temporal profiles both with and without the application of reverse DC bias to the loss section were identical to those obtained from device number four, (Figure 2.2.6.).

2.2.2. Spatial management.

It well known that single mode operation of a simple Fabry-Perot diode laser is only possible for stripe widths of a few micrometres. Such stripe widths limit the optical output power to several hundred milliwatts, depending on the exact structure and the mounting technique employed. A high optical output power can be achieved by increasing the stripe width, but this results in the existence of multiple transverse modes unless some elaborate structure is used.[7] If it were possible to modify a broad area device to greatly improve the spatial output, whilst not detrimentally affecting the optical output power, this would be of significant interest where high power, high brightness diode laser sources are required.

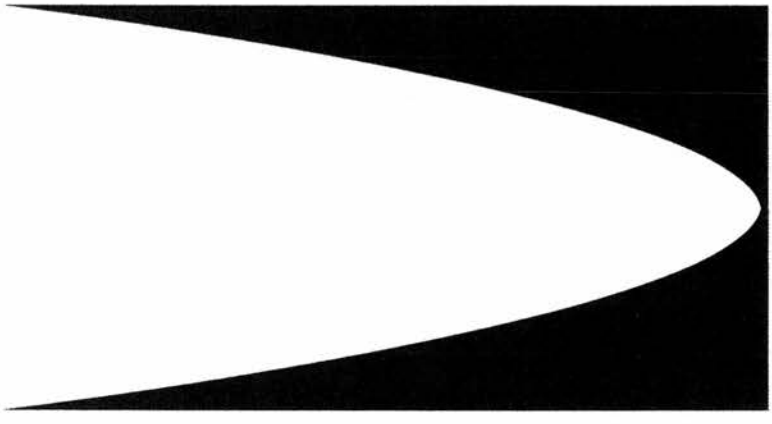

Figure 2.2.7. Illustration of the mask used for lens etching.

A technique used successfully to improve the spatial output from a broad area device was the fabrication of an intracavity lens etched in relief over the active

region of a broad area device.[8] The influence on the spatial characteristics by a focusing of the optical mode within the diode laser cavity, are brought about by the refractive index difference thus produced by the etch.

The mask for the etching machine incorporated a positive lens is shown in Figure 2.2.7. In Figure 2.2.7. the black area corresponds to material that will subsequently be removed during etching. The lens was designed through the use of modelling in Matlab.

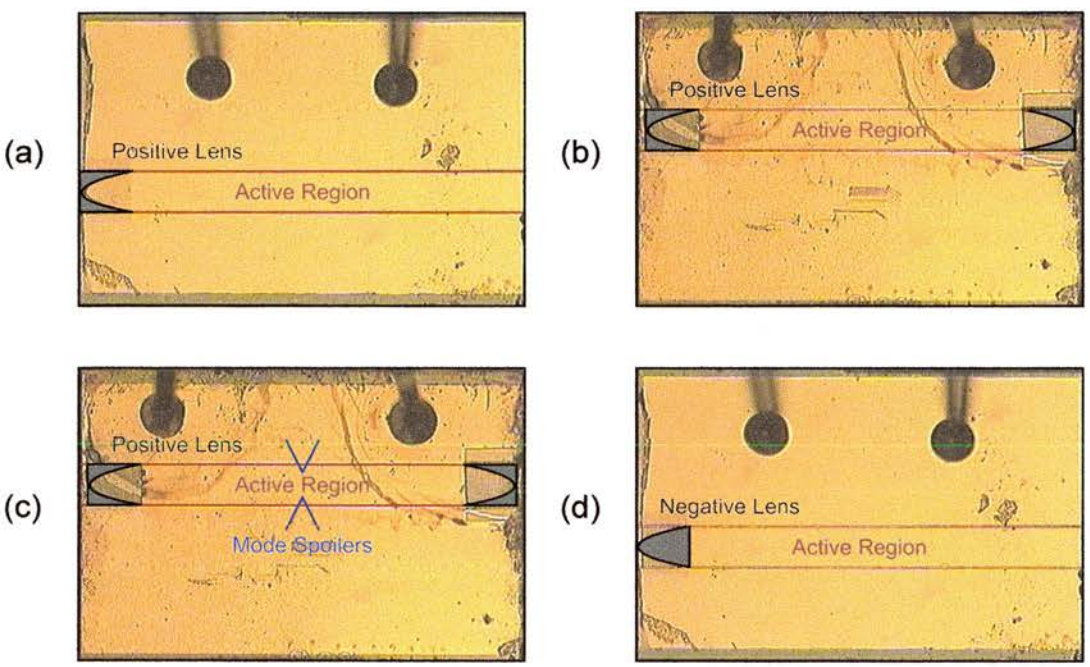

Figure 2.2.8. Devices etched with (a) one or (b), (c) two positive lenses, and (d) one negative lens.

The broad area devices on which spatial refinement would be evaluated were based on the AlGaAs structure, with an emission wavelength of 850nm. The cavity length was $\sim 800\mu m$, with a stripe width of $80\mu\text{m}$. Etching was performed over the active region of the device. The level of accuracy required to etch over the active region could be achieved because details of the structure for this device were known. Several distinct configurations, illustrated in Figure 2.2.8 (a) through (d) were etched using the lens mask shown in Figure 2.2.7. These configurations included (a) single lens, (b) & (c) two lenses, and (d) one negative lens. Mode-spoilers, with a separation of $20\mu m$ were included in device (c) such that high losses would be encountered by the optical modes

perpendicular to the diode laser facets. Shown in Figure 2.2.9. is a SEM image of the lens etched into the device (a).

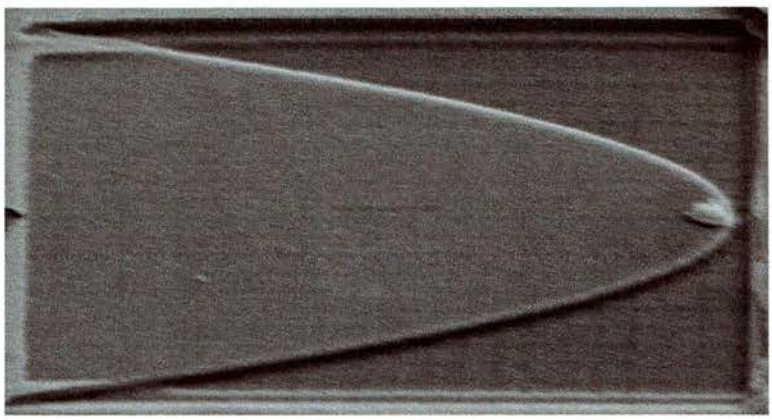

Figure 2.2.9. SEM image of the positive lens etched into device (a).

The etching parameters used for the above devices were a dose of $3000 pC * \mu m^{-2}$ and a beam current of $3nA$. These devices were tested under pulsed operation, $\left(\mathrm{I}_{\max} = 1.50A, \tau = 1\mu s, f = 10kHz\right)$ both in conditions of pre- and post-etching, where the output power and far field parallel to the junction were recorded.

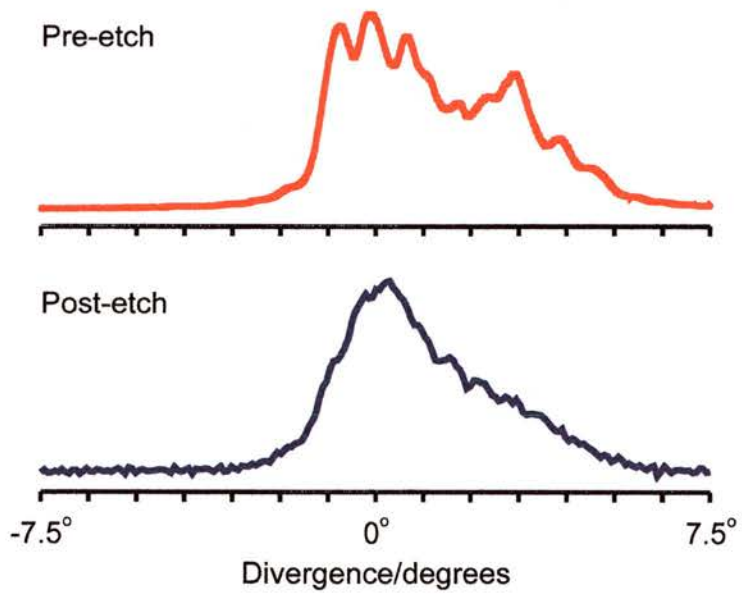

Figure 2.2.10. Pre- and post-etch far-field characteristics of the broad area device.

Of the devices etched, only the single positive lens design demonstrated any significant improvement in the far field (Figure 2.2.10.) The peak output powers with the aforementioned electrical pulse were $500mW$ (pre-etch) and $460mW$

(post-etch). This represents just an 8% reduction in the optical output power compared with the unetched device.

The optical output power of the devices in which two lenses were etched was severely affected.

2.3. Conclusions.

Focussed ion beam etching offers a versatile system that can be utilised for the post processing of a broad range of diode laser devices with the realisation of elaborate structures.

Etching was used for the enhancement of two diode laser characteristics, being temporal and spatial. In both applications, an improvement in the intended characteristic was observed, though at the expense of the optical output power.

When a reverse DC bias was applied to the loss section created on narrow stripe devices, the resultant pulse duration was reduced, to a minimum of $120 ps$. The creation of an intracavity lens in a broad area device resulted in a significantly improved far field profile. However, the flexibility offered by the technique brings with it an unpredictability of attempting to etch to within micrometres of the device active region. This uncertainty has the consequence that the results obtained can vary dramatically, with device failure in the worst cases.

FIBE is an interesting and versatile technique, and its application has been successfully demonstrated for the enhancement of diode laser performance. However, the unpredictability and failure of processed devices resulted in the exploitation of other options to obtain a pulsed output from narrow stripe diode lasers. To this end gain-switching was employed, which proved to be significantly more successful, with the consequence that etching was ceased. The realisation of gain-switching will be discussed in the next chapter, followed by the applications of such pulsed devices.

2.4. References.

1. Camacho, F., Barrow, D. A., Avrutin, E. A., Bryce, A. C. & Marsh, J. H., "Two-contact semiconductor mode-locked lasers," *International Journal of Optoelectronics*, vol. 10, pp. 433-437, 1995.
2. White, I. H., Griffin, P. S., Fice, M. J. & Whiteaway, J. E. A., "Line Narrowed Picosecond Optical Pulse Generation Using 3 Contact InGaAsP/InP Multiquantum Well Distributed Feedback Laser Under Gain Switching," *Electronics Letters*, vol. 28, pp. 1257-1258, 1992.
3. Schrans, T., Sanders, S. & Yariv, A., "Broad-Band Wavelength Tunable Picosecond Pulses From CW Passively Mode-Locked 2-Section Multiple Quantum-Well Lasers," *IEEE Photonics Technology Letters*, vol. 4, pp. 323-326, 1992.
4. Sanders, S., Yariv, A., Paslaski, J., Ungar, J. E. & Zarem, H. A., "Passive-Mode Locking of a 2-Section Multiple Quantum-Well Laser At Harmonics of the Cavity Round-Trip Frequency," *Applied Physics Letters*, vol. 58, pp. 681-683, 1991.
5. Bouchoule, S., Lourtioz, J. M., Kazmierski, C. & Ougazzaden, A., "Transform-Limited Pulses From Low Chirp DFB Lasers With External Feedback," *Electronics Letters*, vol. 29, pp. 518-520, 1993.
6. Williams, K. A. *et al.*, "Design of high-brightness tapered laser arrays," *IEEE Journal of Selected Topics in Quantum Electronics*, vol. 5, pp. 822-831, 1999.
7. Sokolovskii, G. S., Rafailov, E. U., Birkin, D. J. L. & Sibbett, W., "High-power laser structures incorporating novel curved-gratings," *Optical and Quantum Electronics*, vol. 31, pp. 215-221, 1999.
8. Rashed, A. M., Williams, K. A., Heard, P. J., Penty, R. V. & White, I. H., "Intracavity lens for low-divergence high-power laser diode operation," *Applied Physics Letters*, vol. 76, pp. 279-281, 2000.

Chapter 3.
Picosecond pulse generation from diode laser sources.

3.1. Introduction.

Numerous experimental schemes have been developed specifically for the production of short optical pulses from diode lasers, and some practical approaches were discussed in Chapters 1. and 2. A single-contact diode laser repetitively gain-switched[1-3] by direct application of large signal sinusoidal modulation[2,4-6] remains the simplest methodology for the generation of picosecond optical pulses. Such a laser can be used as either a separate pulsed source or in a master-oscillator/amplifier combination.[7]

Obtaining high optical power and a single transverse mode simultaneously from a diode laser source in a compact package was a key objective for the work discussed in this chapter. Due to this self-imposed constraint that the experimental scheme should be compact, the extended cavity required for practical mode-locking was not a viable option. Also, whilst mode-locking may provide optical pulses with the shortest duration, its flexibility is somewhat limited because the external cavity length determines the repetition frequency, or the harmonics thereof. In contrast, an external cavity is not required for gain-switched operation, and the only modulation frequency limitation is electrical.

Gain-switching of single-contact, narrow stripe diode lasers has been used successfully for the direct generation of optical pulses with picosecond durations.[4,8-13] When such a gain-switched diode laser is used in a suitable external cavity, femtosecond pulse durations can also be demonstrated.[14-16]

3.2. Experimental.

The diode lasers used though-out the course of the work that follows were commercially available InGaAs/GaAs quantum well ridge waveguide devices. The laser chips were designed to be operated in the CW regime and had nominal emission wavelengths around $980nm$, a stripe width of $3\mu m$ and a cavity length of $750\mu m$. The devices available had CW output powers of $180mW$ or $210mW$ respectively. However, commercial diode lasers are usually under rated to increase lifetime and so it should have been possible to obtain higher output powers if required but this was not explored.

The facets of the laser chip were asymmetrically coated, AR-coated $(<3\%)$ on the front facet, and HR-coated $(>95\%)$ on the rear facet. This commercial device was mounted *p*-side up using sapphire on a copper sub-mount. The assembly supplied by the manufacturer was attached to an in-house designed copper mount using silver epoxy before being wire bonded. The operational diode laser was maintained at a constant temperature through the use of active stabilisation by a thermoelectric cooler and a Marlow C5010 PID temperature controller, with a stability of $0.1^{o}C$.

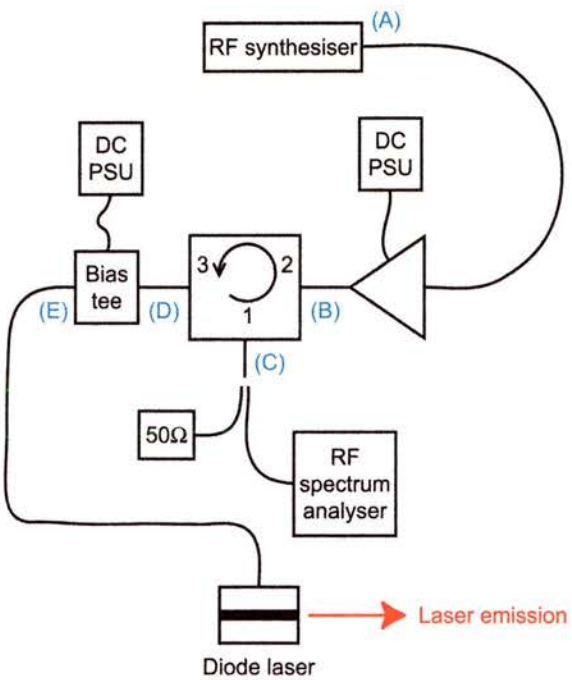

Figure 3.2.1. Schematic of electronics used for gain-switched operation.

The lasers available for this study were designed as pump sources for erbium-doped fibre amplifiers, which are widely used in the telecommunications industry. A result of this was that the device packaging had not been designed to be compatible with high speed modulation. This is in contrast to the $1.55\mu m$ telecommunications lasers that are suitable for high speed modulation. If efficient gain-switched operation is to be achieved through the application of large amplitude sinusoidal modulation, then such packaging is beneficial to ensure efficient use of the available radio frequency (RF) power. Otherwise the mis-matched impedance between the diode laser and 50Ω microwave

transmission line leads to high losses and a reduction in the power applied to the device.

Illustrated in Figure 3.2.1. is the generic electrical scheme used for gain-switching of the narrow stripe diode lasers by large signal sinusoidal modulation. The frequency synthesiser was of crucial importance because its signal quality would directly affect the quality of the pulsed diode laser output. An Anritsu MG3633A synthesiser was used, and according to the manufacturers specifications the output was low noise. The maximum power output was $24dBm$. (See Appendix A. for the conversion of dBm into volts and watts). The only drawback of this synthesiser was the upper frequency limit of $2.70GHz$. The power at point (A) was limited to $4dBm$, this being the maximum input power for the Mini Circuits ZHL-42 amplifier. A lower limit of $1.70GHz$ was placed on the useable sinusoidal modulation frequency range by the power amplifier. Note that when the electron-optical streak camera was used a directional coupler (Mini Circuits ZEDC-15-2B) was inserted between the synthesiser and amplifier to provide the necessary drive signal.

After the Mini Circuits amplifier (point (B)) a maximum output power of $29dBm$ was obtained. To protect the output stage of the amplifier from electrical reflections that might occur due to the mis-matched load presented by the diode laser, its output was connected to the input (port 2) of a Mica C-601S13 circulator. (A circulator is akin to the opto-isolators that are routinely used to stop unwanted reflections affecting the pulsed output of many laser sources.) The arrow on the representation of the circulator in Figure 3.2.1. refers to the path taken through the device. That is, the output from port 2 is port 3. The circulator had the useful property that it could be used to monitor the reflected power, by connecting a suitable RF spectrum analyser to port 1 (point (C)). When the RF spectrum analyser was not in use, correct termination was assured via a 50Ω load, with a power handling capacity of $30dBm$. A DC bias from a power supply unit (PSU) was applied to the diode laser through the use of a Hewlett-Packard (HP) 33150A bias tee. The bias tee decoupled the DC power supply and RF synthesiser through the use of an inductor and capacitor. It was connected to the diode laser using low loss 50Ω microwave cable. The

resulting optical output from the device was collimated using a New Focus 5723-B-H 30X aspheric objective, AR-coated for the near-infrared.

Two pulse measurement schemes were routinely used throughout the course of this work. The first was a New Focus 1024 fibre coupled InGaAsP photodiode with an impulse response of $12ps$ $\left(f_{3dB} = 26GHz\right)$, in combination with a digital sampling oscilloscope, consisting of a HP-54750A mainframe and HP-54752B $50GHz$ plug-in.

Using Equation 1.33, τ_{FWHM} for the $50GHz$ digital sampling oscilloscope is estimated at $8.8ps$. This however, is not the minimum pulse duration that could be measured by the system as a whole, because this depends upon the convolution of several bandwidths. Consider a Gaussian pulse, with FWHM duration of $15ps$ incident on the photodiode. The pulse duration observed on the digital sampling oscilloscope may be estimated by summing the squares of the individual impulse responses. The measured pulse duration, τ_m, will therefore have an approximate duration of:

$$\tau_m = \sqrt{15^2 + 8.8^2 + 12^2} \approx 21.1 \qquad 3.1$$

The temporal resolution limit illustrated above is unavoidable, but may be accounted for given that it is constant, although other factors may exist that have not been considered above, such as any adapters. It follows from 3.1 that the *real* pulse duration, τ_r, may be given by:

$$\tau_r = \sqrt{\tau_m^2 - \left(\tau_{pd}{}^2 + \tau_{dso}{}^2\right)} \qquad 3.2$$

where τ_{pd} and τ_{dso} are respectively the impulse responses for the photodiode and digital sampling oscilloscope.

Another factor that must be considered when using a fast photodiode and digital sampling oscilloscope is the pulse-to-pulse timing jitter. The trace on a digital sampling oscilloscope is made up of the contribution from many independent pulses and so any timing jitter between the pulses will tend to increase the measured duration. As jitter is random it is not easily eliminated, but for small values its influence on the pulse measurement can be minimised through the use of averaging.

The second methodology with which the pulse duration was determined was by using an electron-optical streak camera. The in-house assembled streak camera had an advantage over the fast photodiode and digital sampling oscilloscope combination in that it was significantly more sensitive at the wavelength of interest. The streak camera also offered a reduced temporal resolution of $4ps$, compared with $18ps$ of the fast photodiode and digital sampling oscilloscope combination. However, as a result of the streak cameras design, operation was only possible over a small range of diode laser modulation frequencies, before it was necessary to adjust the resonant frequency to maintain impedance matching with the drive electronics.

3.3. Operational characteristics.

Several narrow stripe devices were used over the course of this work; the operational characteristics that follow are typical of those obtained for these devices. When being evaluated, the device under test was tested under both CW and pulsed conditions, a situation easily accomplished by removable of the sinusoidal modulation.

The characteristics presented and discussed include, electrical, temporal, spectral and spatial features. The electrical measurement consists of the light/current (L/I), voltage/current (V/I) and efficiency $\left(P_{opt}/P_{elec}\right)$ curves. The spatial characteristic of a device was not routinely measured when a new device was evaluated, because it was known from manufacturers specification that the output was single-mode. For the operational characteristics that follow, the temperature of the copper block on which the diode laser submount was mounted was maintained at a constant $20^{o}C$.

Acquisition of the electrical and high resolution spectral characteristics for any given device were automated through the use of instruments equipped with the IEEE488.1 control interface. Using the HP-VEE instrument control program, the programs presented in Appendices B. and C. were written such that these repetitive and extensive measurements could be completed swiftly, with the resulting data being saved for further analysis.

3.3.1. Electrical characteristics.

The electrical characteristics typical of a narrow stripe device with a CW optical output power of $210mW$ are illustrated in Figure 3.3.1. In the figure, the black lines refer to the CW regime, whereas the blue and red lines correspond to the gain-switched regime achieved by the application of a sinusoidal modulation to the diode laser in conjunction with a forward DC bias.

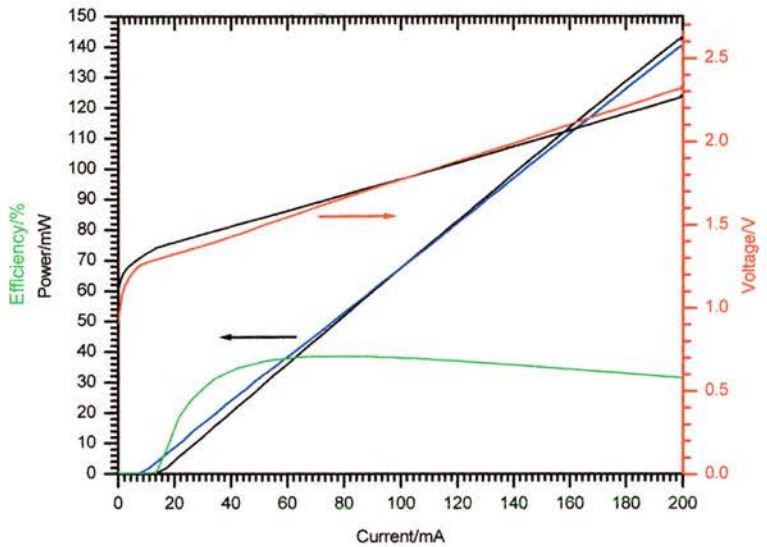

Figure 3.3.1. Electrical characteristics typical of the narrow stripe devices. The L/I, V/I and efficiency curves are shown in blue, red and green respectively.

From Figure 3.3.1. the threshold current of the device when operating CW can be seen to be $17mA$, the slope efficiency is $0.77mW/mA$ and the maximum electrical to optical efficiency 37.9%. Figure 3.3.1. illustrates that the addition of supplementary sinusoidal modulation had little effect upon the electrical characteristics of the device. Under gain-switched operating conditions, the threshold current and slope efficiency were reduced to $\sim 7mA$ and $0.67mW/mA$. To safeguard against device failure, the maximum operation optical output power specified by the manufacturer was not routinely exceeded.

3.3.2. Temporal characteristics.

As previously stated, temporal measurements were routinely performed using the digital sampling oscilloscope and fibre-coupled photodiode, due to the convenience of this scheme. The temporal resolution of the combination was $\approx 18ps$. It was possible to obtain a real-time readout of the FWHM pulse

duration, though for an absolute value a deconvolution had to be performed (Equation 3.2). The minimum optical launch power for efficient detection was $\approx 1mW\,@\,980nm$.

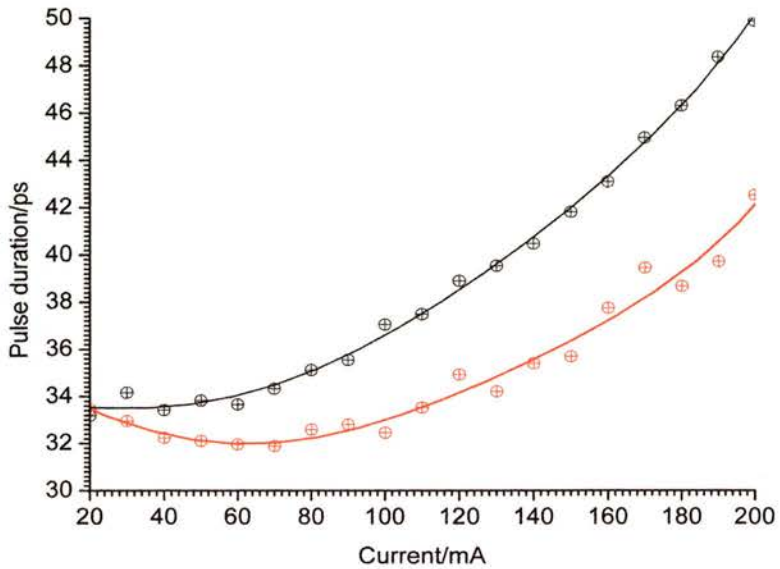

Figure 3.3.2. Variation of the pulse duration from the gain-switched diode laser for increasing DC bias at a modulation frequency of $2.00GHz$ (black) and $2.60GHz$ (red).

Illustrated in Figure 3.3.2. is the variation of the FWHM pulse duration obtained from the gain-switched laser when forward DC biased in the range 20 → $200mA$.

A constant sinusoidal modulation frequency of $2.00GHz$ (black) or $2.60GHz$ (red) was also applied with maximum power output from the amplifier. The minimum pulse duration observed from the gain-switched diode laser was $30ps$ with average optical output powers up to $100mW$.

$2.00GHz$ and $2.60GHz$ represented the two extreme frequencies of the sinusoidal modulation typically applied to the diode laser. Selected temporal profiles are shown in Figure 3.3.3. for a modulation frequency of $2.60GHz$ illustrating that the pulse shape was, within a small approximation, constant with increasing DC bias.

Measurements of the pulse duration were repeated, with a constant DC bias of $100mA$ and a variable modulation frequency in the range $1.70GHz$ → $2.70GHz$, with the results illustrated in Figure 3.3.4. The pulse duration did not vary

smoothly with the applied modulation frequency, but tended to jump as shown in Figure 3.3.4.

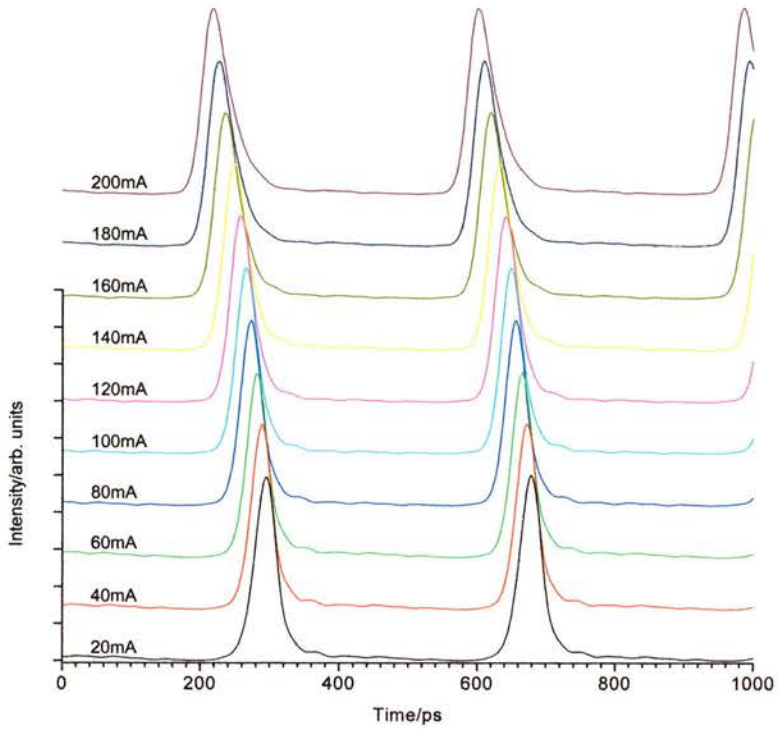

Figure 3.3.3. Temporal profiles obtained from the gain-switched diode laser for increased DC bias at a constant modulation frequency of $2.60GHz$.

It should be clear from Figures 3.3.2. and 3.3.4. that the modulation frequency applied to the diode laser to affect gain-switched operation was key in determining the pulse duration.

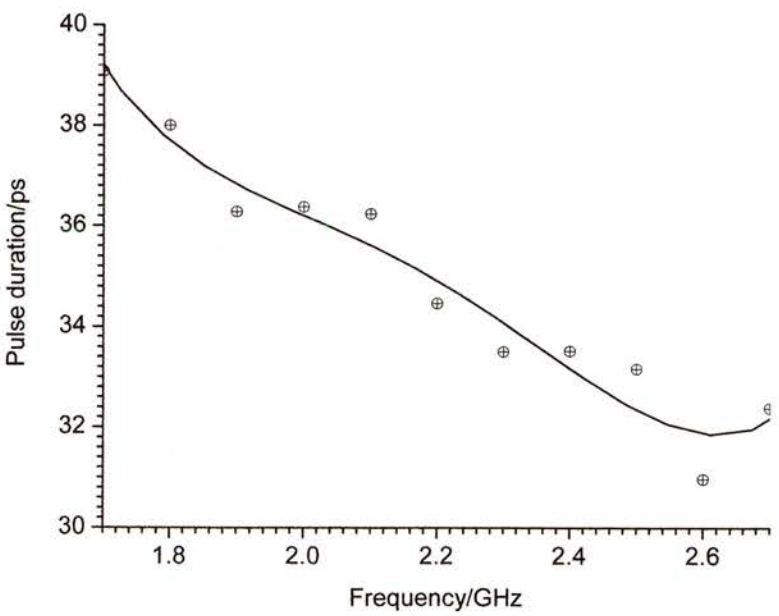

Figure 3.3.4. Pulse duration obtained from the gain-switched diode laser for a constant modulation DC bias and a variable modulation frequency.

It should also be noted that the pulse duration obtained for any given DC bias and modulation frequency would vary, by $\approx 5ps$, from day-to-day.

With operational conditions of a sinusoidal modulation in the frequency range $1.70GHz$ to $2.20GHz$ and $I_{DC} \approx I_{th}$, the well-known period doubling effect was observed in the temporal output.[17] Illustrated in Figures 3.3.5a. and 3.3.5b. are the pulse sequences for a modulation frequency of $1.80GHz$, with a DC bias of $14mA$ and $28mA$ respectively. Period doubling of the optical output to $0.9GHz$ is clearly visible in Figure 3.3.5a. when compared with Figure 3.3.5b. No further stages of the route to chaos[18-21] were observed, such as period tripling or quadrupling.[22,23]

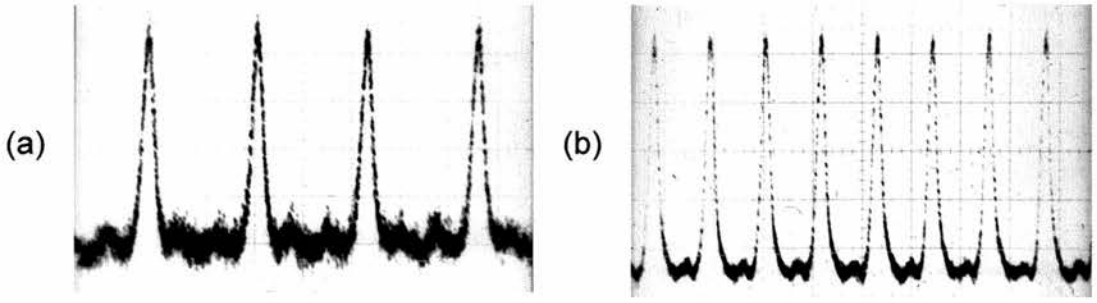

Figure 3.3.5. Pulse trains for a modulation frequency of $1.80GHz$ illustrating (a) period doubled and (b) fundamental optical outputs.

As the effect of period doubling was only observed for DC bias levels of $I_{DC} \approx I_{th}$ it was not an issue for the results subsequently discussed since the typical operational DC bias level was $I_{DC} \geq 6I_{th}$.

3.3.3. Spectral characteristics.

Routine spectral measurements were performed using a spectrometer providing a real-time visualisation of the spectral profile, at a resolution of $\approx 0.3nm$.

With a forward DC bias in the range $20 \rightarrow 200mA$ the centre wavelength and FWHM spectral bandwidth of the output from the diode laser were recorded for CW and gain-switched regimes. In common with the temporal measurements, gain-switched operation was achieved through the application of a constant sinusoidal modulation frequency of $2.00GHz$ and maximum power output from the amplifier.

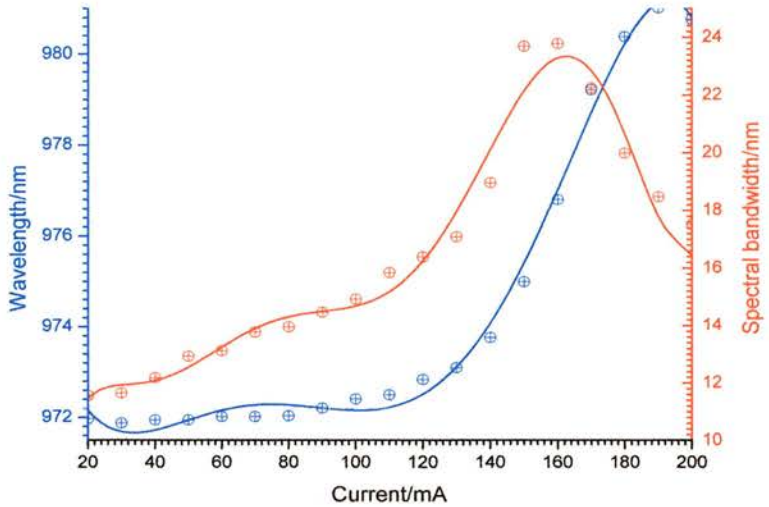

Figure 3.3.6. Variation of the gain-switched diode laser centre wavelength (blue) and spectral bandwidth (red) for an increasing DC bias at a constant modulation frequency of $2.00GHz$.

The spectral bandwidth of the diode laser when operated CW was typically $<1nm$, whereas Figure 3.3.6. illustrates the variation of the centre wavelength (blue line) and spectral bandwidth (red line) from the gain-switched with selected spectral profiles illustrated in Figure 3.3.7.

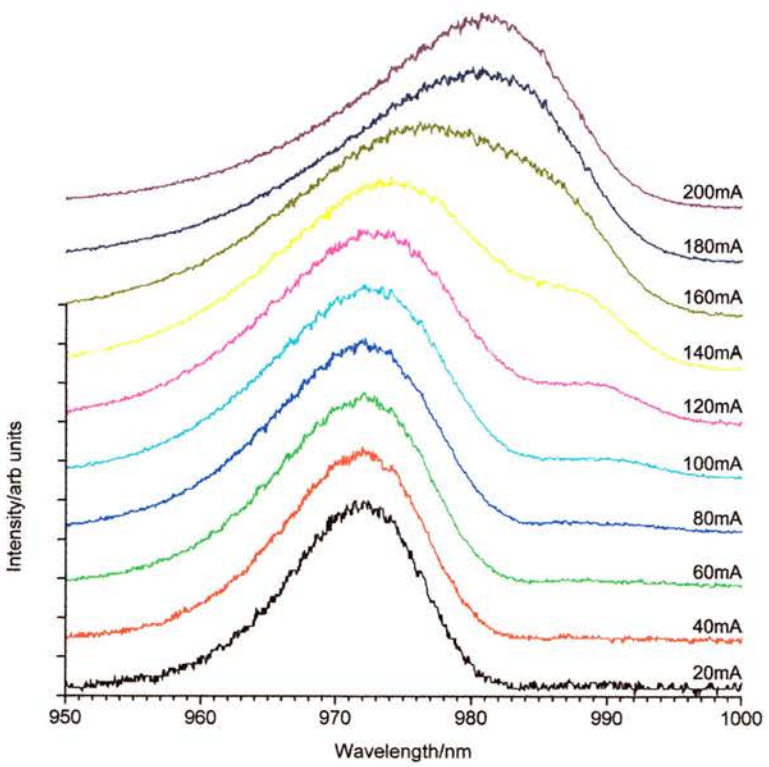

Figure 3.3.7. Spectral profiles obtained from the gain-switched diode laser for increased DC bias at a constant modulation frequency of $2.00GHz$.

Figures 3.3.6. and 3.3.7. demonstrate a gradual increase in both the centre wavelength and spectral bandwidth of the output.

The reduction in spectral bandwidth for a DC bias greater than $160mA$ was due to the imbalance of the DC to RF power. If continued to higher DC bias the optical pulse would start to degrade, eventually resulting in pseudo-CW operation. This regime of operation was not of interest except for the limit it placed on the maximum average power that could be obtained from any particular device. Methodologies through which higher average power operation may be achieved are outlined in section 3.4.

High resolution measurements of the gain-switched diode laser spectrum were performed using a computer-controlled CVI monochromator, operated by a custom written HP-VEE program. Detection of the optical signal transmitted through the monochromator was by a reverse DC biased large area photodiode connected to a Stanford Research 810 lock-in amplifier. An optical chopper connected to the lock-in was positioned before the input to the monochromator. Such a level of detection sensitivity was required because the entrance and exit slits had been reduced to around $10\mu m$ to ensure that the maximum resolution of $0.01nm$ could be obtained.

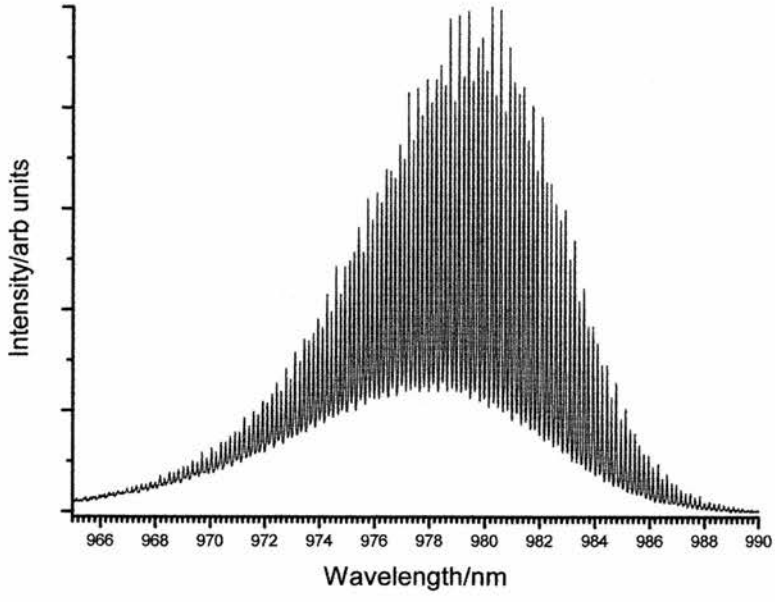

Figure 3.3.8. High resolution scan of the gain-switched diode laser spectrum.

The spectrum shown in Figure 3.3.8. was recorded for a DC bias of $100mA$ and a sinusoidal modulation frequency of $2.00GHz$. Under such operational

conditions the pulse duration was $\sim 30ps$ with an average optical output power of $70mW$. The Fabry-Perot mode structure imparted upon the spectrum by the diode laser cavity is clearly visible, manifesting as a deep modulation. Such modulation was only visible when the monochromator was utilised for spectral measurements since the real-time spectrometer had insufficient resolution. The corresponding FWHM spectral bandwidth of the *envelope* was $11nm$, with a Fabry-Perot mode bandwidth of $\sim 0.04nm$, and separation of $0.17nm$ between adjacent modes. This observed value of the Fabry-Perot mode separation is in agreement with the value of $\Delta\lambda \approx 0.18\mu m$ deduced for a centre wavelength of $980nm$, cavity length of $750\mu m$ and active region refractive index of 3.45.

From the temporal and spectral data presented in Figures 3.3.2. and 3.3.6. respectively, the time-bandwidth product of the optical pulses obtained from the gain-switched diode was calculated.

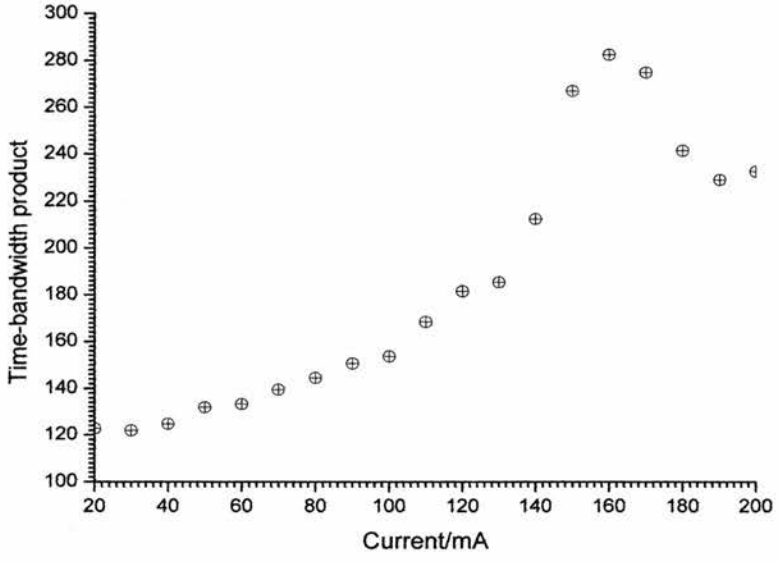

Figure 3.3.9. Time-bandwidth product variation with DC bias for a constant modulation frequency of $2.60GHz$.

As Figure 3.3.9. illustrates, the values thus obtained are significantly higher than that of the Fourier transform-limit. The time-bandwidth product for the minimum pulse duration of $30ps$ was ≈ 103. Throughout the course of the work discussed henceforth, experimental schemes were devised in order to minimise the time-bandwidth product. A dramatic reduction was accomplished by utilising optical feedback from an element external to the diode laser cavity. This work is discussed in Chapters 5, 6, and 7.

3.3.4. Spatial characteristics.

The spatial output of each laser setup was measured to confirm that the diode laser was single mode. Spatial profiles were recorded by scanning a large area silicon photodiode and slit through the output with no collimating optics, using a computer controlled translation stage. It was also possible to manually adjust the distance of the slit from the diode laser to enable an accurate determination of the divergence and the related M^2 values. The in-house developed software saved the resultant profiles and determined the FWHM divergence. Measurements of the far-field beam profile parallel to the junction were performed at a distance of $100mm$ from the output facet, for DC bias of $20mA$ $(4mW)$ and $100mA$ $(70mW)$, with a constant modulation frequency of $1.80GHz$ where applicable. The resultant profiles are shown in Figures 3.3.10 and 3.3.11. Far-field profiles were not performed perpendicular to the junction because in this direction the spatial output of a diode laser is typically diffraction limited due to the active region thickness.

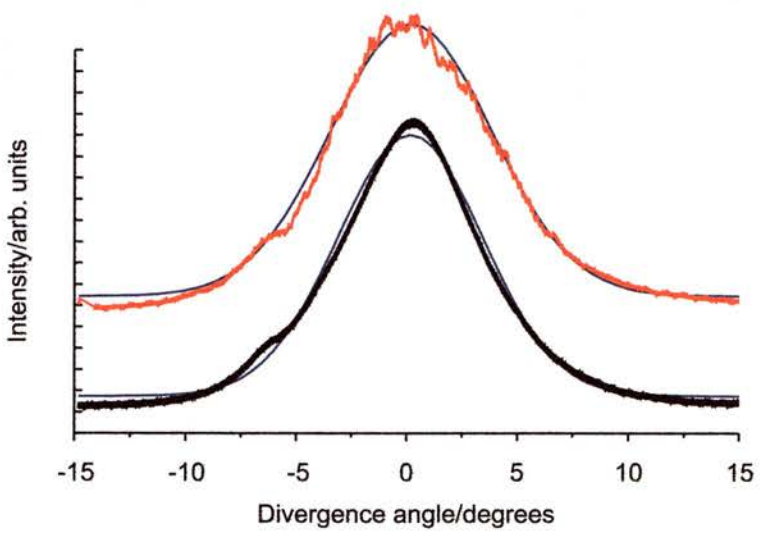

Figure 3.3.10. Far field profiles measured under CW operating conditions for a DC bias of $20mA$ (black) and $100mA$ (red).

Illustrated in Figure 3.3.10. are the far-field profiles measured under CW conditions. The lower black line was for a DC bias of $20mA$, whereas the upper red line was for a DC bias of $100mA$. In both profiles the blue line refers to a Gaussian fit of the data.

The far-field profiles shown in Figure 3.3.11. were taken under the same conditions, as described above for those in Figure 3.3.10., except for the addition of a $1.80GHz$ sinusoidal modulation used to gain-switch the diode laser.

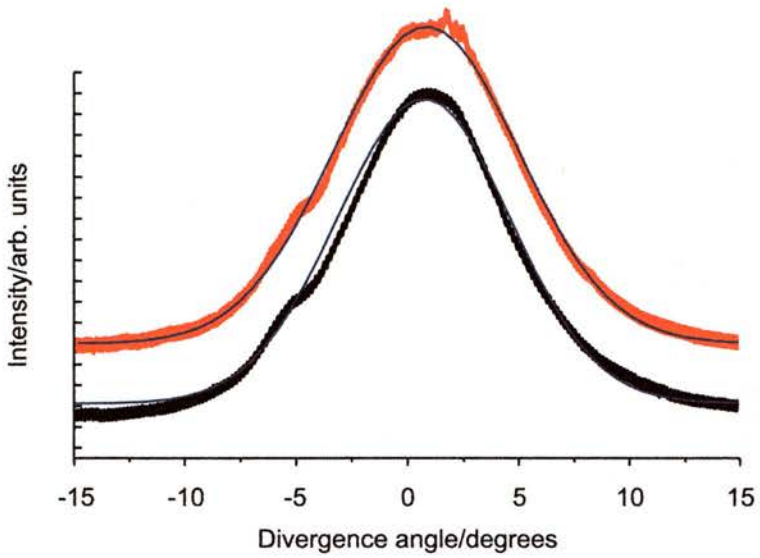

Figure 3.3.11. Far field profiles measured under pulsed operating conditions for a DC bias of $20mA$ (black) and $100mA$ (red).

It is clear from Figures 3.3.10. and 3.3.11. that gain-switching had a negligible effect on the far field, and that the output was near Gaussian. Single mode operation was also achieved over a broad range of DC bias, with an insignificant increase in the divergence. An M^2 value was determined to be ≈ 1.1 in the plane parallel to the junction.

3.3.5. Fibre-coupled narrow stripe diode lasers.

The narrow stripe diode lasers discussed above were also obtained as single-mode optical fibre pigtailed devices. In this case the diode laser was mounted in a small butterfly package, and coupled into a length of single-mode optical fibre, terminated with a standard optical connector. It should be noted that this butterfly package was not optimised for high speed modulation. The electrical characteristics illustrated in Figure 3.3.12. demonstrate the severe effect single-mode optical fibre coupling had upon the optical output power of the device.

The V/I characteristic of the optical fibre-coupled narrow stripe device was largely unaffected when compared with the solitary device (Figure 3.3.1.) The threshold current was $16mA$, reducing to $11mA$ with the application of sinusoidal

modulation. Due to the losses inherent with coupling into a single-mode optical fibre, the maximum output power and electrical to optical efficiency were both reduced, to $60mW$ and $0.44mW/mA$ respectively. When gain-switched, the optimum pulse duration obtained from the fibre coupled laser chip was for a DC bias of $70mA$ and sinusoidal modulation frequency of $2.40GHz$. Under these operational conditions the minimum pulse duration was $32.5ps$, with a corresponding spectral bandwidth of $\sim 6nm$. The time-bandwidth product was ~ 60.

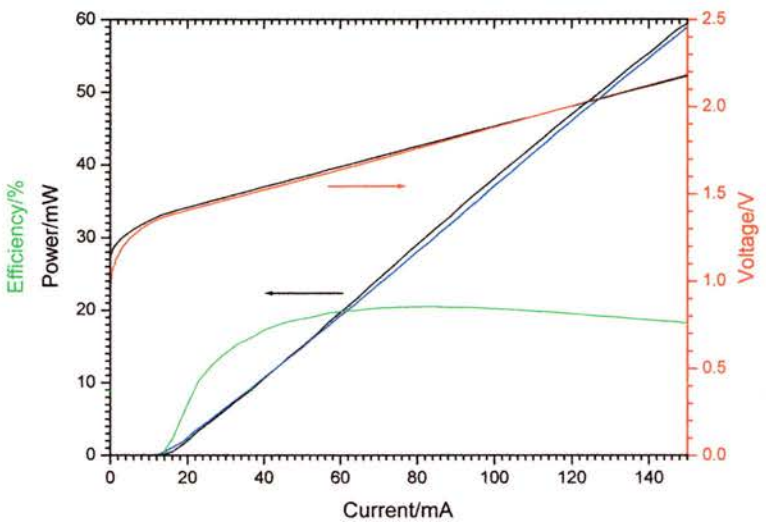

Figure 3.3.12. Electrical characteristics typical of a single-mode optical fibre-coupled narrow stripe devices. The L/I, V/I and efficiency curves are shown in blue, red and green respectively.

Even though the optical output power of the fibre-coupled diode laser was significantly reduced compared with the solitary device, it could be of future use to the work with fibre gratings discussed in Chapter 6.

3.4. Continual development.

Throughout the course of the work discussed in this thesis there has been a consistent desire to obtain the highest average power with the shortest pulse durations, thereby increasing the peak output power. An increased peak power would be of great significance for the second harmonic generation work discussed in Chapter 7. As illustrated in this chapter, a fine balance exists between the DC bias and the amplitude of the supplementary sinusoidal modulation if the peak power is to be maximised. Increasing the DC bias alone

results in optical pulses with an increased duration (Figures 3.3.2 and 3.3.3.). Therefore, to maintain a minimal pulse duration it is necessary to increase both the DC bias and sinusoidal modulation amplitude simultaneously. This requirement translates to the situation where the RF power applied to the diode laser must be increased. An increased RF power delivery to the diode laser may be achieved through three main methodologies, although the last two are essentially equivalent. These are: (i) the use of a RF amplifier with an increased power output. (ii) optimal impedance matching of the microwave cable to the diode laser to make better use of the existing power available. (iii) a diode laser chip suitably incorporated into a high speed modulation package.

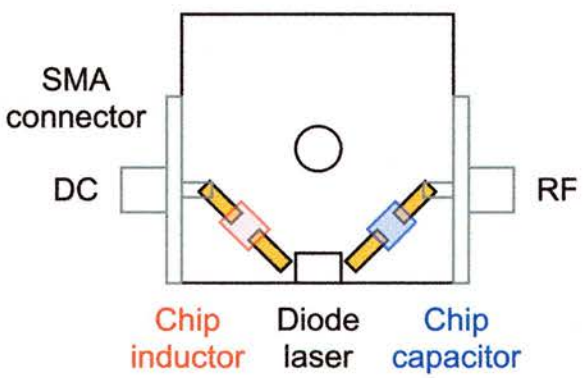

Figure 3.4.1. Proposed dual-contact mounting technique to enable use of the stub tuner.

With the above in mind, the Mini Circuits $29dBm$ amplifier was replaced by a Stealth Microwave SM1727-37H unit. Its power output of $37dBm$, represented a $5X$ increase in output power over the Mini Circuits device. The amplifier bandwidth of $1.70GHz$ to $2.70GHz$ corresponded well to the operational frequency range typically used for gain-switching the diode laser. Despite the higher output power of the replacement power amplifier, the increase in the RF power applied to the diode laser is still limited by the impedance mis-match present between the 50Ω microwave cable and the diode laser. This mis-match results in power being reflected and subsequently discarded by the circulator. A simple way by which this situation can be rectified is through the use of a passive device referred to as a stub tuner, which enables the diode laser to be impedance matched to the 50Ω microwave cable resulting in a decreased reflection. The stub tuner employed, a Maury Microwave 1819B, matched the impedance inductively by adjustment of three sliders. A

consequence of inductive tuning was that the DC supply shown in Figure 3.2.1. used to forward bias the diode laser was short-circuited.

To solve this problem, the dual-contact mounting arrangement shown in Figure 3.4.1. is proposed. Rather than using a bias tee to combine the DC and RF components before application to the diode laser, they are applied individually. As Figure 3.4.1. illustrates, this will be achieved by placing a chip inductor between the DC bias connector and diode laser, or a chip capacitor for the RF. Importantly the capacitor is *invisible* to the RF, being equivalent to a closed circuit, whereas to DC it is equivalent to an open circuit, and hence the stub tuner no longer shorts out the DC power supply. To maintain optimal matching between the 50Ω microwave cable and diode laser, the stub tuner must be *tuned* as the modulation frequency is altered. This can be readily achieved by connecting a RF spectrum analyser to port 3 of the circulator and adjusting the stub tuner to minimise the reflected power.

3.5. Future work.

Recently, the versions of the diode lasers used in this work have become available as single-mode InGaAs/GaAs ridge waveguide devices producing CW output powers of $450mW$. Although gain-switched operation of these devices has been demonstrated akin to its lower power counterparts, it is not reasonable to utilise them until an increased RF power can be applied and its full potential exploited. This will be achieved by impedance matching a $42dBm$ RF power amplifier. An increased average power would result as a consequence of the elevated DC bias required to maintain a short pulse duration.

3.6. Conclusions.

Optical pulses with picosecond pulse durations were demonstrated through the simultaneous application of a forward DC bias and supplementary sinusoidal modulation to a single-contact diode laser.

The operational characteristics of the device were presented for both CW and gain-switched regimes. The threshold current was reduced from $17mA$ to $\sim 7mA$ when gain-switched, with the slope efficiency being reduced from

$0.77mW/mA$ to $0.67mW/mA$. Under optimum operational conditions the minimum pulse duration was measured to be $30ps$, with a spectral bandwidth of $11nm$ and time-bandwidth product of ≈ 103. The average and peak optical output powers for such a pulse duration were $70mW$ and $\approx 1.2W$ respectively. The maximum average and peak powers were limited by the application of the RF power to the diode laser, and suggestions have been made to improve this performance.

Single-mode, fibre-coupled diode lasers were also evaluated. Though the slope efficiency of $0.44mW/mA$ obtained from this laser format was rather low when compared with its non-pigtailed counterpart, it could prove an interesting proposition for future developments.

In conclusion, gain-switching of single-mode, narrow stripe InGaAs/GaAs ridge waveguide devices represents a practical and robust technique for the reliable production of picosecond pulses from diode lasers where reasonably high average and peak output powers are required.

3.7. References.

1. Griffin, R. A., Jackson, D. A. & Sampson, D. D., "Coherence and Noise Properties of Gain-Switched Fabry-Perot Semiconductor-Lasers," *IEEE Journal of Selected Topics in Quantum Electronics*, vol. 1, pp. 569-576, 1995.
2. Sayin, M. & Ozyazici, M. S., "Effect of gain switching frequency on ultrashort pulse generation from laser diodes," *Optical and Quantum Electronics*, vol. 29, pp. 627-638, 1997.
3. Lau, K. Y., "Gain Switching of Semiconductor Injection Lasers," *Applied Physics Letters*, vol. 52, pp. 257-259, 1988.
4. Ito, H., Yokoyama, H., Murata, S. & Inaba, H., "Generation of Picosecond Optical Pulses With Highly RF Modulated Algaas Dh Laser," *IEEE Journal of Quantum Electronics*, vol. 17, pp. 663-670, 1981.
5. Wiesenfeld, J. M. *et al.*, "Gain-Switched GaAs Vertical-Cavity Surface-Emitting Lasers," *IEEE Journal of Quantum Electronics*, vol. 29, pp. 1996-2005, 1993.
6. Tarucha, S. & Otsuka, K., "Response of Semiconductor-Laser to Deep Sinusoidal Injection Current Modulation," *IEEE Journal of Quantum Electronics*, vol. 17, pp. 810-816, 1981.
7. Poelker, M., "High-Power Gain-Switched Diode-Laser Master Oscillator and Amplifier," *Applied Physics Letters*, vol. 67, pp. 2762-2764, 1995.
8. Auyeung, J., "Picosecond Optical Pulse Generation At Gigahertz Rates By Direct Modulation of a Semiconductor-Laser," *Applied Physics Letters*, vol. 38, pp. 308-310, 1981.
9. Klein, H. J., Bimberg, D., Beneking, H., Kuhl, J. & Gobel, E. O., "High Peak Power Picosecond Light-Pulses From a Directly Modulated Semiconductor-Laser," *Applied Physics Letters*, vol. 41, pp. 394-396, 1982.
10. Ong, J. T. *et al.*, "Subpicosecond Soliton Compression of Gain-Switched Diode-Laser Pulses Using an Erbium-Doped Fiber Amplifier," *IEEE Journal of Quantum Electronics*, vol. 29, pp. 1701-1707, 1993.
11. Arakawa, Y., Sogawa, T., Nishioka, M., Tanaka, M. & Sakaki, H., "Picosecond Pulse Generation (<1.8 ps) in a Quantum- Well Laser By a Gain Switching Method," *Applied Physics Letters*, vol. 51, pp. 1295-1297, 1987.
12. Sogawa, T. & Arakawa, Y., "Picosecond Lasing Dynamics of Gain-Switched Quantum-Well Lasers and Its Dependence On Quantum-Well Structures," *IEEE Journal of Quantum Electronics*, vol. 27, pp. 1648-1654, 1991.
13. Li, S. P., Chan, K. T. & Lou, C. Y., "Wavelength-tunable picosecond pulses generated from stable self-seeded gain-switched laser diode with linearly chirped fibre Bragg grating," *Electronics Letters*, vol. 34, pp. 1234-1236, 1998.
14. Ahmed, K. A., Chan, K. C. & Liu, H. F., "Femtosecond Pulse Generation From Semiconductor-Lasers Using the Soliton-Effect Compression Technique," *IEEE Journal of Selected Topics in Quantum Electronics*, vol. 1, pp. 592-600, 1995.
15. Lourtioz, J. M. *et al.*, "(Sub)Picosecond Laser-Diodes," *Annales De Physique*, vol. 20, pp. 1-10, 1995.
16. Yatsu, R., Taira, K. & Tsuchiya, M., "High-quality sub 100 fs optical pulse generation by fiber-optic soliton compression of gain-switched distributed-feedback laser-diode pulses in conjunction with nonlinear optical fiber loops," *Optics Letters*, vol. 24, pp. 1172-1174, 1999.
17. Chusseau, L., Hemery, E. & Lourtioz, J. M., "Period Doubling in Directly Modulated InGaAsP Semiconductor- Lasers," *Applied Physics Letters*, vol. 55, pp. 822-824, 1989.
18. Carpintero, G. & Lamela, H., "Influence of noise in the route to chaos of directly modulated semiconductor lasers," *Journal of Applied Physics*, vol. 82, pp. 2766-2772, 1997.
19. Cohen, J. S. & Lenstra, D., "Noise, Chaos and Coherence Collapse in Semiconductor-Lasers," *Philips Journal of Research*, vol. 44, pp. 43-55, 1989.

20. Kikuchi, N., Liu, Y. & Ohtsubo, J., "Chaos control and noise suppression in external-cavity semiconductor lasers," *IEEE Journal of Quantum Electronics*, vol. 33, pp. 56-65, 1997.

21. Hohl, A. & Gavrielides, A., "Experimental control of a chaotic semiconductor laser," *Optics Letters*, vol. 23, pp. 1606-1608, 1998.

22. Lamela, H., Carpintero, G. & Mancebo, F. J., "Period tripling and chaos in the dynamic behavior of directly modulated diode lasers," *IEEE Journal of Quantum Electronics*, vol. 34, pp. 1797-1801, 1998.

23. Chesnoy, J., Klein, M. C., Chusseau, L. & Lourtioz, J. M., "Period-Doubling and Period-Quadrupling For an Actively Mode- Locked Laser Diode With Extended Cavity," *Journal of Applied Physics*, vol. 67, pp. 7615-7617, 1990.

Chapter 4.
Indirect characterisations of picosecond pulses.

4.1. Introduction.

Although the direct pulse characterisation techniques discussed in Chapter 1. are capable of providing some relevant temporal information regarding a pulse, it is often helpful to deduce complementary characteristics. Notably, these include temporal phase, or its the derivative, frequency chirp.

The picosecond optical pulses from the gain-switched diode lasers discussed in the previous chapter did not have a Fourier transform-limited time-bandwidth product. Given their large spectral bandwidths it is reasonable to infer that these optical pulses were seriously frequency chirped. A knowledge of the spectral and temporal characteristics of the optical pulses from the gain-switched diode laser is required if measures are to be taken which would compensate for the frequency chirp in a controlled manner. Also, in a more general sense, an understanding of picosecond diode laser sources is of crucial importance for high bandwidth optical communications and optoelectronic signal processing due to the data rate limitations arising from frequency chirping effects.

Time-resolved measurements of frequency chirp from the pulsed output of a single-mode diode laser were first reported by Lin and co-workers.[1] Since then various characterisation techniques have been employed with pulsed diode lasers sources to determine the sign and magnitude of the frequency chirp present in the optical output.[1-7] An electron-optical streak camera and monochromator were used successfully by Stelmakh and Lourtioz[4] and Bresson *et al*[7] for frequency chirp measurements of the pulses from Q-switched diode lasers. Tsuchiya and co-workers[6] used a similar experimental scheme for characterising the output from a gain-switched diode laser.

4.2. Frequency chirping of diode laser pulses.

At this point it may prove useful to provide an overview of frequency chirp, and the mechanisms by which it originates. Due to the large spectral bandwidth required to support an ultrashort optical pulse, the dispersion inherent to all materials cannot be ignored. As a consequence of this, careful consideration must be taken when designing ultrashort pulse lasers to minimise (or

compensate for) the resulting frequency chirp. The mechanisms responsible for chirp differ between diode and solid-state lasers. Because the work discussed in this thesis is concerned with diode lasers, only those processes responsible for frequency chirp in diode lasers will be discussed here. (An overview of the processes involved in solid-state lasers is widely available in the referenced literature.[8-12])

In the following discussion a pulse with a Gaussian profile is assumed, though such an assumption does not affect the overall validity of this description.

An optical pulse with a carrier frequency ω_0 and a complex Gaussian envelope can be described by the following:[13]

$$\varepsilon(t) = \exp\left(-at^2\right)\exp j\left(\omega_0 t + bt^2\right) \qquad 4.1$$

The intensity $I(t)$ of the pulse described by Equation 4.1. is:

$$I(t) = \left|\varepsilon(t)\right|^2 = \exp\left(-2at^2\right) = \exp\left[-(4\ln 2)\left(\frac{t}{\tau_p}\right)^2\right] \qquad 4.2$$

where the FWHM pulse duration τ_p is:

$$\tau_p = \sqrt{\frac{2\ln 2}{a}} \qquad 4.3$$

The phase shift of the carrier wave within the Gaussian pulse is:

$$\varepsilon(t) \propto \exp j\left(\omega_0 + bt^2\right) = \exp\left[j\phi(t)\right] \qquad 4.4$$

where the total phase is given by:

$$\phi(t) = \omega_0 t + bt^2 \qquad 4.5$$

The instantaneous frequency in radians per second is:

$$\omega_i(t) = \frac{d\phi(t)}{dt} \qquad 4.6$$

which in complex form yields:

$$\omega_i(t) = \frac{d}{dt}\left(\omega_0 t + bt^2\right) = \omega_0 + 2bt \qquad 4.7$$

From Equation 4.7, in a Gaussian pulse with a zero b value there exists an even distribution of the frequency components within that optical pulse centred

about ω_0 (Figure 4.2.1a.). If b is non-zero then a linearly varying shift of the frequency components occurs across the pulse. Such a pulse is referred to as one having a linear frequency chirp (or just chirped) with b being a measure of this chirping magnitude.

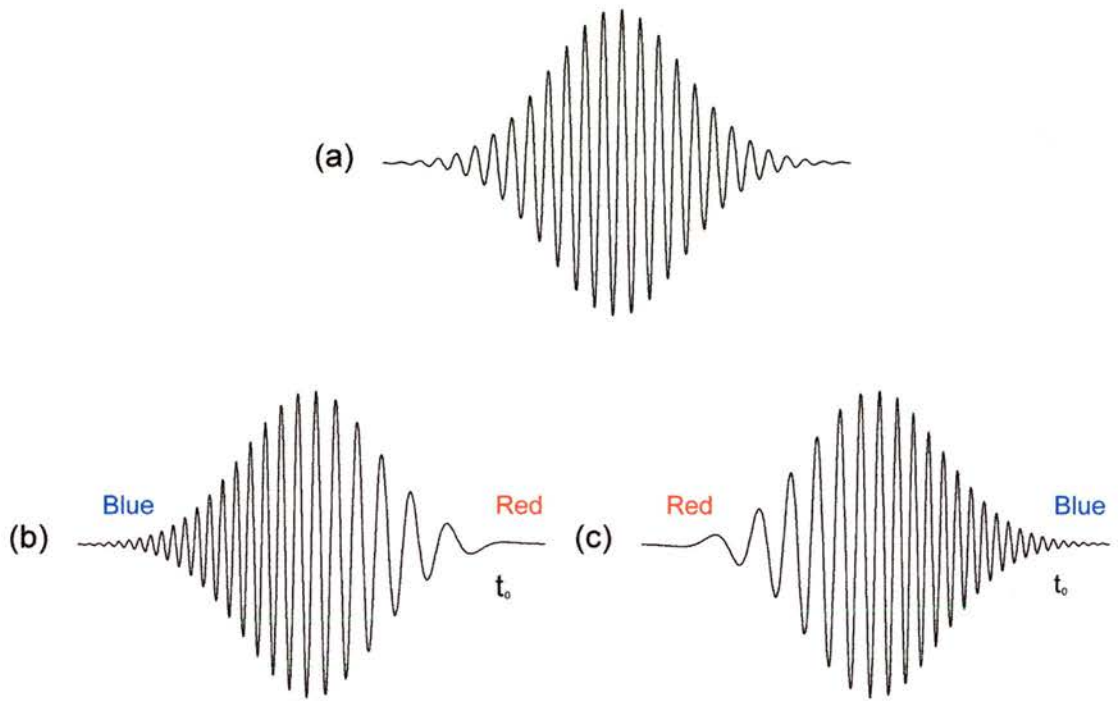

Figure 4.2.1. Gaussian pulse with (a) zero, (b) positive or (c) negative frequency chirp.

Through simulations using Equation 4.1. with various values of b, the three optical pulses shown in Figure 4.2.1. were generated. These figures clearly illustrate the frequency shift discussed above. Figure 4.2.1a. is a chirp free (or transform-limited) pulse where the instantaneous frequency is the same at all time across the pulse. For the frequency chirped pulses of Figure 4.2.1b. and 4.2.1c, the instantaneous frequency chirp varies linearly across the pulse. For positive frequency chirp (Figure 4.2.1b.), the lower frequency components are at the leading edge (t_0) of the pulse with the higher frequency components at the trailing edge. This situation is reversed for the case of negative frequency chirp, illustrated in Figure 4.2.1c.

The mechanisms underlying the chirped optical output obtained from a gain-switched diode laser were discussed in Chapter 1. However, for the benefit of the reader the key points will be reviewed here.

Consider a transient carrier injection, in the form of either an electrical pulse or sinusoidal modulation, applied to the diode laser for the purposes of achieving gain-switching. There are two main effects that should be considered. The first is device heating: such heating leads to a gradual *red-shift* of the diode laser emission wavelength. This effect was demonstrated experimentally, albeit for a change of the DC bias, in Figures 3.3.6. and 3.3.7. but the underlying cause is the same.

The second effect is due to a dynamic response of the inverted carrier density due to the transient electrical pulse. The net increase of the inverted carrier density results in a reduction of the refractive index in the local active region. This reduction of the refractive index, results in a shortening of the effective optical cavity length, with a resultant spectral shift to the shorter wavelengths. As lasing action reduces the inverted carrier density, there is a linear increase in the refractive index with a similar spectral shift of the centre wavelength. The wavelength modulation during the evolution of an optical pulse typically occurs as a *"red" shift* for pulsed diode lasers, otherwise known as negative chirp. A *"blue" shift*, otherwise known as positive chirp, has also been observed from passively mode-locked lasers,[5] though by varying the α parameter of the absorber[14-16] to approaching that of the gain section, negative chirp was observed. These two types of chirp are illustrated in Figure 4.2.1. Frequency chirp on the output of a pulsed diode laser is thus inevitable but steps can be taken to minimise its magnitude either through device design[17-21] or by external dispersion compensation.[22-29]

4.3. The sonogram.

The sonogram is a very useful diagnostic tool, because it can provide information about an optical pulse that is not readily obtained with direct measurement techniques. Unlike the pulse measurement methodologies discussed in Chapter 1, a sonogram is an *indirect* technique, in that the information is not immediately available, but is instead deduced through the use of an algorithm operated on the experimental data.

Compared with other indirect pulse characterisation techniques, such as frequency-domain phase measurement (FDPM)[30] and second harmonic

generation-frequency resolved optical gating (SHG-FROG),[31,32] the sonogram can be used to visualise the sign and magnitude of the frequency chirp in an optical pulse.

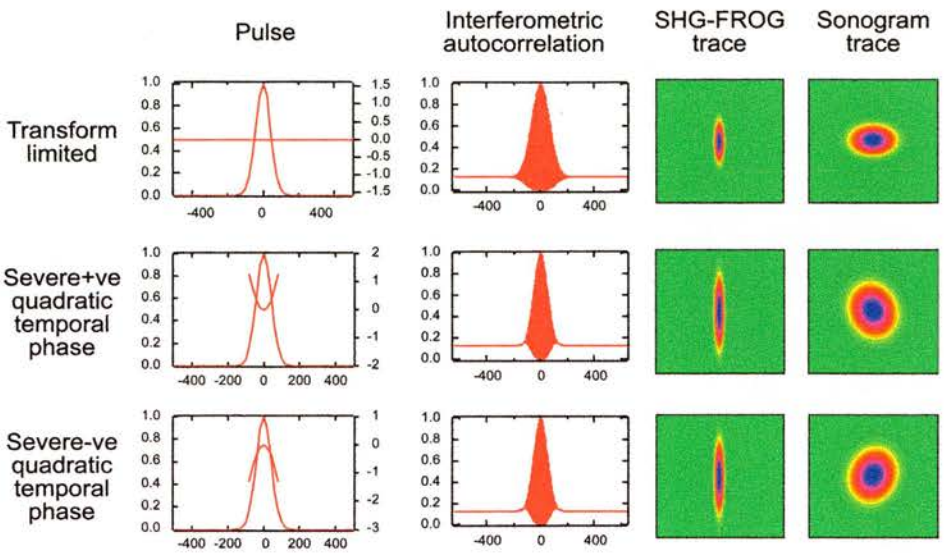

Figure 4.3.1. Comparison of various pulse and phase profiles as measured with interferometric autocorrelation, SHG-FROG and sonogram.[33]

To illustrate the differences between the sonogram and FROG measurement schemes, consider Figure 4.3.1. For an optical pulse with temporal and phase profiles given in the first column, the subsequent columns illustrate the interferometric autocorrelation, SHG-FROG and sonogram traces that would be obtained. The sonogram for a Fourier transform-limited pulse is symmetrical about the horizontal centre line. Any deviation of the sonogram from this position illustrates the presence of temporal phase on the optical pulse. When compared with SHG-FROG, the sonogram offers an intuitive insight regarding the sign and magnitude of the phase information. Such phase information that can be provided by the sonogram makes it an exceedingly useful tool in the arsenal of pulse characterisation techniques.

A sonogram can be realised experimentally by temporal measurement of the optical pulses after they have passed through a narrow band spectral filter $g(\omega-\Omega)$ with a variable centre frequency Ω. The relative position of the spectral filter across the complete spectral bandwidth of the pulse determines the arrival time and intensity of the various components according to the mathematical form:[34]

$$S(t,\Omega)=\left|\int_{-\infty}^{\infty}E(\omega)g(\omega-\Omega)\mathrm{e}^{-j\omega t}\,d\omega\right|^2 \qquad 4.8$$

The action of the spectral filter is to essentially *slice* the optical pulse in the frequency domain. By scanning the spectral filter, and recording the transmitted optical pulses in the temporal domain, it is possible after suitable reconstruction, to produce a plot of frequency (or wavelength) versus time. Any frequency chirping in the optical pulse is then clearly evident on the resultant sonogram, as Figure 4.3.1. illustrates.

Phase information can be obtained from the experimental sonogram through the use of a suitable retrieval algorithm. The basic principles behind such an algorithm will be outlined in the next section.

4.3.1. Sonogram algorithm.

Temporal phase information contained within the experimental sonogram was retrieved by operation of an algorithm developed by Reid[34] that was based on principal component generalised projections.[35] The algorithm has been successfully demonstrated in various experimental applications.[33,36,37]

The flow chat in Figure 4.3.2. represents the procedure used by the pulse retrieval algorithm.[34]

First reasonable trial guesses based on a Gaussian envelope are generated for both the pulse and filter. Outer products are formed from these initial starting conditions, to which row rotation is applied. The resulting matrix is then Fourier transformed before the intensity of the resultant sonogram is replaced with that of the experimental measurement. The next guess for the pulse amplitude and filter transmission are determined by manipulating the sonogram into outer product form before principal component decomposition.

Constraints used within the algorithm are that the filter phase is zero. Also, the spectral intensity retrieved after each iteration was replaced by that measured experimentally. Both of these constraints served to improve convergence.

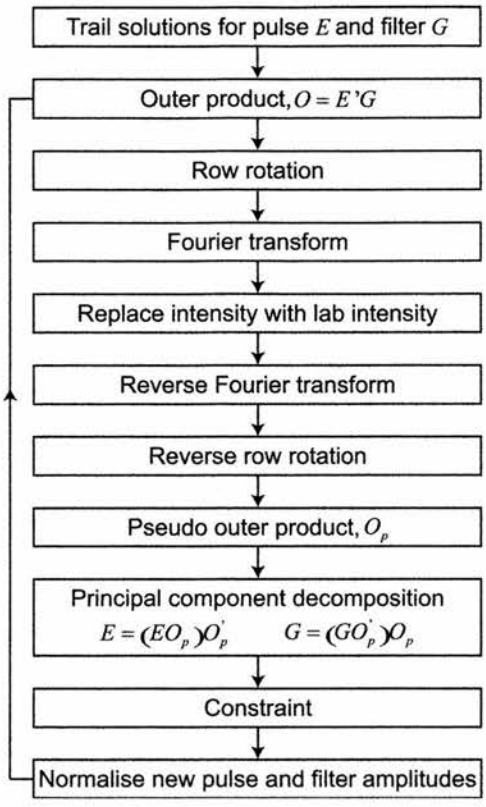

Figure 4.3.2. Sonogram pulse retrieval algorithm.[34]

In practice it was arranged that the passband of the frequency filter was about five times narrower than the spectral bandwidth of the pulse being characterised.

4.4. Experimental.

Two optical schemes were investigated during the course of the work discussed in this chapter.

The first scheme, illustrated in Figure 4.4.1. utilised diffraction gratings aligned such that the optical output from the diode laser was dispersed perpendicular to the plane of the optical bench. (The diffraction gratings are shown as providing dispersion in the plane for illustrative purposes only.) Stelmakh and co-workers[4] successfully demonstrated such an approach of using a single diffraction grating and a streak camera when performing an analysis of the modal chirp in Q-switched diode lasers. Using this technique Stelmakh and co-workers were able to successfully determine the chirp magnitude from various devices.[4] Unlike Stelmakh, two gratings were used in an attempt to increase the dispersion. An adjustable slit was placed in the dispersed beam (parallel to

the optical bench) such that wavelength regions of the output could be selectively blocked. In this way, the slit served to provide spectral calibration.

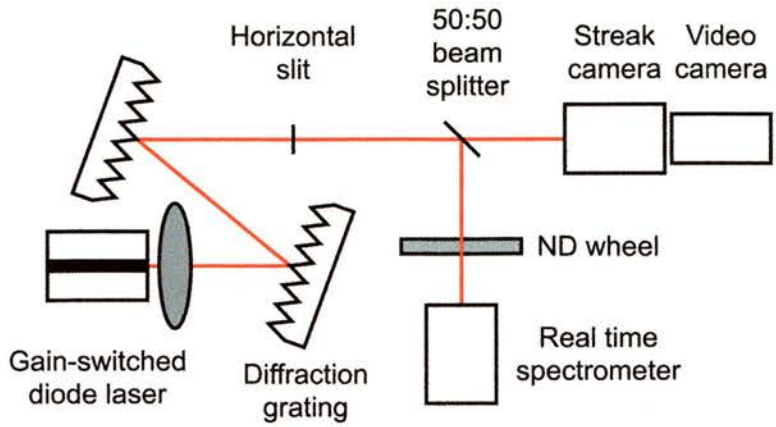

Figure 4.4.1. Experimental sonogram using two diffraction gratings, and a video camera for real-time, full frame readout.

After the horizontal slit, a $50:50$ beam splitter was used such that the output could be simultaneously monitored spectrally and temporally, using an optical spectrum analyser (OSA) and electron-optical synchroscan streak camera. Using the OSA it was possible to determine the spectral width of the bandpass filter compared with the unfiltered output. A vertical slit placed in front of the streak camera objective lens served to improve the spatial, and consequently, the cameras temporal resolution. A high sensitivity charge coupled device (CCD) video camera was used to directly image the output of the streak camera. The video camera was connected to a frame grabber running custom written software on a personal computer. With such a system, it was possible to obtain a sonogram in a single step. A video monitor provided a real-time output from the CCD camera for optimisation purposes.

The two diffraction gratings and slit were subsequently replaced with a computer-controlled CVI high resolution monochromator. Other groups have successfully demonstrated such a scheme, employing a monochromator and electron-optical synchroscan streak camera. For example, Bresson and co-workers[7] used this method for a study of the chirp in the optical pulses from a Q-switched diode laser, and Tsuchiya *et al*[6] used the technique for an analysis of the linear and nonlinear chirp from a gain-switched DFB laser prior to the use of fibre optic pulse compression. Both groups successfully determined the magnitude of the frequency chirp in the pulsed output. The high sensitivity CCD

camera had the obvious advantage that a complete sonogram was displayed in real-time. However, it was replaced with an optical mulitchannel analyser (OMA), which was capable of the real-time detection of low intensity pulses, thereby providing a larger signal-to-noise ratio than the CCD video camera. The temporal calibration was significantly simplified. Real-time, full frame acquisition of a sonogram was not possible with the OMA, and as a result it was necessary to construct a sonogram from the individual temporal profiles recorded by the OMA. The loss of real-time readout was unfortunate but unavoidable.

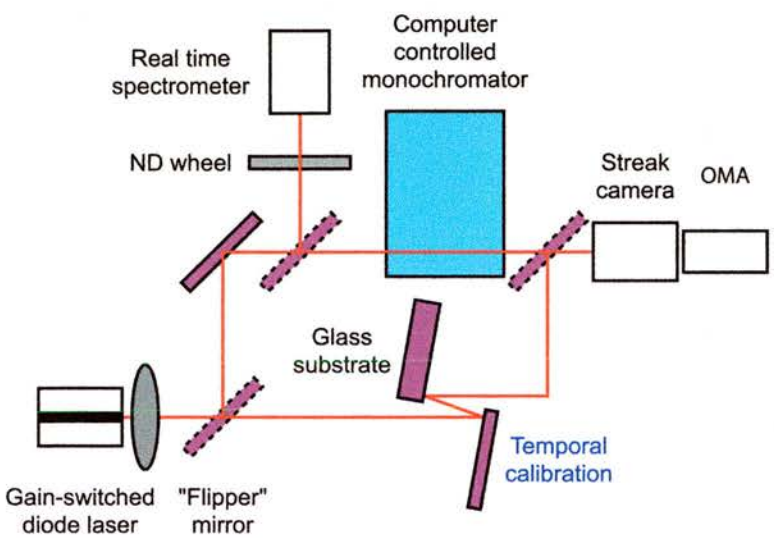

Figure 4.4.2. Experimental sonogram using a monochromator as a scanning bandpass filter.

As Figure 4.4.2. illustrates, the experimental configuration was reasonably straightforward and comprised a monochromator, electron-optical synchroscan streak camera and a personal computer. A real-time spectrometer was also utilised to determine the necessary start and stop points for the wavelength scan. The use of a computer-controlled monochromator gave precise control over the entrance and exit slit widths. No calibration of the wavelength axis was required because this information was obtained automatically from the monochromator through its computer interface.

To realise the full automation of the sonogram retrieval and construction, programs were developed in the equipment control language HP-VEE. The two programs that were written have been included as appendices D. and E. The first program interfaced the computer with the monochromator and oscilloscope

on which the OMA output was displayed. The program scanned the monochromator between user-defined start and stop wavelengths in increments down to the monochromator resolution of $0.01nm$. At each monochromator position, the resultant streak camera trace was saved to the computer hard disc for later analysis. The second program loaded from disc the individual temporal profiles, removed the previously measured background noise, and "stacked" them in increasing wavelength, thereby creating an array with increasing time along the *x*-axis and increasing wavelength along the *y*-axis. Therefore, by scanning the monochromator over the complete pulse spectral bandwidth, typically $30nm$, and after reconstruction, a sonogram of the optical pulse was obtained. The sonogram was in the form of a 2D array that was displayed in the computer program Matlab as a false colour contour map representation of the optical pulse.

Representative experimentally measured sonograms from the gain-switched diode laser are illustrated in Figure 4.4.3. for an applied DC bias of (a) $70mA$, (b) $140mA$ and (c) $190mA$. For such operational DC bias levels the average output powers were $45mW$, $98mW$ and $132mW$ respectively. It is possible to make out the reduced rise-time of the leading edge of the pulse compared with the fall-time. When measurements of the temporal profile for elevated DC bias levels were performed with the streak camera, the extended tail that resulted is clearly visible in Figure 4.4.3c. The variation of the spectral bandwidth is also evident from this sonogram measurement. Furthermore, from these experimental sonograms a measurement of the sign and magnitude of the frequency chirp can be deduced by determining the gradient of the sonogram. Such measurements were preformed on a range of experimental sonograms yielding a frequency chirp magnitude of $\sim 1.8ps/nm$, $\sim 2.1ps/nm$ and $\sim 2.2ps/nm$ for DC bias of $70mA$, $140mA$ and $190mA$ respectively. In agreement with theory, the sign of the frequency chirp was negative (red shift) in all three instances.

The $30nm$ scan of the monochromator performed during the acquisition of an experimental sonogram required the measurement of 1000 individual temporal profiles. During the time period required to perform a monochromator scan it was essential that the equipment and laser output remain stable.

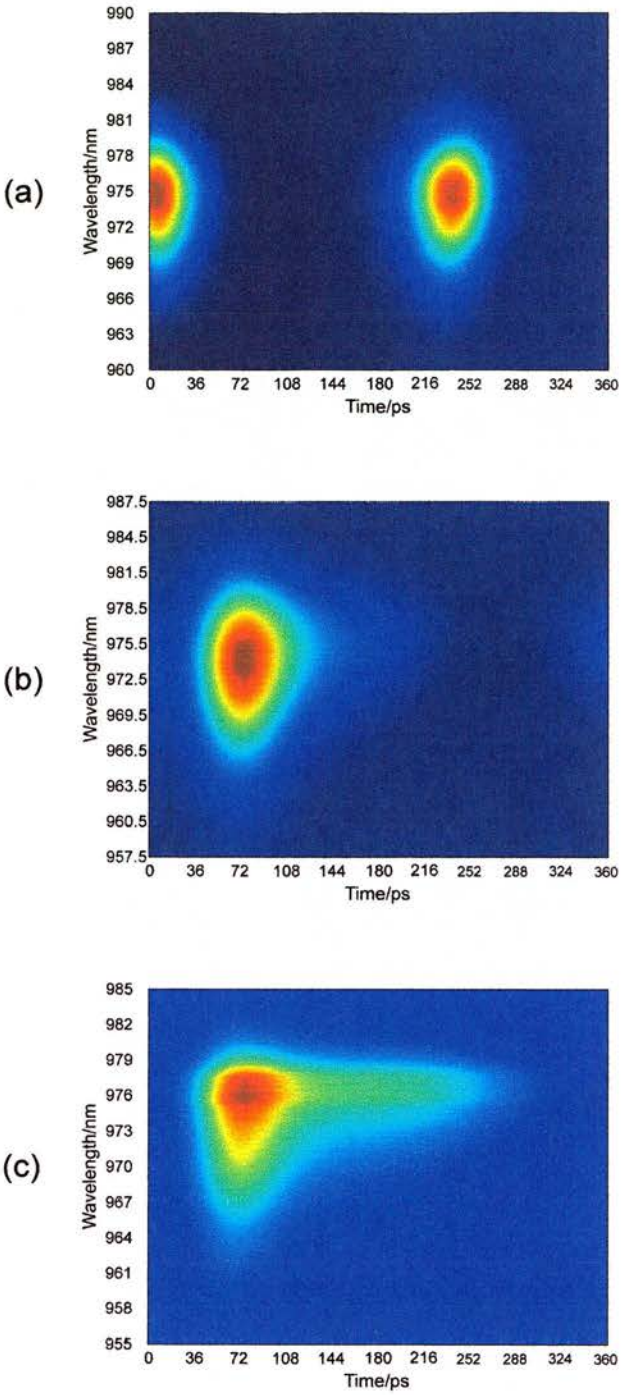

Figure 4.4.3. Experimental sonograms obtained for a DC bias of (a) $70mA$, (b) $140mA$ and (c) $190mA$.

Although the output of the gain-switched diode laser was extremely stable, the streak camera had to be calibrated, then left running to secure a full data-run. By optimising the HP-VEE program, an attempt was made to decrease the scan time, but the monochromator limited the ultimate scan speed.

Due to the frequency of operation of the syncroscan streak camera, two optical pulses were typically observed in the readout. One was recorded on the positive-going edge of the sinusoidal modulation applied to the deflection plates, and the other recorded on the negative-going edge. These streaks were therefore mirror images of one another.

4.5. Sonogram retrieval.

The experimental data were loaded into Matlab where it was displayed as a false colour contour plot. An experimental sonogram was prepared for retrieval through the following procedure. It was first arranged that the *x* and *y*-axes increased in wavelength and time respectively. (The experimental sonogram increased in time and wavelength respectively). To achieve this the matrix of the experimental sonogram was simply transposed in Matlab. The sonogram of the pulse was then isolated, and extracted in accordance with the calibration data, before being re-sampled to a 1024*1024 matrix. A matrix of 1024*1024 was chosen to prevent the under-sampling that would arise in a smaller array.

4.5.1. Calibration.

Calibration of the sonogram was of prime importance if the results from the acquisition were to have validity. The required calibrations were spectral, temporal and filter, otherwise referred to as the gate.

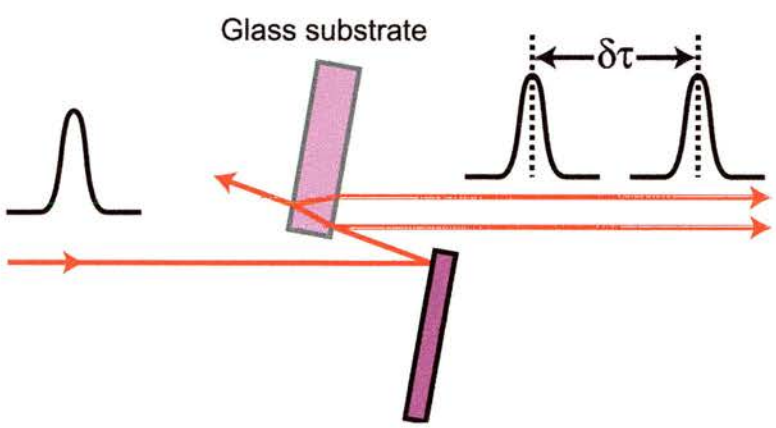

Figure 4.5.1. Experimental scheme for temporal calibration of the streak camera.

Due to the way in which an experimental sonogram was obtained spectral calibration was automatic. That is, a temporal profile was taken for each wavelength position of the computer-controlled monochromator. This temporal

profile was then saved to hard disc with a filename corresponding to that monochromator wavelength. In this way the exact spectral "reference" of any temporal profile was known, limited only by the calibration of the monochromator.

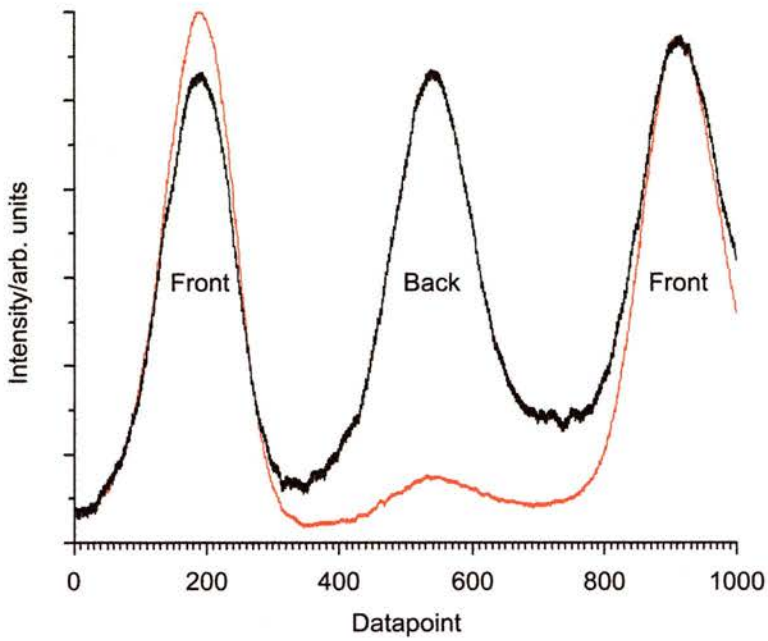

Figure 4.5.2. Temporal calibration using a glass substrate, demonstrating both reflections (black) and front reflection only (red).

Temporal calibration involved the implementation of the scheme illustrated in Figure 4.5.1. The direct output from the diode laser was first reflected by a high reflectance silver mirror before passing through a thick, optically polished glass substrate of known thickness, $(t = 12.88mm)$. Both optics were set such that the angle between the laser output and surface normal was small, and that the output beam was parallel to the input beam. The lateral displacement was of no consequence. After the substrate, two optical sub-pulses were obtained, the temporal separation between which was the extra optical path difference encountered by the pulse reflecting of the rear surface. The optical path difference between the two sub-pulses was therefore $pathlength = 2tn$, where n is the refractive index of glass. The corresponding temporal separation $\delta\tau$ was $128.8ps$. When viewed on the streak camera, multiple temporal profiles were obtained due to its scanning nature. It was necessary to ascertain which of the pulses corresponded to pairs. By adjusting the glass substrate it was possible to image either reflection, or both simultaneously. With the pulses due to the

reflections from both surfaces displayed, (black line in Figure 4.5.2.) the reflection corresponding to the rear surface could be established by the application of acetone to the rear surface of the substrate. This had the effect that the corresponding pulses were suppressed, with only the front face reflections remaining. (red line in Figure 4.5.2.).

Temporal profiles from the streak camera were viewed using a $500MHz$ sampling oscilloscope, with the traces recorded by the HP-VEE program and having a constant length of 1000 data points. After establishing a pair of pulses the number of data points between the two maxima could be determined. The temporal separation between these two points was known and so the temporal calibration could be established

It should be noted that the temporal calibration obtained by following the above procedure was only applicable whilst the streak camera remained stable, or the diode laser modulation frequency remained constant. For this reason, calibration data were verified before commencing each experimental sonogram acquisition.

The final calibration required was associated with the spectral filter. In this scheme, the monochromator was performing the function of a scanning bandpass filter. It was therefore necessary to determine the FWHM spectral bandwidth after the monochromator, which represents the passband of the filter. The centre of a given spectrum was determined using the real-time spectrometer, $(\delta\lambda \approx 0.3nm)$ and the monochromator set to this wavelength. The spectrometer was then positioned after the monochromator, monitoring the transmitted spectrum with both the entrance and exit slits set to $500\mu m$. The wavelengths at the 50% points were recorded. The exit slit was then reduced such that the transmitted spectrum, as measured on the spectrometer, had a FWHM bandwidth of $\sim 1nm$. The spectrum thus recorded formed the gate.

4.5.2. Results.

Using the iterative phase-retrieval algorithm discussed in the Section 4.3.1, pulse and temporal phase profiles were extracted from the calibrated experimental sonogram.

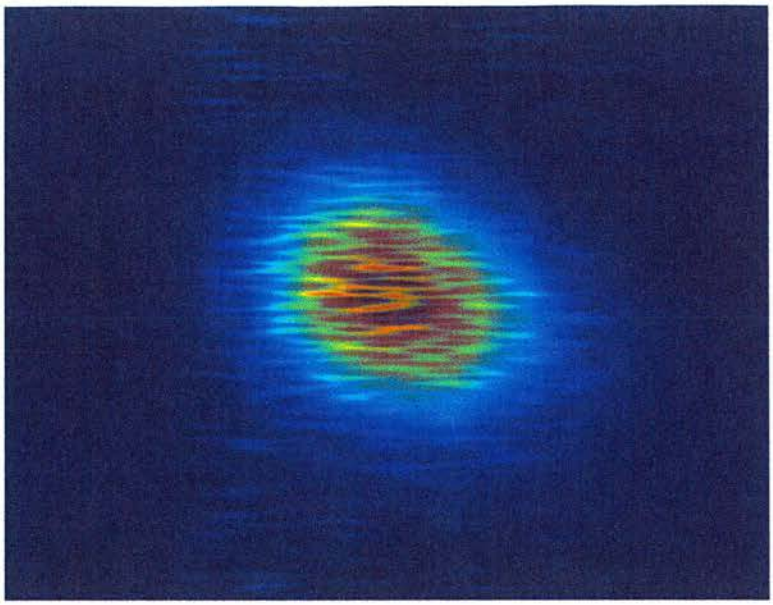

Figure 4.5.3. Retrieved sonogram with a 50% overlay of the experimental sonogram.

Illustrated in Figure 4.5.3. is the retrieved sonogram trace with a 50% opacity overlay of the experimental sonogram. This demonstrates a good correlation between the retrieved and calibrated experimental sonogram.

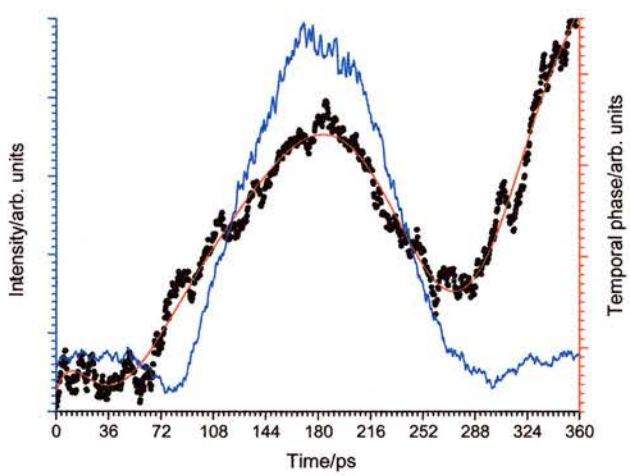

Figure 4.5.4. Retrieved pulse (blue) with the associated temporal phase (black) and polynomial fit (red).

Figure 4.5.4. illustrates the retrieved pulse (blue line) and temporal phase (black dots). The polynomial fit (red line) demonstrates the existence of severe negative temporal phase, consistent with both theory and the experimentally observed results.

When observing the temporal phase in Figure 4.5.4. only that which lies within the pulse duration is of significance. The FWHM pulse duration inferred from the retrieval is $\approx 100ps$, which has the correct order of magnitude when compared with the experimentally measured pulse duration of $\approx 35ps$.

4.6. Conclusions.

In this chapter the temporal characteristics of the picosecond optical pulses obtained from the gain-switched diode laser were investigated. This was achieved using the sonogram technique which is an extremely useful pulse diagnostic. The sign and magnitude of the frequency chirp in the picosecond optical pulses was successfully determined. Further validity is offered because the sign of the experimental and retrieved temporal phase agree well with that expected from the theory.

Such temporal phase information is of crucial importance for the design and realisation of aperiodic grating structures that would fully utilise the spectral bandwidth of the frequency chirped optical pulses. The knowledge gleaned from the work of this chapter was used to form the basis for the design of aperiodic fibre Bragg grating structures in core of germanosilicate optical fibres. (See Chapters 6.)

Additionally, based on the measurements suitable aperiodically-poled gratings were fabricated in lithium niobate crystals enabling highly efficient second harmonic conversion of the output from the gain-switched diode laser, as discussed in Chapter 7.

4.7. References.

1. Lin, C., Lee, T. P. & Burrus, C. A., "Picosecond Frequency Chirping and Dynamic Line Broadening in InGaAsP Injection-Lasers Under Fast Excitation," *Applied Physics Letters*, vol. 42, pp. 141-143, 1983.
2. Koch, T. L. & Bowers, J. E., "Nature of Wavelength Chirping in Directly Modulated Semiconductor-Lasers," *Electronics Letters*, vol. 20, pp. 1038-1040, 1984.
3. Wiesenfeld, J. M., Tucker, R. S. & Downey, P. M., "Picosecond Measurement of Chirp in Gain-Switched, Single-Mode Injection-Lasers," *Applied Physics Letters*, vol. 51, pp. 1307-1309, 1987.
4. Stelmakh, N. & Lourtioz, J. M., "Analysis of Modal Chirp in Q-Switched Semiconductor-Lasers," *Electronics Letters*, vol. 27, pp. 1856-1858, 1991.
5. Schell, M., Tsuchiya, M. & Kamiya, T., "Chirp and stability of mode-locked semiconductor lasers," *IEEE Journal of Quantum Electronics*, vol. 32, pp. 1180-1190, 1996.
6. Tsuchiya, M., Takeshita, H. & Kamiya, T., "Precise analysis of linear and non-linear chirp parameters of gain-switched distributed feedback laser pulses for the fibre optic compression scheme," *Optical and Quantum Electronics*, vol. 28, pp. 975-982, 1996.
7. Bresson, A., Stelmakh, N., Lourtioz, J. M., Shen, A. & Froehly, C., "Chirp measurement of multimode Q-switched laser diode pulses by use of a streak camera and a grating monochromator," *Applied Optics*, vol. 37, pp. 1022-1025, 1998.
8. Szipocs, R. & KohaziKis, A., "Theory and design of chirped dielectric laser mirrors," *Applied Physics B-Lasers and Optics*, vol. 65, pp. 115-135, 1997.
9. Dudley, J. M., Boussen, S. F., Cameron, D. M. J. & Harvey, J. D., "Complete characterization of a self-mode-looked Ti:sapphire laser in the vicinity of zero group-delay dispersion by frequency-resolved optical gating," *Applied Optics*, vol. 38, pp. 3308-3315, 1999.
10. Koch, F., Chernikov, S. V. & Taylor, J. R., "Characterization of dispersion in components for ultrafast lasers," *Optics Communications*, vol. 180, pp. 133-135, 2000.
11. Cormack, I. G., Baumann, F. & Reid, D. T., "Measurement of group velocity dispersion using white light interferometry: A teaching laboratory experiment," *American Journal of Physics*, vol. 68, pp. 1146-1150, 2000.
12. Walmsley, I., Waxer, L. & Dorrer, C., "The role of dispersion in ultrafast optics," *Review of Scientific Instruments*, vol. 72, pp. 1-29, 2001.
13. Seigman, A. E. *Lasers* (University science books, 1986).
14. Henry, C. H., "Theory of the Linewidth of Semiconductor-Lasers," *IEEE Journal of Quantum Electronics*, vol. 18, pp. 259-264, 1982.
15. Osinski, M. & Buus, J., "Linewidth Broadening Factor in Semiconductor-Lasers - an Overview," *IEEE Journal of Quantum Electronics*, vol. 23, pp. 9-29, 1987.
16. Vahala, K., Chiu, L. C., Margalit, S. & Yariv, A., "On the Linewidth Enhancement Factor-Alpha in Semiconductor Injection-Lasers," *Applied Physics Letters*, vol. 42, pp. 631-633, 1983.
17. Feng, J., Chen, T. R. & Yariv, A., "On Chirp Control in 2 Section Distributed-Feedback Semiconductor-Lasers," *Applied Physics Letters*, vol. 67, pp. 2913-2915, 1995.
18. Sudoh, T. K., Funabashi, M., Nakano, Y., Tada, K. & Hirata, T., "Origin of Low Dynamic Wavelength Chirp in Short Optical Pulses From Absorptive-Grating Gain-Coupled Distributed-Feedback Semiconductor-Lasers," *Electronics Letters*, vol. 31, pp. 108-109, 1995.
19. White, I. H., Griffin, P. S., Fice, M. J. & Whiteaway, J. E. A., "Line Narrowed Picosecond Optical Pulse Generation Using 3 Contact InGaAsP/InP Multiquantum Well Distributed Feedback Laser Under Gain Switching," *Electronics Letters*, vol. 28, pp. 1257-1258, 1992.

20. Feng, J., Chen, T. R., Zhao, B. & Yariv, A., "Reduction of the Frequency Chirp of 2 Section Distributed- Feedback Laser By Nonuniform Current Injection," *Applied Physics Letters*, vol. 66, pp. 2028-2030, 1995.

21. Shiraz, H. G. & Chu, C. Y. J., "Chirp Reduction in 3-Cavity Semiconductor-Laser Diodes," *Optics and Laser Technology*, vol. 24, pp. 73-76, 1992.

22. Carter, G. M., Zheng, L. & Huang, K. Y., "Compression of Pulses From a Mode-Locked Gaas-Laser Diode in an Extended Cavity With a Fiber Grating Reflector," *Applied Physics Letters*, vol. 61, pp. 379-380, 1992.

23. Li, S. P. *et al*, "Self-seeding of Fabry-Perot laser diode for generating wavelength-tunable chirp-compensated single-mode pulses with high-sidemode suppression ratio," *IEEE Photonics Technology Letters*, vol. 12, pp. 1441-1443, 2000.

24. Eggleton, B. J., Krug, P. A., Poladian, L., Ahmed, K. A. & Liu, H. F., "Experimental Demonstration of Compression of Dispersed Optical Pulses By Reflection From Self-Chirped Optical-Fiber Bragg Gratings," *Optics Letters*, vol. 19, pp. 877-879, 1994.

25. Chung, J., Kikuchi, N. & Sasaki, S., "Generation of Transform-Limited Optical Pulses Using a Combination of a Gain-Switched Diode-Laser and a Semiconductor Optical Amplifier," *IEEE Photonics Technology Letters*, vol. 7, pp. 860-862, 1995.

26. Barry, L. P., Debeau, J. & Boittin, R., "Simple Technique to Improve the Spectral Quality of Gain- Switched Pulses From a DFB Laser," *Electronics Letters*, vol. 30, pp. 2143-2145, 1994.

27. Vonderweid, J. P., Passy, R. & Gisin, N., "Chirp and Feedback-Control in Semiconductor Pigtailed DFB Lasers Without Integrated Isolator," *Electronics Letters*, vol. 29, pp. 50-52, 1993.

28. Bouchoule, S., Lourtioz, J. M., Kazmierski, C. & Ougazzaden, A., "Transform-Limited Pulses From Low Chirp DFB Lasers With External Feedback," *Electronics Letters*, vol. 29, pp. 518-520, 1993.

29. Ahmed, K. A., Eggleton, B. J., Liu, H. F., Krug, P. A. & Ouellette, F., "Simultaneous Mode Selection and Pulse-Compression of Gain- Switched Pulses From a Fabry-Perot Laser Using a 40-Mm Chirped Optical-Fiber Grating," *IEEE Photonics Technology Letters*, vol. 7, pp. 158-160, 1995.

30. Chilla, J. L. A. & Martinez, O. E., "Direct Determination of the Amplitude and the Phase of Femtosecond Light-Pulses," *Optics Letters*, vol. 16, pp. 39-41, 1991.

31. Trebino, R. & Kane, D. J., "Using Phase Retrieval to Measure the Intensity and Phase of Ultrashort Pulses - Frequency-Resolved Optical Gating," *Journal of the Optical Society of America a-Optics Image Science and Vision*, vol. 10, pp. 1101-1111, 1993.

32. Kane, D. J. & Trebino, R., "Characterization of Arbitrary Femtosecond Pulses Using Frequency-Resolved Optical Gating," *IEEE Journal of Quantum Electronics*, vol. 29, pp. 571-579, 1993.

33. Reid, D. T., "Few cycle EM pulses," *Contemporary Physics*, vol. 40, pp. 193-204, 1999.

34. Reid, D. T., "Algorithm for complete and rapid retrieval of ultrashort pulse amplitude and phase from a sonogram," *IEEE Journal of Quantum Electronics*, vol. 35, pp. 1584-1589, 1999.

35. Kane, D. J., "Real-time measurement of ultrashort laser pulses using principal component generalized projections," *IEEE Journal of Selected Topics in Quantum Electronics*, vol. 4, pp. 278-284, 1998.

36. Reid, D. T., Thomsen, B. C., Dudley, J. M. & Harvey, J. D., "Sonogram characterisation of picosecond pulses at 1.5 mu m using waveguide two photon absorption," *Electronics Letters*, vol. 36, pp. 1141-1142, 2000.

37. Loza-Alvarez, P., Reid, D. T., Faller, P., Ebrahimzadeh, M. & Sibbett, W., "Simultaneous second-harmonic generation and femtosecond-pulse compression in aperiodically poled KTiOPO4 with a RbTiOAsO4- based optical parametric oscillator," *Journal of the Optical Society of America B-Optical Physics*, vol. 16, pp. 1553-1560, 1999.

Chapter 5.
Self-injection seeding of picosecond diode lasers.

5.1. Introduction.

As discussed in Chapter 3., the pulses from the gain-switched diode laser had a spectral bandwidth considerably broader than that of Fourier transform-limited pulses having the same duration. This excess bandwidth led to the conclusion that the pulses were frequency-chirped, a topic that was discussed in Chapter 4. There is considerable interest in reducing the time-bandwidth product of the pulses to that of the Fourier transform limit and there are two possible ways of achieving this: either by decreasing the spectral bandwidth or duration.

It has been demonstrated on numerous occasions that optical feedback into a diode laser may be either detrimental or advantageous. The effects of feedback may include coherence collapse,[1-4] accelerated ageing, and various effects on the spatial, spectral and temporal output.

Consider, as illustrated schematically in Figure 5.1.1., a gain-switched diode laser in an extended cavity terminated by a reflective surface at an arbitrary distance of L_{ext} from the output facet of the diode laser. A three-mirror coupled-cavity is thereby formed, comprising the two facets of the diode laser and the external reflector. There are two cavities of importance, the intrinsic diode laser cavity and that formed by the output facet and external reflector. If the exit facet of the diode laser chip was sufficiently well AR-coated then only one cavity would exist.

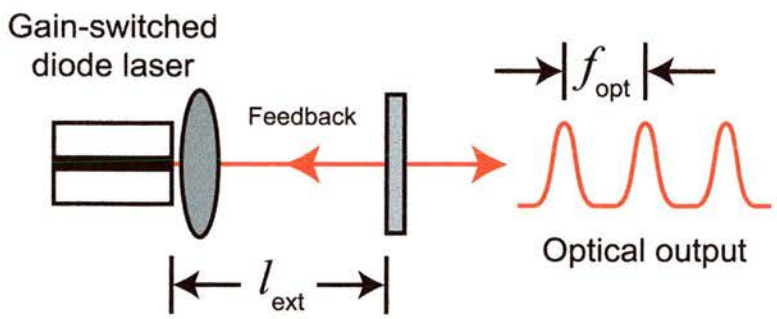

Figure 5.1.1. Basic configuration for optical feedback, consisting of a Fabry-Perot diode laser and a planar reflector.

As shown in Figure 5.1.1. the external-cavity formed by the external reflector has a frequency of $f_{ext} = c/2L_{ext}$, which is independent of the electrical modulation and resultant optical frequencies $f_{mod} = f_{opt}$. Although in Figure

5.1.1. a planar surface is assumed, schemes have been demonstrated utilising the wavelength specific feedback obtained from a diffraction grating.[5-15]

Normally a gain-switched pulse evolves from amplified spontaneous emission, but if optical feedback is present this can serve to assist one particular mode at the expense of the others. As a result of the optical injection, the assisted mode dominates the noise driven modes. Since the diode laser emission is responsible for the optical injection back into the device it is referred to as *self-injection seeding*.[5,16-33] An prerequisite for low-level $(\leq 4\%)$ self-injection seeding is that the optical injection must interact with the optical field within the diode laser during the evolution of a pulse.[18] (This is not the situation for high-level[26,34,35] optical feedback). Low-level self-injection seeding also requires that the roundtrip frequency of the external-cavity f_{ext} must be close to, and slightly greater than the electrical modulation frequency f_{mod} applied to the diode laser, or a harmonic thereof.[11,18]

Bouchoule and co-workers[11] discuss how, under the influence of optical feedback, the dynamics of diode laser operation are affected. (1) The laser emission typically occurs at wavelengths longer than the feedback wavelength. (2) For weak optical feedback the gain-switched pulse is temporally advanced compared with a solitary device. This is due to the optical injection driving the device more quickly into saturation, though this was not observed for high-level optical feedback. (3) Changing the modulation frequency is equivalent to adjusting the external-cavity length, in that both affect the arrival time of the feedback pulse. (4) Gain variations during the pulse emission result in a pulse duration that increases proportionally with the optical feedback intensity.

If a diffraction grating is used to terminate the external-cavity, then a spectrally selective optical feedback obtained can result in the injection seeding of a single longitudinal mode. From work carried out by other groups it is well understood that self-injection seeding of a laser diode may have a profound influence on the spectral output of that device.[5,7,13-15,30,36-40] Schell and co-workers[26,27] demonstrated how the pulse-to-pulse jitter of a gain-switched diode laser can be reduced through the use of self-injection seeding due to the deterministic nature of the optical feedback compared with the random spontaneous noise. In the

context of the study discussed in this chapter, it was desired that the spectral output of the gain-switched diode laser would be significantly reduced as has been achieved previously through the use of self-injection seeding.[10,24,30,31,33,41-47]

5.2. Optical feedback without spectral selectivity.

The simplest form of optical feedback is that derived from an uncoated planar glass surface placed at some arbitrary distance from the facet of a diode laser. The difference in refractive indices at the air-glass interface results in an approximately 4% reflection with the production of a three-mirror compound cavity. Optical feedback from uncoated air-glass surfaces is typically undesirable due to the effect it can have on the output wavelength of a diode laser. For example, the $980nm$ InGaAs/GaAs diode lasers discussed in this work were also used as the pump source for a solid-state laser based on Yb:YCOB that has an absorption at $976nm$ with a bandwidth of $2.3nm$.[48] If optical feedback into the pump diode laser occured, the resultant spectral jump, led to a reduction in the absorption in the Yb:YCOB crystal with the consequent lasing performance being severely compromised.

5.2.1. Low-level self-injection feedback.

Low-level feedback in the context of this study refers to the 4% reflection obtained from an uncoated glass surface. The optical feedback required for self-injection seeding was obtained through the use of an uncoated glass microscope slide as an external-cavity element. The necessary level of optical feedback was not surprising because coherent photon seeding (CPS)[49-55] has been observed in mode-locked solid-state lasers for optical feedback levels of $\ll 1\%$, although the mechanisms here are quite distinct.

As shown in Figure 5.2.1., the scheme for self-injection seeding of the gain-switched diode laser was simple in its implementation and consisted of the diode laser, a 30X collimating lens and an uncoated glass microscope slide that terminated the external-cavity. The entire glass slide assembly was mounted on a translation stage such that it could be moved through $25mm$ without adversely affecting the linear alignment of the system. The optimum facet to

slide distance, L_{ext}, was determined from $(f = c/2L_{ext})$ where f was either the cavity frequency, or the modulation frequency applied to the diode laser.

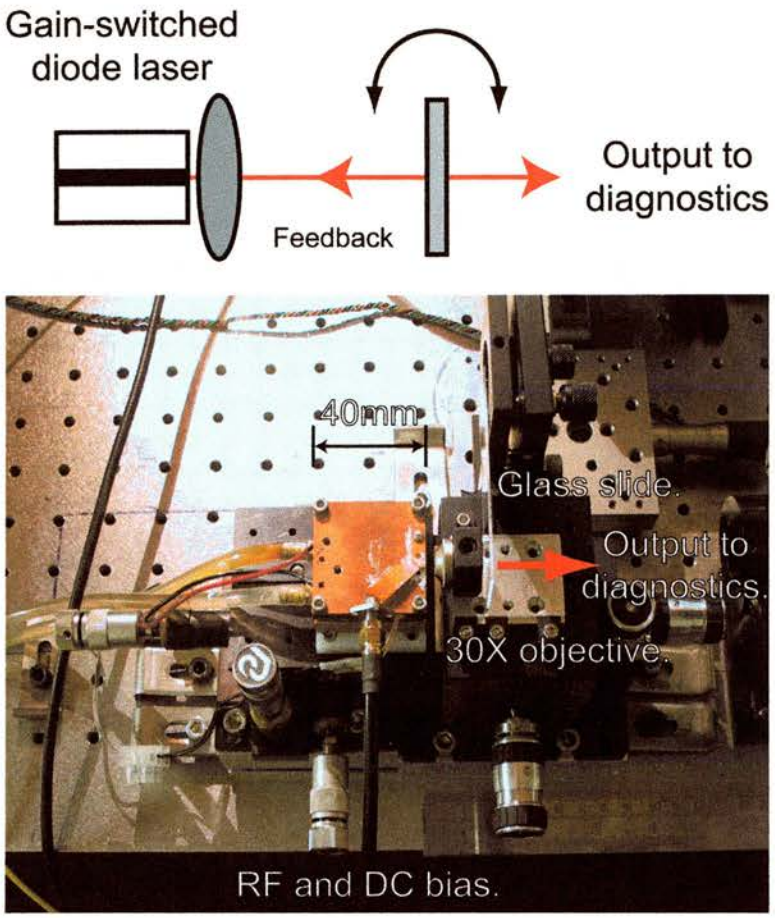

Figure 5.2.1. Optical scheme used for non-selective low-level self-injection optical feedback utilising an uncoated glass slide.

It seemed reasonable given the subject matter available in the literature that initial measurements should be performed with the glass-slide at a distance of $76mm$ from the diode laser facet. The resultant cavity length of $\sim 150mm$ would be the fundamental harmonic of the typical diode laser modulation frequency f_{opt} of $2.00GHz$. The use of a $25mm$ translation stage meant that the glass-slide could be positioned at a distance, L_{ext}, in the range 87 to $63mm$ from the laser diode facet. This range corresponded to an external-cavity round-trip frequency, f_{ext}, from 1.72 to $2.38GHz$.

It was important that the output of the diode laser be nearly collimated because it was required that the reflection from the surface of the glass-slide be imaged back through the collimating lens onto the diode laser facet. If the diode laser

were not collimated this re-imaging would not be optimal, thereby adversely affecting the self-injection seeding. Alignment was achieved by initially ensuring that the reflection was directed along the path of the laser emission. This rough alignment was verified by observing the reflected output illuminating the diode laser. By observing the spectrum on a real-time Rees Instruments spectrometer E202 precise alignment of the external-cavity was performed. When optical feedback was not present the emission was the characteristic broad spectrum, as shown in Figure 5.2.2. However, as the optical feedback provided by the uncoated glass slide started to influence the diode laser emission, several discrete longitudinal modes were observed. These longitudinal modes were subsequently reduced to one in optimum alignment. The output spectrum thus obtained was repeatable and extremely stable when compared with CW operation. It was observed that this alignment was more critical in the plane perpendicular to the junction than it was parallel to the plane of the junction. This is consistent with the fact that the junction is of the order of $\sim 10nm$ thick compared to $3\mu m$ wide.

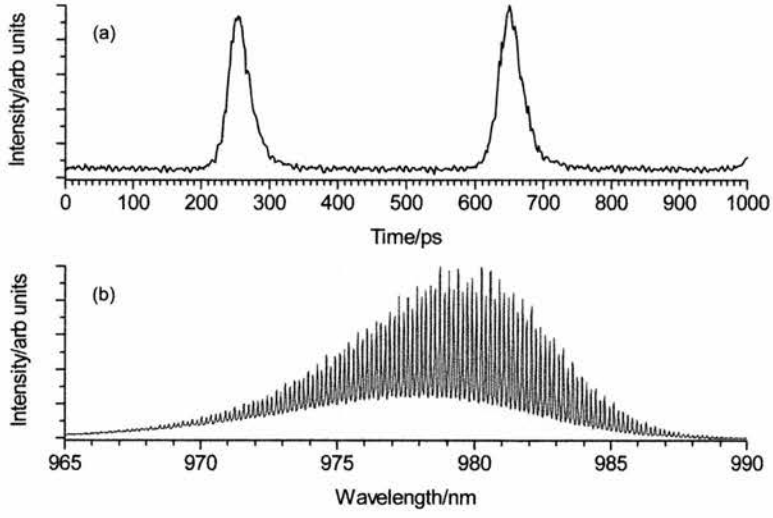

Figure 5.2.2. Temporal and spectral output from the gain-switched diode laser without optical feedback.

In order to determine whether Fabry-Perot filtering was responsible for the observed spectral bandwidth reduction, an experiment was also performed in which an uncoated thick 3^o glass wedge replaced the glass slide and where the optical feedback to the diode laser was obtained from the front face of the wedge. Given that the spectral narrowing observed with the wedge was

identical to that obtained with the glass slide, this confirmed that any Fabry-Perot etalon properties exhibited by the glass slide were not essential for the spectral narrowing and this effect was induced entirely by self-injection optical feedback.

The small amount of feedback from the glass slide, of the order of 4%, was sufficient to have a profound affect on the spectral bandwidth, reducing its value from $\sim 11nm$ to $\sim 0.05nm$. Figures 5.2.2b. and 5.2.3b. illustrate, on the same wavelength scale, the comparative reduction in the spectral bandwidth for the case of no optical feedback and self-injection optical feedback. This reduction in spectral bandwidth yielded a similar, $\sim 220X$, improvement in the time-bandwidth product. There was only a slight reduction in the average output power, decreasing from $68mW$ to approximately $65mW$, a reduction of $\sim 7\%$. There was a slight increase in the pulse duration from $31ps$ to $\sim 36ps$, although the pulse shape remained largely unchanged.

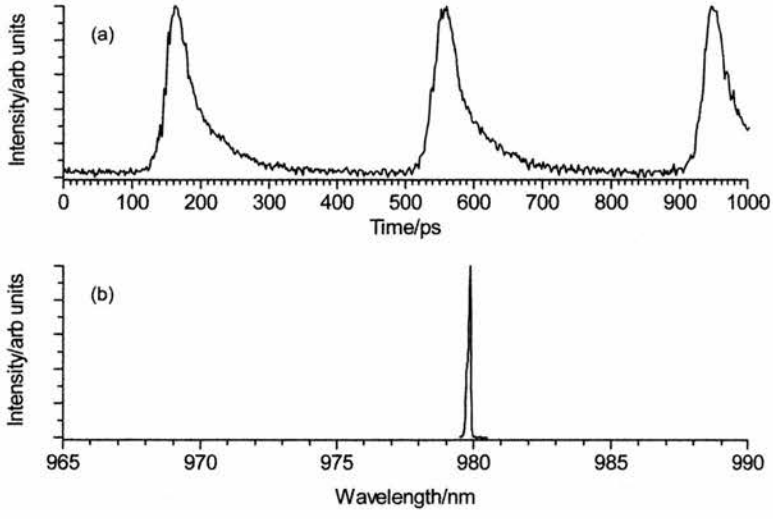

Figure 5.2.3. Temporal and spectral output from the gain-switched diode laser with optical feedback.

There are two significant differences between the results discussed here and those reported earlier for the well-known technique of self-seeding in gain-switched lasers.[8] The effect of spectral narrowing as described above is different from the standard self-seeding techniques where the strong spectral selectivity of the external reflector is crucial in achieving single-frequency operation; consider for example a distributed Bragg reflector (DBR) diode laser. With standard self-seeding, strong spectral selectivity is always introduced

either explicitly,[27] by using a selective external reflector, or implicitly,[56] by using a dispersive fibre in the external-cavity and thus making the crucial timing of the seeding pulse spectrally dependent. Also, in contrast with the referenced published work pertaining to self-injection seeding, spectral narrowing was only observed in this case for *non-resonant* operation. That is, when the round-trip frequency of the external-cavity f_{ext} was significantly detuned from the laser modulation frequency f_{opt}. The external-cavity had no discernible effect on the output spectrum of the gain-switched diode laser for $f_{mod} = f_{ext} \pm 200MHz$. This was also true within approximately the same frequency range around other even harmonics of f_{ext}.

The spectral narrowing due to self-injection seeding had a negligible effect on the temporal and spatial characteristics of the laser output. The significant reduction in the spectral bandwidth was sufficient such that the time-bandwidth product was decreased from 103 by $220X$ to 0.44 resulting in near Fourier-transform limited pulses, strongly suggesting single-frequency operation. The resonance condition observed when an external-cavity length was such that $f_{ext} = f_{opt}$ required that $L_{ext} = 74mm$ be adjusted to ensure the resonance frequency $f_{ext} \neq Nf_{opt}$, where N is an even harmonic number. Since a compact system was desired the external cavities of several metres reported previously[11,18,27,56] were not acceptable. It was therefore arranged that the external-cavity would be made as small as engineering constraints would allow, whilst allowing for free angular adjustment of the glass-slide. The resultant scheme illustrated in Figure 5.2.1. had a cavity length of $22mm$ and a fundamental frequency of $6.81GHz$. Such a cavity frequency placed the second and fourth harmonics at $3.40GHz$ and $1.70GHz$ respectively, clear of the typical modulation frequencies used. As anticipated, spectral narrowing was observed for all modulation frequencies between $1.90GHz$ and $2.70GHz$. An interesting observation regarding the short external-cavity was that when compared with the longer cavities the spectrum was more stable and easier to tune. The use of such a short external-cavity demonstrated that operating at large sub-harmonics of the fundamental cavity frequency does not adversely affect the

output, indeed quite the contrary, because larger sub-harmonics increase the frequency spacing between the neighbouring resonances.

It was observed that for any given external-cavity length the spectral output of the self-injection seeded gain-switched diode laser could be tuned by two entirely independent mechanisms. The first technique was to adjust the frequency of the modulation applied to the gain-switched diode laser. This technique was far from ideal for a number of reasons. First, the output would not tune smoothly with modulation frequency. This erratic behaviour is shown in Figure 5.2.3. for three external-cavity lengths with several different modulation frequencies. Although the tuning is not continuous, the wavelength of the output was seen to bunch up around several regions. A second consequence of modulation frequency tuning was, as discussed earlier, the existence of frequency regions for any given cavity length where no spectral bandwidth reduction was evident. It should however be noted that modulation frequency tuning was a useful technique through which certain wavelengths could readily be obtained, although it might require some "hunting".

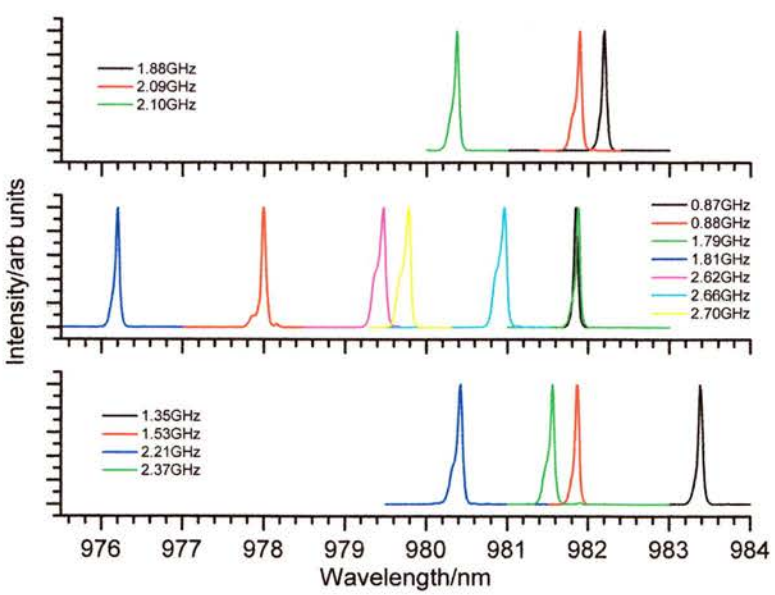

Figure 5.2.4. Erratic spectral behaviour of the self-injection seeded gain-switched diode laser for changes in the modulation frequency.

A second methodology through which the spectral output of the self-injection seeded diode laser could be tuned was preformed with a constant modulation frequency. Therefore the pseudo-random spectral jumps caused by changes in the modulation frequency were not an issue. A periodic step-tuning over $6nm$

was achieved by introducing a small variation of the angle of the glass slide in either direction. The spectral output did not tune continuously between the two extremes of glass slide angle but instead demonstrated a periodicity within a small wavelength region.

Illustrated in Figure 5.2.5. is the centre wavelength versus glass slide angle. Beyond the two extremes shown in Figure 5.2.5., the angle of the glass slide was such that optical feedback was lost and the distinctive broad gain-switched spectrum was observed.

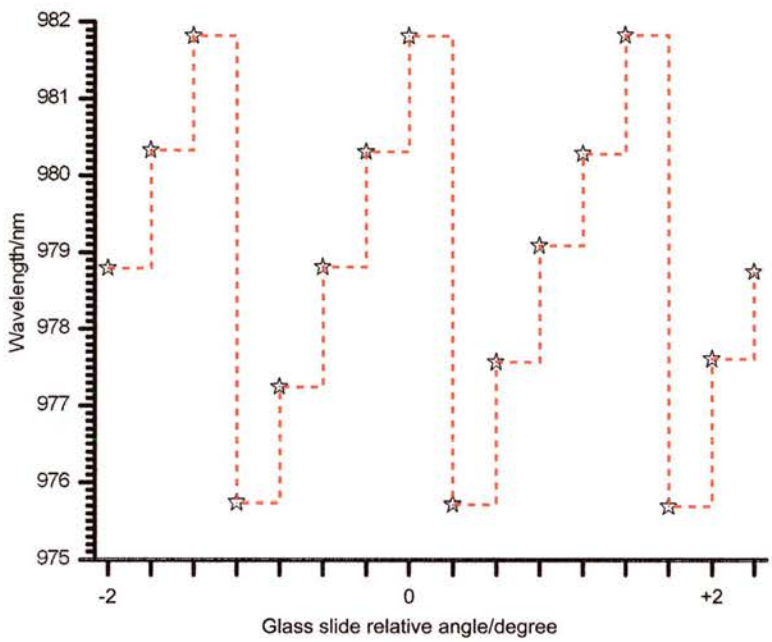

Figure 5.2.5. Glass slide angle tuning of a diode laser output operated under non-resonant self-injection optical feedback.

Given that in the absence of self-injection optical feedback, the spectral bandwidth increased with DC bias, the potential spectral range over which the output can be tuned was also increased. Although this tuning effect was observed for any external-cavity length, the output spectra demonstrated the most stability for the shorter cavities. A similar tunable operation was previously reported in a more complex laser system using coherent photon seeding in actively mode-locked laser diodes.[57-59]

5.2.2. Modelling of low-level self-injection feedback.

The external-cavity length L_{ext} in the work discussed here is several (at least 2-3) orders of magnitude smaller (and the external-cavity round-trip frequency

$f_{ext} = c/2L_{ext}$ therefore greater by the same factor) than those typically used in the cavity configurations described in references.[8,11,27,56] It was shown[11,27] that a timing detuning ΔT between the seeding and lasing pulses, within a certain window of the order of several tens of picoseconds, is required for successful self-seeding. The frequency detuning Δf corresponding to this timing detuning may be estimated as:

$$\Delta f = f_{mod} - N f_{ext} \approx f_{mod} f_{ext} \Delta T \qquad 5.1$$

where $N = (f_{mod}/f_{ext})$ is the modulation harmonic number. With, say, $\Delta T = 50 ps$ and $f_{mod} = f_{ext} = 2GHz$, we get $\Delta f = 200MHz$, consistent with the non-resonant nature of operation in our short external-cavity.

Also, as the optical path difference between the lengths of the laser and external-cavity is reduced, the spectral selectivity in the compound cavity formed by the external and intrinsic (facet) reflectors is of increased importance. Indeed, the output loss of the *k*-th (intrinsic) laser cavity mode in the presence of the short external-cavity terminated by a weak reflector (with an effective intensity reflectance $R_{ext} \ll 1$) may be estimated as:[60]

$$a_{ck} \approx a_0 + \Delta a_{ck} \qquad 5.2$$

where $a_0 = \frac{1}{2L}\log\frac{1}{R_1 R_2} + a_i$ is the cavity loss without the presence of any external reflector. The first term of is the outcoupling loss, with R_1 and R_2 the higher and lower reflectances respectively, L the intrinsic laser cavity length, and a_i is the dissipative loss. This intrinsic loss is independent of the mode number *k*. The spectral variation was introduced by the presence of the external reflector, described by the second term in Equation 5.2:

$$\Delta a_{ck} = -\frac{1-R_2}{L\sqrt{R_2}}\sqrt{R_{ext}}\cos\left(\frac{2\pi k L_{ext}}{nL} + \psi\right) = -\frac{1-R_2}{L\sqrt{R_2}}\sqrt{R_{ext}}\cos\left(\frac{2\pi k}{N} + \psi\right) \qquad 5.3$$

The cosine term describes the strength of coupling to the external-cavity. If L_{ext}/nL is not an integer, then Equation 5.3 describes spectral selectivity with a period of:

$$N = 1/\left\{\frac{L_{ext}}{nL}\right\} \qquad 5.4$$

where L and L_{ext} are of the order used in the experiment, typically $N \sim 10$, as in seen in Figure 5.2.6. This is consistent with the mode hopping that was observed experimentally (the vertical step magnitude in Figure 5.2.5.).

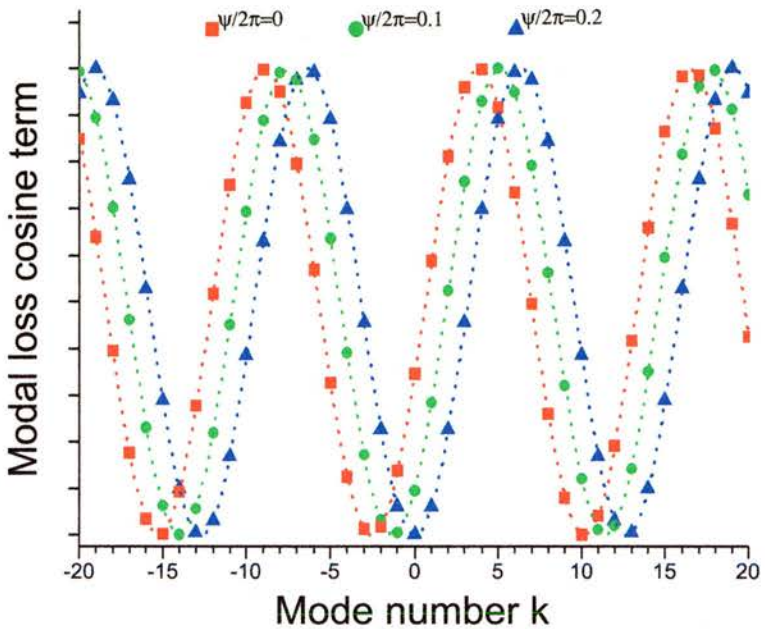

Figure 5.2.6. Calculated spectral variation of the cavity output losses in a weak cavity.

The phase ψ in Equation 5.3 is

$$\psi = \frac{2L_{ext}\omega_0}{c} \qquad 5.5$$

where ω_0 is the reference optical frequency, usually taken to be close to the frequency of the mode with *k*=0). The phase changes strongly with sub-micron variations in the external reflector position, which can occur when the reflector angle is adjusted. As seen from Figure 5.2.6., variations of the phase may result in the global spectral minimum in threshold losses shifting from one local minimum to another, implying a possibility of step tuning.

Equations 5.2, 5.3 and 5.4 are only valid for very small R_{ext}. Experimentally, spectral narrowing and mode hopping due to external cavity adjustments were observed during CW operation, but were plagued with poor stability and repeatability in stark contrast to the robust tuning of modulated lasers. This

implies that the spectral selectivity mechanism is significantly modified, and benefits from, modulation.

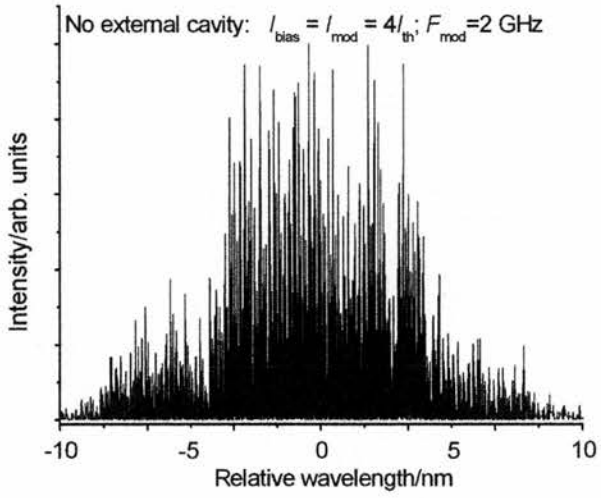

Figure 5.2.7. Simulated spectral characteristics for a gain switched diode laser without an external cavity. Geometrical parameters as in the experiment.

To perform a more quantitative comparison with the experimental results, numerical simulations were performed using a distributed time-domain model (DTDM) adapted to compound cavities.[61]

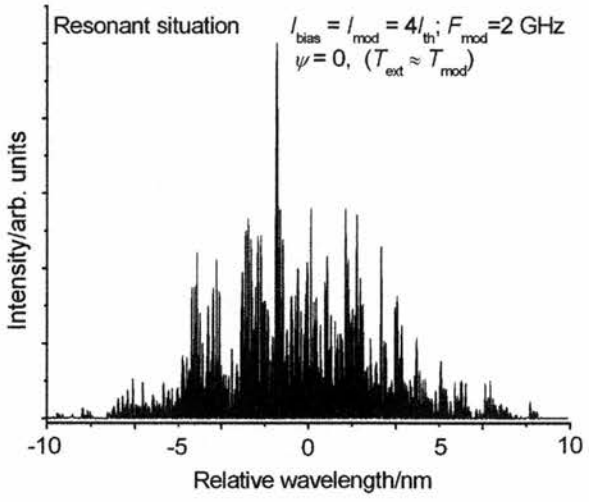

Figure 5.2.8. Simulated spectral characteristics for an external-cavity gain-switched diode laser under resonant conditions.

The model solves one-dimensional propagation equations for slow amplitudes of left and right propagating light waves, coupled with co-ordinate-dependent

rate equations for carrier density, and takes into account effects such as self-phase modulation, gain and group velocity dispersion, shift of gain peak with carrier density, fast gain suppression, and spontaneous noise.

Lasing spectra were calculated by a fast Fourier transform of the resulting temporal profiles, after discarding the initial transient following turn on. The results are shown in Figures 5.2.6. through 5.2.10.

Under CW operation, the simulated lasing spectra are narrow, as are the experimentally observed spectra, but reliable single-frequency operation was not obtained either with or without the external reflector.

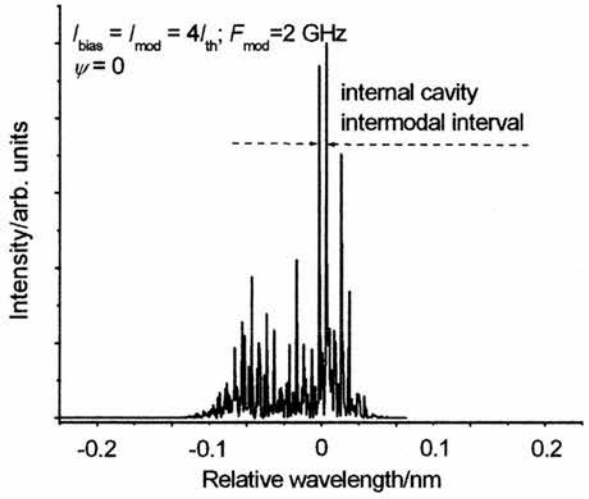

Figure 5.2.9. Simulated spectral characteristics for an external-cavity gain-switched diode laser under non-resonant conditions.

With large-signal modulation applied to a solitary laser to achieve gain-switching, the experimentally observed broad spectrum was reproduced theoretically (Figure 5.2.7.). Also in agreement with the experiment, no spectral narrowing was seen in the external-cavity configuration under the conditions of resonant modulation (Figure 5.2.8.).

Under non-resonant modulation conditions with $R_{ext} \sim 0.001$, and consistent with the experiment, the simulations predicted a dramatic spectral narrowing (Figure 5.2.9.). This was in good agreement with the experimentally observed behaviour.

As was observed experimentally, spectral narrowing was accompanied by a $30-40\%$ increase in the FWHM pulse duration. The seeding pulse formed a precursor for each of the lasing pulses in the simulated pulse sequence, and the expected position of the lasing pulse without seeding appears as a shoulder following the pulse maximum (Figure 5.2.10.).

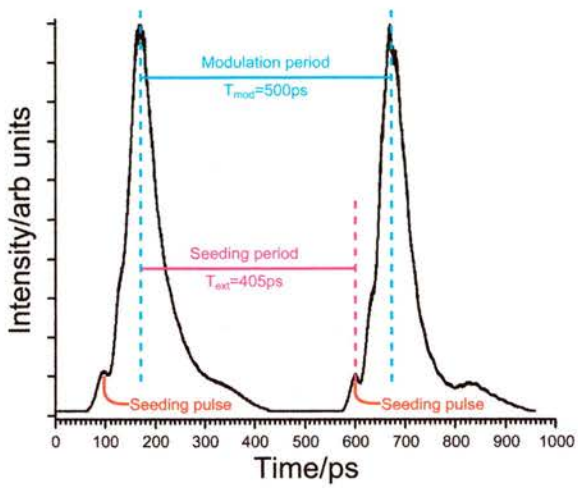

Figure 5.2.10. Simulated optical pulses from an external-cavity gain-switched diode laser under non-resonant conditions.

The simulations show, in qualitative agreement with the experiment, that mode hopping by several (4 to 12) intrinsic cavity modes may occur with variations in either f_{mod}, L_{ext} (of the order of $10-20\mu m$), or the phase of the external mirror reflectance (the latter modelling sub-wavelength variations in L_{ext}, as in Figure 5.2.9. The detailed shape of the step-tuning curve (Figure 5.2.4.) was, unfortunately, not reproduced in the simulations.

5.2.3. High-level self-injection seeding.

As discussed in the previous section, self-injection seeding provided by an uncoated air-glass interface was considered low-level $(\leq 4\%)$. In contrast, the study discussed in this section is concerned with what is described as high-level self-injection seeding $(\leq 25\%)$.

The scheme for high-level non-selective self-injection seeding was unlike that for its low-level counterpart, where the glass-slide formed an *inline* external reflector, which was *on axis* with the diode laser emission. Instead, the high-level scheme (Figure 5.2.11.) used a $50mm$ diameter, $1mm$ thick AR-coated

$50:50$ beam splitter after the 30X AR-coated aspheric objective lens. Nonetheless, in common with the low-level scheme, the output was along the diode laser axis. After alignment to ensure that the reflected portion from the beam splitter was both parallel to the optical bench and perpendicular to the diode laser emission axis, a silver coated mirror held in a gimbal mount was positioned at a similar distance from the beam splitter as the diode laser facet, approximately $125mm$. (Total cavity length $\sim 250mm$.)

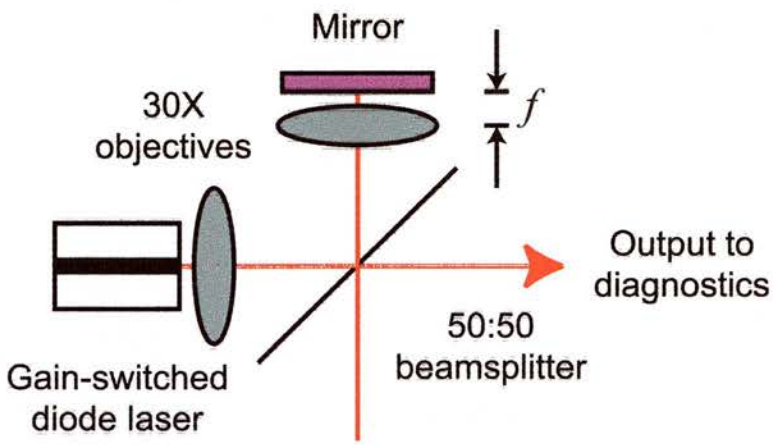

Figure 5.2.11. High-level self-injection optical feedback scheme utilising one mirror.

In common with the low-level optical feedback provided by the glass-slide, alignment then involved adjustment of the mirror until optical feedback was observed as initially characterised by instability in the spectral output before a stable reduction in the bandwidth. With the mirror aligned it was locked in position. A second AR coated 30X aspheric objective was added and adjusted such that there was a distance of approximately f between the lens and mirror surface, where the focal distance $f = 5.2mm$. The second objective was utilised to ensure that the optical feedback of $\leq 25\%$ was focussed back on to the diode laser facet. This was not the case in the low-level scheme where the reflection was free to diverge. That output perpendicular to the mirror surface was useful for two reasons; first, for alignment of the optical feedback to the diode laser, and second, to check that the second lens was at a distance of approximately one focal length from the mirror surface. When this was the case, the reflection from the mirror would be re-collimated after transmission through the beam splitter. Henceforth, as depicted in Figure 5.2.11., the feedback path through the beam splitter caused by the reflection from the silver mirror will be called the

feedback arm. The position of the objective lens was adjusted in the 2-dimensional plane parallel to the mirror surface such that self-injection seeding was re-established. Adjustment of the lens perpendicular to the mirror surface effected the re-collimation of the *feedback arm* and hence the re imaging back onto the diode laser facet. Following optimal adjustment of the objective lens its position was locked. Although not marked in the Figure 5.2.11., there existed a line of symmetry perpendicular to the surface of the beam splitter.

The optical output power of $\sim 70mW$ after the first 30X objective lens for a DC bias of $100mA$ inferred a maximum optical feedback power of $\sim 17.5mW$, significantly greater than the $\sim 2.8mW$ that was obtained with the glass-slide. (It should be noted that due to divergence following reflection from the glass-slide surface this level is probably over-estimated.) The optical feedback power could be monitored from the *feedback arm*, where it was measured to be $17mW$. One consequence of separating the optical feedback from the output path was that it became possible to stop the self-injection seeding simply by blocking the *feedback arm*, something that was not possible when the glass-slide was used as an external reflector.

Figure 5.2.12. illustrates the temporal and spectral output from the gain-switched diode laser with no optical feedback, where the pulse duration and spectral bandwidth were $\sim 30ps$ and $11nm$ respectively.

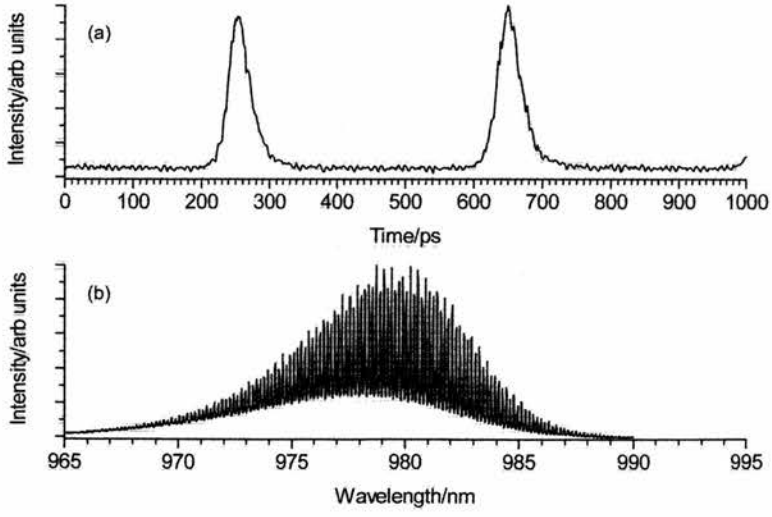

Figure 5.2.12. Temporal and spectral output from the gain-switched diode laser without optical feedback.

Low-level self-injection seeding resulted in the spectral bandwidth being reduced to $< 0.1nm$ (Figure 5.2.3b.), with only a slight increase in the pulse duration to $\sim 40ps$ (Figure 5.2.3a.). However, as Figure 5.3.13. illustrates for high-level self-injection seeding the spectral bandwidth was reduced to $0.11nm$ while there was an increase in the pulse duration to $\sim 60ps$. These observations are in line with those of Bouchoule and co-workers.[11]

An interesting consequence of the high-level self-injection seeding was the $15nm$ red shift to $995nm$ when optical feedback was present (Figure 5.2.13.). Again this is in agreement with the observation of Bouchoule and co-workers.[11]

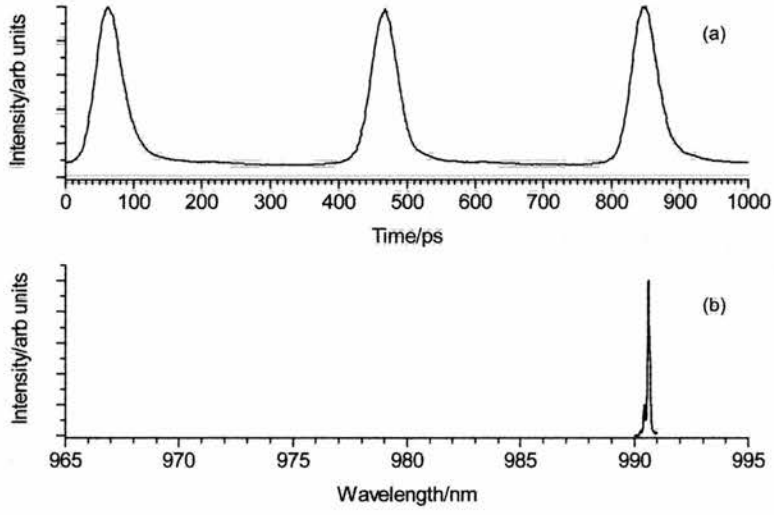

Figure 5.2.13. Temporal and spectral output from the gain-switched diode laser with optical feedback.

The emission wavelength could be tuned by very fine focussing adjustment of the second 30X objective but the spectral output exhibited the greatest stability around $990nm$. Also, the emission wavelength was, for the most part, unaffected by small angular adjustment of the silver mirror. The long-term spectral stability was greatly improved over the low-level scheme, which must be partly arbitrated to the improved mounts that were used. However, the low-level scheme suffers less of an optical power penalty and lends itself very well to miniaturisation, something that is currently being exploited.

5.3. Spectrally selective optical feedback.

It is well documented in the literature that a diffraction grating, when used as an external reflector, can have a major influence on the spectral characteristics of a diode laser, be it CW[5-7] or pulsed.[8-15] Also, wavelength tuning has been demonstrated, with up to 88 nm being obtained from specially designed multi-quantum well laser structures.[62] Dual-wavelength operation has also been achieved for mode-locked laser diodes with different configurations[63] as well as for gain-switched diode lasers.[43]

5.3.1. Single grating.

Figure 5.3.1. is an illustration of the scheme based on non-resonant self-injection seeding investigated for single wavelength selective operation. Based on the configuration shown in Figure 5.3.1., the mirror and aspheric objective were replaced with a diffraction grating having 1600 lines/mm. The small amount of optical feedback obtained from the grating first-order diffraction was sufficient to induce non-resonant self-injection seeding and its characteristic reduction of the spectral bandwidth. The output from the resultant external-cavity diode laser was inline with the device.

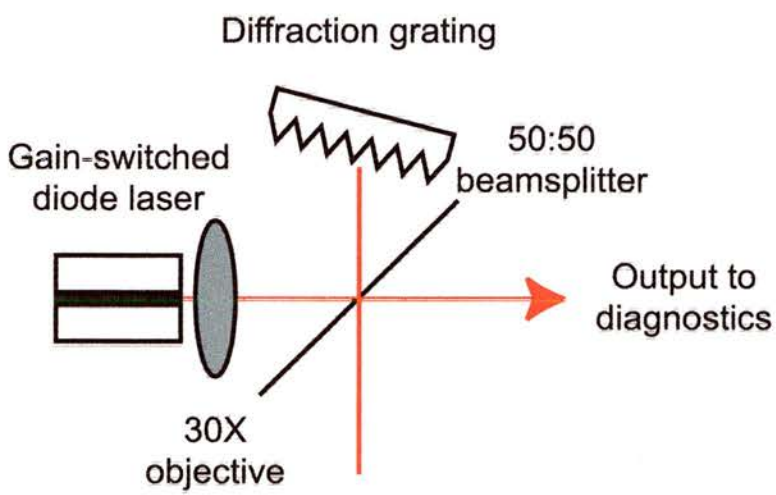

Figure 5.3.1. Self-injection optical feedback scheme utilising one spectrally selective element.

In common with the previous arrangements utilising non-resonant self-injection seeding, optical feedback resulted in a considerable reduction in the spectral bandwidth of the pulses obtained from the gain-switched diode laser. Figure

5.3.2. shows the spectral (a) and temporal (b) output profiles both with (blue line) and without (red line) the presence of optical feedback. The relative intensities of the two spectral profiles are directly comparable, clearly demonstrating the reduction in the spectral bandwidth from $\sim 10nm$ to $\sim 0.8nm$.

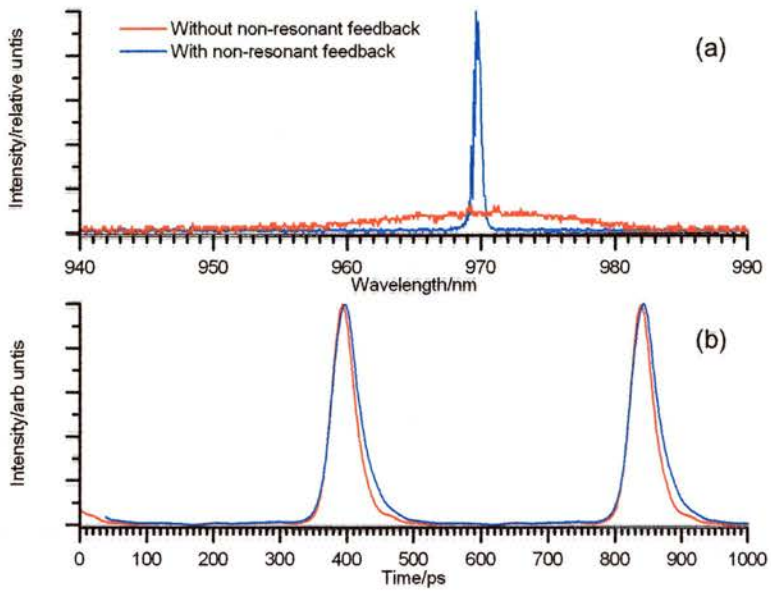

Figure 5.3.2. Temporal and spectral output from a gain-switched diode laser when self-injection seeded by a diffraction grating.

As for the other schemes where non-resonant self-injection seeding was present, there was a slight increase in the pulse duration from $\sim 30ps$ to $39ps$.

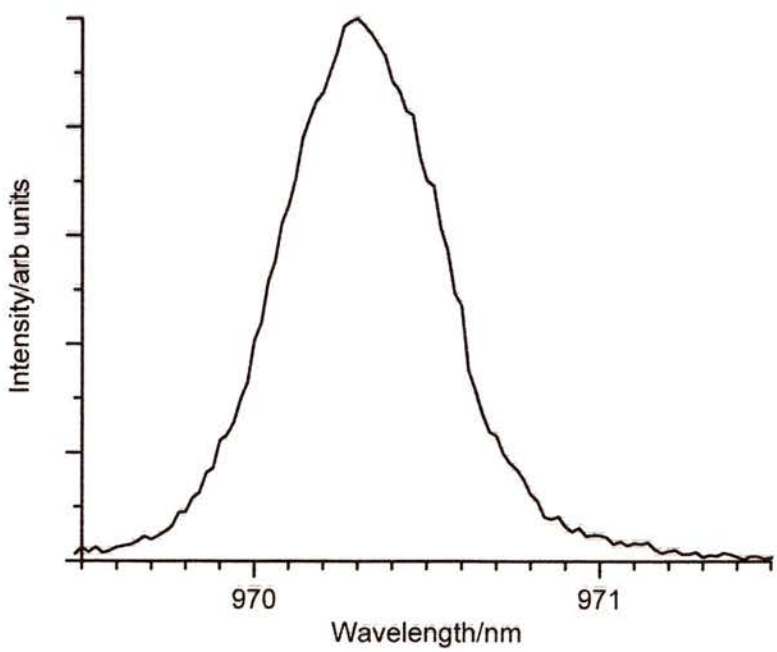

Figure 5.3.3. Spectral output from the injection seeded gain-switched diode laser at $200mA$.

This slight increase in the pulse duration when compared with that obtained when a mirror was used, can be attributed to the small fraction of the diode laser optical output power available in the first-order diffraction. The average and peak output powers, with optimal feedback present, for a DC bias of $100mA$ were $\sim 50mW$ and $625mW$ respectively. When the DC bias was increased to, $200mA$ the output powers increased to $102mW$ and $580mW$. The pulse durations became $88ps$ and $47ps$, with and without optical feedback respectively.

There was only a slight increase in the spectral bandwidth to $0.54nm$ (Figure 5.3.3.) which was notable considering the bandwidth of the isolated gain-switched diode laser at such a bias current was $\sim 25.5nm$ (Figure 3.3.6.).

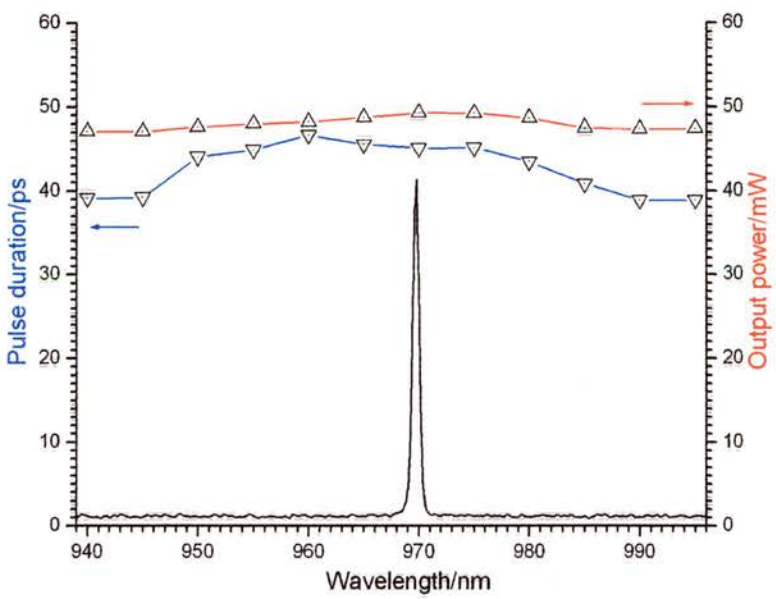

Figure 5.3.4. Pulse duration (blue) and output power (red) wavelength dependence of the injection-seeded diode laser, and a typical spectrum.

In contrast to those schemes not utilising wavelength selective optical feedback, the spectral output from the self-injection seeded gain-switched diode laser was smoothly tunable. Tuning was achieved by varying the angle of the diffraction grating in the plane parallel to the diode laser junction. When the configuration was optimised for maximum tuning capability, the spectral output was smoothly tunable over a range of $70nm$, from 935 to $1005nm$ with little variation in the output characteristics (Figure 5.3.4.). At either extreme of the spectral tuning range, the angle of the diffraction grating was such that optical feedback to the diode laser was lost and the output spectrum reverted back to that typical of a

solitary gain-switched device. Figure 5.3.4. represents a typical spectrum in the middle of the tuning range, along with the pulse duration and output power at a constant DC bias of $100mA$.

The optimum pulse duration and output power from the single wavelength external-cavity diode laser were $45ps$ and $49mW$ respectively and, as Figure 5.3.4. illustrates, their values remained consistent, within 15%, over the range where non-resonant self-injection seeding was observed.

5.3.2. Dual gratings.

As Figure 5.3.5. illustrates, a second diffraction grating identical to the first, was added to the scheme of Figure 5.3.1. The configuration was arranged such that there existed a line-of-symmetry parallel to the surface of the beam splitter, resulting in the use of the ± 1 diffraction orders. One diffraction grating was mounted on a $25mm$ translation stage such that the two cavity lengths could be varied with respect to one another.

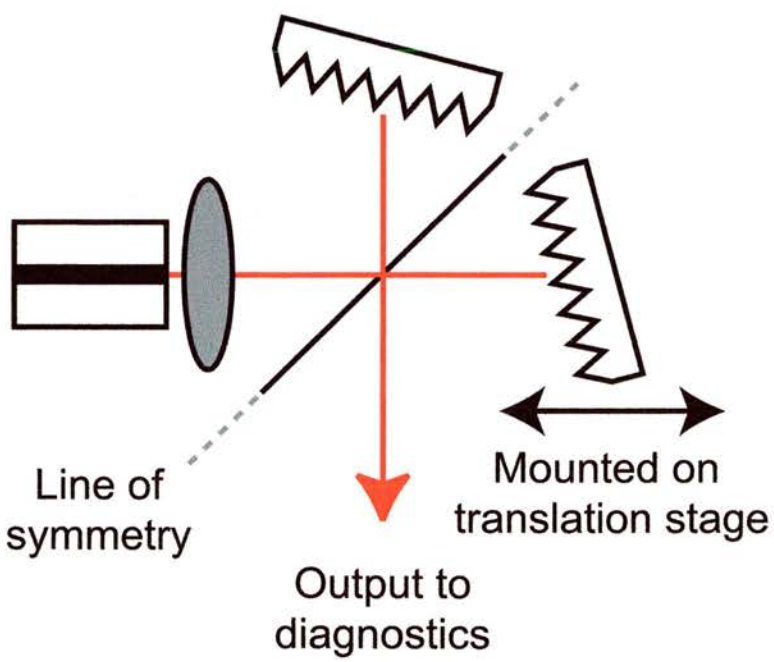

Figure 5.3.5. Symmetrical self-injection optical feedback scheme utilising two spectrally selective elements.

This was of importance due to the narrow diode laser modulation frequency range over which non-resonant self-injection seeding was observed. As a consequence of this narrow frequency range, if the two cavity lengths were too dissimilar there was the distinct possibility that one of the cavity frequencies

may coincide with a harmonic, and as a result of which stable dual wavelength operation could not be obtained.

By blocking either of the optical feedback arms, the spectral and temporal output of the gain-switched diode laser reverted to that of single diffraction grating operation as illustrated in Figure 5.3.1. The emission wavelengths determined by the two optical feedback arms were independently and continuously variable by adjusting the angle of the individual diffraction gratings in the plane parallel to the diode laser junction. The maximum wavelength separation between the emissions resulting from the two independent optical feedback arms was $\sim 53nm$. Figure 5.3.6. illustrates three different longitudinal mode separations that could be readily obtained up to a maximum separation of $53nm$.

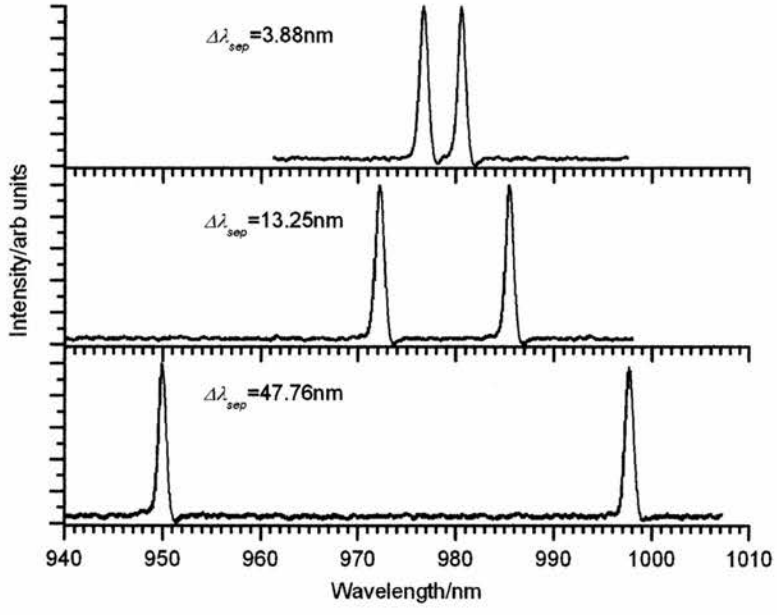

Figure 5.3.6. Various longitudinal mode separations for the dual-wavelength self-injection seeded diode laser.

By adjusting the angle of either diffraction grating (typically that mounted on the translation stage) in the plane perpendicular to the diode laser junction, the relative intensities of the two spectral outputs could be varied, to the greater part independently. This was of use to balance the output.

It is believed that the separation for dual wavelength operation was less than the tunable range observed for single wavelength operation due to laser gain being unable to support simultaneously the two extreme wavelengths.

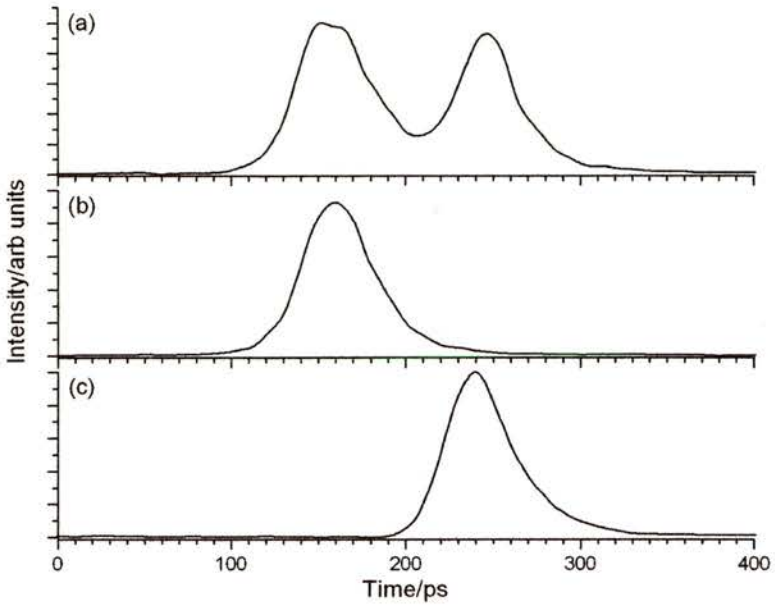

Figure 5.3.7. Temporal output from the non-resonantly self-injection seeded diode laser with (a) feedback from both arm and (b)(c) feedback from one arm.

Not only was a dual spectral output observed with the dual diffraction grating configuration of Figure 5.3.5., but for a limited range of modulation frequencies and grating separations a dual temporal output resulted. The dual temporal output was less stable than its spectral counterpart and depended more heavily on the operational parameters.

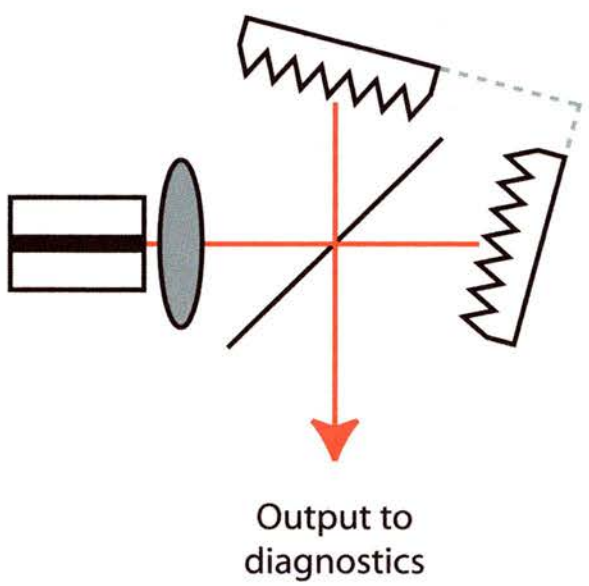

Figure 5.3.8. Asymmetrical self-injection optical feedback scheme utilising two spectrally selective elements.

Temporal separation of the two pulses depended on the linear position of the diffraction gratings relative to each other. Figure 5.3.7. illustrates a dual-

temporal output from the non-resonant self-injection seeded diode laser. It should be noted that a dual temporal output could only be obtained for modulation frequencies that satisfied the non-resonant conditions for both arms simultaneously, including harmonics. The corresponding emission wavelengths for the individual temporal outputs, determined by the diffraction gratings, were independently and continuously variable by adjusting the angle of the individual gratings.

An experimental scheme was tested which made use of the $+1$ diffraction order from both gratings (Figure 5.3.8.) but the performance was inferior to that obtained with the ± 1 diffraction orders (Figure 5.3.1.).

5.4. Conclusions.

Self-injection seeding of a picosecond gain-switched diode laser has been discussed along with the resultant reduction in the spectral bandwidth obtained from such a source. The effect of terminating an external-cavity with either an uncoated glass-slide or conventional diffraction grating(s) was investigated.

Use of a glass-slide as an external reflector offered a scheme that was extremely compact and simple in it implementation. The spectral bandwidth of the gain-switched diode laser was reduced from $11nm$ to $0.05nm$, a $220X$ improvement. There was a negligible effect on the output power of the device and only a slight increase in the pulse duration. It was demonstrated that tuning was possible simply by adjusting the angle of the glass-slide. A theoretical study was performed which demonstrated good agreement with the experimental results reproducing the observed effects.

The glass-slide was subsequently replaced with a $50:50$ beam splitter and silver coated planar mirror. With this arrangement an extremely stable spectral output was observed.

When the mirror was replaced with a single diffraction grating the spectral bandwidth reduction was accompanied with an output that was continuously and smoothly tunable over a range of $70nm$. The addition of a second grating resulted in two outputs that were independently tunable, with spectral separations of between $3.5nm$ and $53nm$ being demonstrated. A dual temporal

output was also observed, the separation between the two pulses being easily adjustable by varying the diffraction grating separation.

All of the aforementioned configurations resulted in the generation of optical pulses with near Fourier transform-limited durations. Self-injection seeding, and its accompanying spectral reduction, would be of significant use in those applications where narrow spectral bandwidths, and the possibility of a tunable output are necessary.

One such example where self-injection seeding was successfully utilised is discussed in Chapter 7. Efficient second harmonic generation was obtained from a nonlinear waveguide crystal incorporating a Bragg section for optical feedback at the fundamental wavelength, thereby effecting a spectral bandwidth reduction of the picosecond optical pulses obtained from the gain-switched diode laser.

5.5. Future Work.

Work is on going to further reduce the footprint and long-term spectral stability of the schemes. Consideration is also being given as to how the tunable range from the gratings configurations might be increased.

5.6. References.

1. Hohl, A. & Gavrielides, A., "Experimental control of a chaotic semiconductor laser," *Optics Letters*, vol. 23, pp. 1606-1608, 1998.
2. Fukuchi, S., Ye, S. Y. & Ohtsubo, J., "Relaxation oscillation enhancement and coherence collapse in semiconductor lasers with optical feedback," *Optical Review*, vol. 6, pp. 365-371, 1999.
3. Lawrence, J. S. & Kane, D. M., "Injection locking suppression of coherence collapse in a diode laser with optical feedback," *Optics Communications*, vol. 167, pp. 273-282, 1999.
4. Ohtsubo, J., "Feedback induced instability and chaos in semiconductor lasers and their applications," *Optical Review*, vol. 6, pp. 1-15, 1999.
5. Goldberg, L., Taylor, H. F., Dandridge, A., Weller, J. F. & Miles, R. O., "Spectral Characteristics of Semiconductor-Lasers With Optical Feedback," *IEEE Journal of Quantum Electronics*, vol. 18, pp. 555-564, 1982.
6. Andrews, J. R., "Electronically Tunable Single-Mode External-Cavity Diode-Laser," *Optics Letters*, vol. 16, pp. 732-734, 1991.
7. Harvey, K. C. & Myatt, C. J., "External-Cavity Diode-Laser Using a Grazing-Incidence Diffraction Grating," *Optics Letters*, vol. 16, pp. 910-912, 1991.
8. Lundqvist, S., Andersson, T. & Eng, S. T., "Generation of Tunable Single-Mode Picosecond Pulses From an AlGaAs Semiconductor-Laser With Grating Feedback," *Applied Physics Letters*, vol. 43, pp. 715-717, 1983.
9. Ahmed, Z., Zhai, L., Lowery, A. J., Onodera, N. & Tucker, R. S., "Locking Bandwidth of Actively Mode-Locked Semiconductor-Lasers," *IEEE Journal of Quantum Electronics*, vol. 29, pp. 1714-1721, 1993.
10. Barry, L. P., Odowd, R. F., Debau, J. & Boittin, R., "Tunable Transform-Limited Pulse Generation Using Self-Injection Locking of an Fp Laser," *IEEE Photonics Technology Letters*, vol. 5, pp. 1132-1134, 1993.
11. Bouchoule, S., Stelmakh, N., Cavelier, M. & Lourtioz, J. M., "Highly Attenuating External-Cavity For Picosecond-Tunable Pulse Generation From Gain Q-Switched Laser-Diodes," *IEEE Journal of Quantum Electronics*, vol. 29, pp. 1693-1700, 1993.
12. Ong, J. T. *et al.*, "Subpicosecond Soliton Compression of Gain-Switched Diode-Laser Pulses Using an Erbium-Doped Fiber Amplifier," *IEEE Journal of Quantum Electronics*, vol. 29, pp. 1701-1707, 1993.
13. Thedrez, B., Lourtioz, J. M., Bouchoule, S. & Kazmierski, C., "Extended tunability of a self-seeded gain-switched InGaAsP laser using an intracavity absorber," *Electronics Letters*, vol. 32, pp. 662-664, 1996.
14. Lee, K. S. & Shu, C., "Stable and widely tunable dual-wavelength continuous-wave operation of a semiconductor laser in a novel Fabry-Perot grating-lens external cavity," *IEEE Journal of Quantum Electronics*, vol. 33, pp. 1832-1838, 1997.
15. Yam, S. P. & Shu, C., "An extended external cavity for the generation of tunable multi-wavelength pulses from a self-seeded laser diode," *Applied Physics Letters*, vol. 71, pp. 3347-3349, 1997.
16. Agrawal, G. P., "Line Narrowing in a Single-Mode Injection-Laser Due to External Optical Feedback," *IEEE Journal of Quantum Electronics*, vol. 20, pp. 468-471, 1984.
17. Ahmed, Z. & Tucker, R. S., "Small-Signal Im Response of Grating-Terminated External-Cavity Semiconductor-Lasers," *IEEE Journal of Selected Topics in Quantum Electronics*, vol. 1, pp. 505-515, 1995.
18. Cavelier, M. *et al.*, "Picosecond (Less-Than-2.5ps) - Wavelength-Tunable (Approximately-20nm) Semiconductor-Laser Pulses With Repetition Rates Up to 12-Ghz," *Electronics Letters*, vol. 28, pp. 224-226, 1992.
19. Hadley, G. R., "Injection Locking of Diode-Lasers," *IEEE Journal of Quantum Electronics*, vol. 22, pp. 419-426, 1986.

20. Kitaoka, Y., Sato, H., Mizuuchi, K., Yamamoto, K. & Kato, M., "Intensity noise of laser diodes with optical feedback," *IEEE Journal of Quantum Electronics*, vol. 32, pp. 822-828, 1996.

21. Kobayashi, S. & Kimura, T., "Injection Locking in AlGaAs Semiconductor-Laser," *IEEE Journal of Quantum Electronics*, vol. 17, pp. 681-688, 1981.

22. Lang, R. & Kobayashi, K., "External optical feedback effects on semiconductor injection laser properties.," *IEEE Journal of Quantum Electronics*, vol. 16, pp. 347-355, 1980.

23. Lang, R., "Injection Locking Properties of a Semiconductor-Laser," *IEEE Journal of Quantum Electronics*, vol. 18, pp. 976-983, 1982.

24. Lee, Y. C. & Shu, C., "Wavelength-tunable nearly transform-limited pulses generated by self-injection seeding of a laser diode at an arbitrary repetition rate," *IEEE Photonics Technology Letters*, vol. 9, pp. 590-592, 1997.

25. Olesen, H., Osmundsen, J. H. & Tromborg, B., "Nonlinear Dynamics and Spectral Behavior For an External Cavity Laser," *IEEE Journal of Quantum Electronics*, vol. 22, pp. 762-773, 1986.

26. Schell, M., Utz, W., Huhse, D., Kassner, J. & Bimberg, D., "Low Jitter Single-Mode Pulse Generation By a Self-Seeded, Gain- Switched Fabry-Perot Semiconductor-Laser," *Applied Physics Letters*, vol. 65, pp. 3045-3047, 1994.

27. Schell, M. *et al.*, "Jitter and Dynamics of Self-Seeded Fabry-Perot Laser-Diodes," *IEEE Journal of Selected Topics in Quantum Electronics*, vol. 1, pp. 528-534, 1995.

28. Spano, P., Piazzolla, S. & Tamburrini, M., "Frequency and Intensity Noise in Injection-Locked Semiconductor-Lasers - Theory and Experiments," *IEEE Journal of Quantum Electronics*, vol. 22, pp. 427-435, 1986.

29. Tromborg, B., Osmundsen, J. H. & Olesen, H., "Stability Analysis For a Semiconductor-Laser in an External Cavity," *IEEE Journal of Quantum Electronics*, vol. 20, pp. 1023-1032, 1984.

30. Wang, D. N. & Shu, C., "Tunable dual-wavelength picosecond pulse generation using multiple-optical-path self-seeding approach," *IEEE Photonics Technology Letters*, vol. 9, pp. 1211-1213, 1997.

31. Wang, D. N. & Shu, C., "Dual-wavelength picosecond pulse generation using a single grating and a Michelson interferometer in a self-injection seeding scheme," *Electronics Letters*, vol. 33, pp. 423-425, 1997.

32. Williams, K. A., White, I. H., Burns, D. & Sibbett, W., "Jitter reduction through feedback for picosecond pulsed InGaAsP lasers," *IEEE Journal of Quantum Electronics*, vol. 32, pp. 1988-1994, 1996.

33. Yam, S. P. & Shu, C., "Fast wavelength-tunable multichannel switching using a self-injection seeding scheme," *IEEE Journal of Quantum Electronics*, vol. 35, pp. 228-233, 1999.

34. Simpson, T. B., Liu, J. M. & Gavreilides, A., "Small-signal analysis of modulation characteristics in a semiconductor laser subject to strong optical injection," *IEEE Journal of Quantum Electronics*, vol. 32, pp. 1456-1468, 1996.

35. Chen, H. F., Liu, J. M. & Simpson, T. B., "Response characteristics of direct current modulation on a bandwidth-enhanced semiconductor laser under strong injection locking," *Optics Communications*, vol. 173, pp. 349-355, 2000.

36. Struckmeier, J. *et al.*, "Electronically tunable external-cavity laser diode," *Optics Letters*, vol. 24, pp. 1573-1574, 1999.

37. Mourat, G., Servagent, N. & Bosch, T., "Optical feedback effects on the spectral linewidth of semiconductor laser sensors using self-mixing interference," *IEEE Journal of Quantum Electronics*, vol. 34, pp. 1717-1721, 1998.

38. Kiguchi, T., Uematsu, A., Kitano, M. & Ogura, H., "Grating external cavity diode lasers with broad tunable range and narrow spectral linewidth for high-resolution spectroscopy," *Japanese Journal of Applied Physics Part 1-Regular Papers Short Notes & Review Papers*, vol. 35, pp. 5890-5895, 1996.

39. Sun, H. Y., Menhart, S. & Adams, A. J., "Development of a Tunable, Grating External-Cavity, Strong Feedback Semiconductor-Laser With Real-Time Wavelength Monitoring," *Optical Engineering*, vol. 34, pp. 2993-2998, 1995.

40. Jongerius, M. J., "Compact Violet Lasers By 2nd-Harmonic Generation in KTP Wave-Guides," *Philips Journal of Research*, vol. 49, pp. 293-313, 1995.

41. Bouchoule, S. & Lourtioz, J. M., "Injection-Seeding and Self-Injection-Seeding of Gain-Switched Fabry-Perot Laser-Diodes," *Annales Des Telecommunications-Annals of Telecommunications*, vol. 49, pp. 595-606, 1994.

42. Burns, D., Critten, M. P. & Sibbett, W., "Low-threshold diode-pumped femtosecond Cr3+:LiSrAlF6 laser," *Optics Letters*, vol. 21, pp. 477-479, 1996.

43. Shu, C. & Lee, Y. C., "Tunable dual-wavelength picosecond optical pulses generated from a self-injection seeded gain-switched laser diode," *IEEE Journal of Quantum Electronics*, vol. 32, pp. 1976-1980, 1996.

44. Wang, D. N. & Shu, C., "Multiple optical paths in a self-seeding scheme for multiwavelength short pulse generation," *Applied Physics Letters*, vol. 71, pp. 1305-1307, 1997.

45. Zhao, Y. & Shu, C., "Single-mode operation characteristics of a self-injection seeded Fabry-Perot laser diode with distributed feedback from a fiber grating," *IEEE Photonics Technology Letters*, vol. 9, pp. 1436-1438, 1997.

46. Calvani, R., Cisternino, F., Girardi, R. & Puleo, M., "All-fiber self-injection seeding for optical timing jitter reduction in a chirp compensated gain-switched DFB laser," *Fiber and Integrated Optics*, vol. 18, pp. 33-40, 1999.

47. Troger, J., Thevenaz, L. & Robert, P., "Frequency-sweep generation by resonant self-injection locking," *Optics Letters*, vol. 24, pp. 1493-1495, 1999.

48. Valentine, G. J. *et al.*, "Femtosecond Yb:YCOB laser pumped by narrow-stripe laser diode and passively modelocked using ion implanted saturable-absorber mirror," *Electronics Letters*, vol. 36, pp. 1621-1623, 2000.

49. Bi, J. Q., Beaud, P., Hodel, W. & Weber, H. P., "Experimental and Theoretical-Study of a New Technique to Stabilize Synchronously Pumped Mode-Locked Lasers," *Institute of Physics Conference Series*, pp. 109-112, 1991.

50. Bi, J. Q., Hodel, W. & Weber, H. P., "Self-Stabilization of a Hybridly Mode-Locked Styryl-9 Dye-Laser Using Coherent Photon Seeding," *Optics Communications*, vol. 89, pp. 240-244, 1992.

51. Weber, H. P., Hodel, W., Bi, J. Q., Beaud, P. & Peter, D. S., "Coherent Photon Seeding - a Scheme For Ultra Stable Ultrashort Pulse Generation," *Institute of Physics Conference Series*, pp. 83-88, 1992.

52. Rzhanov, Y. A. & Moloney, J. V., "Coherent Photon Seeding in a Color-Center Laser," *Optical and Quantum Electronics*, vol. 25, pp. 63-74, 1993.

53. Mollmann, K. & Gellermann, W., "Passive Stabilization of a Synchronously Mode-Locked Nacl Color-Center Laser By Coherent Photon Seeding," *Optics Letters*, vol. 19, pp. 490-492, 1994.

54. Michailov, N. I. & Chamel, M., "Application of the coherent photon seeding technique to synchronously pumped and hybridly mode-locked dye lasers," *Optical and Quantum Electronics*, vol. 28, pp. 653-667, 1996.

55. Riviere, C. J. B., Baribault, R., Gay, D., McCarthy, N. & Piche, M., "Stabilization of terahertz beats from a pair of picosecond dye lasers by coherent photon seeding," *Optics Communications*, vol. 161, pp. 31-36, 1999.

56. Huhse, D. *et al.*, "Generation of Electrically Wavelength Tunable (Delta-Lambda=40nm) Singlemode Laser-Pulses From a 1.3 Mu-M Fabry- Perot Laser By Self-Seeding in a Fiberoptic Configuration," *Electronics Letters*, vol. 30, pp. 157-158, 1994.

57. Langlois, P., Gay, D., McCarthy, N. & Piche, M., "Noise reduction in a mode-locked semiconductor laser by coherent photon seeding," *Optics Letters*, vol. 23, pp. 114-116, 1998.

58. Kawaguchi, H. & Abedin, K. S., "Coherent Photon Seeding of Actively Modelocked Laser-Diodes With Optical-Fiber Cavities," *Electronics Letters*, vol. 29, pp. 832-833, 1993.

59. Kawaguchi, H. & Sarwar, A. K., "Coherent Photon Seeding of Actively Mode-Locked Laser-Diodes," *Applied Physics Letters*, vol. 62, pp. 2164-2166, 1993.

60. Street, M. W. *et al.* in *12th LEOS Annual meeting* CThF3 (San Francisco, 1999).

61. Avrutin, E. A. *et al.*, "Analysis of harmonic (sub)THz passive mode-locking in monolithic compound cavity Fabry-Perot and ring laser diodes," *IEE Proceedings-Optoelectronics*, vol. 146, pp. 55-61, 1999.

62. Krauss, T. F., Hondromitros, G., Vogele, B. & De La Rue, R. M., "Broad spectral bandwidth semiconductor lasers," *Electronics Letters*, vol. 33, pp. 1142-1143, 1997.

63. Zhu, B. & White, I. H., "Variable Delay Dual-Wavelength Picosecond Optical Pulse Generation Using an Actively Mode Locked Multichannel Grating Cavity Laser," *Applied Physics Letters*, vol. 65, pp. 2928-2930, 1994.

Chapter 6.
Fibre Bragg grating external cavity picosecond diode lasers.

6.1. Introduction.

Optical fibres that are used extensively in telecommunications now span the globe and offer the capability of worldwide telephone conversations and high-speed internet access. The demand for these services is set to increase substantially. Given the comparable dimensions of the emission cross-section from a diode laser facet and the core diameter of a single-mode fibre, their combined use offers a scheme that is simple both in concept and implementation. Optical fibres are currently used extensively with diode lasers for pump delivery, where the fibre can offer numerous advantages, which include circularising an otherwise elliptical spatial output beam profile and enabling the diode laser source to be remote from the gain medium. It is also possible to combine the output from many low power emitters into one higher power output. The use of a fibre Bragg grating with a diode laser is not a new concept and has been used successfully in many diverse experimental configurations. These would typically involve an improvement in one of the operational characteristics of the diode laser. Examples cited in the literature include, amongst others, temporal pulse compression. Optical components containing fibre Bragg gratings are also applicable as sensing elements given the sensitivity of the Bragg grating period to variations of many physical parameters, such as changes in stress and temperature.[1-5]

As discussed in Chapter 3, gain-switching is a straightforward technique for obtaining picosecond pulses from a diode laser, where typical pulse durations are a few tens of picoseconds. The optical pulses obtained from the diode lasers described were frequency chirped, did not have transform-limited durations and although the temporal profile was near symmetrical, the spectral profile was not because of a Fabry-Perot structure which manifested itself as a deep modulation. Schemes to simultaneously improve the temporal and spectral profiles are of practical interest and thus the study described here was undertaken.

It was shown in Chapter 5. that the single-mode, narrow stripe InGaAs/GaAs ridge-waveguide lasers used in this work responded favourably to non-resonant self-injection optical feedback and demonstrated a marked improvement in the

time-bandwidth product. Although the scheme utilising self-injection optical feedback using the glass slide or beamsplitter/mirror combination worked well, the feedback elements were not wavelength selective or engineered to a known specification. Also, the lasing wavelength was essentially random, though this technique did allow for limited tuning. The use of bulk gratings did allow for continuous and smooth tuning of the output, but the overall footprint of the arrangement was increased. A big observation from the self-injection optical feedback studies was that the time-bandwidth product improvement was attributable solely to a reduction in the spectral bandwidth. Indeed, a slight worsening of the pulse duration was observed and this is not desirable in many instances. A practicable configuration based on a diode laser that yields temporally compressed transform-limited pulses would be of considerable interest due to the increased peak powers that would be available or the increased data rate that could be achieved in an optical time division multiplexed (OTDM) telecommunications system. Ideally, any such optical arrangement should be precise and rugged, preferably comprising only the diode laser and optical fibre. This would lend itself very well to a permanent assembly through the manufacture of a fibre pigtailed device that would also be opto-mechanically robust.

It has long been understood that the use of a grating (be it bulk or fibre Bragg) in an external cavity configuration can have a considerable effect on the operational characteristics of a diode laser.[6-13] The resultant effects may be advantageous, detrimental, or a trade-off of one characteristic against another. However, those schemes that rely upon the use of bulk optics cannot result in a particularly compact or intrinsically simplistic design. All this changed with the advent of the ability to directly write gratings into the cores of photosensitised optical fibres.[14,15] The output power that may be obtained from a diode laser will be influenced detrimentally by the use of such an optical fibre containing a fibre Bragg grating, although upon transmission through the fibre, the beam is spatially circular rather than elliptical. When compared with the output from a similar free-space device, the maximum power transmitted through an optical fibre is up to 90% of the launched power.[16,17]

6.2. Fabrication of fibre Bragg gratings in optical fibres.

The first demonstration of photosensitivity in silica optical fibres was by Hill and co-workers[14] in 1978. Ge-doped single-mode silica (germanosilicate) optical fibres were employed. By utilising two counter-propagating beams, at 488 or $514.5nm$, such that a standing wave interference pattern was set up, the first permanent fibre Bragg gratings were fabricated.[15]

Subsequently Meltz and co-workers[18] demonstrated the fabrication of fibre Bragg gratings in Ge-doped single-mode silica optical fibres by use of a two-beam holographic writing technique. The output of a tunable dye laser $(486-500nm)$ was frequency doubled and the Bragg gratings were written perpendicularly to the optical fibre rather than longitudinally as with the technique proposed by Hill and co-workers. The technique of transverse holographic exposure has several advantages that will be discussed further later in the section.

Photosensitivity in optical fibres may be brought about by doping standard silica single-mode telecommunications optical fibre with germania (GeO_2) at concentrations of approximately $\sim 3mol\%$.[19] The photoinduceable refractive index change, Δn, in such doped optical fibres is positive, increases with Ge concentration and has typical values of $\sim 3*10^{-5}$, though values $\approx 10^{-3}$ have been reported from optical fibres with a Ge concentration in the range ~ 10 to $\sim 20mol\%$.[20,21]

Although this topic will not be covered within the subject matter of this chapter, there are many relevant publications[21-31] which explain the processes involved in the origins of the photosensitivity employed for writing fibre Bragg gratings in germanosilicate optical fibres.

An alternative method for photosensitisation of optical fibres was proposed by Lemaire and co-workers,[32] where standard telecommunications optical fibre (the core of which was not Ge-doped) was subjected to a hydrogen atmosphere with pressures in the range $20-750$ atmospheres. A similar technique was suggested by Bilodeau and co-workers[33] and involved exposure of an optical fibre to a hydrogen-oxygen burner at temperatures up to $1700^{o}C$.

Although there exist many techniques for the writing of Bragg gratings in optical fibres, these can be categorised into one of two groups, being (i) two-beam interference[15,18,34,35] and (ii) phase-mask.[36] Two-beam interference techniques are of particular interest because the Bragg grating period can easily be varied simply by adjusting the wavelength of the writing beam. Phase-mask writing is useful for commercial applications because unlike the two-beam interference technique the period of the Bragg grating is determined by the pitch of the phase-mask and not the wavelength of the write beam. Whichever technique is employed the grating manifests itself as a varying refractive index profile along the exposed region.

The optical fibres containing fibre Bragg gratings used in this work were produced using the transverse holographic method, so a brief in context discussion of this technique follows. The arrangement used for the fabrication of these fibre Bragg gratings is illustrated below in Figure 6.2.1.[5,15,18]

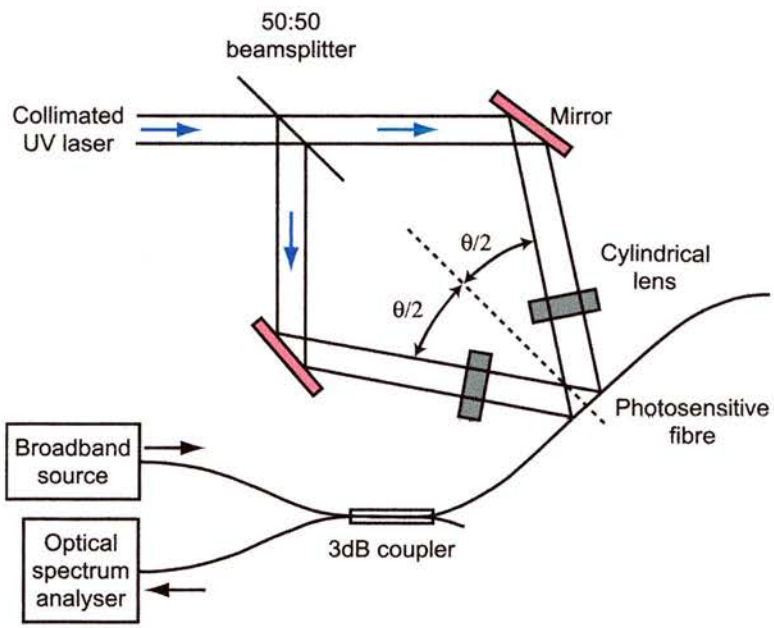

Figure 6.2.1. Illustration of the scheme used for transverse fibre Bragg grating fabrication.[19]

As discussed previously the refractive index increase in the photosensitised optical fibre is induced through an increased sensitivity to ultraviolet light $(\lambda < 400nm)$. The incident UV writing beam from the laser source is initially split using a $50:50$ beam-splitter, after which mirrors steer the two beams toward the optical fibre at equal angles with respect to the normal to the optical fibre. Cylindrical lenses focus these write beams along the region of the optical fibre

core into which the Bragg grating is to be written. To ensure a near uniform intensity profile of the write beams, only the centre of the Gaussian UV laser output is utilised.[19]

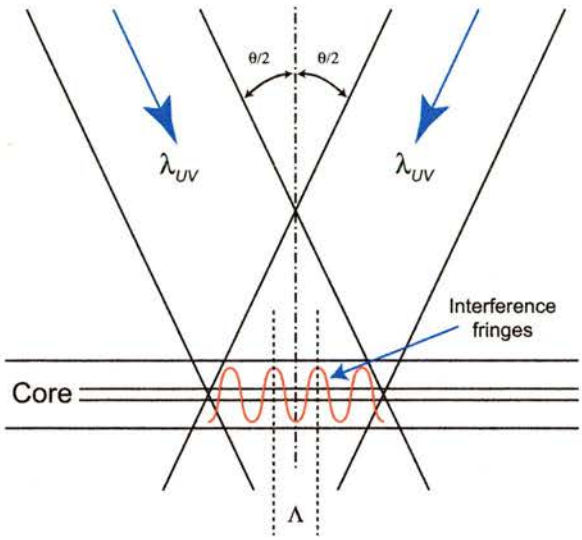

Figure 6.2.2. Writing of a Bragg grating into the core of an optical fibre.[19]

The grating to be written into the core of the optical fibre is determined through the following analysis. The two UV writing beams are incident on the fibre at angles of $\pm\theta/2$ with respect to the normal to the fibre. The grating that is subsequently written into the core of the optical fibre exists as a spatial modulation of the refractive index with a period of Λ, which is governed by the equation:[19]

$$\Lambda = \frac{\lambda_{UV}}{2\sin\left(\theta/2\right)} \qquad 6.1$$

λ_{UV} is the free-space wavelength of the incident UV writing beam.

According to Bragg's law, only one wavelength will be selected by such a grating with a period, Λ, where the Bragg wavelength, λ_B, is satisfied by equation:[37]

$$\lambda_B = 2n\Lambda \qquad 6.2$$

The grating written into the core of the optical fibre may, as illustrated in Figure 6.2.2., be considered as a uniform sinusoidal modulation of the core refractive index, n, with distance, z, that can be described as:[37]

$$n(z) = n_0 + \Delta n \cos\left(\frac{2\pi z}{\Lambda}\right) \qquad 6.3$$

n_0 is the refractive index of the untreated fibre core, and Δn is the magnitude of the photoinduced index change.

The reflectivity, *R*, for a guided wave interacting with such a grating may be determined from the following equations:[19]

$$R = \frac{\kappa^2 \sinh^2(SL)}{\delta\beta \sinh^2(SL) + S^2 \cosh^2(SL)} \qquad \kappa^2 > \delta\beta^2 \qquad 6.4$$

and

$$R = \frac{\kappa^2 \sin^2(QL)}{\delta\beta - \kappa^2 \cos^2(QL)} \qquad \kappa^2 < \delta\beta^2 \qquad 6.5$$

The parameters have the following meanings: L is the grating length, κ is the coupling coefficient of the grating, $\delta\beta = \beta - p\pi/\Lambda$, where p is an integer and Λ is the grating period, $\beta = 2\pi\eta_{eff}/\lambda$, being the mode propagation constant.

The maximum reflectivity occurs when $\delta\beta = 0$, for which condition:

$$p\lambda = 2\eta_{eff}\Lambda \equiv \lambda_B \qquad 6.6$$

Equation 6.6 denotes the Bragg condition for a given free-space wavelength, where $\delta\beta$ is a measure of the detuning from this optimum condition, and the strongest interaction occurs when $p = 1$.

When $\delta\beta = 0$ the maximum reflectivity value may be obtained from equation 6.4 to be:

$$R_{\max} = \tanh^2(\kappa L) \qquad 6.7$$

An approximate expression for the FWHM bandwidth of a Bragg grating may be obtained from:[38]

$$\Delta\lambda = \lambda_B s \sqrt{\left(\frac{\Delta n}{2n}\right)^2 + \left(\frac{1}{N}\right)^2} \qquad 6.8$$

Where $s \sim 1$ for strong Bragg gratings, ie, those with a reflectivity $\sim 100\%$, and $s \sim 0.5$ for weak Bragg gratings and N is the number of planes contained within the Bragg grating.

The fibre Bragg gratings considered thus far contain a periodic structure. Although periodic fibre Bragg gratings may be designed to have a large bandwidth, $\Delta\lambda_{FWHM}$, such gratings have a significant loss on the shorter-wavelength side of λ_B.[39] Designing a fibre Bragg grating in which the period is aperiodic[40-44] - also known as chirped gratings – leads to an increased grating bandwidth without introducing significant losses. Such aperiodic fibre Bragg gratings have a Bragg condition that varies (either continuously or quasi-continuously) along their length.

Based on Equation 6.2, the Bragg condition for an aperiodic fibre Bragg grating is denoted by:

$$\lambda_B(z) = 2n_{eff}(z)\Lambda(z) \qquad 6.9$$

This infers that an aperiodic structure can be realised by making either $n_{eff}(z)$ or $\Lambda(z)$ vary with distance z along the grating.

The techniques used for the fabrication of aperiodic fibre Bragg grating in optical fibres are very similar to those used for periodic fibre Bragg gratings with schemes employed to either alter the refractive index[40,43] or Bragg period[42] with distance.

Such aperiodic fibre Bragg gratings are of interest because their grating bandwidths are sufficient to encompass the large spectral bandwidth of either chirped or short duration pulsed laser outputs and have been used extensively with diode lasers as an external reflector for the manipulation of the output in both the spectral and temporal domains.[8,12] Given that the output of a pulsed diode laser will often be frequency chirped, an aperiodic fibre Bragg grating can be used to compensate for this chirp, with the result of near-Fourier-transform-limited pulses.[45]

6.3. Experimental.

Three methodologies for the diode laser-to-optical fibre coupling were initially investigated. The two techniques that were subsequently rejected are illustrated in Figure 6.3.1.

The first of the configurations shown in Figure 6.3.1a utilised two microscope objectives (typically 30X). One objective collimated the output from a free-space device with a second objective focussing into the optical fibre. This scheme was abandoned due to the low overall transmission and the serious difficulties in alignment. However, due to the nature of the coupling, there was no risk of damage to either the diode laser facet or the fibre end.

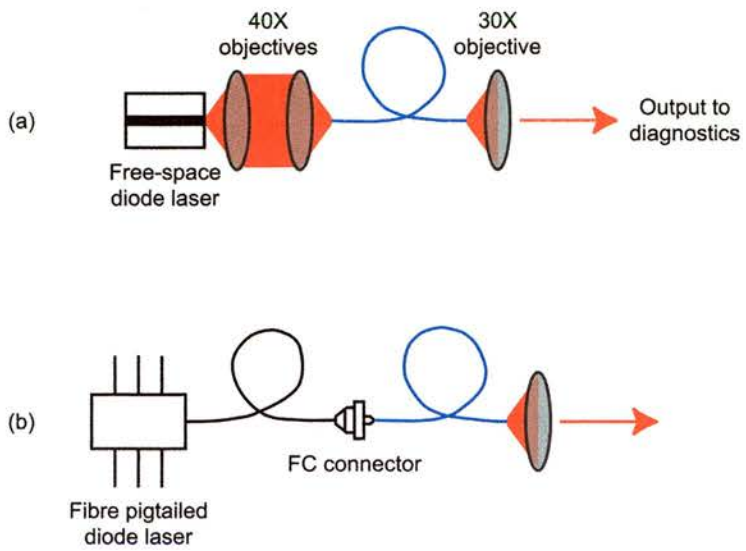

Figure 6.3.1. Coupling schemes considered and rejected.

The free-space single-mode laser chips that have been used in the work were also obtained in a FC-connectorised fibre pigtailed butterfly package as might be used in the telecommunications industry. The electrical and optical characteristics of these fibre-coupled devices (which can be found in section 3.3.5.) were essentially identical to those of the free-space devices, discussed in the same chapter.

The coupling mechanism for the second scheme, illustrated in Figure 6.3.1b, involved the alignment of the pigtail and the optical fibre containing the fibre Bragg grating. Although the coupling was somewhat simplified, aided by a reflection of the optical fibre end in the FC connector, the $<50\%$ overall transmission was deemed unsatisfactory. The fibre pigtailed devices suffered two sets of optical losses due to the laser-to-fibre coupling and the subsequent fibre-to-fibre coupling. However, the fibre pigtailed devices could be of future exploitability, as discussed at the end of this chapter, if a length of optical fibre

containing a fibre Bragg grating were fusion spliced directly into the fibre pigtail. This would represent a compact and robust opto-mechanical assembly.

The scheme that was decided upon for the optical fibre Bragg grating experiments that follow, is illustrated in Figure 6.3.2. For clarity, the RF drive electronics to the diode laser are not shown. To summarise though, the RF electronics consisted of a frequency synthesiser, $37dBm$ power amplifier, circulator and bias tee. The operational range of the modulation frequency applied to the diode laser was limited by the $1GHz$ bandwidth of the power amplifier. The gain-switched diode laser module was mounted on a piezo-electric controlled *xyz* stage that had an adjustment resolution of $20nm$.

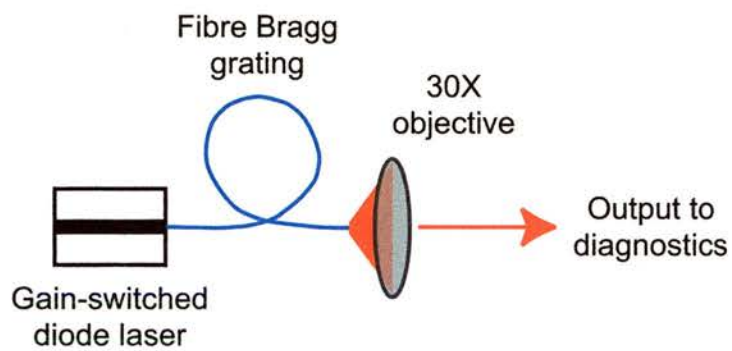

Figure 6.3.2. Experimental scheme used for the optical fibre Bragg grating experiments.

The optical fibre under investigation first had a section of its outer polymer jacket removed from each end using methylene chloride prior to being cleaved perpendicular to the core using a York FK11 automated cleaver. The cleaves were visually inspected for quality before the fibre ends were mounted in v-groove clamps on differential *xyz* stages. The laser emission was launched into the optical fibre using a *butt-coupling* technique, which involved no additional optics, and as a result this incurred no avoidable losses. This butt coupling of the laser output to the optical fibre was performed manually and an optical microscope was used as an alignment aid. Coupling was established by initially moving the fibre into close proximity with the diode laser facet but still with a perceptible gap between the two. Whilst observing the laser transmission through the fibre, alignment of the fibre parallel to the diode laser junction was optimised, after which the fibre alignment was optimised perpendicular to the junction. The fibre was then moved closer to the facet after which the parallel

and perpendicular alignments were re-optimised. Course coupling adjustments were performed using a differential micrometer stage whilst the piezo-electric stage was utilised for precise and fine adjustments. This arrangement worked well except that the alignment was sensitive to minor external perturbations. Extreme care had to be exercised to ensure that the fibre end did not crash into the diode laser facet thereby destroying the device and the fibre cleave. For a very small range of fibre end to diode laser facet separations, optical feedback from the fibre cleave was observed to influence the spectral output from the diode laser. The spectral reduction was akin to that which was observed due to the non-resonant optical feedback discussed in Chapter 5.

On existing the optical fibre, the laser emission was collimated with an AR coated 30X aspheric objective, before being steered to the diagnostics that were used to determine how the presence of the optical fibre might have affected the diode laser pulse characteristics. In common with previous experiments, the temporal measurements were performed with a HP 54750A digital sampling oscilloscope with a HP-54752B $50GHz$ plug-in and a New Focus 1024 InGaAs single-mode fibre-coupled photodiode (FWHM resolution $12ps$). The temporal resolution of the assembly (including connectors) was approximately $18ps$. Real-time spectral measurements were performed using a Rees Instruments E202 spectrometer (specified resolution $\sim 0.3nm$). For high resolution spectral measurements, a CVI DK480 computer-controlled monochromator (specified resolution $0.01nm$) operated by a custom written HP-VEE program (Appendix C) was used. Given the time required by the computer-controlled monochromator to perform a scan at the highest resolution (~10 minutes), it was used only for high-resolution spectral measurements for a centre wavelength previously determined through use of the real-time spectrometer.

6.3.1. Diode laser characterisation using a standard fibre.

To determine the maximum optical transmission that could be expected from an optical fibre containing a Bragg grating, a reference measurement needed to be performed. Therefore, for comparative purposes, the laser emission was butt-coupled, in the manner described in the previous section, into a $50cm$ length of

standard monomode optical fibre of the type in which the fibre Bragg gratings would subsequently be fabricated. Such an evaluation was crucial, in that it not only established the transmitted optical power that could be realistically obtained, but it would also demonstrate whether optical fibre transmission had any effect - detrimental or otherwise - on the pulse characteristics, other than the expected reduction in laser output power.

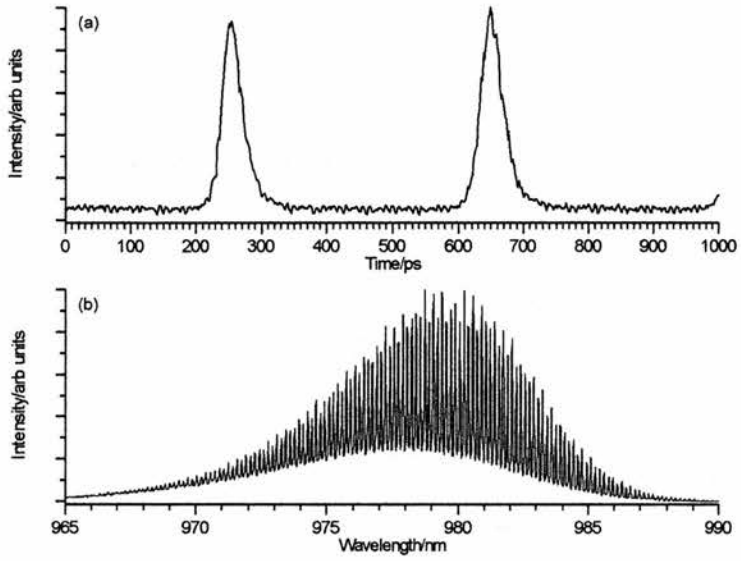

Figure 6.3.3. Temporal (a) and spectral (b) characteristics for the pulses transmitted through the standard optical fibre.

The temporal and spectral characteristics of the pulses transmitted through the standard optical fibre are shown in Figures 6.3.3a and 6.3.3b respectively. These were identical to those obtained for the free-space device, for which data are included as Figures 3.3.3. and 3.3.7. respectively. For a diode laser DC bias $100mA$, the optical output power from the free-space diode laser was measured to be $70mW$, whereas the optical power transmitted through the standard fibre was $35mW$, indicating a transmission efficiency of 50%. It should be noted that the optical coupling, and hence the transmission through the optical fibre, were determined by the distance between the diode laser facet and the fibre end. Obviously this distance is variable so the transmission efficiency is not absolute, but is instead a guide as to what is achievable. The optical power transmitted through the standard fibre was unaffected by either the RF power level applied to the diode laser or its modulation frequency. Given the limitation of the launch methodology used, and considering the non-optimised nature of the coupling, the degree of diode laser to fibre coupling

observed was encouraging. As discussed in the previous section, due to the diode laser facet to fibre distances involved, extreme caution had to be exercised to avoid damaging the laser facet, and thereby destroying the device.

There is scope for a marked improvement in the fibre launch efficiency using methods that will be discussed in the future work section at the end of this chapter.

6.3.2. Optical fibres containing periodic fibre Bragg gratings.

Having established what can be considered the typical transmitted power, the standard optical fibre was replaced with an optical fibre containing a periodic fibre Bragg grating. The optical fibres containing periodic fibre Bragg gratings that were initially assessed had gratings of length $6mm$, with a spatial periodicity of $0.35\mu m$, and measured peak reflectivites ranging from 20% to 50%. A typical optical transmission versus wavelength measurement for an optical fibre containing a periodic fibre Bragg grating is illustrated in Figure 6.3.4. The Bragg grating had a design wavelength of approximately $979nm$ with a corresponding FWHM spectral reflectivity of $\sim 0.1nm$, both of which are clearly visible in the transmission measurement. Given that the Bragg gratings in these initial optical fibres were periodic, they were orientation non-specific, but for consistency one end of the optical fibre was marked such that it could be similarly positioned should they subsequently be re-used.

The first optical fibre to be cleaved and mounted was one containing a periodic Bragg grating that provided a peak reflectivity of 50%. Initially the fibre end was positioned some distance from the diode laser facet to avoid any unwanted optical feedback into the laser. The spectra of the transmitted pulses was highly stable and centred at $979nm$ (the design transmission centre wavelength for the periodic fibre Bragg gratings contained within the optical fibres.) Following optimisation of the coupling, subsequent measurements of the transmitted spectra were made using the computer-controlled monochromator that yielded a centre wavelength of $978.5nm$ and a FWHM spectral bandwidth of $0.1nm$. For a diode laser DC bias of $150mA$, it was not possible to obtain a satisfactory temporal pulse profile and duration since the output was erratic and the duration unstable. This was rectified when the DC bias was reduced to

$100mA$, where the pulses were symmetrical and stable. The minimum pulse duration was $26ps$, and the maximum transmitted optical power was $23mW$. This apparent increase over 50% of the reference value could be explained by an enhancement due to the optical feedback, or the fibre end being closer to the diode laser facet than was the case when the standard fibre measurements were performed.

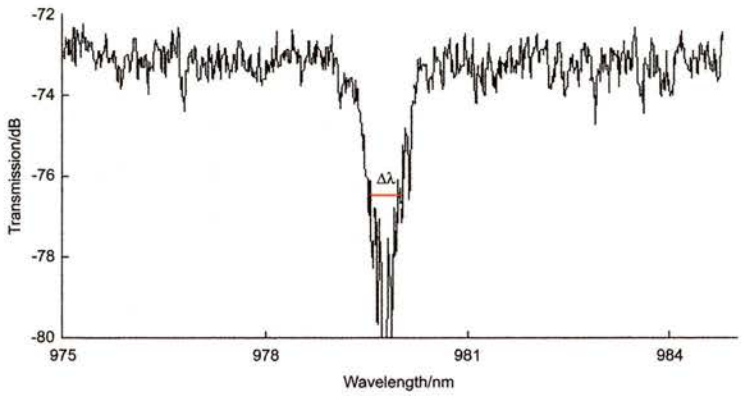

Figure 6.3.4. Typical transmission characteristic for an optical fibre containing a periodic fibre Bragg grating.

The power transmitted through the optical fibre containing the fibre Bragg grating with a 50% peak reflectivity was highly dependent upon the modulation frequency and RF power applied to the laser. A minimum of $0.94mW$ was observed even though the DC bias was unchanged at $100mA$, indicating significant spectral filtering effects. This is similar to what was observed with self-injection optical feedback, where if the frequency of the modulation applied to the diode laser coincided with a harmonic of the cavity frequency, the output power was reduced to a minimum. It is reasonable to conclude therefore, that if the modulation frequency applied to the diode laser was a harmonic of the external cavity frequency, terminated by the Bragg grating the resulting broad spectral output from the gain-switched diode laser, would be filtered by the narrow bandpass fibre Bragg grating. The optical fibres containing the Bragg gratings with peak reflectivities of 40% and 30% exhibited a similar behaviour and minimum pulse durations.

Compared with the others, transmission through the optical fibre containing the Bragg grating that provided a 20% peak reflectivity, showed a somewhat reduced pulse duration of $18ps$, as illustrated in Figure 6.3.5a. It should be

noted that $18ps$ is the minimum pulse duration that could be reliably measured by the sampling oscilloscope/photodiode combination. The construction of a slow scan auto-correlator, such that the pulse duration might be re-measured to determine whether the equipment was indeed limiting the temporal measurements, should be considered. The FWHM spectral bandwidth, as measured with the monochromator, was $0.1nm$, being centred at $978.5nm$, as illustrated Figure 6.3.5b. These results show a substantial improvement over the characteristics of the pulses transmitted through the standard optical fibre, which were illustrated in Figure 6.3.3.

The observed spectral and temporal improvement corresponded to a time-bandwidth product of < 0.49, representing a reduction of $210X$ over the free-space product.

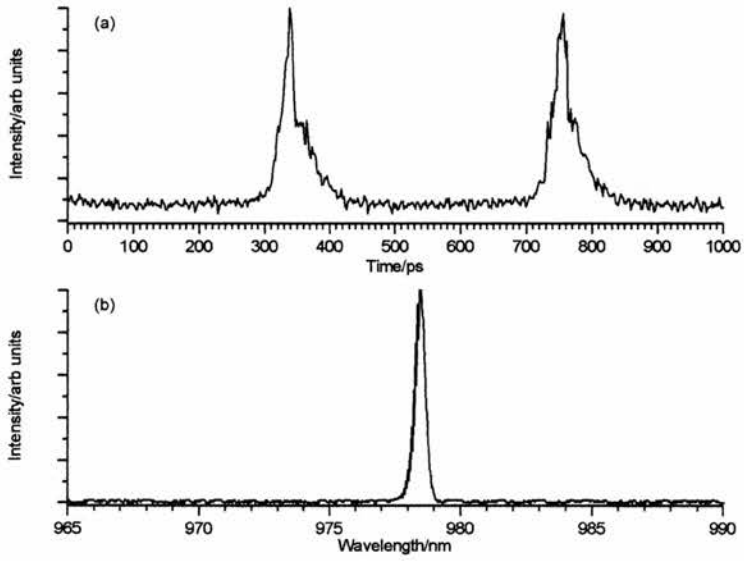

Figure 6.3.5. Temporal (a) and spectral (b) characteristics of the pulses transmitted through an optical fibre containing a periodic FBG with a 20% peak reflectivity.

It was observed that a variation in the peak reflectivity of the periodic Bragg grating did not significantly affect the characteristics of the transmitted pulse, with the exception of optical output power. Given that the transmitted optical power was determined by the fibre Bragg gratings peak reflectivity, it is reasonable to conclude that an external cavity was formed with the diode laser and fibre Bragg grating, rather than being purely a spectral filtering configuration. Assuming a linear scaling, if spectral filtering were responsible for the reduction in the spectral bandwidth, then for a similar reduction in the

spectral bandwidth the transmitted optical power would have been reduced to $\sim 0.31mW$. This was clearly not the situation.

The power transmitted through an optical fibre containing a periodic Bragg grating was dependent upon the frequency of the modulation applied to the diode laser. This was not the case when the device was operated either free-space or coupled into the standard fibre. With the modulation applied to the diode laser, such that it was operating in the picosecond pulse regime, the power transmitted through an optical fibre containing a fibre Bragg grating with a 20% peak reflectivity was $27mW$, whereas this was reduced to $8mW$ when the modulation was removed. To investigate this observation further the optical power through the fibre was recorded as a function of modulation frequency.

The coupling of the diode laser output to the optical fibre containing the Bragg grating with a 20% peak reflectivity was optimised. The modulation frequency was then scanned at a rate of $100MHz/s$ with a constant DC bias of $100mA$ $(70mW)$. In the usual manner, the light transmitted through the optical fibre was collimated using a 30X objective, after which the optical power was measured. The power meter used had an electrical output connector, which was connected to a chart recorder.

When viewing the scans of transmitted power versus modulation frequency, it was observed that there were dips and peaks in the transmitted power that were periodic with frequency (Figures 6.3.7.). This was interesting given that for the free-space device, the optical output power was unchanged as the modulation frequency applied to the diode laser was varied. Before any conclusion could be reached regarding any effect the fibre Bragg gratings may have had on the pulsed output of the diode laser, it was necessary to determine whether the laser operating regime or the modulation frequency had any pronounced effect on the laser-to-fibre coupling. To assess this, the modulation frequency applied to the diode laser was increased until a maximum in the power transmitted through the optical fibre was observed. With the modulation frequency applied to the diode laser such that the power transmitted through the optical fibre was maximised, the laser-to-fibre coupling was optimised. After coupling optimisation, the power transmitted through the optical fibre was

$21mW$ for a modulation frequency of $1.99GHz$. In the absence of the modulation - such that the diode laser was operating CW - the transmitted optical power dropped to $7.70mW$. The modulation frequency was further increased to $2.46GHz$, the location of a minimum in the transmitted optical power, where the pulsed and CW transmitted powers were $4.76mW$ and $5.80mW$ respectively. The coupling was then re-optimised for pulsed operation after which the transmitted powers were $6.10mW$ and $4.80mW$ respectively, but the output was unstable. With the laser-to-fibre coupling still optimised for transmission at the minimum located at $2.46GHz$ the modulation frequency was returned to $1.99GHz$. The transmitted power was now $16.40mW$, which increased to $19.35mW$ after re-alignment. This demonstrates that the laser-to-fibre coupling was not influenced adversely by changes in the modulation frequency.

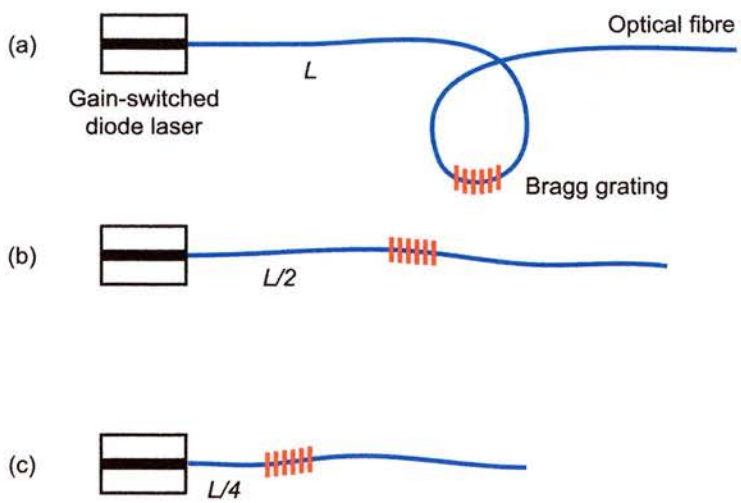

Figure 6.3.6. An illustration of the methodology used in the fibre cut-back experiment.

Finally, a "cut-back" experiment was performed on the optical fibre containing the 40% reflectivity fibre Bragg grating. This involved taking three sets of transmitted power versus modulation frequency scans. An arbitrary end of the optical fibre was chosen as the input. The initial length of the optical fibre between this arbitrary end and the fibre Bragg grating was $L \approx 47cm$, as depicted in Figure 6.3.7a. The length of the optical fibre, L, was subsequently halved, $(L/2 \approx 25cm)$, and quartered, $(L/4 \approx 12cm)$, as indicated in Figures 6.3.7b. and 6.3.7c. respectively.

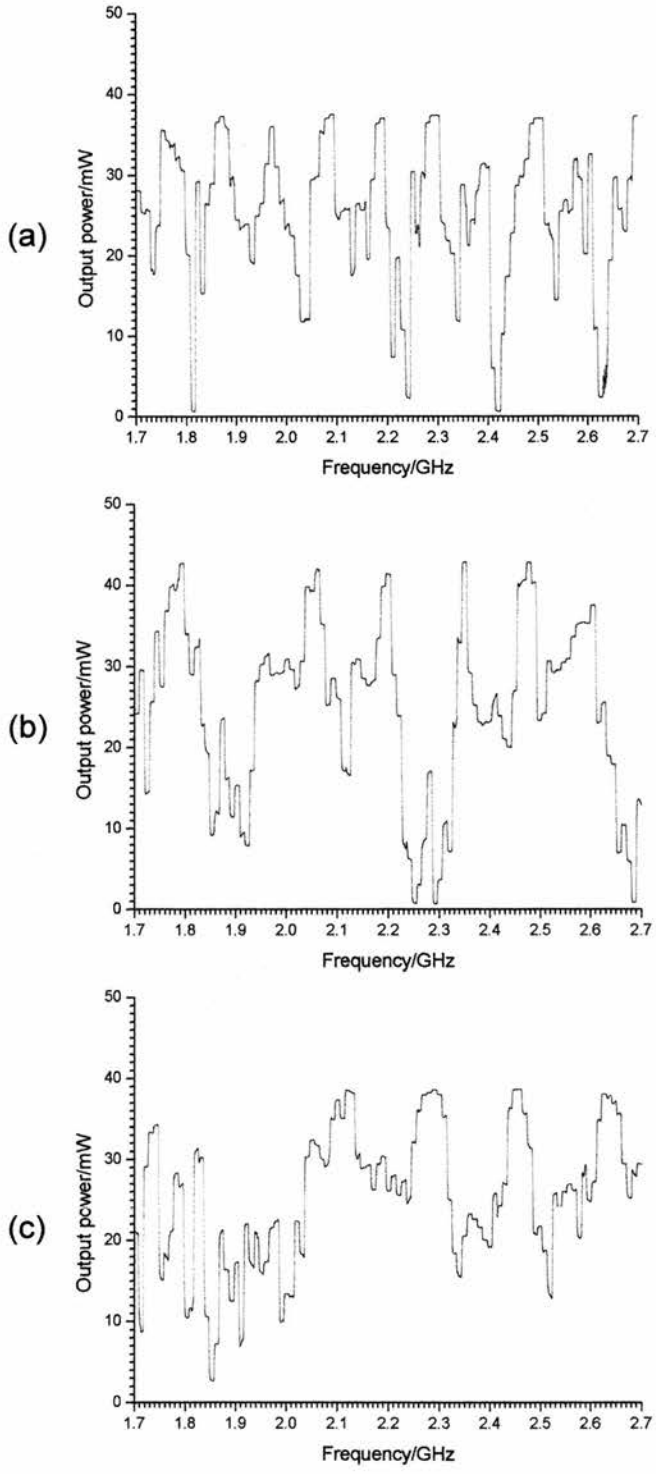

Figure 6.3.7. Transmitted power versus frequency for different *cavity lengths* of (a) $\approx 47cm$, (b) $\approx 25cm$ and (c) $\approx 12cm$.

The resultant scans of transmitted power versus modulation frequency are shown in Figures 6.3.7a, 6.3.7b. and 6.3.7c. for L, $L/2$ and $L/4$ respectively. These figures illustrate that the number of points corresponding to maximum

transmission were reduced with external cavity length, though their respective width in terms of modulation frequency increased.

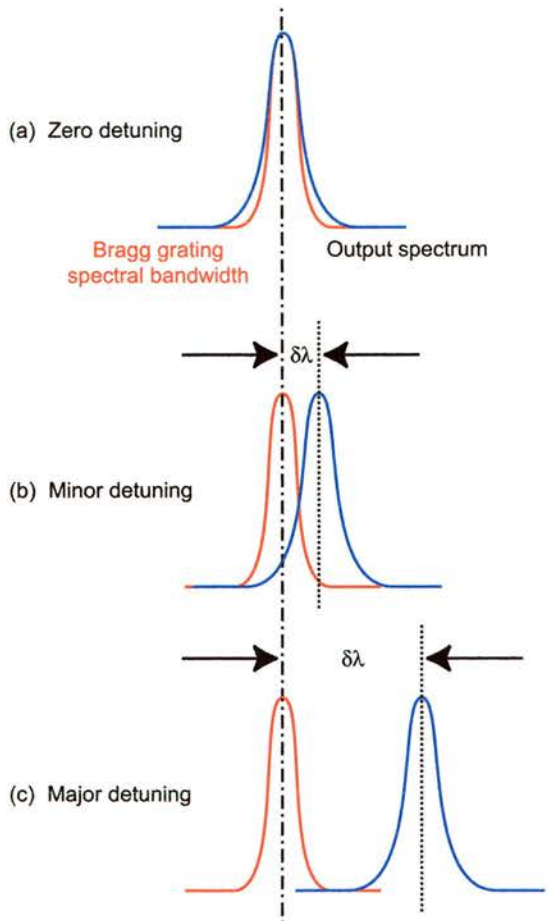

Figure 6.3.8. Illustration of spectral detuning and filtering due to variation of the modulation applied to the diode laser.

As it was demonstrated that the reduction in the power transmitted through the optical fibres containing fibre Bragg gratings that resulted from a change in the modulation frequency applied to the diode laser was not attributed to a degradation of the laser-to-fibre coupling another explanation needed to be sought. Recall that the spectral bandwidth of the periodic grating within the optical fibre core was very narrow at $<0.1nm$. Also, by its very nature, a fibre Bragg grating is wavelength selective, in this case for $\sim 979.5nm$, as observed experimentally. Referring to the work discussed in Chapter 5. on self-injection seeding with no wavelength selective elements (glass-slide and beam-splitter/mirror), it was demonstrated how a similar reduction in the spectral bandwidth was observed. However, unlike the periodic fibre Bragg gratings, as the modulation frequency applied to the diode laser was varied, the output

wavelength would jump around pseudo-randomly with little influence on the output optical power observed from the diode laser. Similar pseudo-random jumps in the output wavelength are not permitted when an optical fibre containing a periodic fibre Bragg grating is utilised due to the strong wavelength selectivity imposed by the Bragg grating structure. If a change in the modulation frequency attempts to force a shift in the output wavelength, then weak spectral filtering results and the power transmitted through the optical fibre is severely compromised. This is shown schematically in Figure 6.3.8. where the fibre grating and transmitted spectral bandwidths are indicated in red and black respectively. For zero detuning, $\delta\lambda$, (a) there exists a good overlap between the Bragg grating reflection centre wavelength and the lasing spectrum of the diode laser favoured by the applied modulation frequency. The resultant optical power transmitted through the fibre is maximised. However, a periodic fibre Bragg grating is spectrally selective, so, unlike a glass slide or beam-splitter/mirror, an attempted spectral jump of the diode laser output, due to a variation of the applied modulation frequency, is not permitted. As the detuning of the laser output increases from that of the fibre Bragg grating reflection centre wavelength (b and c) the spectral filtering effect is enhanced with a resultant decrease in the optical power transmitted through the fibre.

It can be seen from Figure 6.3.5 that the periodic fibre Bragg gratings had a pronounced effect on the spectral characteristics of the laser, reducing the bandwidth from $11nm$ to $0.1nm$, representing a reduction of $110X$. However, the pulse duration was only slightly decreased from $30ps$ to, an equipment-limited minimum of $18ps$, although the pulse was slightly asymmetric. If optimum temporal compression could be achieved to produce Fourier-transform-limited pulses, then the $11nm$ bandwidth would imply that durations as short as $\sim 150fs$ might be obtained. One methodology that could be considered to achieve this objective would be the fabrication of fibre Bragg gratings with the aim of maximising pulse compression. This is discussed in the next section.

6.3.3. Optical fibres containing aperiodic fibre Bragg gratings.

The magnitude of the frequency chirp in the output of gain-switched diode lasers obtained from sonogram experiments (discussed in chapter 4.) was used as a basis for the design of an optical fibre containing an aperiodic fibre Bragg grating structure that could accommodate the entire spectral bandwidth of the pulse. Such aperiodic structures are routinely utilised in nonlinear frequency conversion to enable temporal pulse compression.[46-50] It was therefore reasonable to presume that an optical fibre containing a suitably designed aperiodic fibre Bragg grating, used in an external cavity configuration with the gain-switched diode laser, might yield temporal pulse compression.

The aperiodic fibre Bragg gratings (a-FBG) were fabricated with this objective of temporal - rather than spectral - pulse compression in mind. They contained a chirped grating that was $6mm$ long with a $10nm$ spectral bandwidth and a peak reflectivity of 50%.[51] A typical optical transmission versus wavelength measurement for an optical fibre containing an aperiodic fibre Bragg grating is illustrated in Figure 6.3.9. The fibre was prepared, mounted and aligned using the techniques described in Section 6.3.

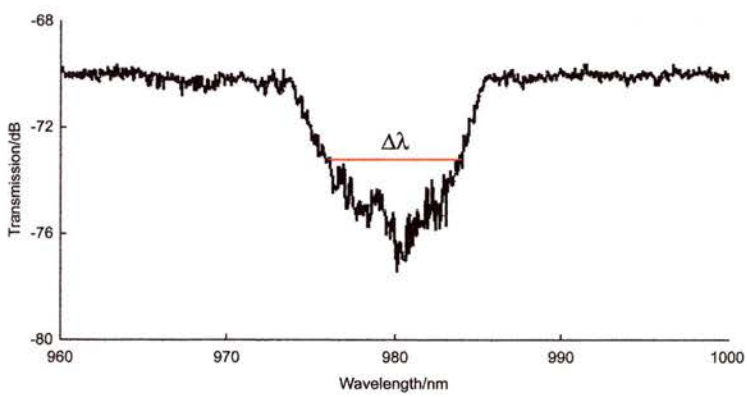

Figure 6.3.9. Typical transmission characteristic for the optical fibre containing an aperiodic fibre Bragg grating.

Given the negative sign of the frequency chirp on the diode laser pulses, the fibre was mounted such that the longer-period end of the grating was initially near the emission facet of the diode laser chip. Figure 6.3.10 shows an illustration of a negatively chirped pulse entering such an aperiodic grating. With the grating in such an orientation the structure results in the external cavities experienced by the blue and red wavelength components being

$l_B^{ext} > l_R^{ext}$. Due to the different group velocities for the blue leading edge, and the red trailing edge of the pulse, the fibre was orientated so the blue components of the pulse travel farther into the grating. Thus after reflection, the blue edge of the pulse has been retarded with respect to the red edge, thereby compensating for the frequency chirp on the pulse. Ideally, if the measurement of the frequency chirp and grating fabrication were precise, then near-Fourier-transform limited pulses could be obtained. Obviously, in a real system, the frequency chirp present in the gain-switched pulse is dynamic in that it varies with DC bias.[52-55] Also, there may exist imperfections in the grating structure.

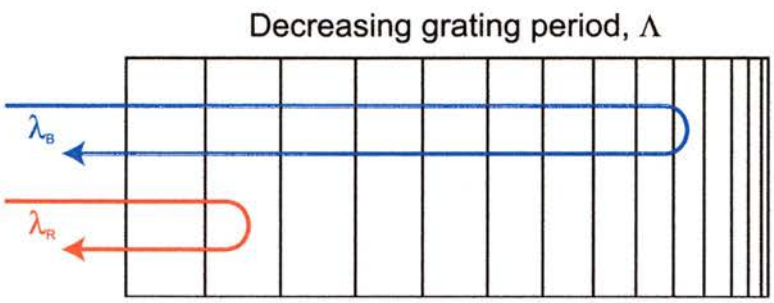

Figure 6.3.10. Reflection profile for an aperiodic fibre Bragg grating structure.[37]

For an output power of $70mW$ from the gain-switched diode laser, the maximum power transmitted through the optical fibre containing the aperiodic fibre Bragg grating, following optimisation of the laser-to-fibre coupling, was $20mW$. This figure was consistent with that expected when the transmission through the standard fibre was used as a calibration reference. Analogously, with the optical fibre containing the periodic fibre Bragg gratings, when the modulation applied to the diode laser was removed, the power transmitted through the optical fibre was significantly reduced to $\leq 5mW$. The transmitted power also depended on by the frequency of the modulation applied to the diode laser.

The spectrum of the pulse after transmission through the optical fibre containing the aperiodic fibre Bragg grating is shown in Figure 6.3.11b. The optical fibre was oriented such that the longer-period end of the fibre Bragg grating was at the input from the diode laser. The spectrum was centred at $984nm$ with a bandwidth of $0.08nm$. With the optical fibre in this orientation, the pulses had an equipment limited duration of $18ps$, a typical profile of which, as measured with the sampling oscilloscope, is shown in Figure 6.3.11a.

The time-bandwidth product associated with the pulses after transmission through the optical fibre containing the aperiodic fibre Bragg grating was 0.45, which is Fourier-transform-limited if a Gaussian profile is assumed. Such a value represented a reduction of 230 when compared with the time-bandwidth product of the pulses from the free-space device.

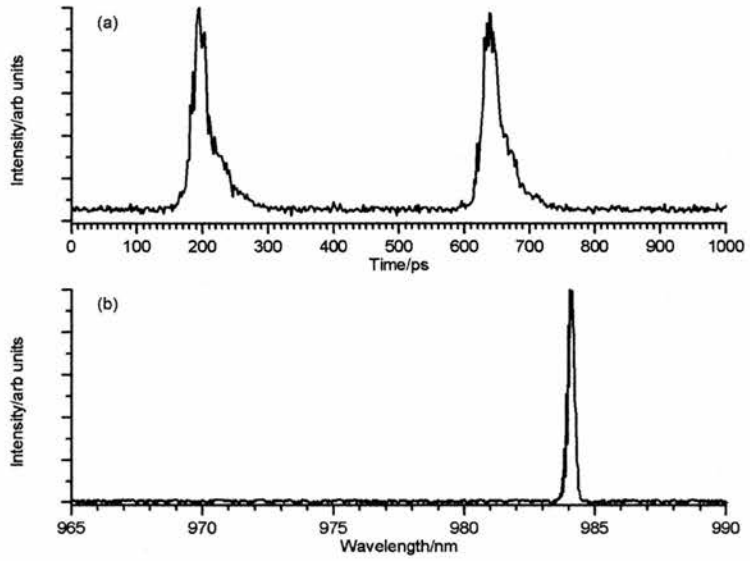

Figure 6.3.11. Temporal (a) and spectral (b) characteristics of the pulse transmitted through an optical fibre containing an aperiodic FBG with the longer-period end as the input.

The optical fibre was then reversed, such that the shorter-period end of the aperiodic fibre Bragg grating was now nearer the input from the diode laser.

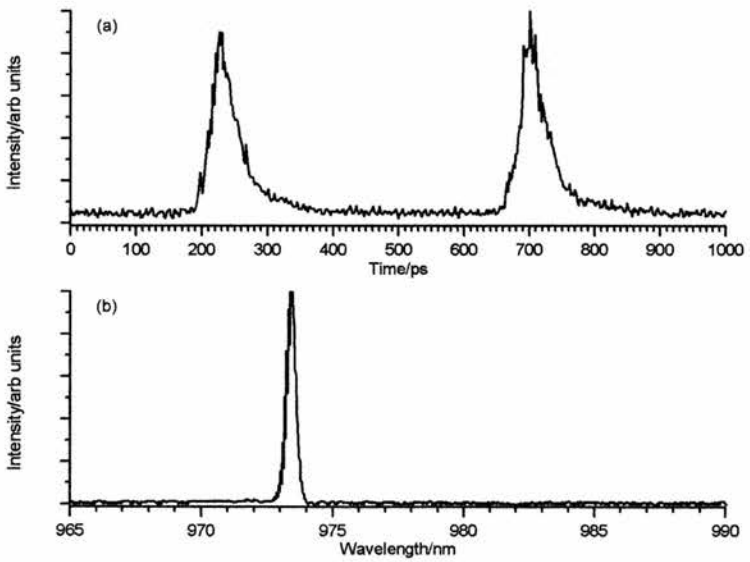

Figure 6.3.12. Temporal (a) and spectral (b) characteristics of the pulse transmitted through an optical fibre containing an aperiodic FBG with the shorter-period end as the input.

In this orientation, the transmitted spectrum was centred at $973.5nm$, as shown Figure 6.3.12b, and had a corresponding FWHM spectral bandwidth of $0.1nm$. A pulse duration of $22ps$ was recorded which had a typical pulse profile as illustrated in Figure 6.3.12a.

The time-bandwidth product of the pulses transmitted through the aperiodic fibre Bragg grating in this orientation was 0.68. The reduction of the time-bandwidth product compared to that obtained from the free-space device was 150.

However, the emission was spectrally unstable and would jump randomly between 974 and $984nm$, this range being the bandwidth of the aperiodic fibre Bragg grating contained within the optical fibre. The average output power was $20mW$, with the peak power being $455mW$. The output power dropped to $2.0mW$ when the modulation applied to the diode laser was removed.

6.4. Conclusions.

In this chapter the spectral and temporal compressions of the output from gain-switched diode lasers have been described for configurations where optical fibres containing periodic and aperiodic fibre Bragg gratings were used as external cavity elements.

For an optical fibre containing a periodic fibre Bragg grating it was demonstrated that a spectral narrowing to $\approx 0.1nm$ and a minimum pulse duration of $18ps$ were observed, with a corresponding time-bandwidth product of 0.56. The average power transmitted through the fibre was $27mW$ representing an efficiency of 40%.

An optical fibre containing an aperiodic Bragg grating was then utilised as the external cavity element. The degree of temporal compression was rather poor (factor of ~2) when compared with the reduction in the spectral bandwidth (factor of ~210). An explanation as to why significant temporal compression was not observed was based on the fact that the Bragg grating period closest to the laser was dominating the reflection. This is consistent with the observation of the two extreme transmitted wavelengths that occurred when the optical fibre containing the aperiodic fibre Bragg grating was reversed. A summary of this is

illustrated in Figure 6.4.1. This situation could possibly be rectified with a suitably designed Bragg grating structure, for which a proposed design is outlined in the "future work" section at the end of this chapter.

A measurement equipment-limited pulse duration of $18ps$ was observed with a corresponding time-bandwidth product of 0.45, which is Fourier-transform-limited if a Gaussian profile is assumed.

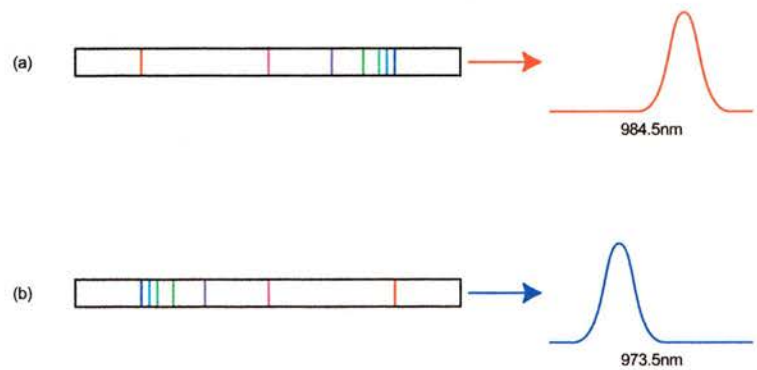

Figure 6.4.1. Summary of the experimental results from the optical fibre containing the aperiodic fibre Bragg grating.

Illustrated in Table 6.4.1. is a summary of the results obtained when optical fibres containing Bragg gratings were used in conjunction with the gain-switched single-mode InGaAs/GaAs diode lasers. Worthy of note is the significant reduction in the time-bandwidth product.

Table 6.4.1. Summary of the results presented in this chapter.

	Pulse duration $\Delta\tau/ps$	Spectral bandwidth $\Delta\lambda/nm$	Time-bandwidth product $\Delta\tau\Delta\nu$	Modulation frequency f/GHz	CW output power P_{CW}/mW	Average output power P_{AV}/mW	Peak output power P_{PK}/mW
Free-space.	30	11	103	2.00	68	68	1135
Standard fibre.	30	11	103	2.00	68	~35	583
Periodic FBG	18[1]	0.1	0.562	1.95	8.0	27	769
Aperiodic FBG. Longer period.	18[1]	0.08	0.45	1.87	2.6	22	653
Aperiodic FBG. Shorter period.	22	0.1	0.687	2.00	2.0	20	455

[1] Measurement at equipment limit.

In conclusion, the combination of a gain-switched diode laser and fibre Bragg grating results in a source of near-transform limited picosecond optical pulses that is spectrally stable and through optomechanical engineering has significant potential to be compact and robust.

6.5. Future work.

Although the butt-coupling technique used for the free-space diode laser-to-fibre coupling was simple, the associated overall transmission efficiency was not an optimum. An increase in this coupling efficiency could be realised through the use of one of two methodologies. A fibre lens could be fusion spliced to the input end of the grating, as illustrated in Figure 6.5.1a. Alternatively, a 0.29 pitch GRIN lens could be utilised. This would relay the laser emission from the diode facet to a focal point, where the fibre would be positioned, as illustrated in Figure 6.5.1b. Not only would each of these improvements yield an increased coupling efficiency, they would also protect the laser facet from possible damage as a consequence of the increased working distance between the diode facet and fibre. Neither scheme was investigated in the work discussed here due to time constraints.

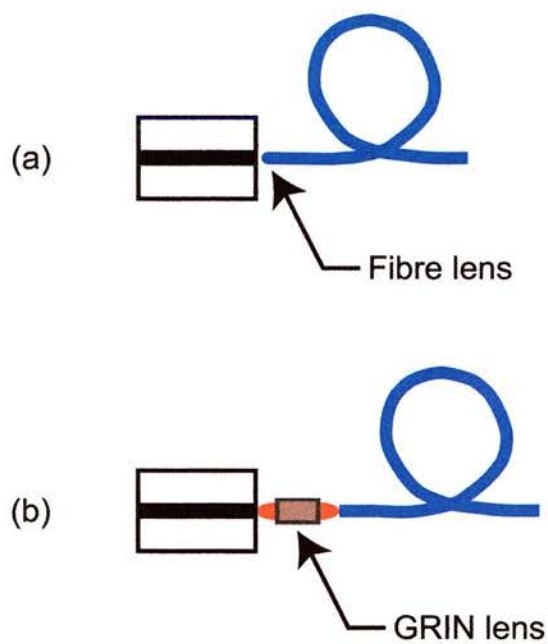

Figure 6.5.1. Possible schemes for improved coupling between laser and optical fibre.

The minimum pulse duration that the digital sampling oscilloscope/high-speed photodiode combination could reliably measure was $18ps$. In order to ascertain whether the equipment limited the temporal measurement, the pulse duration after transmission through the optical fibre containing the periodic fibre Bragg grating with 20% peak reflectivity should be determined. A suitable scheme would be the use of a slow scan auto-correlator, which would be realised by

mounting one of the mirrors of a Michelson-type delay stage on a computer-controlled translation stage.

The free-space diode lasers used in the experiments discussed above were also obtained as connectorised single-mode fibre pigtailed devices. Although the output power from the fibre was somewhat lower than that obtained from the free-space device, it would nonetheless be conceivable that a grating could be fusion spliced directly into the pigtail with a high overall coupling efficiency. Given the high efficiency of fusion splicing, this should result in an efficient methodology. Furthermore, being completely fibre based, the re-alignment required when using the free-space devices would no longer be an issue such that the overall system would be extremely compact and robust.

Li and co-workers demonstrated that when using an optical fibre containing an aperiodic fibre Bragg grating with an optical delay it was possible obtain pulse compression and tune the centre wavelength of the transmitted pulses.[8] It is reasonable to conclude that if a similar optical delay were used, centre wavelengths other than those corresponding to the two extreme grating periods of the aperiodic fibre Bragg grating might be obtained.

The stable spectral output when the periodic fibre Bragg grating was combined with the gain-switched diode laser, along with the circular spatial profile that results from transmission through a fibre, are qualities that would make the combination desirable for frequency conversion.

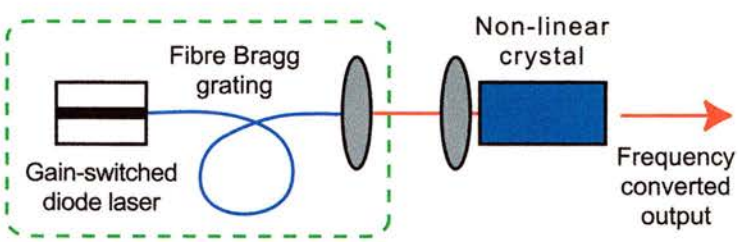

Figure 6.5.2. Proposed frequency conversion scheme utilising a periodic fibre Bragg grating in an external cavity picosecond diode laser.

As discussed in Section 6.3.3, when the optical fibre containing the aperiodic fibre Bragg grating was used, only two emission wavelengths were observed which depended on the orientation of the Bragg grating. These two emission wavelengths corresponded to those transmitted by the extreme period of the Bragg grating that was closest to the emitting diode laser facet. A possible

solution to this problem would be to design and fabricate an optical fibre containing an aperiodic Bragg grating, the reflectivity of which increases uniformly along the length of the grating, as illustrated schematically in Figure 6.5.3.

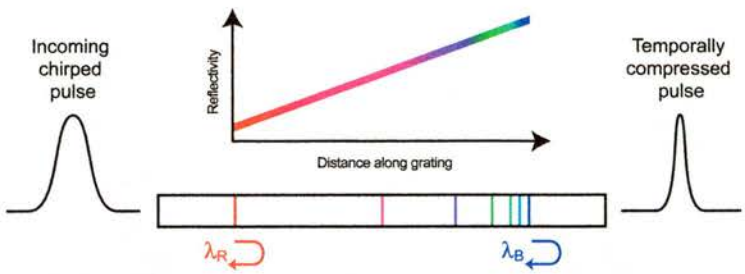

Figure 6.5.3. Proposed design for an optical fibre containing a non-uniform reflectivity aperiodic fibre Bragg grating.

The longer (input) period end of the grating would have a low reflectivity, increasing as required throughout the grating to the shorter (output) period end. The design of the grating would be such that a flat reflectivity characteristic would be achieved for all wavelengths within the spectral bandwidth of the diode laser pulse. It is anticipated that such a Bragg grating design would result in temporal rather than the spectral compression that was observed with the aperiodic fibre grating.

Kashyap[10,56] proposed a design for *step-chirped* Bragg gratings. Rather than having a period that gradually increases throughout the length of the Bragg grating the step-chirped design consists of, N, discrete periodic sections each of equal length, δl, with a different period, $\delta\Lambda$. Up to 200 sections were considered with an overall grating length of up to $100nm$. The total length of each section was dependent on the overall length, L, and the number of sections, whereas the period step was determined by the total chirp desired and the number of steps. Such a grating design could prove of interest if employed with the non-uniform reflectivity aperiodic fibre Bragg grating described above.

It can therefore be deduced that there are a range of choices for future configurations of these diode laser cavity arrangements. The expectation can thus be that "fully engineered" versions of robust picosecond diode lasers can be made available in the future both for fundamental wavelengths and for the frequency up/down converted systems.

6.6. References.

1. Rao, Y. J., Cooper, M. R., Jackson, D. A., Pannell, C. N. & Reekie, L., "Simultaneous measurement of displacement and temperature using in-fibre-Bragg-grating-based extrinsic Fizeau sensor," *Electronics Letters*, vol. 36, pp. 1610-1612, 2000.
2. Rao, Y. J., Cooper, M. R., Jackson, D. A., Pannell, C. N. & Reekie, L., "Absolute strain measurement using an in-fibre-Bragg-grating- based Fabry-Perot sensor," *Electronics Letters*, vol. 36, pp. 708-709, 2000.
3. Rao, Y. J., "Recent progress in applications of in-fibre Bragg grating sensors," *Optics and Lasers in Engineering*, vol. 31, pp. 297-324, 1999.
4. Rao, Y. J., Henderson, P. J., Jackson, D. A., Zhang, L. & Bennion, I., "Simultaneous strain, temperature and vibration measurement using a multiplexed in-fibre-Bragg-grating/fibre-fabry-Perot sensor system," *Electronics Letters*, vol. 33, pp. 2063-2064, 1997.
5. Rao, Y. J., "In-fibre Bragg grating sensors," *Measurement Science & Technology*, vol. 8, pp. 355-375, 1997.
6. Matsui, Y., Pelusi, M. D. & Suzuki, A., "Generation of 20-fs optical pulses from a gain-switched laser diode by a four-stage soliton compression technique," *IEEE Photonics Technology Letters*, vol. 11, pp. 1217-1219, 1999.
7. Li, S. P., Chan, K. T. & Lou, C. Y., "Wavelength switching of picosecond pulses in a self-seeded Fabry-Perot semiconductor laser with external fiber Bragg grating cavities by optical injection," *IEEE Photonics Technology Letters*, vol. 10, pp. 1094-1096, 1998.
8. Li, S. P., Chan, K. T. & Lou, C. Y., "Wavelength-tunable picosecond pulses generated from stable self-seeded gain-switched laser diode with linearly chirped fibre Bragg grating," *Electronics Letters*, vol. 34, pp. 1234-1236, 1998.
9. Yu, J. *et al.*, "Fourier-Transform-Limited 2.5ps Light-Pulses With Electrically Tunable Wavelength (15nm) By Hybridly Modelocking a Semiconductor-Laser in a Chirped Bragg Grating Fiber External- Cavity," *Electronics Letters*, vol. 31, pp. 2008-2009, 1995.
10. Gunning, P., Kashyap, R., Siddiqui, A. S. & Smith, K., "Picosecond Pulse Generation of Less-Than-5ps From Gain-Switched Dfb Semiconductor-Laser Diode Using Linearly Step-Chirped Fiber Grating," *Electronics Letters*, vol. 31, pp. 1066-1067, 1995.
11. Ding, H., Li, S. P., Fang, Z. J. & Chan, K. T., "Wavelength switching of semiconductor laser pulses by self- seeding from a chirped fiber Bragg grating," *IEEE Photonics Technology Letters*, vol. 9, pp. 901-903, 1997.
12. Ozyazici, M. S., Morton, P. A., Zhang, L. M. & Mizrahi, V., "Theoretical-Model of the Hybrid Soliton Pulse Source," *IEEE Photonics Technology Letters*, vol. 7, pp. 1142-1144, 1995.
13. Schell, M. *et al.*, "20 Nm Wavelength Tunable Singlemode Picosecond Pulse Generation At 1.3-Mu-M By Self-Seeded Gain-Switched Semiconductor-Laser," *Electronics Letters*, vol. 28, pp. 2154-2155, 1992.
14. Hill, K. O., Fujii, Y., Johnson, D. C. & Kawasaki, B. S., "Photosensitivity in optical fibre waveguides: Application to reflection filter fabrication," *Applied Physics Letters*, vol. 32, pp. 647-649, 1978.
15. Kawasaki, B. S., Hill, K. O., Johnson, D. C. & Fujii, Y., "Narrow-band Bragg reflectors in optical fibres," *Optics Letters*, vol. 3, pp. 66-68, 1978.
16. Vakhshoori, D. *et al.*, "980nm spread index laser with strain compensated InGaAs/GaAsP/InGaP and 90% fibre coupling efficiency," *Electronics Letters*, vol. 32, pp. 1007-1008, 1996.
17. Verdiell, J. M., Ziari, M. & Welch, D. F., "Low-loss coupling of 980 nm GaAs laser to cleaved singlemode fibre," *Electronics Letters*, vol. 32, pp. 1817-1818, 1996.
18. Meltz, G., Morey, W. W. & Glenn, W. H., "Formation of Bragg Gratings in Optical Fibers By a Transverse Holographic Method," *Optics Letters*, vol. 14, pp. 823-825, 1989.
19. Bennion, I., Williams, J. A. R., Zhang, L., Sugden, K. & Doran, N. J., "UV-written in-fibre Bragg gratings," *Optical and Quantum Electronics*, vol. 28, pp. 93-135, 1996.

20. Fertein, E. *et al.*, "Shifts in Resonance Wavelengths of Bragg Gratings During Writing or Bleaching Experiments By Uv Illumination Within Germanosilicate Optical Fiber," *Electronics Letters*, vol. 27, pp. 1838-1839, 1991.

21. Xie, W. X. *et al.*, "Experimental-Evidence of 2 Types of Photorefractive Effects Occurring During Photoinscriptions of Bragg Gratings Within Germanosilicate Fibers," *Optics Communications*, vol. 104, pp. 185-195, 1993.

22. Hand, D. P. & Russell, P. S., "Photoinduced Refractive-Index Changes in Germanosilicate Fibers," *Optics Letters*, vol. 15, pp. 102-104, 1990.

23. Simmons, K. D., Larochelle, S., Mizrahi, V., Stegeman, G. I. & Griscom, D. L., "Correlation of Defect Centers With a Wavelength-Dependent Photosensitive Response in Germania-Doped Silica Optical Fibers," *Optics Letters*, vol. 16, pp. 141-143, 1991.

24. Tsai, T. E., Friebele, E. J. & Griscom, D. L., "Thermal-Stability of Photoinduced Gratings and Paramagnetic Centers in Ge-Doped and Ge/P-Doped Silica Optical Fibers," *Optics Letters*, vol. 18, pp. 935-937, 1993.

25. Tsai, T. E., Askins, C. G. & Friebele, E. J., "Photoinduced Grating and Intensity Dependence of Defect Generation in Ge-Doped Silica Optical Fiber," *Applied Physics Letters*, vol. 61, pp. 390-392, 1992.

26. Atkins, R. M. & Mizrahi, V., "Observations of Changes in Uv Absorption-Bands of Singlemode Germanosilicate Core Optical Fibers On Writing and Thermally Erasing Refractive-Index Gratings," *Electronics Letters*, vol. 28, pp. 1743-1744, 1992.

27. Atkins, R. M., Mizrahi, V. & Erdogan, T., "248 Nm Induced Vacuum Uv Spectral Changes in Optical-Fiber Preform Cores - Support For a Color Center Model of Photosensitivity," *Electronics Letters*, vol. 29, pp. 385-387, 1993.

28. Xie, W. X. *et al.*, "2nd-Order Diffraction Efficiency of Bragg Gratings Written Within Germanosilicate Fibers," *Optics Communications*, vol. 101, pp. 85-91, 1993.

29. Cordier, P. *et al.*, "Tem Characterization of Structural-Changes in Glass Associated to Bragg Grating Inscription in a Germanosilicate Optical-Fiber Preform," *Optics Communications*, vol. 111, pp. 269-275, 1994.

30. Niay, P. *et al.*, "Behavior of Spectral Transmissions of Bragg Gratings Written in Germania-Doped Fibers - Writing and Erasing Experiments Using Pulsed or Cw Uv Exposure," *Optics Communications*, vol. 113, pp. 176-192, 1994.

31. Williams, D. L., Davey, S. T., Kashyap, R., Armitage, J. R. & Ainslie, B. J., "Direct Observation of UV Induced Bleaching of 240-Nm Absorption-Band in Photosensitive Germanosilicate Glass-Fibers," *Electronics Letters*, vol. 28, pp. 369-371, 1992.

32. Lemaire, P. J., Atkins, R. M., Mizrahi, V. & Reed, W. A., "High-Pressure H-2 Loading As a Technique For Achieving Ultrahigh Uv Photosensitivity and Thermal Sensitivity in Geo2 Doped Optical Fibers," *Electronics Letters*, vol. 29, pp. 1191-1193, 1993.

33. Bilodeau, F. *et al.*, "Photosensitization of Optical-Fiber and Silica-On-Silicon Silica Wave-Guides," *Optics Letters*, vol. 18, pp. 953-955, 1993.

34. Douay, M. *et al.*, "Formation of Bragg Gratings in Germanium Doped Optical Fibers Using a Prism Interferometer," *Journal De Physique Iv*, vol. 1, pp. 529-532, 1991.

35. Zhang, Q., Brown, D. A., Reinhart, L. & Morse, T. F., "Simple Prism-Based Scheme For Fabricating Bragg Gratings in Optical Fibers," *Optics Letters*, vol. 19, pp. 2030-2032, 1994.

36. Hill, K. O., Malo, B., Bilodeau, F., Johnson, D. C. & Albert, J., "Bragg Gratings Fabricated in Monomode Photosensitive Optical- Fiber By Uv Exposure Through a Phase Mask.," *Applied Physics Letters*, vol. 63, pp. 424-424, 1993.

37. Othonos, A. & Kalli, K. *Fibre Bragg gratings: fundamentals and applications in telecommunications and sensing* (Artech House, 1999).

38. Russell, P. S. J., Archambault, J. L. & Reekie, L., "Fiber Gratings," *Physics World*, vol. 6, pp. 41-46, 1993.

39. Mizrahi, V. & Sipe, J. E., "Optical-Properties of Photosensitive Fiber Phase Gratings," *Journal of Lightwave Technology*, vol. 11, pp. 1513-1517, 1993.

40. Byron, K. C., Sugden, K., Bricheno, T. & Bennion, I., "Fabrication of Chirped Bragg Gratings in Photosensitive Fiber," *Electronics Letters*, vol. 29, pp. 1659-1660, 1993.

41. Byron, K. C. & Rourke, H. N., "Fabrication of Chirped Fiber Gratings By Novel Stretch and Write Technique," *Electronics Letters*, vol. 31, pp. 60-61, 1995.

42. Sugden, K., Bennion, I., Molony, A. & Copner, N. J., "Chirped Gratings Produced in Photosensitive Optical Fibers By Fiber Deformation During Exposure," *Electronics Letters*, vol. 30, pp. 440-442, 1994.

43. Farries, M. C. *et al.*, "Very Broad Reflection Bandwidth (44nm) Chirped Fiber Gratings and Narrow Bandpass-Filters Produced By the Use of an Amplitude Mask," *Electronics Letters*, vol. 30, pp. 891-892, 1994.

44. Putnam, M. A., Williams, G. M. & Friebele, E. J., "Fabrication of Tapered, Strain-Gradent Chirped Fiber Bragg Gratings," *Electronics Letters*, vol. 31, pp. 309-310, 1995.

45. Birkin, D. J. L. *et al.*, "Near-transform-limited pulses from a diode laser with an aperiodic fibre Bragg grating.," *eCLEO*, CWF75, 2000.

46. Arbore, M. A., Marco, O. & Fejer, M. M., "Pulse compression during second-harmonic generation in aperiodic quasi-phase-matching gratings," *Optics Letters*, vol. 22, pp. 865-867, 1997.

47. Arbore, M. A., Galvanauskas, A., Harter, D., Chou, M. H. & Fejer, M. M., "Engineerable compression of ultrashort pulses by use of second- harmonic generation in chirped-period-poled lithium niobate," *Optics Letters*, vol. 22, pp. 1341-1343, 1997.

48. Loza-Alvarez, P. *et al.*, "Simultaneous femtosecond-pulse compression and second-harmonic generation in aperiodically poled KTiOPO4," *Optics Letters*, vol. 24, pp. 1071-1073, 1999.

49. Imeshev, G. *et al.*, "Ultrashort-pulse second-harmonic generation with longitudinally nonuniform quasi-phase-matching gratings: pulse compression and shaping," *Journal of the Optical Society of America B-Optical Physics*, vol. 17, pp. 304-318, 2000.

50. Imeshev, G., Arbore, M. A., Kasriel, S. & Fejer, M. M., "Pulse shaping and compression by second-harmonic generation with quasi-phase-matching gratings in the presence of arbitrary dispersion," *Journal of the Optical Society of America B-Optical Physics*, vol. 17, pp. 1420-1437, 2000.

51. Williams, J. A. R., Bennion, I. & Zhang, L., "The Compression of Optical Pulses Using Self-Phase-Modulation and Linearly Chirped Bragg-Gratings in Fibers," *IEEE Photonics Technology Letters*, vol. 7, pp. 491-493, 1995.

52. Wiesenfeld, J. M., Tucker, R. S. & Downey, P. M., "Picosecond Measurement of Chirp in Gain-Switched, Single-Mode Injection-Lasers," *Applied Physics Letters*, vol. 51, pp. 1307-1309, 1987.

53. Schell, M., Tsuchiya, M. & Kamiya, T., "Chirp and stability of mode-locked semiconductor lasers," *IEEE Journal of Quantum Electronics*, vol. 32, pp. 1180-1190, 1996.

54. Tsuchiya, M., Takeshita, H. & Kamiya, T., "Precise analysis of linear and non-linear chirp parameters of gain-switched distributed feedback laser pulses for the fibre optic compression scheme," *Optical and Quantum Electronics*, vol. 28, pp. 975-982, 1996.

55. Dellunde, J., Torrent, M. C., Sancho, J. M. & SanMiguel, M., "Frequency dynamics of gain-switched injection-locked semiconductor lasers," *IEEE Journal of Quantum Electronics*, vol. 33, pp. 1537-1542, 1997.

56. Kashyap, R., "Design of step-chirped fibre Bragg gratings," *Optics Communications*, vol. 136, pp. 461-469, 1997.

Chapter 7.
Frequency conversion of picosecond diode lasers.

7.1. Introduction.

There is considerable interest in compact lasers operating in the blue spectral region for various applications in science, technology and medicine. The preferred laser source for these applications would be a one with its fundamental wavelength in the blue, such as the GaN-based diode laser developed by Nakamura and co-workers.[1-3] Although such devices are now commercially available, their output powers were, at the time of writing, rather low $(\sim 5mW)$, their unit cost relatively high $(\sim \$2000)$ and their specified operational lifetime rather short $(< 5000h)$, when compared to more established material structures. Obviously this situation will improve as the technology matures. However, in the mean time an alternative methodology is required to gain access to the blue spectral region if diode lasers are to be utilised. The frequency doubling of near-infrared diode lasers using a suitable nonlinear crystal represents a competitive methodology.

The realisation of a compact blue light source based on a frequency-doubled near-infrared diode laser was made practicable by the recent development of good quality lasers.[4-13] Commercial diode lasers can have near-diffraction-limited spatial outputs and narrow spectral bandwidths, using, for example (Distributed Bragg Reflector/Distributed Feed Back) DBR/DFB configurations.[14-16] It is also possible to obtain multi-watt output powers with high beam quality using master oscillator power amplifier (MOPA) combinations.[17,18] However, DBR/DFB and MOPA systems have their respective drawbacks, the major one common to both being their high unit cost. By contrast, the InGaAs/GaAs diode lasers used in this work are selectively low cost, volume-produced commercial devices having continuous wave (CW) output powers $\geq 210mW$ with a nominal emission wavelength of $980nm$. A blue laser source incorporating such a laser diode and suitably designed nonlinear crystal could thus be compact, stable, self-contained and have an attractively competitive overall cost.

The successful frequency doubling of diode laser depends upon the use of a suitable nonlinear crystal and although various materials have been demonstrated to exhibit second harmonic generation capabilities,[19-34] the crystals of interest for this study should be economical, readily available, easy

to process and offer efficient second harmonic generation. The crystal characteristics include, optical quality, nonlinear coefficients, likelihood for periodic poling for quasi-phase-matching and the compatibility with waveguide formation.

With the aforementioned considerations in mind the crystals chosen for investigated were lithium niobate ($LiNbO_3$) and potassium titanyl phosphate (KTP). Both of these crystals are commercially available with established fabrication techniques for obtaining efficient second harmonic conversion. The discussion that follows will be limited to these crystals from which the samples investigated in this study were fabricated.

7.1.1. Phase matching.

Efficient second harmonic generation requires the use of a technique to correct for the different propagation velocities of the fundamental and its second harmonic that result from the refractive index variation with wavelength in a material. Such a technique is referred to as phase matching, and we can consider the two main types of birefringent- and quasi-phase matching (QPM).

7.1.1.1. Non-phase matched second harmonic generation.

Due to the different refractive indices experienced by the electromagnetic radiation at a fundamental frequency, ω, and its second harmonic, 2ω, when traversing a given (nonlinear) material a phase mismatch, Δk, occurs between the two. Δk is given by:

$$\Delta k = k_{2\omega} - 2k_{\omega} \qquad 7.1$$

where $k_{2\omega}$ and k_{ω} relate to:[35]

$$k_{2\omega} = \frac{2\pi n_{2\omega}}{\lambda_{2\omega}} \qquad 7.2$$

$$k_{\omega} = \frac{2\pi n_{\omega}}{\lambda_{\omega}} \qquad 7.3$$

Optimum conversion to the second harmonic frequency is obtained when $\Delta k = 0$, i.e. in a phase-matched condition.

The second harmonic power generated at a distance l from the input facet of the crystal is given by the equation:[35]

$$P_{2\omega} = \frac{2\pi^2 \omega_\omega^{\ 2} \mu_0 d_{eff}^2 l^2}{n_\omega^2 n_{2\omega}} P_\omega^2 \operatorname{sinc}^2\left(\frac{\Delta k l}{2}\right) \qquad 7.4$$

where d_{eff} is the effective nonlinear coefficient.

For perfect phase matching, at $\Delta k = 0$, it follows from Equation 7.4 that the converted power $P_{2\omega}$ increases quadratically with l, as illustrated in curve (a) of Figure 7.1.1.

If, as illustrated in curve (b) of Figure 7.1.1., $\Delta k \neq 0$ there exists a periodic cycling of the intensity of the generated second harmonic signal governed by the $\operatorname{sinc}^2(x)$ function, with a period of π.

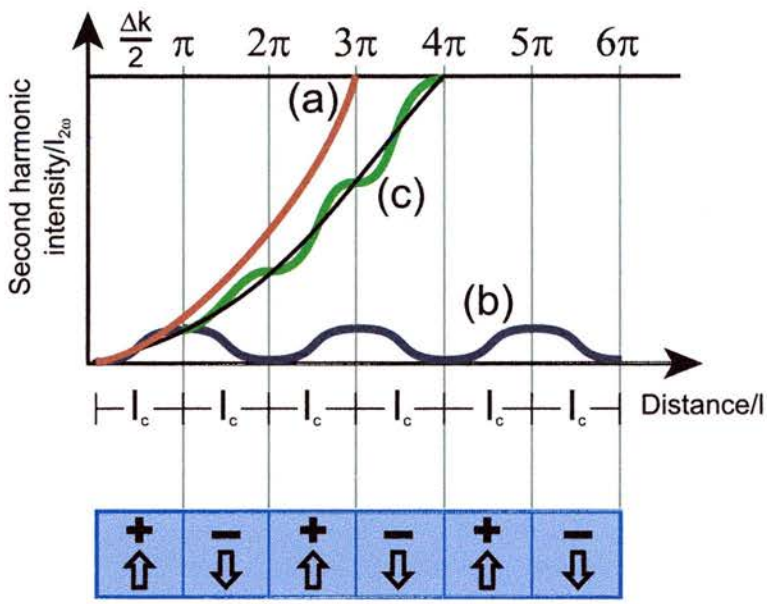

Figure 7.1.1. Generated second harmonic as a function of propagation distance for (a) non-phase matched, (b) ideally phase matched, and (c) quasi-phase matched.[36]

The distance over which the accumulated phase mismatch between the two propagating frequencies becomes π with respect to one another is referred to as the coherence length, and is defined as:

$$l_c = \frac{\pi}{\Delta k} = \frac{\lambda_\omega}{4(n_{2\omega} - n_\omega)} \qquad 7.5$$

where λ_ω is the free space wavelength of the fundamental.

7.1.1.2. Birefringent phase matching.

A method by which the phase matching condition of $\Delta k = 0$ may be satisfied is to utilise the birefringence that arises in anisotropic crystals. Birefringence occurs when the refractive indices of the axes in a crystal are not all equal. If there exist two unique refractive index values then the crystal is said to be uniaxial, whereas if there exist three unique values then the crystal is biaxial. The ordinary and extraordinary axes are defined for the polarisation of the light wave traversing the crystal as being normal (for ordinary) or perpendicular (for extraordinary) to the plane formed by the optic (z-) axis and wave vector. By utilising birefringence, the fundamental and its second harmonic can be phase matched if it can be arranged that they propagate along the ordinary and extraordinary axes of a suitable crystal. This is illustrated in the index ellipsoid shown in Figure 7.1.2.

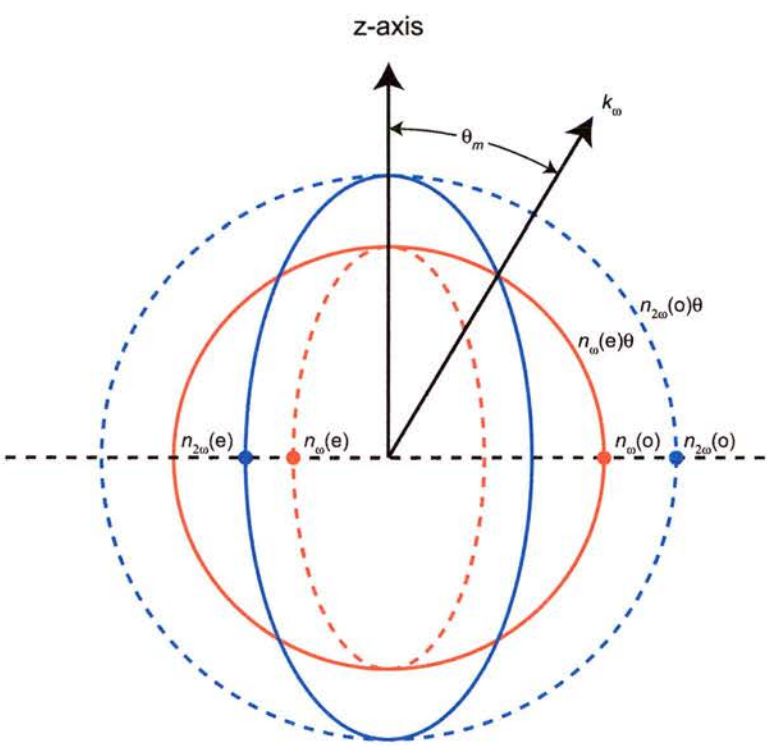

Figure 7.1.2. Index ellipsoid for a birefringent crystal with an ordinary frequency of ω (red) and an extraordinary of 2ω (blue).[35]

The refractive indices encountered by a given frequency propagating as the ordinary or extra-ordinary wave are denoted as n_o and n_e respectively. If $n_e > n_o$ the crystal is said to be positive uniaxial, whereas it is negative uniaxial if $n_e < n_o$. The refractive index dependence of the extraordinary wave on the

angle θ between the optic (-z) axis and the generated second harmonic is given by:[37]

$$\frac{1}{n_e^{\,2}(\theta)} = \frac{\cos^2\theta}{n_o^{\,2}} + \frac{\sin^2\theta}{n_e^{\,2}} \qquad 7.6$$

Assuming $n_e^{2\omega} < n_o^{\omega}$ there exists an angle θ_m where $n_e^{2\omega}(\theta_m) = n_o^{\omega}$. A fundamental beam propagating as an ordinary ray will result in second harmonic propagating in the same direction as an extraordinary ray. As illustrated in Figure 7.1.2. the angle θ_m is determined by the intersection of the surfaces for n_o^{ω} and $n_e^{2\omega}$, and is obtained from 7.6 as being:[37]

$$\frac{1}{\left(n_o^{\omega}\right)^2} = \frac{\cos^2\theta_m}{\left(n_o^{2\omega}\right)^2} + \frac{\sin^2\theta_m}{\left(n_e^{2\omega}\right)^2} \qquad 7.7$$

Solving for θ_m yields:[37]

$$\sin^2\theta_m = \frac{\left(n_o^{\omega}\right)^{-2} - \left(n_o^{2\omega}\right)^{-2}}{\left(n_e^{2\omega}\right)^{-2} - \left(n_o^{2\omega}\right)^{-2}} \qquad 7.8$$

The technique of birefringent phase matching is limited because the largest nonlinear coefficient cannot be successfully phase matched for certain wavelengths.

7.1.1.3. Quasi-phase matching.

The limited phase matching wavelength range of birefringent phase matching can be overcome by the use of quasi-phase matching (QPM). The concept of quasi-phase matching was independently suggested in 1962 by Armstrong and co-workers[38] and then in 1963 Franken and Ward.[39] Interestingly, although quasi-matching was suggested long before birefringent phase matching, the technology was not available to make use of the discovery. Quasi-phase matching involves accepting the phase mismatch which occurs between the fundamental and its second harmonic as they propagate co-linearly through a given crystal and correcting the resultant phase mismatch at regular intervals. This correction can be achieved by a periodic inversion of either the nonlinear coefficient, d_{eff}, or the spontaneous polarisation.[36] A region having the same properties of nonlinear coefficient or spontaneous polarisation is typically

referred to as a domain. Every coherence length, l_c, once the accumulated mismatch reaches π, the domain is reversed thereby bringing the fundamental and second harmonic back into phase. This domain reversal is effected periodically along the length of the crystal and is referred to as a grating period. Quasi-phase matching results in a step-type nonlinear conversion as depicted by curve (c) of Figure 7.1.1., with the domain structure illustrated in the lower portion of the figure.

For quasi-phase-matched nonlinear conversion, the phase mismatch of Equation 7.1 between the fundamental and its second harmonic becomes:[9,35]

$$\Delta k = k_{2\omega} - 2k_{\omega} - k_g \qquad 7.9$$

where k_g is the grating wave vector:

$$k_g = \frac{2\pi m}{\Lambda} \qquad 7.10$$

and m is the order of the phase matching and Λ is the grating poling period.

As discussed above, the optimum nonlinear conversion occurs when $\Delta k = 0$. This occurs when the grating period is:[9]

$$\Lambda = 2ml_c \qquad 7.11$$

Equation 7.11 corresponds to a domain reversal every length l_c along the crystal when the phase between the fundamental and second harmonic equals $m\pi$. When $m = 1$, this is described as a first-order grating although other higher odd orders maybe considered with a subsequent reduction in the nonlinear conversion efficiency.[40] However, such higher orders ease the fabrication requirement for frequency conversion of shorter wavelength sources – for example, near-infrared diode lasers.

7.2. Frequency conversion in lithium niobate.

7.2.1. Introduction.

Lithium niobate is particularly suitable as the nonlinear crystal for second harmonic generation partly because of its modest cost, but more importantly, because it can be readily poled to satisfy the quasi-phase matching conditions discussed in the previous section. In fact, a conversion efficiency of up to 83% has been observed for a pulsed laser with single spatial and spectral mode characteristics.[41]

7.2.2. Fabrication.

There are several techniques that have been employed for the post crystal growth fabrication of periodically poled lithium niobate (PPLN), which include chemical indiffusion,[9,42-44] electron beam writing[45] and external electric fields.[40,46,47] Of these, electric field poling is most commonly employed due to its simplicity and the maturity of the photolithographic techniques used to impart the mask on the lithium niobate wafer. As elecric field poling was used to fabricate the crystals used in this study a brief overview of the technique will be presented, though further elaboration is available in the literature.[48-54]

The grating structure to be produced within the lithium niobate crystal is first deposited on to the +z surface of a wafer using standard lithographic techniques. This mask may either consist of a conductor or an insulator (typically aluminium and photoresist are employed). The mask is then covered with an insulator for a conductive mask or a conductor for an insulating mask.[48] The –z surface of the wafer is untreated. The prepared wafer is held between two O-rings with electrical connection to the poling circuitry being achieved through the use of liquid electrodes, typically consisting of an electrolyte (such as LiCl or KCl) dissolved in deionised water. Such an arrangement of electrodes allows for the application of very high electric fields without breakdown of the sample. The poling circuit is relatively simple and consists of a HV power supply, a current limiting resistor with voltage and current monitors. Periodic poling is thus formed by the application of a single high-voltage pulse (slightly exceeding the coercive field of $\sim 22kV/mm$) along the z-axis.

7.2.3. Experimental.

A PPLN crystal was fabricated for initial evaluation. The crystal was $20mm$ long, $500\mu m$ thick and contained one first-order grating that had a width of $1mm$ and constant period of $5.06\mu m$. This grating period corresponded to frequency conversion of a fundamental wavelength of $980nm$. The facets of the crystal were optically polished but were not AR-coated.

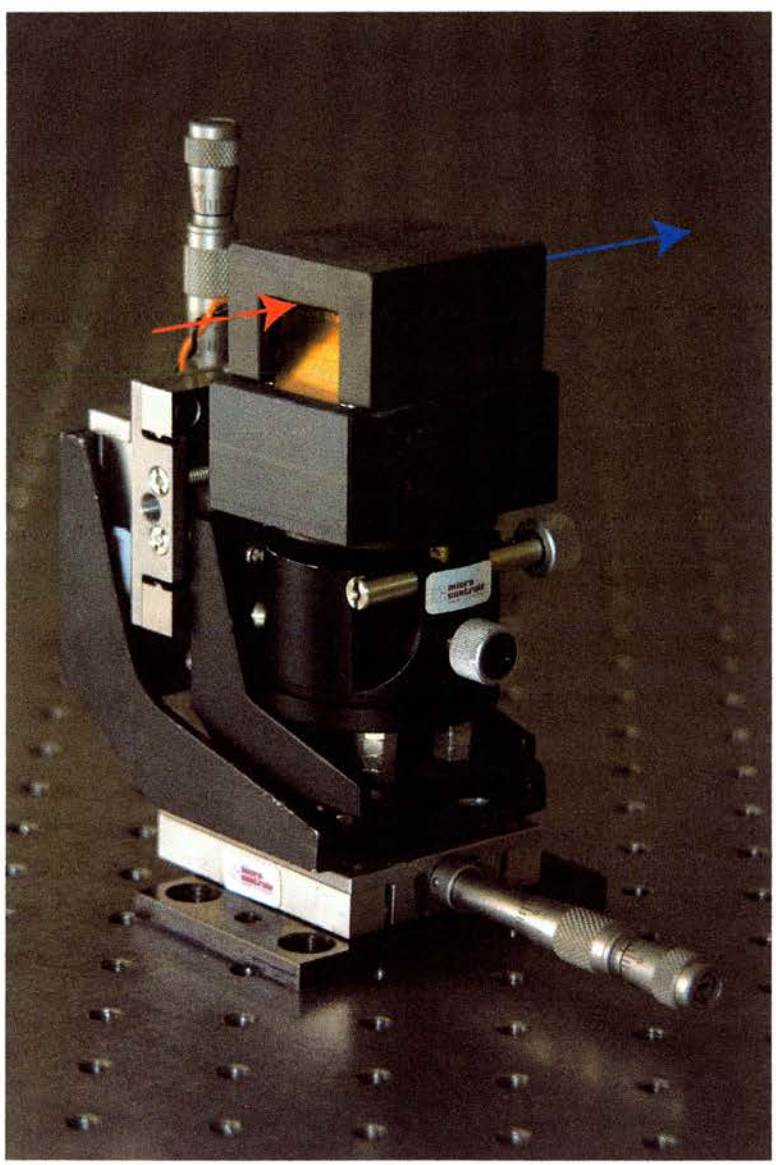

Figure 7.2.1. Photograph of the crystal mount used for PPLN frequency conversion.

To overcome the likelihood of photorefractive damage from the generated second harmonic, the crystal was maintained at a constant temperature, within the phase-matching temperature range of $110 \rightarrow 150^{o}C$, by enclosure in an oven which was stabilised through the use of a thermoelectric cooler (TEC).

The typical temperature drift, as observed on the TEC controller, was $\sim 0.1^{o}C$, which was achieved through the use of the low conductivity material Torlon to isolate the oven from the environment. As shown in Figure 7.2.1., the crystal mount was designed such that it had 6 degrees of freedom to allow maximum flexibility in adjustment of the crystal.

7.2.3.1. Preliminary evaluation with Ti:sapphire laser.

The frequency doubling efficiency of the PPLN crystal was evaluated initially using a Ti:sapphire laser operating in either CW or mode-locked regimes. When mode-locked, the pulse duration was $\sim 1ps$ when measured with an autocorrelator and assuming a Gaussian pulse profile.

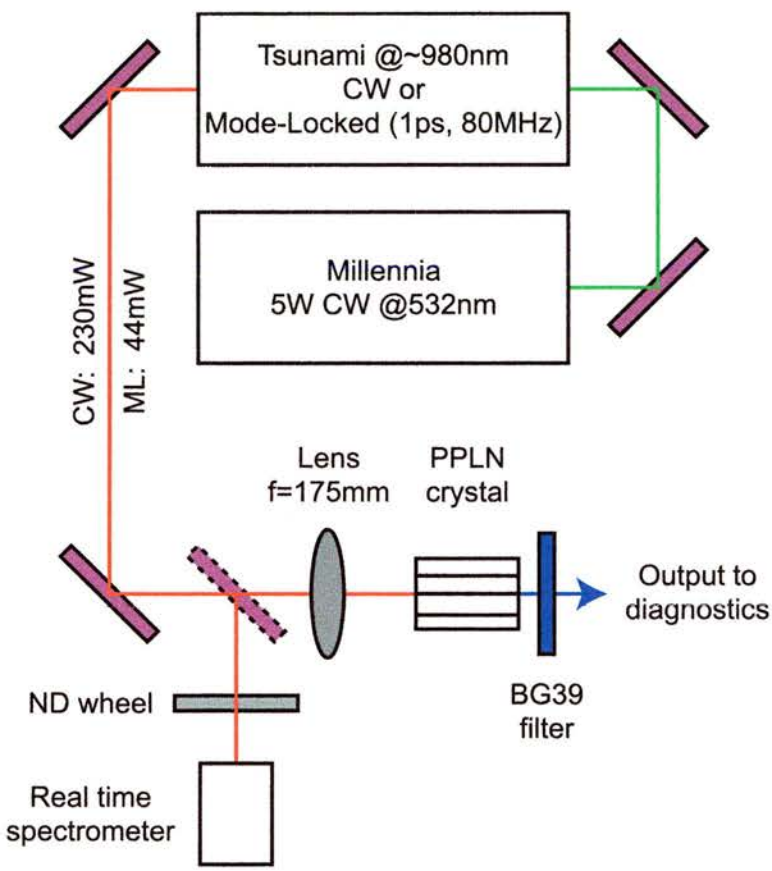

Figure 7.2.2. Optical scheme for PPLN evaluation with Ti:sapphire laser.

The pulse repetition rate was $80MHz$. The emission wavelength of the Ti:sapphire laser was tuned to $980nm$ where the CW and mode-locked output powers were $230mW$ and $44mW$ respectively. The significantly reduced average output power for mode-locked operation can be explained by the difficulty of obtaining stable operation at $980nm$ due to the decreased gain of

Ti:sapphire at such wavelengths, and because of the use of an optical-isolator to prevent feedback which might adversely affect the laser's performance. The experimental scheme used for the assessment is illustrated in Figure 7.2.2. The output from the Ti:sapphire laser was focussed into the crystal by a $175mm$ AR-coated spherical lens. The laser output could also be steered into a real-time spectrometer that was used to monitor the lasing wavelength. The frequency doubled power was measured using a wavelength specific optical power meter, in front of which was attached a BG39 filter to block any unconverted fundamental.

For optimum focussing of the laser and alignment of the PPLN crystal, a maximum frequency doubled power of $3.45mW$ for CW operation was obtained for an incident power of $230mW$. The lasing wavelength was $977nm$ and the oven temperature was $110^{o}C$.

The laser was then mode-locked, with all other conditions of laser focussing, crystal temperature and alignment remaining constant. Under mode-locked operation, an average frequency doubled power of $5.1mW$ was obtained, from a fundamental power of $44mW$. The corresponding peak power of the generated second harmonic was $90W$.

The frequency doubled output power compared favourably with that predicted by a simplified model based on a monochromatic fundamental signal with the above conditions of input power (CW and pulsed operations), wavelength and temperature.

7.2.3.2. Crystal evaluation using a diode laser.

Figure 7.2.3. illustrates the optical scheme used for the frequency doubling of a gain-switched InGaAs diode laser in which a 30X AR-coated aspheric lens was used to collimate the laser output and a $25.4mm$ focal length cylindrical lens was used to focus the beam, in the crystal plane, into the PPLN crystal. Since the PPLN crystal required a vertically polarised input, a $\lambda/2$ waveplate was positioned between the diode laser and PPLN crystal.

For an incident CW power of $108mW$, the maximum second harmonic output power observed was $150\mu W$. When the diode laser was gain-switched the

maximum average second harmonic output was approximately $100\mu W$. The simplified model based on a monochromatic fundamental signal predicted that for input powers of $108mW$ for CW and the same average power for pulsed operation (peak power of $1.1W$) the average second harmonic output powers should have been $0.5mW$ and $3.35mW$ respectively.

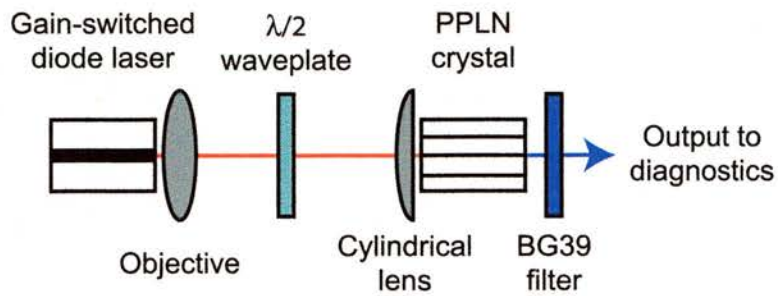

Figure 7.2.3. Optical scheme used for frequency doubling a diode laser with a PPLN crystal.

Both of the observed frequency doubled output power levels were significantly lower than those implied by theory and for the previously recorded experimental results obtained using the Ti:sapphire laser. These observations are explained by the fact that the spectral beam quality of the Ti:sapphire laser is much superior to that of the diode laser. Also, the spatial beam quality of the diode laser is slightly inferior to that of the Ti:sapphire laser, although in diode laser terms, it is very good $\left(M^2 \approx 1.1\right)$. Given that both the spatial and spectral beam quality are of crucial importance for efficient second harmonic conversion, this explains why the second harmonic generation was compromised for the gain-switched diode laser because it had an enlarged spectral bandwidth when operating in this regime. Specifically, the wavelength bandwidth over which second harmonic conversion will efficiently occur, as determined by the spectral acceptance bandwidth of the PPLN was $\sim 1nm$, whereas the spectral bandwidth of our gain-switched diode laser was $11nm$ for a DC bias of $100mA$.

It therefore follows that to achieve more efficient second harmonic generation with a gain-switched diode laser a scheme was required whereby the complete spectral bandwidth of the output could be properly accommodated. To achieve this, a crystal was and fabricated with a grating for which the period increased smoothly and uniformly with length. The resultant aperiodically-poled lithium niobate (a-PPLN) crystal was designed to be compatible with the spectral

characteristics that were obtained from the sonogram experiments of Chapter 4. for a gain-switched diode laser.

7.2.3.3. Aperiodically poled lithium niobate crystal.

Whereas frequency conversion from the single period of a periodically-poled structure will only be efficient over a narrow wavelength range, the varying grating period of an a-PPLN crystal can be designed to yield efficient second harmonic generation over an enlarged spectral range. This is due to the fact that each section of the aperiodic grating is tailored to a specific wavelength range, such that an aperiodically-poled grating can be thought of as many "component" periodically-poled gratings. The acceptance spectral bandwidth can thus be engineered by simply altering the grating design.

Grating number	Entrance period Λ_i /μm	Chirp ps/nm	Spectral bandwidth nm		Exit period Λ_f/μm
8	5.304	1	23	8	4.906
7	5.129	8	3	7	5.077
6	5.138	6	4	6	5.069
5	5.144	5	5	5	5.062
4	5.155	4	6	4	5.052
3	5.172	3	8	3	5.035
2	5.205	2	12	2	5.002
1	5.103	-	<1	1	5.103

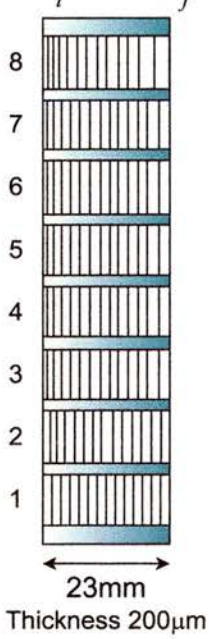

Figure 7.2.4. Grating parameters for the a-PPLN crystal.

The a-PPLN crystal fabricated for this work, which is illustrated in Figure 7.2.4., was $23mm$ long, $200\mu m$ thick and contained 8 gratings each of $0.5mm$ width corresponding to different crystal spectral acceptance bandwidths. Grating one was for reference purposes and was periodic with a period of $5.103\mu m$. The remaining seven gratings were aperiodic centred on a spatial period of $5.103\mu m$ and designed for laser spectral bandwidths that ranged from $3nm$ to $23nm$.

For an incident average power of $108mW$ from the gain-switched laser diode, a maximum second harmonic power of $3.6mW$ was obtained from grating 2. This grating had a spectral bandwidth of $12nm$, which was similar to that of the laser spectrum at that output power. The corresponding second harmonic peak power was $83mW$. Measurements using an electron-optical streak camera yielded a second harmonic pulse duration of $\sim 22ps$. It should be noted that the uncoated crystal had facet reflectivities of $\sim 14\%$, resulting in an actual launched fundamental power of $90mW$. As expected, it was observed that the a-PPLN crystal exhibited a considerably larger temperature acceptance bandwidth than the PPLN counterpart, ($\sim 10^{o}C$ compared with $\sim 0.1^{o}C$) and this provided a greater stability for frequency doubling.

7.3. Frequency conversion using KTP waveguides incorporating a Bragg reflector.

Potassium titanyl phosphate (KTP) is a near-ideal nonlinear crystal for the frequency doubling of diode laser sources since it can be phase matched within the operational temperature of most commercial devices. It is also less prone to photorefractive damage than lithium niobate. It has a modest cost, and can be periodically poled to satisfy the quasi-phase matching conditions that offer increased second harmonic conversion efficiencies for pulsed sources.

Nonlinear crystals having waveguide structures[42,43,55] can be readily fabricated and provide confinement of the pump and second harmonic radiation to the grating throughout the crystal length. Such waveguides are of great interest due to the reduced interaction area and resultant increase in second harmonic generation efficiency that can be obtained. Given the comparable dimensions of the emission cross-section from a diode laser and the typical waveguide dimension, efficient coupling can be achieved through the use of two suitable microscope objectives. The waveguide also negates the need for confocal focussing.

7.3.1. KTP-crystal considerations.

The potassium (P) ions in KTP are losely bonded in an anistropic orthorhombic unit cell structure. As shown in Figure 7.3.1.[56] the KTP crystal structure as

viewed along the -z to +z axis clearly illustrates *channels* along which potassium ions (red circles) may diffuse. The channels result in an ionic conductivity along the z-axis that is many orders of magnitude greater than that along any other lateral direction. This increased ionic conductivity along the z-axis means that electric-field poling[57-60] of KTP is complicated due to the resultant increased poling currents. However, the lose bonding of the potassium ions make KTP an ideal nonlinear crystal for the ion exchange[61-65] process used in the fabrication of the waveguide structures discussed in the subsequent sections.

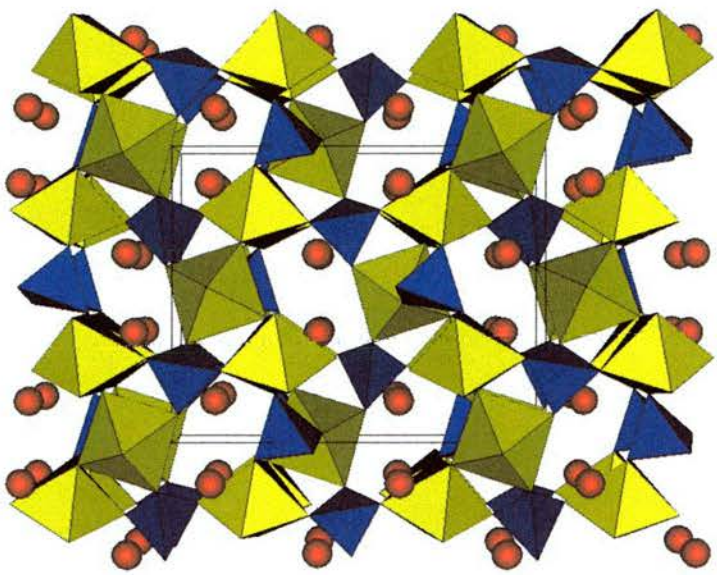

Figure 7.3.1. KTP crystal structure viewed along the –z to +z axis.[56]

The work of the previous section related to the PPLN crystals illustrated how the second harmonic efficiency was severally compromised if the acceptance bandwidth of the grating structure contained within the crystal was not comparable to the spectral bandwidth of the laser output. The solution there was to design an aperiodic grating that could handle the entire spectral bandwidth from the gain-switched diode laser. Interestingly, from the work discussed in Chapter 5. it was demonstrated that the spectral bandwidth obtained from the gain-switched diode laser could be substantially reduced if optical feedback was present, whether or not that feedback was spectrally selective. Therefore, if it were somehow possible to combine such an optical feedback element with the second harmonic generation structure[66,67] then the

spectral bandwidth of the gain-switched diode laser would be significantly reduced such that a periodic grating could be utilised for second harmonic conversion and the acceptance bandwidth limitation would not longer be an issue.

To achieve efficient second harmonic generation from the gain-switched diode laser used in this work, a two-section KTP waveguide crystal was designed and fabricated by Adv-R Inc. The waveguide that provided 2D confinement, had a periodic grating structure for quasi-phase matched second harmonic conversion and a Bragg grating structure for spectrally selective optical feedback. A Bragg grating structure is a key element in the design of this crystal, and follows from the work of Chapters 5. and 6. where it was discussed how the gain-switched diode laser responded favourably to wavelength selective optical feedback. In Chapter 5. it was shown that non-resonant self-injection seeding of the diode laser could yield a marked reduction of the spectral bandwidth of the pulses resulting in near Fourier-transform-limited durations. The crystal discussed here makes use of this effect, which means that a periodically poled grating can now be used for the second harmonic conversion. It is believed that such a PP-KTP waveguide crystal with a Bragg reflector currently marks the apogee of crystal design for use with diode lasers.

7.3.2. Fabrication.

The steps undertaken in the fabrication of the PP-KTP waveguide crystals used in this study are illustrated in Figure 7.3.2. The KTP wafer with dimensions of approximately $25*25mm$ is first spin coated with a layer of photoresist. (Step (i) in Figure 7.3.2.) A mask designed and fabricated with the desired grating structure was then imaged onto the photoresist using a 5 to 1 photolithographic technique, step (ii) in Figure 7.3.2. The wafers were subsequently developed (step (iii)) to remove the exposed regions of photoresist before being coated with a thin layer of aluminium (step (iv)). The patterned wafer that may contain up to 8 distinct waveguide configurations was then cleaved using a manual scriber before the end facets are optically polished with a Logitech LP30 polishing machine. The individual crystals were $10mm$ long, $3mm$ wide, $1mm$ thick and contained up to 50 waveguides. Ion exchange (step (v)) of the

potassium ions is performed by immersion of the individual crystals in a molten nitrate salt bath of MNO_3, where M is typically barium, caesium, potassium, rubidium, sodium, titanium or some combination, though in this case rubidium (Rb) and barium (Ba) were used. The addition of divalent ions in the form of $BaNO_3$ alters both the diffusion rate and the resultant waveguide refractive index profile. Other divalent ions, such as calcium or strontium may be substituted in place of barium resulting in different refractive index profiles.[56] The crystals are submerged in the salt bath with a temperature of $\sim 350^{o}C$ for approximately 30 minutes, during which ions from the nitrate bath exchange with potassium ions from beneath the unmasked regions of the KTP crystal along the *z*-axis channels. The regions where ion exchange has occurred have a slightly increased refractive index compared with that of the bulk material. This raised refractive index profile results in a 2D optical waveguide, bounded above by air. The completed PP-KTP crystal contains a segmented Bragg grating section with a Bragg wavelength determined by the ion exchange parameters and the physical dimensions of the waveguide, that is, period, width and depth.

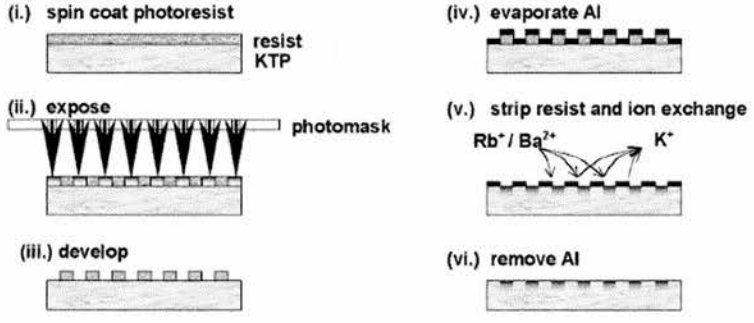

Figure 7.3.2. Steps for the fabrication of a PP-KTP waveguide crystal.

The waveguides fabricated for this work had a section designed for quasi-phase-matched (QPM) second harmonic generation followed by a Bragg grating section designed to reflect $30-40\%$ of the fundamental at the QPM wavelength. The crystal contained ~ 50 waveguides in three groups, with a spacing of $\sim 30\mu m$ between adjacent waveguides. Figure 7.3.3. illustrates a section of the crystal, in which the waveguides are clearly visible. Each group had a different Bragg grating period, and the spacing between adjacent groups was $\sim 50\mu m$.

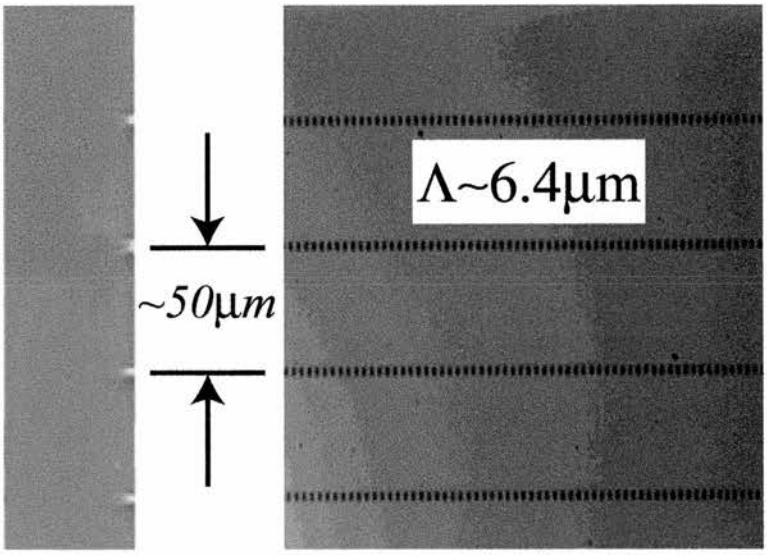

Figure 7.3.3. PP-KTP waveguide crystal.

The $3\mu m$ wide ridge-waveguide of the commercial InGaAs/GaAs single-mode devices used in this work was directly comparable to the KTP waveguide dimensions of $\sim 4*4\mu m$. The PP-KTP crystals fabricated for this study contained 3 grating periods for the fundamental Bragg wavelengths of 972, 976, and $982nm$.

7.3.3. Experimental.

The experimental scheme for frequency doubling of the near-infrared diode lasers using a KTP Bragg waveguide crystal is illustrated in Figure 7.3.4. It consisted of the gain-switched diode laser that was collimated by an AR-coated 30X aspheric objective lens and a second aspheric objective lens to couple into the waveguide. Different objectives in the range 10X to 40X were evaluated, with 30X demonstrating the best performance as determined by the observed second harmonic efficiency. Because the KTP crystal required a vertically polarised input, a $\lambda/2$ waveplate was positioned between the diode laser and KTP crystal. The KTP crystal was mounted such that its temperature could be controlled precisely through the use of a thermo-electric cooler, the typical temperature drift being $\sim 0.1^{o}C$. The crystal temperature also gave a small degree of control over the fundamental emission wavelength by altering the Bragg grating period. Due to the small dimensions of the waveguide structure the KTP crystal assembly was mounted on a piezo-controlled waveguide stage

that greatly assisted with the optical coupling between the diode laser and the waveguides in the nonlinear crystal.

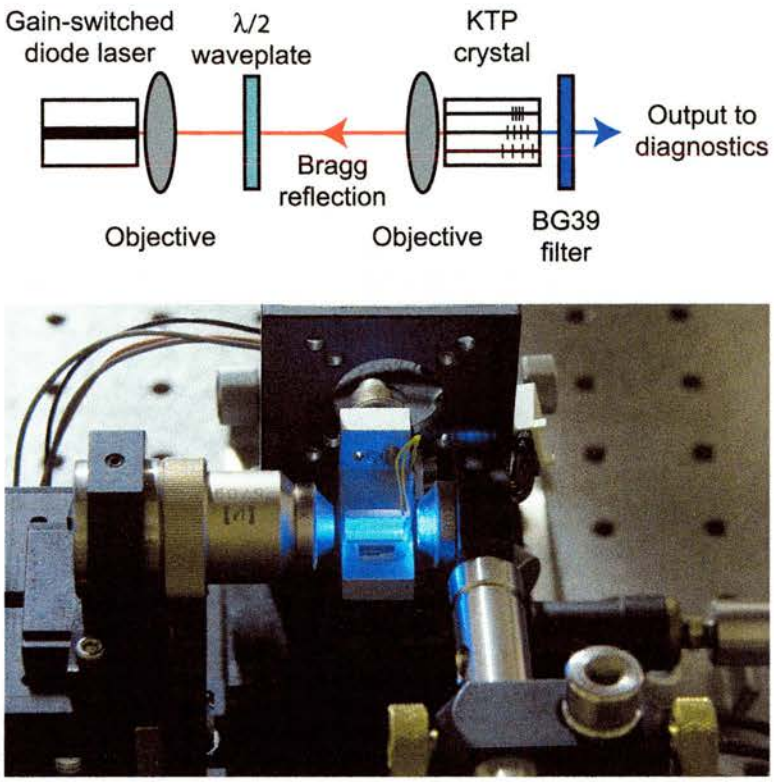

Figure 7.3.4. Optical scheme used for frequency doubling a diode laser with a KTP Bragg waveguide crystal.

As previously discussed the maximum CW output power from the InGaAs/GaAs ridge waveguide diode lasers used in this study was $210mW$, with a corresponding FWHM spectral bandwidth of $<1nm$. When gain switched the maximum average and peak powers were $150mW$ and $1.45W$ respectively, with a corresponding FWHM spectral bandwidth of $\sim 25nm$. Operation of the diode laser at a DC bias of $210mA$ resulted in a duration slightly increased from its minimum value of $30ps$. The peak output power was not unduly compromised by the increase in pulse duration due to the increased average output power. For DC bias levels $\gg 150mA$ gain-switched operation of the diode laser would be compromised due to insufficient amplitude of the supplementary sinusoidal modulation, resulting in both spectral and temporal instability. Stable gain-switched operation at such elevated DC bias levels could easily be achieved by application of increased modulation amplitude to the diode laser, with practical solutions discussed in Chapter 3.

Figure 7.3.5. illustrates the temporal (upper) and spectral (lower) output from the gain-switched diode laser at $150mW$ with no KTP crystal present, and hence no optical feedback.

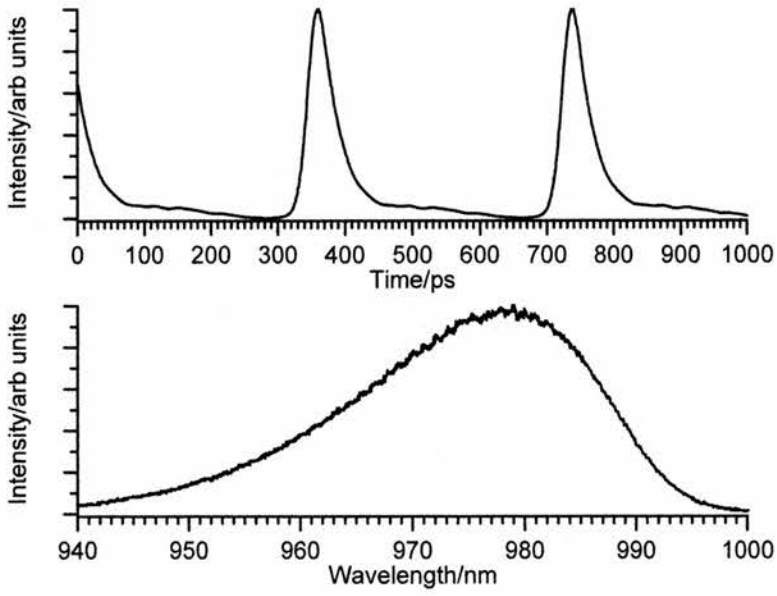

Figure 7.3.5. Diode laser temporal (upper) and spectral (lower) output profiles without optical feedback.

The corresponding FWHM values of pulse duration and spectral bandwidth were $39ps$ and $24nm$ respectively. The asymmetry and slight tail present on the trailing edge of the temporal profile were due to the elevated DC bias required for an output power of $150mW$.

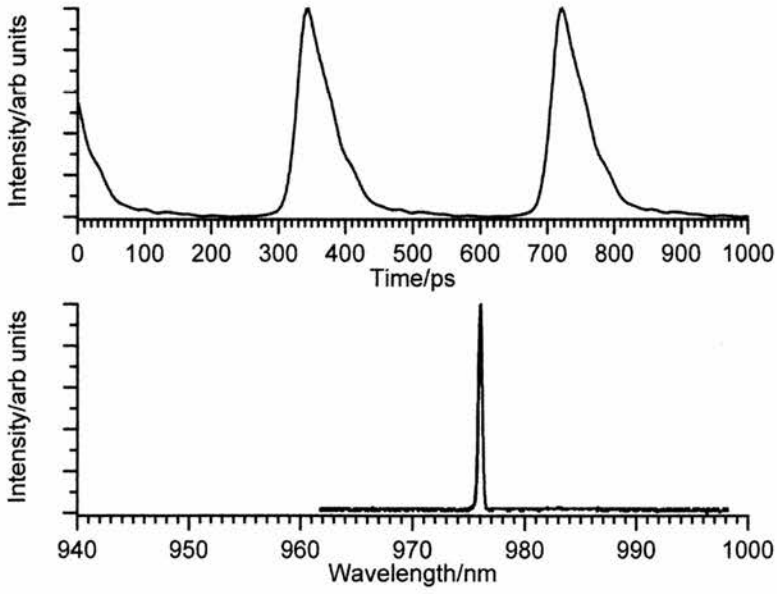

Figure 7.3.6. Diode laser temporal (upper) and spectral (lower) output profiles with optical feedback.

These temporal features that were not so pronounced for lower DC bias levels. (The Fabry-Perot mode structure is not evident in the spectrum due to the limited resolution of the real-time spectrometer used for the measurement.)

Temporal and spectral outputs typical of those observed under optimum operating conditions of the gain-switched diode laser may be found in Figures 3.3.3. and 3.3.7.

When the KTP crystal was aligned such that non-resonant optical feedback from the Bragg section was present there was an increase in the pulse duration, to $\sim 48ps$ (Figure 7.3.6 upper) and a marked reduction in the spectral bandwidth, to $\sim 0.40nm$ (Figure 7.3.6 lower). These results are illustrated in Figure 7.3.6. and were as expected when compared with the self-injection optical feedback effect obtained when "bulk" optics were used. Similarly, with the schemes that utilised bulk optics the there was a significant reduction in the spectral bandwidth and a slight increase in the pulse duration. The increase in the pulse duration appeared to be directly proportional to the optical feedback level and/or coupling efficiency. There was no apparent effect on the spatial characteristics of the gain-switched diode laser due to the optical feedback from the Bragg grating section. The Bragg grating structure within the PP-KTP waveguide resulted in the formation of an external cavity with a length of $\sim 250mm$, and a corresponding cavity frequency of $0.60GHz$. Due to the non-resonant nature of the optical feedback provide by the Bragg grating in the KTP waveguide there existed certain diode laser modulation frequencies that could not be used due to them being a harmonic of the cavity frequency. For such harmonic frequencies the spectral output of the gain-switched diode laser reverted back to that characteristic of the solitary device, and as a consequence of which the second harmonic efficiency was compromised.

The non-resonant condition of the modulation frequency imposed by the nature of the optical feedback was not an issue so long as it was considered. Decreasing the length of the external cavity, which serves to increase the cavity frequency, will reduce the effect of harmonics by increasing the harmonic spacing. The harmonic frequency issue does however place a constraint on the maximum external cavity length that can successfully be used, since for long cavities the fundamental frequency is sufficiently low that exist very few

"windows" where a spectral reduction is observed. This long cavity issue was not a problem since a compact footprint was an experimental objective.

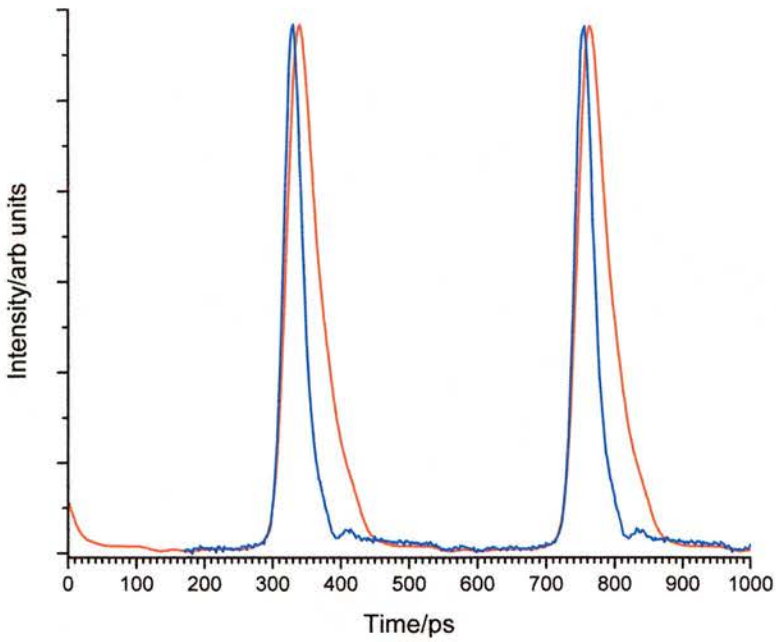

Figure 7.3.7. Temporal output from the injection-seeded gain-switched diode laser for (red) fundamental and (blue) its second harmonic.

Illustrated in Figure 7.3.7. is the temporal output from the gain-switched diode laser when injected-seeded by the Bragg section of the PP-KTP waveguide crystal. The fundamental is shown as the red line whereas its second harmonic is shown as the blue line, with pulse durations of $48ps$ and $24ps$ respectively.

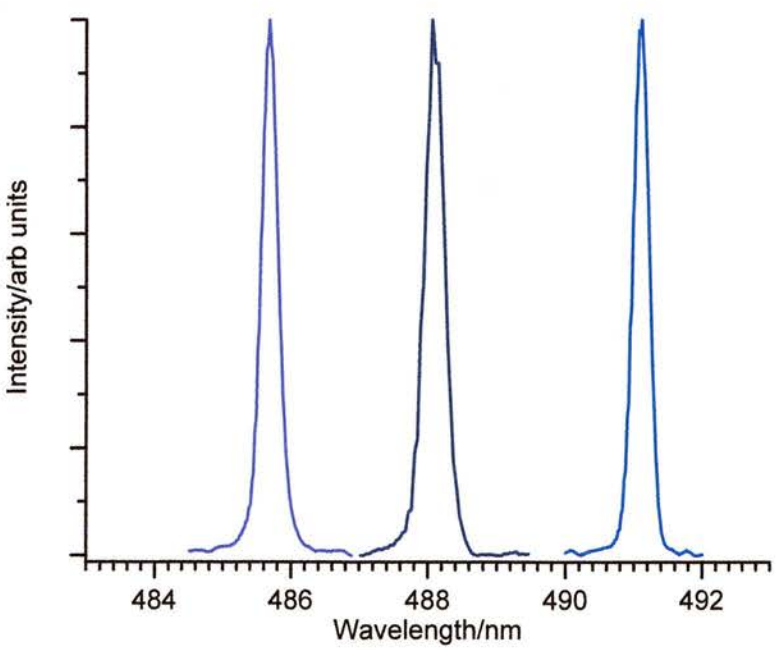

Figure 7.3.8. Second harmonic spectra corresponding to different Bragg grating periods.

Figure 7.3.8. illustrates the three distinct second harmonic wavelengths that were obtained by utilising waveguides that had a Bragg section with a period at different fundamental centre wavelengths. The average spectral bandwidth of the second harmonic was $0.30nm$.

Table 7.3.1. summarises the frequency doubled results obtained from the gain-switched diode laser using the PP-KTP waveguide crystal. These results were all for an average incident fundamental power of $144mW$. It should be noted that the quoted fundamental power does not take into account the reflection from the input facet of the PP-KTP crystal.

Table 7.3.1. Summary of the results obtained from a diode laser that was frequency doubled with a PP-KTP waveguide crystal.

Fundamental wavelength. λ_ω / nm	972	976	982
Second harmonic wavelength. $\lambda_{2\omega} / nm$	486	488	491
Second harmonic pulse duration. $\tau_{2\omega} / ps$	~24	~24	~24
Crystal temperature. $T / °C$	29.6	25.6	22.4
Average second harmonic power. $P_{2\omega} / mW$	6.2 (7.3)	3.5 (4.1)	2.4 (2.9)
Peak second harmonic power. $P_{2\omega} / mW$	130 (152)	73 (85)	50 (60)

The second harmonic powers quoted in parenthesis are those that take account of the losses due to the BG39 filter required for the optical power meter.

The maximum second harmonic average and peak powers were $7.3mW$ and $152mW$ respectively for the $486nm$ spectral range. The variation in the observed second harmonic output powers obtained for the different wavelengths might be attributed to the quality of the individual waveguides.

7.4. Conclusions.

The work described in this chapter illustrated that frequency doubling of a near-infrared diode laser is a simple and cost effective method that enables the blue spectral region to be readily accessed. The resultant schemes discussed in the context of this work have the potential to be compact and opto-mechanically robust.

The aperiodically-poled lithium niobate crystal that was designed and fabricated enabled the entire spectral bandwidth of the gain-switched diode laser output to be efficiently utilised. The average output power of the second harmonic was

$3.6mW$ (with a corresponding peak power of $82mW$) for an incident fundamental power of $108mW$, as summarised in Table 7.4.1.

Blue light was also generated using a periodically poled KTP waveguide crystal incorporating a Bragg grating section for self-injection optical feedback of the diode laser. Impressively increased average powers up to $7.3mW$ with picosecond pulse durations of $\sim 24ps$ were obtained from the frequency-doubled gain-switched diode laser utilising a relatively simple optical scheme that only consisted of two AR-coated 30X aspheric objectives and a $\lambda/2$ waveplate.

Table 7.4.1. Summary of results obtained from frequency doubling of a gain-switched diode laser.

	a-PPLN	PP-KTP		
Fundamental wavelength. λ_ω/nm	980	972	976	982
Second harmonic wavelength. $\lambda_{2\omega}/nm$	490	486	488	491
Second harmonic pulse duration. $\tau_{2\omega}/ps$	22	~24	~24	~24
Crystal temperature. $T/°C$	129	29.6	25.6	22.4
Average second harmonic power. $P_{2\omega}/mW$	3.1 (3.6)	6.2 (7.3)	3.5 (4.1)	2.4 (2.9)
Peak second harmonic power. $P_{2\omega}/mW$	70 (82)	130 (152)	73 (85)	50 (60)

The second harmonic powers quoted in parenthesis are those that take account of the losses due to the BG39 filter required for the optical power meter.

The waveguides in the periodically-poled KTP crystal incorporated a Bragg grating section for reflection at one of three different fundamental wavelengths. This enabled the frequency doubled output of one diode laser to be assessed at three different second harmonic wavelengths, as summarised in Table 7.4.1.

Such a PP-KTP waveguide crystal incorporating a Bragg grating section represents the pinnacle of second harmonic generation studies with the gain-switched diode lasers. The optical feedback from the Bragg grating means that the broad spectral bandwidth usually associated with such a laser source is no longer an issue of concern. There is also significant scope for further improvement in the design of the crystal and optical configuration.

KTP crystals have an advantage over the lithium niobate counterparts in that high crystal temperatures are not required with KTP that can be phase matched

successfully at room temperature. By contrast, lithium niobate requires temperatures in the range $110 \rightarrow 150^{o}C$ for phase matching. The lower phase matching temperatures of KTP make it entirely feasible to mount a PP-KTP crystal and diode laser together on the same assembly, resulting in an exceedingly compact blue laser source. However, lithium niobate does have a slightly higher nonlinear optical coefficient (d_{33}), of $\sim 34 pm/V$ compared with that of KTP $(\sim 17 pm/V)$, such that if temperature control is not an issue then schemes utilising lithium niobate nonlinear crystals would be the superior.

7.5. Future work.

Improvements in the overall second harmonic efficiency could be obtained through the application of appropriate anti-reflection coatings to the crystal facets, such that residual reflectivities could be reduced. Also, the single-mode InGaAs/GaAs ridge waveguide diode lasers used in this study are now available with CW output powers up to $450mW$. An increased second harmonic output would result from the increased power available at the fundamental frequency if such a device were suitably gain-switched. In this context "suitably gain-switched" relates to an increase in the amplitude of the sinusoidal modulation applied to the diode laser. The impedance mismatch between the 50Ω microwave cable and the diode laser results in a reflection, reducing the RF power that is actually applied to the diode laser. This RF power delivered to the laser can be increased by either (i) improved impedance matching of the present $37dBm$ amplifier, which is currently underway or (ii) an amplifier with a higher output power.

The fabrication of waveguide structures in periodically-poled lithium niobate crystals to provide confinement of the pump beam to the grating throughout the crystal length is under consideration. As demonstrated with PP-KTP, such a waveguide structure eases focussing and thereby offers the potential to increase substantially the efficiency of the second harmonic conversion.

7.6. References.

1. Nakamura, S., "High-power InGaN-based blue laser diodes with a long lifetime," *Journal of Crystal Growth*, vol. 195, pp. 242-247, 1998.
2. Nakamura, S., "Present status of InGaN-based laser diodes," *Physica Status Solidi a-Applied Research*, vol. 176, pp. 15-22, 1999.
3. Nakamura, S., "InGaN-based blue light-emitting diodes and laser diodes," *Journal of Crystal Growth*, vol. 202, pp. 290-295, 1999.
4. Ohya, J., Tohmon, G., Yamamoto, K., Taniuchi, T. & Kume, M., "Picosecond Blue-Light Pulse Generation By Frequency Doubling of a Gain-Switched GaAlAs Laser Diode With Saturable Absorbers," *Applied Physics Letters*, vol. 56, pp. 2270-2272, 1990.
5. Ohya, J., Tohmon, G., Yamamoto, K., Taniuchi, T. & Kume, M., "Generation of Picosecond Blue-Light Pulse By Frequency Doubling of a Gain-Switched GaAlAs Laser Diode Having Saturable Absorber," *IEEE Journal of Quantum Electronics*, vol. 27, pp. 2050-2059, 1991.
6. Goldberg, L. & Mehuys, D., "Blue-Light Intensity Modulation in a Frequency-Doubled Tapered Amplifier Modelocked Laser," *Electronics Letters*, vol. 30, pp. 1296-1297, 1994.
7. Kitaoka, Y., Yokoyama, T., Mizuuchi, K., Yamamoto, K. & Kato, M., "Modulated blue second harmonic generation using direct modulation of distributed Bragg reflector laser diode," *Electronics Letters*, vol. 33, pp. 1638-1639, 1997.
8. Uchiyama, Y., Tsuchiya, M., Liu, H. F. & Kamiya, T., "Efficient ultraviolet-light (345-nm) generation in a bulk LiIO3 crystal by frequency doubling of a self-seeded gain-switched AlGaInP Fabry-Perot semiconductor laser," *Optics Letters*, vol. 22, pp. 78-80, 1997.
9. Webjorn, J., Siala, S., Nam, D. W., Waarts, R. G. & Lang, R. J., "Visible laser sources based on frequency doubling in nonlinear waveguides," *IEEE Journal of Quantum Electronics*, vol. 33, pp. 1673-1686, 1997.
10. Batchko, R. G. *et al.*, "Continuous-wave quasi-phase-matched generation of 60 mW at 465 nm by single-pass frequency doubling of a laser diode in backswitch-poled lithium niobate," *Optics Letters*, vol. 24, pp. 1293-1295, 1999.
11. Sugita, T., Mizuuchi, K., Kitaoka, Y. & Yamamoto, K., "31%-efficient blue second-harmonic generation in a periodically poled MgO : LiNbO3 waveguide by frequency doubling of an AlGaAs laser diode," *Optics Letters*, vol. 24, pp. 1590-1592, 1999.
12. Uchiyama, Y. & Tsuchiya, M., "Generation of ultraviolet (335-nm) light by intracavity frequency doubling from active mode-locking action of an external-cavity AlGaInP diode laser," *Optics Letters*, vol. 24, pp. 1148-1150, 1999.
13. Cheng, Z. X., Zhang, S. J., Zhou, G. Y., Han, J. R. & Chen, H. C., "Magnesium-doped potassium lithium niobate crystal and its properties," *Progress in Crystal Growth and Characterization of Materials*, vol. 40, pp. 153-160, 2000.
14. Takigawa, S. *et al.*, "780 Nm GaAlAs Distributed Feedback Lasers," *Solid-State Electronics*, vol. 32, pp. 577-581, 1989.
15. Takigawa, S. *et al.*, "50 Mw Stable Single Longitudinal Mode-Operation of a 780nm GaAlAs DFB Laser," *IEEE Journal of Quantum Electronics*, vol. 25, pp. 1489-1494, 1989.
16. Oberg, M. *et al.*, "Wide Continuous Wavelength Tuning of a Narrow Linewidth DBR Laser," *IEEE Photonics Technology Letters*, vol. 4, pp. 230-232, 1992.
17. Goldberg, L. & Mehuys, D., "Blue-Light Generation Using a High-Power Tapered Amplifier Mode-Locked Laser," *Applied Physics Letters*, vol. 65, pp. 522-524, 1994.
18. Woll, D. *et al.*, "1 W of blue 465-nm radiation generated by frequency doubling of the output of a high-power diode laser in critically phase- matched LiB3O5," *Optics Letters*, vol. 24, pp. 691-693, 1999.
19. Nayfeh, M. H. *et al.*, "Second harmonic generation in microcrystallite films of ultrasmall Si nanoparticles," *Applied Physics Letters*, vol. 77, pp. 4086-4088, 2000.

20. Goncalves, A. L. & Konotop, V. V., "Second harmonic generation in a two-dimensional diatomic lattice," *Physical Review B*, vol. 62, pp. 14105-14112, 2000.

21. Yamauchi, T. *et al.*, "Second harmonic generation in CdTe plate by free electron laser," *Japanese Journal of Applied Physics Part 1-Regular Papers Short Notes & Review Papers*, vol. 39, pp. 5912-5913, 2000.

22. Clark, H. A., Campagnola, P. J., Wuskell, J. P., Lewis, A. & Loew, L. M., "Second harmonic generation properties of fluorescent polymer- encapsulated gold nanoparticles," *Journal of the American Chemical Society*, vol. 122, pp. 10234-10235, 2000.

23. Liu, Q. M., Zhao, X. J. & Gan, F. X., "Second harmonic generation in the system Ge-As-S and analysis of the poling mechanism," *Acta Physica Sinica*, vol. 49, pp. 1726-1730, 2000.

24. Yu, J. *et al.*, "Second harmonic generation in a LiNbO3 crystal fiber," *Journal De Physique Iv*, vol. 10, pp. 113-114, 2000.

25. Misuryaev, T. V. *et al.*, "Second harmonic generation in the lamellar ferrielectric CuInP2S6," *Solid State Communications*, vol. 115, pp. 605-608, 2000.

26. Niedermeier, S., Schillinger, H., Sauerbrey, R., Adolph, B. & Bechstedt, F., "Second-harmonic generation in silicon carbide polytypes," *Applied Physics Letters*, vol. 75, pp. 618-620, 1999.

27. Hoshi, H., Chung, D. H., Ishikawa, K. & Takezoe, H., "Second-harmonic generation in distributed feedback ferroelectric liquid crystal cells," *Bulletin of Materials Science*, vol. 22, pp. 439-441, 1999.

28. Casalboni, M. *et al.*, "Second-harmonic generation in PMMA films doped with organometallic complexes," *Radiation Effects and Defects in Solids*, vol. 150, pp. 237-242, 1999.

29. Fazio, V. S. U., Lagerwall, S. T., Busson, P., Hult, A. & Motschmann, H., "Phase-matched second-harmonic generation in a ferroelectric liquid crystal waveguide," *Applied Physics Letters*, vol. 77, pp. 319-321, 2000.

30. Lammers, D., Betzler, K., Xue, D. & Zhao, J., "Optical second-harmonic generation in benzophenone," *Physica Status Solidi a-Applied Research*, vol. 180, pp. R5-R7, 2000.

31. Mitchell, S. A., Boukherroub, R. & Anderson, S., "Second harmonic generation at chemically modified Si(111) surfaces," *Journal of Physical Chemistry B*, vol. 104, pp. 7668-7676, 2000.

32. Zhang, G. H. *et al.*, "Blue-violet light second harmonic generation with CMTC crystals," *Journal of Materials Science Letters*, vol. 19, pp. 1255-1257, 2000.

33. Champert, P. A., Popov, S. V., Taylor, J. R. & Meyn, J. P., "Efficient second-harmonic generation at 384 nm in periodically poled lithium tantalate by use of a visible Yb-Er-seeded fiber source," *Optics Letters*, vol. 25, pp. 1252-1254, 2000.

34. Goldoni, G., "Optimal design and quantum limit for second harmonic generation in semiconductor heterostructures," *Journal of Applied Physics*, vol. 89, pp. 1755-1758, 2001.

35. Yariv, A. *Optical Electronics* (Saunders College Publishing, 1991).

36. Fejer, M. M., Magel, G. A., Jundt, D. H. & Byer, R. L., "Quasi-Phase-Matched 2nd Harmonic-Generation - Tuning and Tolerances," *IEEE Journal of Quantum Electronics*, vol. 28, pp. 2631-2654, 1992.

37. Hawkes, J. & Latimer, I. *Lasers: Theory and Practice* (Prentice Hall, 1995).

38. Armstrong, J. A., Bloembergen, N., Ducuing, J. & Pershan, P. S., "Interactions between light waves in a nonlinear dielectric," *Physical Review*, vol. 127, pp. 1918-1939, 1962.

39. Franken, P. A. & Ward, J. F., "Optical harmonics and nonlinear phenomena," *Review Modern Physics*, vol. 35, pp. 23-39, 1963.

40. Webjorn, J., Pruneri, V., Russell, P. S., Barr, J. R. M. & Hanna, D. C., "Quasi-Phase-Matched Blue-Light Generation in Bulk Lithium- Niobate, Electrically Poled Via Periodic Liquid Electrodes," *Electronics Letters*, vol. 30, pp. 894-895, 1994.

41. Taverner, D. *et al.*, "Highly efficient second harmonic and sum frequency generation of nanosecond pulses in a cascaded erbium-doped fiber periodically poled lithium niobate source," *Optics Letters*, vol. 23, pp. 162-164, 1998.

42. Cao, X. F., Rose, B., Ramaswamy, R. V. & Srivastava, R., "Efficient Direct Diode-Laser Frequency Doubling in Quasi-Phase- Matched Linbo3 Wave-Guides," *Optics Letters*, vol. 17, pp. 795-797, 1992.

43. Amin, J. *et al.*, "Blue light generation in a periodically poled Ti:LiNbO3 channel waveguide," *Optics Communications*, vol. 135, pp. 41-44, 1997.

44. Shu, H. *et al.*, "Study on domain inversion in LiNbO3 by Ti-indiffusion," *Ferroelectrics*, vol. 197, pp. 691-694, 1997.

45. Ito, H., Takyu, C. & Inaba, H., "Fabrication of Periodic Domain Grating in Linbo3 By Electron- Beam Writing For Application of Nonlinear Optical Processes," *Electronics Letters*, vol. 27, pp. 1221-1222, 1991.

46. Yamada, M., Nada, N., Saitoh, M. & Watanabe, K., "1st-Order Quasi-Phase Matched Linbo3 Wave-Guide Periodically Poled By Applying an External-Field For Efficient Blue 2nd- Harmonic Generation," *Applied Physics Letters*, vol. 62, pp. 435-436, 1993.

47. Burns, W. K., McElhanon, W. & Goldberg, L., "2nd-Harmonic Generation in-Field Poled, Quasi-Phase-Matched, Bulk Linbo(3)," *IEEE Photonics Technology Letters*, vol. 6, pp. 252-254, 1994.

48. Myers, L. E. *et al.*, "Quasi-Phase-Matched Optical Parametric Oscillators in Bulk Periodically Poled Linbo3," *Journal of the Optical Society of America B-Optical Physics*, vol. 12, pp. 2102-2116, 1995.

49. Balakrishnan, A. *et al.*, "Broadly tunable laser-diode-based mid-infrared source with up to 31 mu W of power at 4.3-mu m wavelength," *Optics Letters*, vol. 21, pp. 952-954, 1996.

50. Byer, R. L., "Quasi-phasematched nonlinear interactions and devices," *Journal of Nonlinear Optical Physics & Materials*, vol. 6, pp. 549-592, 1997.

51. Miller, G. D. *et al.*, "42%-efficient single-pass cw second-harmonic generation in periodically poled lithium niobate," *Optics Letters*, vol. 22, pp. 1834-1836, 1997.

52. Batchko, R. G., Shur, V. Y., Fejer, M. M. & Byer, R. L., "Backswitch poling in lithium niobate for high-fidelity domain patterning and efficient blue light generation," *Applied Physics Letters*, vol. 75, pp. 1673-1675, 1999.

53. Laurell, F., "Periodically poled materials for miniature light sources," *Optical Materials*, vol. 11, pp. 235-244, 1999.

54. Shur, V. Y. *et al.*, "Regular ferroelectric domain array in lithium niobate crystals for nonlinear optic applications," *Ferroelectrics*, vol. 236, pp. 129-144, 2000.

55. Lim, E. J., Fejer, M. M., Byer, R. L. & Kozlovsky, W. J., "Blue-Light Generation By Frequency Doubling in Periodically Poled Lithium-Niobate Channel Wave-Guide," *Electronics Letters*, vol. 25, pp. 731-732, 1989.

56. Bierlein, J. D. & Vanherzeele, H., "Potassium Titanyl Phosphate - Properties and New Applications," *Journal of the Optical Society of America B-Optical Physics*, vol. 6, pp. 622-633, 1989.

57. Chen, Q. & Risk, W. P., "Periodic Poling of Ktiopo4 Using an Applied Electric Field," *Electronics Letters*, vol. 30, pp. 1516-1517, 1994.

58. Chen, Q. & Risk, W. P., "High efficiency quasi phasematched frequency doubling waveguides in KTiOPO4 fabricated by electric field poling," *Electronics Letters*, vol. 32, pp. 107-108, 1996.

59. Guan, Q. *et al.*, "The DC conductive property of KTiOPO4 crystal along its z-axis," *Crystal Research and Technology*, vol. 33, pp. 821-825, 1998.

60. Moorthy, S. G., Kumar, F. J., Kannan, C. V., Subramanian, C. & Ramasamy, P., "Conductivity and dielectric studies on flux grown KTiOPO4 single crystals," *Ferroelectrics*, vol. 230, pp. 477-482, 1999.

61. Risk, W. P., "Fabrication and Characterization of Planar Ion-Exchanged KTiOPO4 Wave-Guides For Frequency Doubling," *Applied Physics Letters*, vol. 58, pp. 19-21, 1991.

62. Roelofs, M. G., Morris, P. A. & Bierlein, J. D., "Ion-Exchange of Rb, Ba, and Sr in Ktiopo4," *Journal of Applied Physics*, vol. 70, pp. 720-728, 1991.

63. Jongerius, M. J., Bolt, R. J. & Sweep, N. A., "Blue 2nd-Harmonic Generation in Wave-Guides Fabricated in Undoped and Scandium-Doped Ktiopo4," *Journal of Applied Physics*, vol. 75, pp. 3316-3325, 1994.

64. Guan, Q. C. *et al.*, "Ion exchange in KTiOPO4 crystals by electrolysis," *Progress in Crystal Growth and Characterization of Materials*, vol. 40, pp. 51-55, 2000.

65. Mu, X. D., Zotova, I. B., Ding, Y. J. & Risk, W. P., "Backward second-harmonic generation in submicron-period ion- exchanged KTiOPO4 waveguide," *Optics Communications*, vol. 181, pp. 153-159, 2000.

66. Laurell, F., "Stable Blue 2nd-Harmonic Generation in a KTP Wave-Guide With a Diode-Laser in an External-Cavity," *Electronics Letters*, vol. 29, pp. 1629-1630, 1993.

67. Jongerius, M. J., "Compact Violet Lasers By 2nd-Harmonic Generation in KTP Wave-Guides," *Philips Journal of Research*, vol. 49, pp. 293-313, 1995.

Chapter 8.
General conclusions.

8.1 General conclusions.

The work discussed in this thesis was concerned with the realisation and investigation of pulsed diode laser systems. Enhanced average and peak powers for required with picosecond-pulse operation in a compact laser source. By utilising single-mode narrow stripe InGaAs/GaAs ridge waveguide diode laser two distinct methodologies were investigated in pursuit of this goal.

The first technique for short optical pulse generation made use of a focused ion beam etching machine for the post-fabrication modification of the test single-contact devices. The modification involved etching the devices to form a two-section configuration. It was shown in Chapter 2. how when operated in a Q-switched configuration the appropriate application of DC bias voltages to such a modified device could effect a significant improvement in the pulse duration and its profile, and thus increase the peak powers achieved. The versatile technique of focused ion beam etching was also used to create structures in broad-area diode laser with the intention of improving the spatial output qualities of an otherwise multi-mode device. When an intracavity lens was etched in relief over the active region, a marked improvement was observed in the far-field with only a slight reduction in the optical output power. With further refinement, such a technique could form the basis as a cost-effective means of obtaining a high power, high brightness diode laser source. Currently such levels of performance can only be obtained from the expensive master oscillator/power amplifier (MOPA) configuration.

Due to the simplicity and elegance of its implementation, gain-switching was then evaluated with unmodified single-contact devices. No external optics were required for pulsed operation and the repetition rate of the output was readily adjustable by changing the frequency of the sinusoidal modulation that was utilised to affect gain-switched operation. Pulse durations as short as $30ps$ were observed with average and peak powers up to $150mW$ and $\approx 1.8W$ respectively. Unfortunately, a spectral bandwidth in the range $\approx 11nm$ to $\approx 25nm$ meant that the time-bandwidth product greatly exceeded the Fourier-transform limit. This implied the presence of frequency chirp on the picosecond pulse output.

Although these pulse durations and output powers represent an impressive achievement there has been a continual drive to improve upon these results, with the presentation and discussion of practical schemes.

To determine the exact nature of the temporal phase the recently established sonogram technique was implemented. In common with several other research groups studying the dynamic characteristics of diode laser outputs, an electron-optical streak camera and grating monochromator were combined to obtain the sonogram. From this work the sign and magnitude of the frequency chirp present on the optical pulses was established. Such information proved of significant value in the design of configurations/devices to compensate for the frequency chirp.

It was observed that the gain-switched InGaAs/GaAs ridge waveguide devices used throughout this study responded very favourably to optical feedback. This knowledge would prove extremely important as a consequence of the significant reduction in the spectral bandwidth that was associated with self-injection seeding. A sufficient reflection was obtained from an uncoated glass-slide placed some distance from the diode laser output facet. The spectral bandwidth of the external cavity picosecond diode laser thus obtained was reduced from $\approx 11nm$ to a minimum of $0.05nm$, representing a reduction of 220 times. There was a similar reduction in the time-bandwidth product with 0.45 being observed, indicating near-Fourier-transform limited pulse durations. The spectrally narrowed output could be tuned over $6nm$ simply by adjusting the angle of the glass-slide in either plane. There was no apparent effect on the spatial output of the single-mode device and only a minor degradation of the temporal and optical power output characteristics. Interestingly, unlike previous examples of self-injection seeding, the effect was only observed for non-resonant conditions, that was when $f_{mod} \neq Nf_{ext} \pm 200MHz$, where f_{mod} is the sinusoidal modulation applied to the diode laser, $N = 1, \pm 2, \pm 4...$ and f_{ext} is the external cavity frequency. If this condition was not satisfied then the output characteristics of a solitary device were observed. Theoretical modelling was performed and demonstrated a good agreement with the experimental results.

Optical feedback does not appear to have any detrimental effect on the observed operational lifetime of the device.

To investigate this effect further the glass-slide was replaced with a $50:50$ beam splitter and a standard diffraction grating. With such a configuration it was possible to continuously and smoothly tune the spectrally narrowed output over $70nm$ by varying the angle of the diffraction grating in the plane parallel to the junction. The effect was highly repeatable with only a 15% variation in the pulse duration and output power across the range where self-injection seeding was observed. Similar to the case of the glass-slide, in this external cavity the resultant output was near-Fourier-transform limited.

With the addition of a second grating, identical to the first, dual spectral and temporal outputs were observed. The two outputs were independently tunable. Spectral separations of up to $53nm$ were demonstrated between the two outputs. The temporal separation was adjustable by varying one of the two cavity lengths formed between each of the diffraction gratings and the laser chip. This is an exciting result and could find application wherever a tunable source of picosecond laser pulses is required. This work is currently ongoing and schemes are being evaluated to reduce the footprint of the dual grating configuration as well as attempting to increase its tuning range. The effect of self-injection seeding was also demonstrated successfully as discussed in Chapters 6. and 7. In particular, optical fibres containing Bragg gratings and a nonlinear KTP waveguide crystal incorporating a Bragg section were used for highly efficient second harmonic generation.

The concept of optical feedback was further utilised when optical fibres containing periodic Bragg gratings were fabricated. Several optical fibres were obtained with the reflectivity of the Bragg grating ranging from 20% to 50% at a centre wavelength of $\approx 979nm$. As expected a significant reduction in the spectral bandwidth was observed, however rather than a slight increase in the pulse duration (as with non-resonant self-injection seeding) a factor of two decrease was observed. Intrigued by this result, optical fibres containing aperiodic Bragg gratings were fabricated, the structure of was been designed with the knowledge of the optical pulses gleaned from the sonogram work of Chapter 4. The aperiodic Bragg grating had a 50% reflectivity centred at $979nm$

with a spectral bandwidth of $10nm$. As with its periodic counterpart, a reduction in both the spectral bandwidth and pulse duration was observed. Rather than significant pulse compression, spectral narrowing was observed with a centre wavelength corresponding to that of the Bragg grating period closest to the diode laser output facet. This effect was attributed to the reflectivity profile of the aperiodic Bragg grating and possible solutions were presented in Chapter 6.

A topic of current interest to the photonics community is the use of frequency conversion to access spectral regions not readily available from discrete laser sources. Frequency doubling of the $980nm$ diode lasers used in this study would result in an output in the blue spectral region that could be of use in many aspects of science, technology and medicine. Nonlinear conversion was realised by two distinct approaches, and work is still on going due to the significance.

The first methodology for frequency doubling involved the design of an a-PPLN crystal. Similar to the aperiodic fibre Bragg gratings discussed in Chapter 6., the crystal had a grating structure, designed using the knowledge obtained from the sonogram work, that would fully utilise the complete spectral bandwidth of the frequency chirped optical pulses from the gain-switched diode laser. We demonstrated an average second harmonic power of $3.6mW$ from a single pass fundamental input power of $108mW$. With further optimisation of the coupling optics it is anticipated that this value can be improved upon.

The second scheme for frequency conversion used a specially designed crystal fabricated in KTP. This crystal represents an accumulation of all the previous knowledge and is a major achievement in direct second harmonic generation using a diode laser source.

The crystal contained a 2D waveguide structure with dimensions in the x and y-axes comparable to those of the emission aperture of the diode laser. A consequence of this was that the focusing requirements were eased significantly, when compared with the a-PPLN optical scheme with only two AR coated objectives being required. The waveguide confined the coupled fundamental into a small region of space, increasing the interaction between the quasi-phase matching grating and the fundamental. The resultant second

harmonic efficiency was also guided by the waveguide. A consequence resulting from the use of a symmetrical waveguide was that the output in the blue did not show the same degree of astigmatism as the input at the fundamental. Efficient second harmonic conversion was obtained from a periodic grating by utilising the spectral narrowing associated with self-seeding optical feedback. To achieve optical feedback the latter $3/10th's$ of the waveguide contained a Bragg grating section designed to provide a $\approx 40\%$ reflection of the fundamental. This had the expected effect of reducing the spectral bandwidth of the optical pulse from the gain-switched diode laser $(\Delta\lambda \approx 25nm)$ to a level $(\Delta\lambda \approx 0.05nm)$ where the use of a periodic quasi-phase matched structure was applicable. Further more, the crystal contained waveguides with Bragg sections for a Bragg reflection at three discrete fundamental wavelengths. Changing to a nearby waveguide easily altered the second harmonic wavelength.

The maximum second harmonic was $7.3mW$ for a fundamental input power of $150mW$. Improvements in the second harmonic output power are anticipated by further refinement of the coupling optics, application of suitable AR coatings and the use of diode laser with higher output powers.

It should be noted that neither of the crystal facets were AR-coated so a significant reflection of the fundamental occurred at the input facet to the crystals. An increase in the second harmonic would be achieved simply through the application of suitable coatings to the crystal facets. This solution is currently under review.

There is potential for the commercial exploitation of this work, resulting in a compact and high power source of picosecond optical pulses in the blue spectral region. Using the techniques discussed, second harmonic generation of AlGaAs diode lasers would provide a source in the blue/UV that could be of use for photobiological applications.

Throughout the course of the work discussed in this thesis it has been demonstrated that the gain-switching of single-mode narrow stripe InGaAs/GaAs ridge waveguide diode lasers is a viable method through which picosecond optical pulses with high average peak power can be obtained. With

further improvements in optics it is possible that a blue source of picosecond pulses could be realised having a semi-monolithic design.

Chapter 9.
Acknowledgements.

9.1 Acknowledgements.

First and foremost I wish to extend my sincere gratitude toward my PhD supervisior, Professor Wilson Sibbett. I am grateful for his encouragement and understanding over the past years.

I wish to acknowledge the ever changing *face* of the "W-squad". It has certainly been an interesting ride, if not a little turbulent at times.

In common with most W-squad members of recent years, Dr Sleat deserves special mention for his expert knowledge of all things electronic and for teaching me the basics regarding the operation and set-up of electron-optical streak cameras.

Thanks to the mechanical workshop for bringing my drawings to life, usually as illustrated. What's a couple of extra holes here and there?

In order to keep Morag happy, I'd better mention the secretaries. They do a sterling job, and I'm sure the place would grind to a halt with out them running around after us all.

To my proof reader Dr Kemp I am indebted. Hopefully the bottle of whisky demonstrates my appreciation of your services rendered.

We are grateful to JDS Uniphase for the supply of $980nm$ single-mode, InGaAs diode lasers.

Finally, I should thank the staff from the department of physics and applied physics at the University of Hull. If it weren't for them I wouldn't be here now.

Chapter 2.

I wish to thank the staff at the University of Bristol for the help provided when using the focussed ion beam etching facility. In particular, I am grateful to Dr Williams for his invaluable assistance throughout the course of this work, and Dr Heard for his patience when operating the machine and the image used in Figure 2.1.

I also wish to thank GEC Marconni materials technology (GMMT) for the diode laser arrays, and Dr Yanson from the University of Glasgow for the broad area devices.

Chapter 4.

I am grateful to Dr Reid his assistance in the sonogram work, including experimental realisation, algorithm development, retrieval and numerous discussed. Thanks to Iain Cormack for proof reading the chapter.

Chapter 5.

I wish to thank Dr Avrutin from the York of University for the non-resonant self-injection seeding modelling, and his assistance with the identification of the mechanisms involved.

Chapter 6.

Thanks to Dr Zhang from the University of Aston for fabricating the optical fibre Bragg gratings used in this work.

Chapter 7.

I wish to thank Dr Smith from the Southampton of University for the lithium niobate crystals used in this study. I am grateful to Jonathan Philips for allowing the use of his Ti:sapphire laser with which the lithium niobate crystals were evaluated.

I am indebted to Dr Battle and the company Adv-R Inc (USA) for whom he works for providing the PP-KTP crystals, and their ongoing support on this project. I acknowledge Dr Allan from the University of Edinburgh for supplying the image used in Figure 7.3.1. and Dr Battle from Adv-R Inc for supplying the images used in Figures 7.3.2. and 7.3.3.

Appendix A.
dBm conversion.

Conversion between dBm, volts and watts for a 50Ω system.

dBm	V	P	dBm	V	P
50	70.7	100W	24	3.55	250mW
49	64.0	80W	23	3.20	200mW
48	58.0	64W	22	2.80	160mW
47	50.0	50W	21	2.52	125mW
46	44.5	40W	20	2.25	100mW
45	40.0	32W	19	2.00	80mW
44	32.5	25W	18	1.80	64mW
43	32.0	20W	17	1.60	50mW
42	28.0	16W	16	1.41	40mW
41	26.2	12.5W	15	1.25	32mW
40	22.5	10W	14	1.15	25mW
39	20.0	8W	13	1.00	20mW
38	18.0	6.4W	12	0.90	16mW
37	16.0	5W	11	0.80	12.5mW
36	14.1	4W	10	0.71	10mW
35	12.5	3.2W	9	0.64	8mW
34	11.5	2.5W	8	0.58	6.4mW
33	10.0	2W	7	0.500	5mW
32	9.0	1.6W	6	0.445	4mW
31	8.0	1.25W	5	0.400	3.2mW
30	7.10	1.0W	4	0.355	2.5mW
29	6.40	800mW	3	0.320	2.0mW
28	5.80	640mW	2	0.280	1.6mW
27	5.0	500mW	1	0.252	1.25mW
26	4.45	400mW	0	0.225	1.0mW
25	4.00	320mW			

Appendix B.

HP-VEE electrical characteristics program.

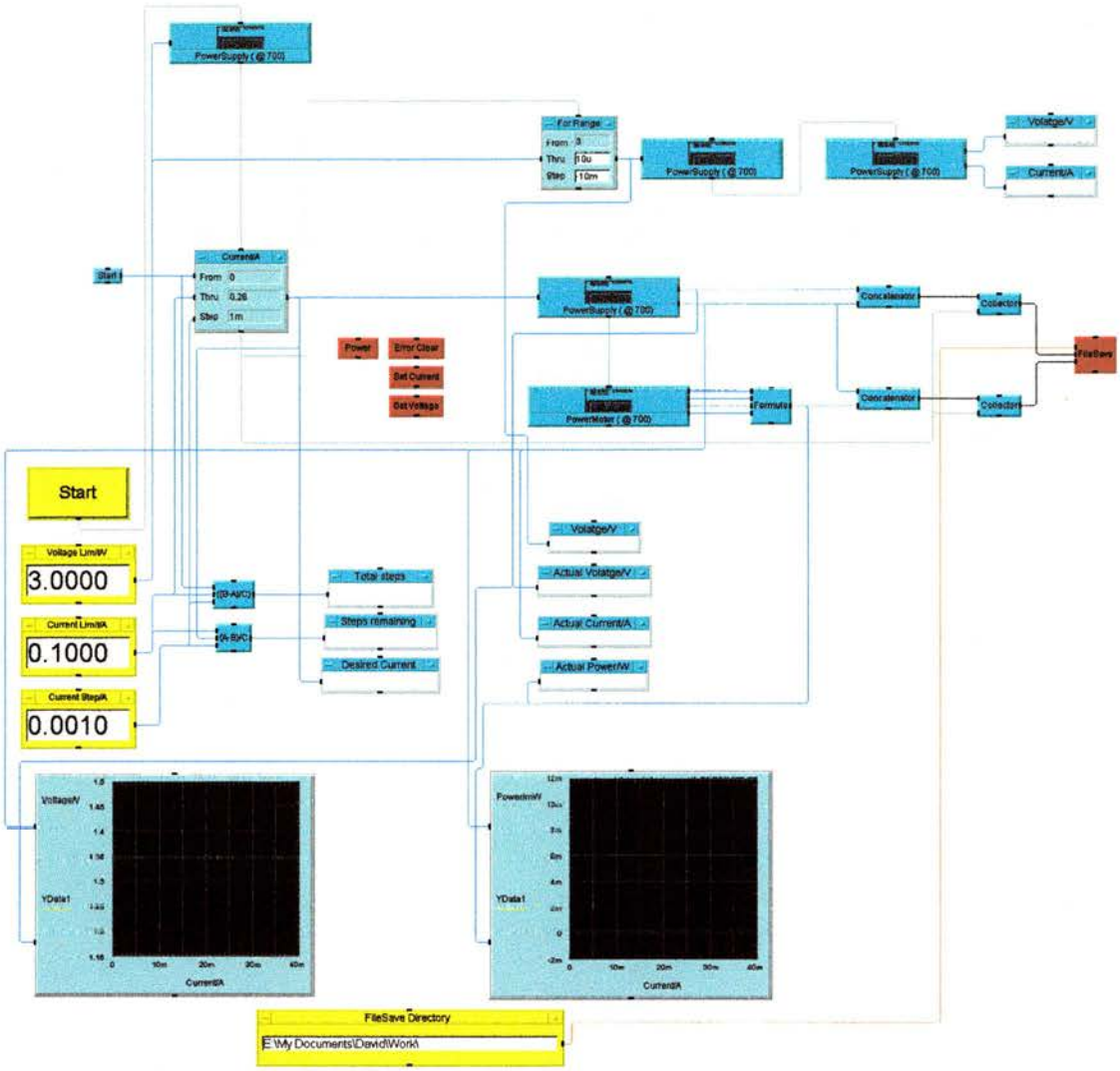

Figure B.1. Main program.

Program to measure the electrical characteristics of any given diode laser, with a maximum current of $8A$. For device protection both voltage and current limits were provided. Three individual measurements of the output power were taken for any DC bias, with the recorded value being the algebraic average.

Measurement of the characteristics was undated in real-time providing a visual representation of the progress. Two data files were saved to hard disc, being light/current and voltage/current curves. The save directory and filenames were user selectable.

Figures B.2 through B.6. illustrate the various sub-routines used within the main program.

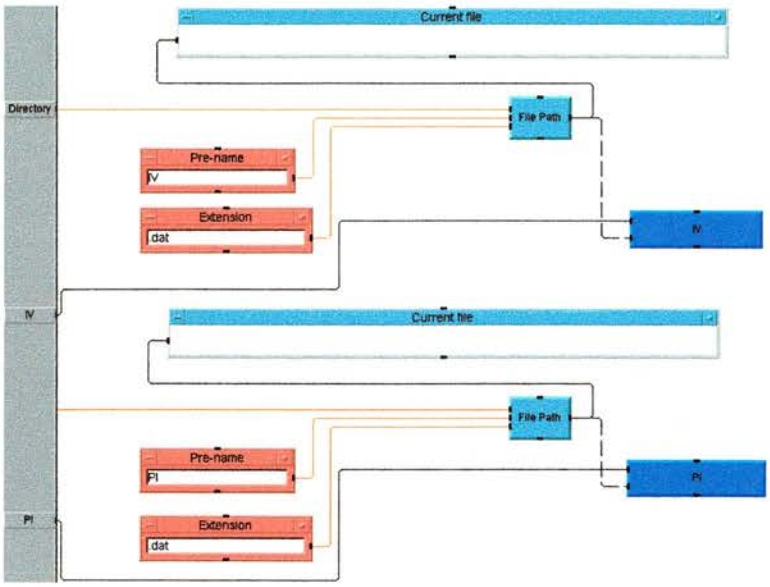

Figure B.2. Save file to disc sub-routine.

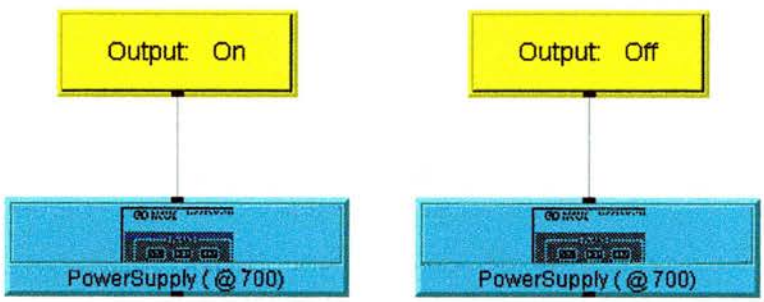

Figure B.3. Manual power supply status sub-routine.

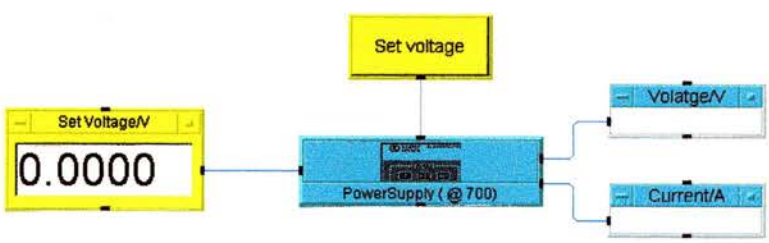

Figure B.4. Manually set voltage sub-routine.

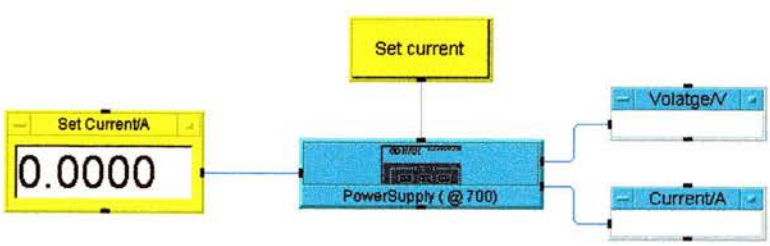

Figure B.5. Manually set current sub-routine.

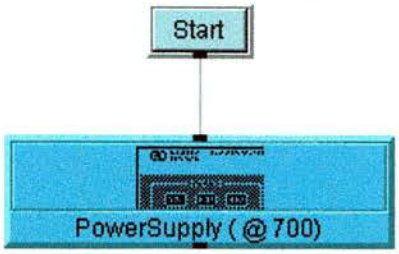

Figure B.6. "Error clear" sub-routine.

Appendix C.

HP-VEE high-resolution monochromator program.

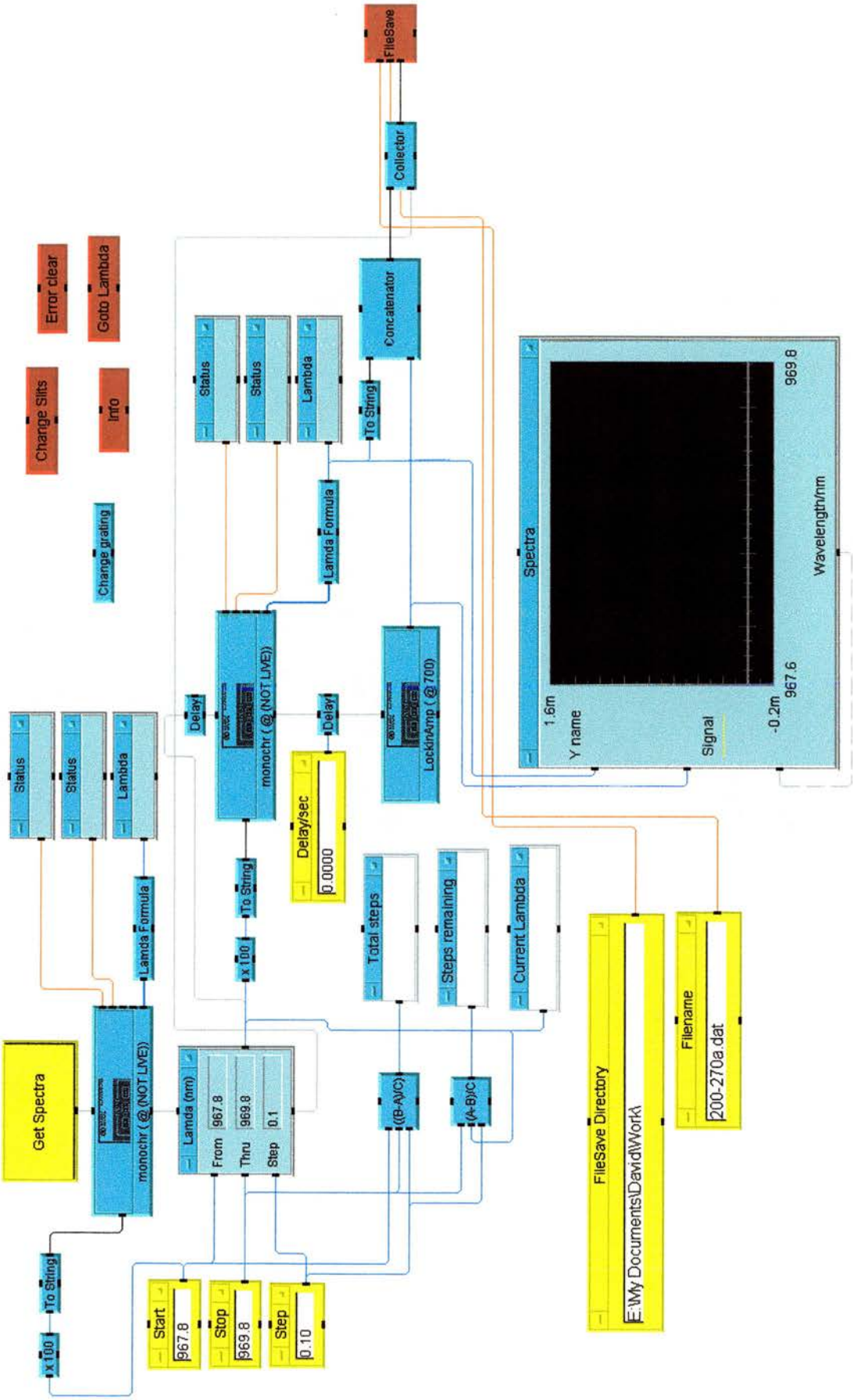

Figure C.1. Main program.

Program to measure a spectrum using the computer-controlled CVI high-resolution monochromator. Manual control of the grating number, slit widths and wavelength was provided.

Measurement of the spectrum was undated in real-time providing a visual representation of the progress. The data file was saved to hard disc, with the save directory and filenames being user selectable.

Figures C.2 through C.8. illustrate the various sub-routines used within the main program

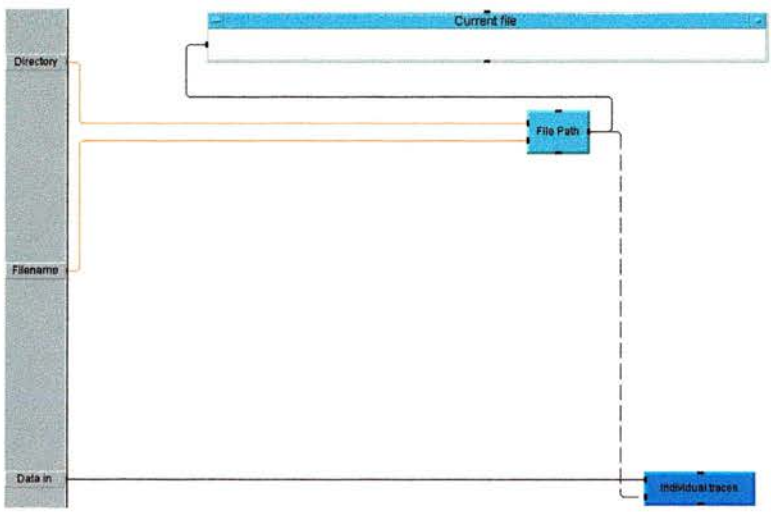

Figure C.2. Save file to disc sub-routine.

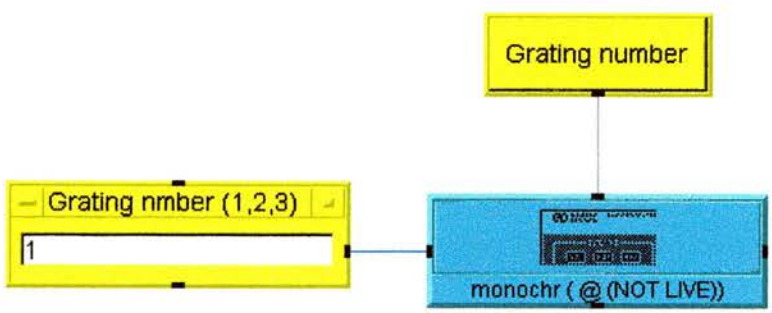

Figure C.3. Change grating sub-routine.

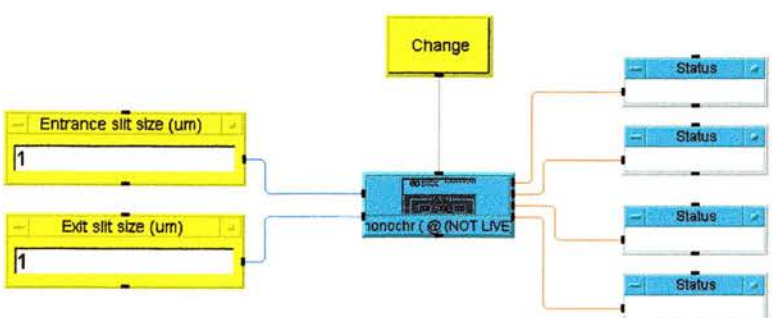

Figure C.4. Change slit width sub-routine.

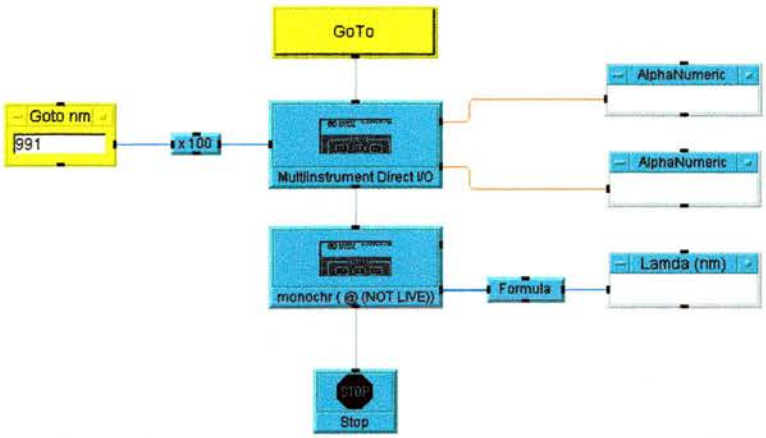

Figure C.5. Go to user specified wavelength sub-routine.

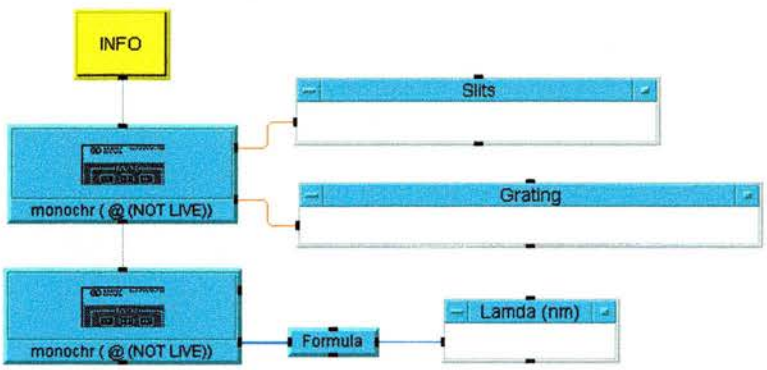

Figure C.6. Monochromator information display sub-routine.

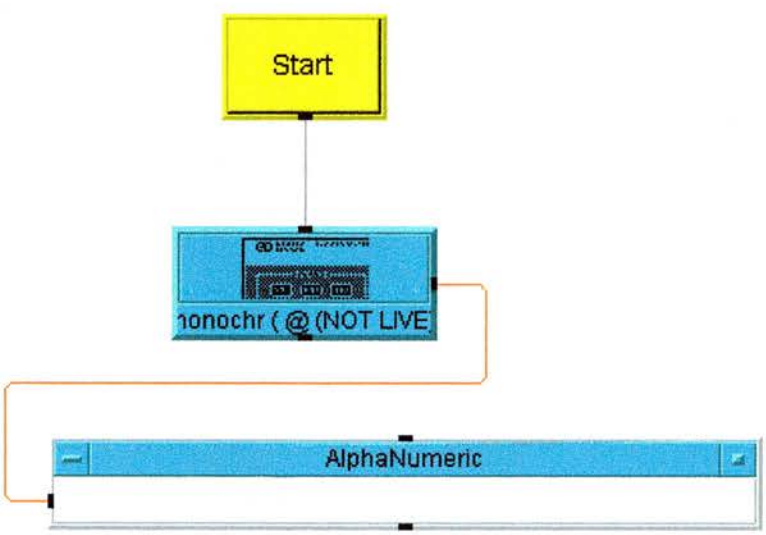

Figure C.7. "Error clear" sub-routine.

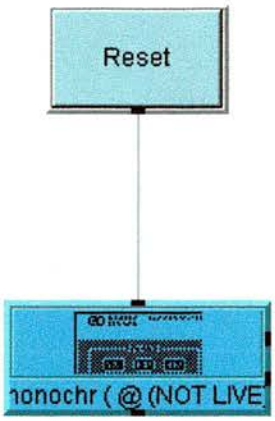

Figure C.8. Monochromator reset sub-routine.

Appendix D.

HP-VEE sonogram data acquisition program.

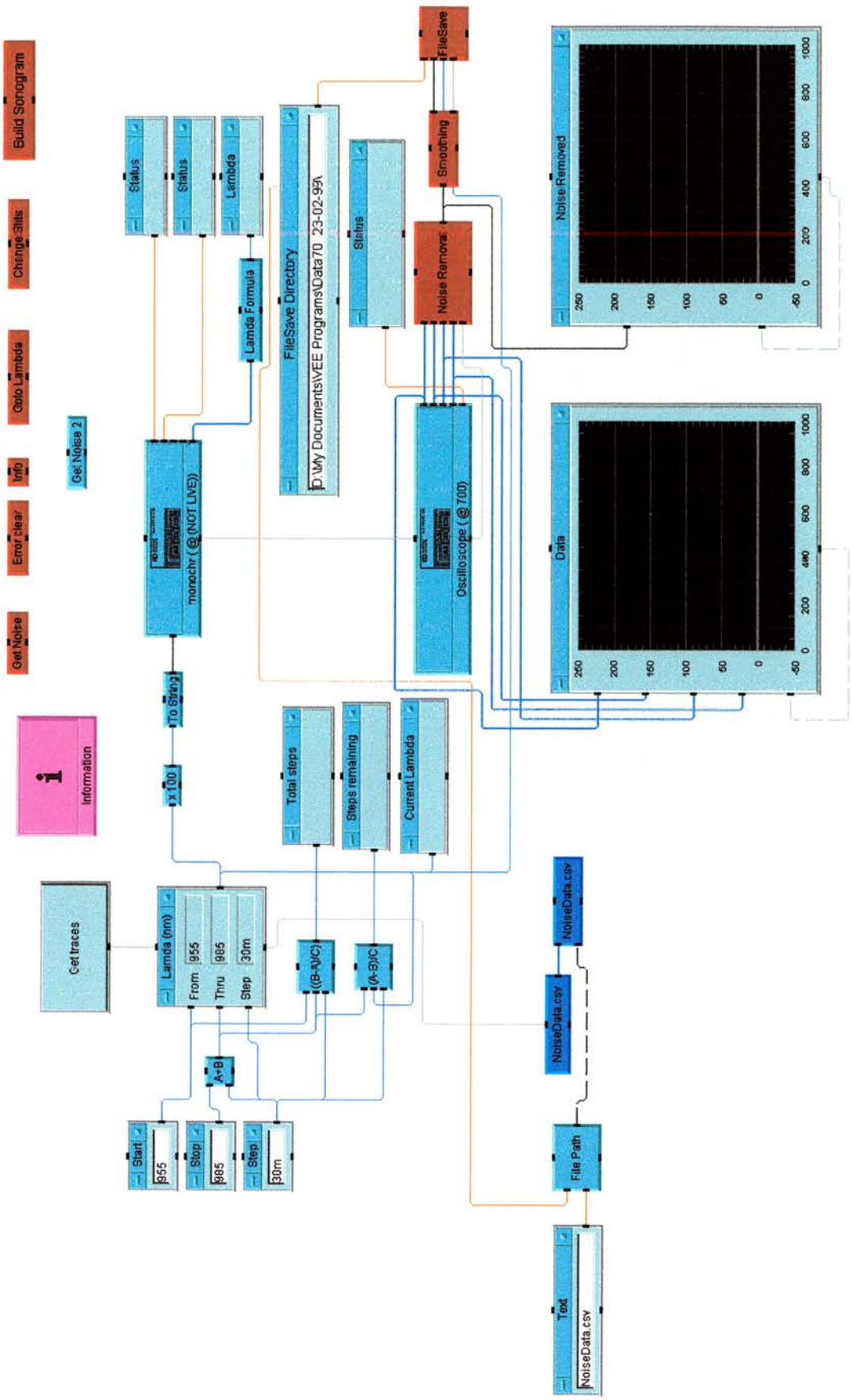

Figure D.1. Main program.

Program to acquire the data necessary to produce an experimental sonogram. The computer-controlled monochromator was used as a scanning bandpass filter, with the temporal profiles recorded by the streak camera displayed in the program and saved to disc with a filename corresponding to the current monochromator wavelength.

Figures D.2. through D.6. illustrate the various sub-routines used within the main program. The program shares the monochromator control sub-routines that were illustrated in Appendix C.

A measurement of the streak camera noise was performed and saved to disc using the sub-routine illustrated in Figure D.2. Four measurements of a temporal profile at a given monochromator wavelength were taken. The previously measured noise was subtracted using the sub-routine in Figure D.3. before the algebraic average was calculated.

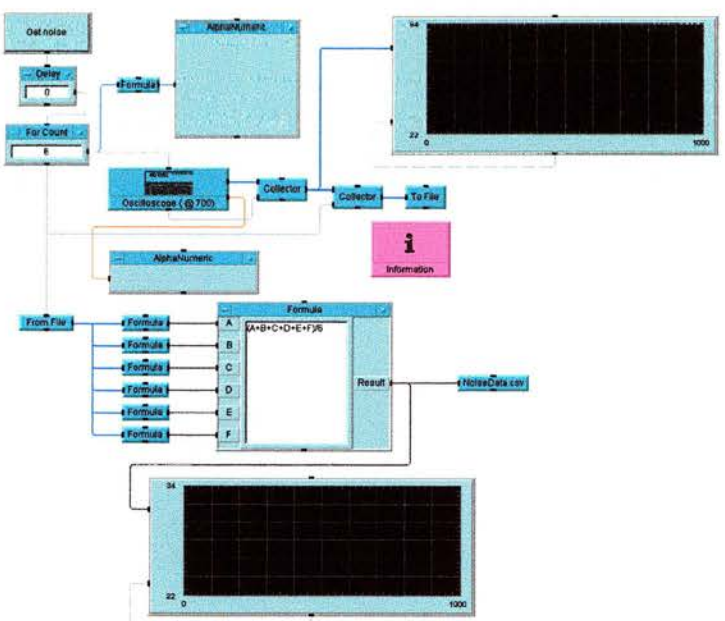

Figure D.2. Get noise sub-routine.

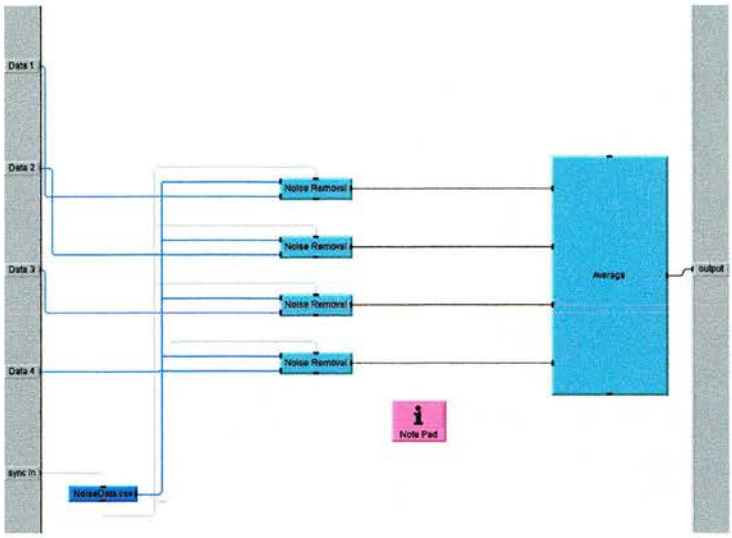

Figure D.3. Noise removal and averaging sub-routine.

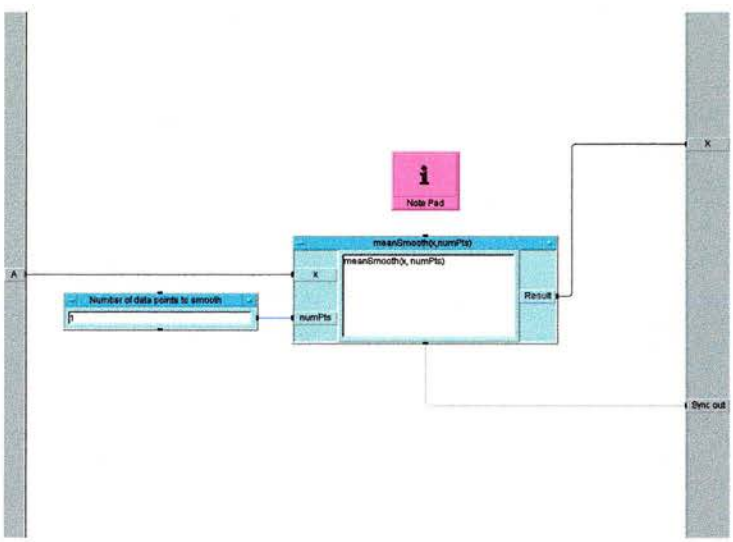

Figure D.4. Smoothing sub-routine.

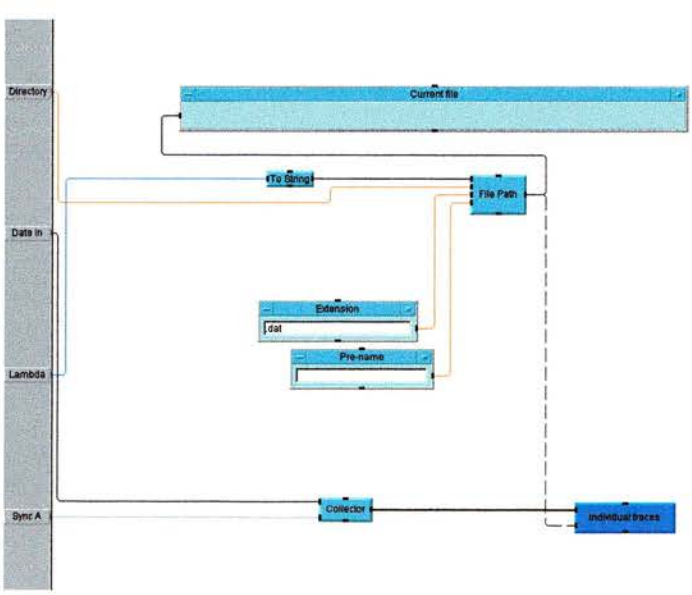

Figure D.5. File save sub-routine.

Appendix E.

HP-VEE sonogram construction program.

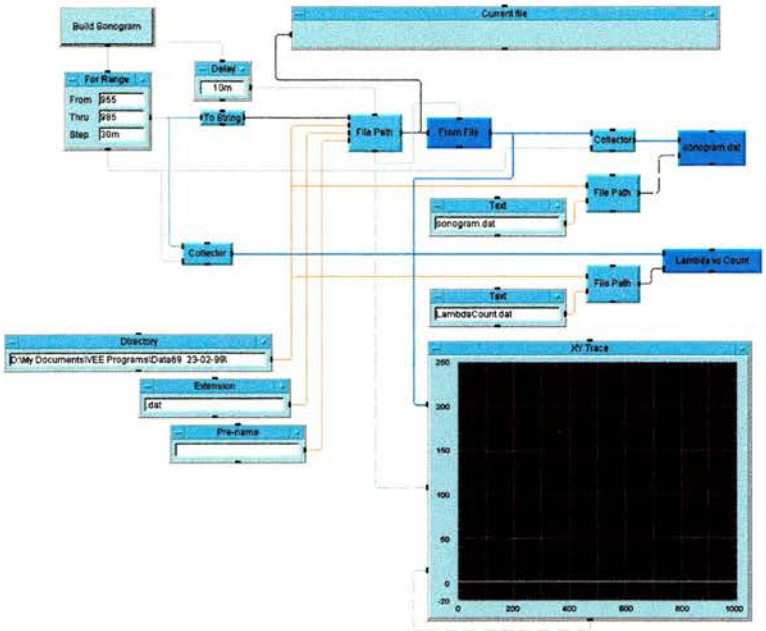

Figure E.1. Main program.

Reads the data from the disc previously saved by the sonogram data acquisition program outline in Appendix D. These individual temporal profiles were then "stacked" in wavelength to create an experimental sonogram. The resulting array was saved to disc with a user selectable filename and target directory.

Appendix F.
Matlab sonogram retrieval program.

```
%                                                    sonogram1024.m

figure(1);
clf reset;
figure(2);
clf reset;
figure(3);
clf reset;
figure(4);
clf reset;
figure(5);
clf reset;
figure(6);
clf reset;
%figure(7);
%clf reset;
%figure(8);
%clf reset;
%figure(9);
%clf reset;



%sonogram must be named "sono1024"
%load spectrum of gain-switched laser "spectra1024.dat"
%load gate function "g_975.dat"
%create freq using freq=[1:1024];



%clear all;                                          % Remove for experimental
%figure(1);
load_sonogram1024                                    % Enable for experimental
%Experimental spectrum
labspec = sqrt(spectra1024);
labspec = labspec';
labspec = abs(labspec);
figure(2);
plot(freq,abs(labspec).*abs(labspec));
%Experimental gate
labgate = sqrt(g_975);
labgate = labgate';
figure(5);
plot(freq,abs(labgate).*abs(labgate));


%break
pause(10);


%create guess pulse and gate in order to produde a synthetic sonogram

% Create Gaussian pulse in time:
tp=2500.;                                            % Original value 32  (10)  (30)
a=1.386/tp/tp;                                       % Original value 1.386
for n=1:1024
t=09.*(n-512);                                       % Original value 09  (09)  (35)
```

```
e(n)=exp(-a*t*t+i*0.00004*t*t);
freq(n)=n;
end

% for n=512:1:1024
% e(n)=e(n)+0.5*e(n-10);
% end
%plot guess pulse
%figure(3);
%plot(freq,abs(e).*abs(e));
%pause(4);
% Transform guess pulse from time to frequency domain
e=fft(e);
e=fftshift(e);
% filter blue end (high freqs);
for n=512:1:1024
%e(n)=e(n)+0.5*e(n-10);
end
% plot guess pulse
%figure(4);
%plot(freq,abs(e).*abs(e));
%                              pause(4);
%break
e=fftshift(e);
e=ifft(e);
%plot(freq,abs(e).*abs(e));
%pause;

% Create Gate in frequency:
a2=0.002;
for n2=1:1024,
 if abs(n2-512)<50                                    %was 40
  g(n2)=1.;
            else
  g(n2)=0;
 end
end
% plot gate function                                  ***Remove if using Experimental gate***
%figure(5);
%plot(freq,abs(g).*abs(g));

% labs=make_sono(e,g);
% pcolor(labs)
% shading interp
% pause
% Transform E into freq domain:
e=fft(e);
e=fftshift(e);

op=e'*g;
op=row_rot_for(op);
op=fftshift(op);
op=ifft(op);
labs=abs(op).*abs(op);
```

```
%Retrieval starts here!!!

figure(1);                                  % Remove for experimental
pcolor(labdata)                             % Change to "labdata" experimental
shading interp                              % Remove for experimental
%break
% Guess field and gate:
ek=labspec;
for n=1:1024
ek(n)=ek(n)*exp(2.*pi*i*rand);
gk(n)=exp(-.0004*(n-512)^2);
%gk(n)=exp(-.08*(n-512)^2);
end
figure(5);
plot(freq,abs(ek).*abs(ek));
ek=fft(ek);
ek=fftshift(ek);

figure(3);
plot(freq,abs(ek).*abs(ek));
figure(6);
plot(freq,abs(gk).*abs(gk));

%                   break                   % plots guess pulse and gate

pause(2);
ok=1
I2=sqrt(labdata);                           % Change to "labdata" experimental
rand('state',0);
for ialg=1:20                               %number of loops to calculate
ialg
% Make sonogram:
% Outer product:
op=ek'*gk;
% Row rotation:
op=row_rot_for(op);
% Fourier transform (freq->time):
op=fftshift(op);
op=ifft(op);


%Sonogram before intensity constraint:
sonok=abs(op).*abs(op);
%pcolor(abs(op).*abs(op))

%g=g_error(labs,sonok)

% Intensity constraint - NOTE using labdata not labs
op=(op./abs(op)).*I2;


% Reverse Fourier transform (time->freq):

op=fft(op);
op=fftshift(op);
% Reverse row rotation:
op=row_rot_rev(op);
```

```
% Principal Component Decomposition:
%ek=ek*(op*op');
%gk=gk*(op'*op);


ek=(ek*op);
ek=ek*op';
gk=(gk*op');
gk=gk*op;

ek=ek/max(ek);
gk=gk/max(gk);

%gk=abs(gk);                                          % Sets gate phase to zero
%Replaces the amplitude with the experimental amplitude
%maintains phase information.
ek=ek.*(labspec./abs(ek));  %labspec=sqrt(lab spectrum)
%gk=gk.*(labgate./abs(gk));
end

%plot retreived sonogram
figure(4);
pcolor(sonok);
shading interp


et=fftshift(ek);
et=ifft(et);

figure(3);
plot(freq,abs(ek).*abs(ek));
figure(5);
[ax, h1, h2]=plotyy(freq,abs(et).*abs(et),freq,unwrap(angle(et)));
figure(6);
plot(freq,abs(gk).*abs(gk));

save sono_freq_05.dat freq  -ascii
save sono_ek_05.dat  ek  -ascii
save sono_et_05.dat  et  -ascii
save sono_gk_05.dat  gk  -ascii
save sono_sonok_05.dat  sonok  -ascii

%pause(4);
%figure(6);
%[ax, h1, h2]=plotyy(freq,abs(gk).*abs(gk),freq,unwrap(angle(gk)));
*****************************************************************************************

%clear all
%load sono1024.dat        %Enable if sono1024.dat is not
for f=1:1024                                %currently loaded
for t=1:1024
ipos=(f-1)*1024+t;
labdata(t,1025-f) = sono1024(ipos);
% Horiz axis is freq shift & vertical is delay
% (ignore variable names!)
% labdata(t,f)=lab_sono(ipos);
```

```
end
end
%pcolor(labdata)
%shading interp
*****************************************************************************************

function [x]=row_rot_for(x)
s=size(x);
m=s(1);
for n=2:m
a=x(n,1:n-1);
b=x(n,n:m);
x(n,1:m+1-n)=b;
x(n,m+2-n:m)=a;
end;
*****************************************************************************************

function [x]=row_rot_rev(x)
s=size(x);
m=s(1);
for n=2:m
a=x(n,m+2-n:m);
b=x(n,1:m+1-n);
x(n,1:n-1)=a;
x(n,n:m)=b;
end;
```

Appendix G.
Publications.

1. Birkin, D. J. L., Rafailov, E. U. & Sibbett, W., "Tunable operation of a gain-switched diode laser by nonresonant self-injection seeding," *Photonics Technology Letters*, pp. (submitted), 2001.

2. Rafailov, E. U. *et al.*, "Efficient direct frequency conversion of a non-resonant injection-seeded diode laser using a periodically-poled KTP waveguide crystal," *Optics Letters*, pp. (submitted), 2001.

3. Rafailov, E. U., Birkin, D. J. L., Avrutin, E. A. & Sibbett, W., "Non-resonant self-injection seeding of a gain switched diode laser," *IEEE Journal of Select Topics of Quantum Electronics*, vol. 7 pp. 287-292, 2001.

4. Rafailov, E. U., Birkin, D. J. L. & Sibbett, W. in *QEP'15* (submitted) (Glasgow, UK, 2001).

5. Birkin, D. J. L. *et al.* in *QEP'15* (submitted) (Glasgow, UK, 2001).

6. Birkin, D. J. L. *et al.*, "Near-transform-limited picosecond pulses from a gain-switched InGaAs diode laser with fiber Bragg gratings," *Applied Physics Letters*, vol. 79, pp. 151-152, 2001.

7. Birkin, D. J. L. *et al.*, "3.6 mW blue light by direct frequency doubling of a diode laser using an aperiodically poled lithium niobate crystal," *Applied Physics Letters*, vol. 78, pp. 3172-3174, 2001.

8. Sokolovskii, G. S. *et al.* in *Int. Symp. Nanostructures: Physics and Technology (NANO-2001)* (St. Petersburg, Russia, 2001).

9. Birkin, D. J. L. *et al.* in *CLEO'00* (Baltimore, USA, 2001).

10. Sokolovskii, G. S., Rafailov, E. U., Birkin, D. J. L. & Sibbett, W., "Novel high-power laser structures incorporating curved gratings," *Ieee Journal of Quantum Electronics*, vol. 36, pp. 1412-1420, 2000.

11. Valentine, G. J. *et al.*, "Femtosecond Yb : YCOB laser pumped by narrow-stripe laser diode and passively modelocked using ion implanted saturable-absorber mirror," *Electronics Letters*, vol. 36, pp. 1621-1623, 2000.

12. Birkin, D. J. L., Rafailov, E. U., Sibbett, W. & Avrutin, E. in *CLEO/Europe'00* CWF76 (Nice, France, 2000).

13. Birkin, D. J. L. *et al.* in *eCLEO* CWF75 (Nice, France, 2000).

14. Sokolovskii, G. S. *et al.* in *CLEO/Europe'00* CWF67 (Nice, France, 2000).

15. Sokolovskii, G. S., Rafailov, E. U., Birkin, D. J. L. & Sibbett, W., "High-power laser structures incorporating novel curved-gratings," *Optical and Quantum Electronics*, vol. 31, pp. 215-221, 1999.

16. Rafailov, E. U., Birkin, D. J. L., Avrutin, E. A., Sleat, W. E. & Sibbett, W., "High average power short-pulse generation from singlemode InGaAs GaAs laser diodes," *Iee Proceedings-Optoelectronics*, vol. 146, pp. 51-54, 1999.

17. Birkin, D. J. L. *et al.* in *CLEO/Europe'00* CThB4 (Nice, France, 2000).

18. Birkin, D. J. L., Rafailov, E. U., Reid, D. T. & Sibbett, W. in *LEOS* (St. Andrews, UK, 2000).

19. Sokolovskii, G. S. *et al.* in *Nanostructures'00* (St. Petersburg, Russia, 2000).

20. Rashed, A. M. *et al.* in *CLEO-Pacific Rim 2000* (2000).

21. Birkin, D. J. L. *et al.* in *CLEO'00* (San Francisco, USA, 2000).

22. Birkin, D. J. L. *et al.* in *CLEO'00* (San Francisco, USA, 2000).

23. Reid, D. T. *et al.*, "Femtosecond pulse compression by second-harmonic generation in aperiodically poled KTP," , 1998.

24. Rafailov, E. U., Birkin, D., Avrutin, E. A. & Sibbett, W., "Short-pulse generation from single-mode InGaAs/GaAs laser diodes by large-signal RF modulation," *Microwave and Optical Technology Letters*, vol. 18, pp. 354-356, 1998.

25. Rafailov, E. U., Birkin, D., Avrutin, E. A. & Sibbett, W. (Cardiff, UK, 2001).